



UNIVERSITY OF
LIVERPOOL

Solid acid catalysts based on heteropoly acids for conversion of renewable feedstocks

Thesis submitted in accordance with the requirements of
the University of Liverpool for the degree of Doctor in
Philosophy by Ali Mohammed Alsalmé

July 2010

Abstract

“Solid acid catalysts based on heteropoly acids for conversion of renewable feedstocks”

PhD thesis by Ali M. Alsalmé

The aim of this work is to investigate homogeneous and heterogeneous catalysis by HPAs for the conversion of renewable feedstocks. This includes the preparation, characterisation and testing of a range of acidic solid materials such as bulk HPAs, $\text{Cs}_{2.5}\text{H}_{0.5}\text{PW}_{12}\text{O}_{40}$ and the acidic composites comprising $\text{H}_3\text{PW}_{12}\text{O}_{40}$ (HPW) supported on Nb_2O_5 , ZrO_2 and TiO_2 .

The HPW supported on TiO_2 , ZrO_2 and Nb_2O_5 were prepared by impregnation method and then characterised regarding their acid properties and the chemical structure of HPA on the catalyst surface, compared to “standard” HPA catalysts such as bulk and silica-supported $\text{H}_3\text{PW}_{12}\text{O}_{40}$ and $\text{Cs}_{2.5}\text{H}_{0.5}\text{PW}_{12}\text{O}_{40}$. In contrast to the parent acid $\text{H}_3\text{PW}_{12}\text{O}_{40}$ and $\text{Cs}_{2.5}\text{H}_{0.5}\text{PW}_{12}\text{O}_{40}$, possessing strong Brønsted acid sites, the catalysts supported on TiO_2 , ZrO_2 and Nb_2O_5 possess both Brønsted and Lewis acid sites, with the latter mainly originating from the oxide support. These catalysts possess weaker acid sites than $\text{H}_3\text{PW}_{12}\text{O}_{40}$ and $\text{Cs}_{2.5}\text{H}_{0.5}\text{PW}_{12}\text{O}_{40}$, with their acid strength being similar to that of acidic zeolites. The catalytic activity (turnover frequency) in gas-phase isopropanol dehydration decreases in the order: $\text{H}_3\text{PW}_{12}\text{O}_{40} > \text{Cs}_{2.5}\text{H}_{0.5}\text{PW}_{12}\text{O}_{40} > 15\%\text{H}_3\text{PW}_{12}\text{O}_{40}/\text{SiO}_2 > 15\%\text{H}_3\text{PW}_{12}\text{O}_{40}/\text{TiO}_2 \gg 15\%\text{H}_3\text{PW}_{12}\text{O}_{40}/\text{Nb}_2\text{O}_5 > 15\%\text{H}_3\text{PW}_{12}\text{O}_{40}/\text{ZrO}_2$, which is in line with the acid strength determined by NH_3 adsorption calorimetry. ^{31}P MAS NMR and FTIR indicate an increasing interaction between support and HPA in the following order: $\text{SiO}_2 < \text{TiO}_2 < \text{Nb}_2\text{O}_5, \text{ZrO}_2$, whilst the strength of acid sites decreases in that order.

Esterification of hexanoic acid and transesterification of ethyl propanoate and ethyl hexanoate with excess methanol (1:20 molar ratio) were tested at 60 °C and ambient pressure with a range of HPA catalysts in homogeneous and heterogeneous systems in comparison with conventional homogeneous and solid acid catalysts such as H_2SO_4 , Amberlyst-15 and zeolites HY and H-Beta. In these reactions, the intrinsic catalytic activity (turnover frequency, TOF) of HPA catalysts is significantly higher than that of the conventional acid catalysts. The TOF values decrease with decreasing catalyst acid strength in the order: $\text{H}_3\text{PW}_{12}\text{O}_{40} \approx \text{Cs}_{2.5}\text{H}_{0.5}\text{PW}_{12}\text{O}_{40} > \text{H}_4\text{SiW}_{12}\text{O}_{40} > 15\%\text{H}_3\text{PW}_{12}\text{O}_{40}/\text{Nb}_2\text{O}_5, 15\%\text{H}_3\text{PW}_{12}\text{O}_{40}/\text{ZrO}_2, 15\%\text{H}_3\text{PW}_{12}\text{O}_{40}/\text{TiO}_2 > \text{H}_2\text{SO}_4 > \text{HY}, \text{H-Beta} > \text{Amberlyst-15}$. Supported HPA catalysts suffer from leaching and exhibit significant contribution of homogeneous catalysis by the leached HPA.

The isomerisation of α -pinene is studied in the gas phase over solid HPA catalysts in a fixed bed continuous flow reactor at 200°C and ambient pressure. The reaction yields camphene as the main product in a mixture with monoterpene by-products such as limonene, terpinolenes, terpinenes, β -pinene, p-cymene and others. The strong Brønsted solid acids exhibit high initial activities, but suffer from catalyst deactivation, resulting in low camphene yields. Conversely, the HPA catalysts supported on Nb_2O_5 , ZrO_2 and TiO_2 , although weaker acids, show more stable performance in α -pinene isomerisation.

Publication

The results presented in this thesis have been published in the following journals and conferences:

- 1- A. Alsalme, E. F. Kozhevnikova, I. V. Kozhevnikov, "Heteropoly acids as catalysts for liquid-phase esterification and transesterification", *Appl. Catal. A* 349 (2008) 170.
- 2- A. M. Alsalme, P. Wiper, Y. Z. Khimyak, E. F. Kozhevnikova, I. V. Kozhevnikov, "Solid acid catalysts based on $H_3PW_{12}O_{40}$ heteropoly acid: acid and catalytic properties at a gas-solid interface", *J. Catal.* in press.
- 3- A. Alsalme, E. F. Kozhevnikova, I. V. Kozhevnikov, Poster day in University of Liverpool, Liverpool, United Kingdom, March 2008.
- 4- A. Alsalme, E. F. Kozhevnikova, I. V. Kozhevnikov, Saudi International Innovation Conference (SIIC), University of Leeds, Leeds, United Kingdom, June 2008.
- 5- A. Alsalme, E. F. Kozhevnikova, I. V. Kozhevnikov, 6th World Congress on Catalysis by Acids and Bases, Genova, Italy, May 2009.
- 6- A. Alsalme, E. F. Kozhevnikova, I. V. Kozhevnikov, 42nd IUPAC Congress, Glasgow, United Kingdom, August 2009.
- 7- A. Alsalme, E. F. Kozhevnikova, I. V. Kozhevnikov, (EuropaCat IX) Catalysis for a Sustainable World, Salamanca, Spain, September 2009.
- 8- A. Alsalme, E. F. Kozhevnikova, I. V. Kozhevnikov, The 10th International Symposium on the "Scientific Bases for the Preparation of Heterogeneous Catalysts", Louvain-la-Neuve, Belgium, July 2010.

Acknowledgements

First of all, I would like to thank my supervisor Professor Ivan V. Kozhevnikov for his support and supervision. He was always there to listen and to give advice. He showed me different ways to approach a research problem and the need to be persistent to achieve any goal.

I am also very grateful to Dr Elena F. Kozhevnikova for her assistance in solving several problems during my work in this project. Thanks are due to Dr Yaroslav Z. Khimyak for valuable discussions.

I appreciate the experimental work carried out by Paul V. Wiper for NMR analysis and Stephen Apter for elemental analysis.

I would also like to thank all members of the technical support team in the Chemistry Department, especially James Mulvihill and Charles Clavering for their assistance relating to the laboratory work.

It is a pleasure to record my thanks to my group members Abdullah Alhanash, Fahd Al-wadaani, Mshari Alotaibi and Robert Hettely.

I thank my parents for unconditional support and encouragement to pursue my interests.

A special thanks to my wife and my children for the many weekends and evenings they patiently allowed me to work. Without their support and encouragement, I would not have been able to complete this thesis.

Finally, I would like to acknowledge the financial support of the King Saud University in Riyadh.

List of abbreviations

HPA	Heteropoly Acid.
FFAs	Free Fatty Acids.
TPD	Temperature Programmed Desorption.
BET	Brunauer-Emett-Teller
TGA	Thermogravimetric Analysis.
IR	Infrared
XRD	X-ray Diffraction.
NMR	Nuclear Magnetic Resonance
MAS	Magic Angle Spinning.
DSC	Differential Scanning Calorimetry.
DTG	Derivative Thermogravimetric.
ICP	Inductively Coupled plasma.
AES	Atomic Emission Spectroscopy.
MS	Mass Spectroscopy.
DRIFT	Diffuse Reflectance Infrared Fourier.
UV	Ultraviolet.
GC	Gas Chromatography.
FTIR	Fourier Transform Infrared.
TOF	Turnover Frequency.
STP	Standard Temperature and Pressure.

Contents

Abstract	i
Publication	ii
Acknowledgements	iii
List of abbreviations	iv
Contents	v
1. Introduction	1
1.1 Heteropoly acids (HPA)	1
1.1.1 Introduction to HPA	1
1.1.2 Structures of HPA	2
1.1.2.1 Primary structure	2
1.1.2.1.1 Keggin structure	2
1.1.2.1.2 Wells-Dawson structure	5
1.1.2.1.3 Anderson-Evans structure	5
1.1.2.1.4 Dexter-Silverton structure	6
1.1.2.2 Secondary structure	6
1.1.2.3 Tertiary structure	8
1.1.3 Stability of heteropoly compounds	9
1.1.3.1 Stability of heteropoly acids in solution	9
1.1.3.2 Thermal stability	10
1.1.4 Acid properties of heteropoly compounds	11
1.1.4.1 Heteropoly acids in solution	11
1.1.4.2 Solid heteropoly acids	12
1.1.4.3 Solid heteropoly salts	15
1.1.4.4 Supported heteropoly acids	17
1.1.5 Acid catalysis by heteropoly acids	19
1.1.5.1 Homogenous acid catalysis	19
1.1.5.2 Acid catalysed reactions in biphasic liquid-liquid systems	21
1.1.5.3 Heterogeneous acid catalysis	22
1.1.5.3.1 Types of heterogeneous catalysis by heteropoly acid	23
1.2 Biodiesel as an alternative fuel	24
1.2.1 Alternative diesel fuels	24

1.2.2	Biodiesel production through transesterification of triglycerides	26
1.2.2.1	Base catalysts	26
1.2.2.2	Acid catalysts	28
1.2.2.2.1	Homogeneous acid catalysis	28
1.2.2.2.2	Heterogeneous acid catalysis	30
1.2.3	Biodiesel production through esterification of free fatty acids (FFAs)	32
1.2.3.1	Homogeneous acid catalysis	32
1.2.3.2	Heterogeneous acid catalysis	34
1.3	Isomerisation of α -pinene	36
1.4	Objectives and thesis outline	40
	References	42
2.	Experimental	50
2.1	Introduction	50
2.2	Chemicals and solvents	50
2.3	Catalyst preparation	50
2.3.1	Preparation of $\text{Cs}_{2.5}\text{H}_{0.5}\text{PW}_{12}\text{O}_{40}$	50
2.3.2	Preparation of supported HPW catalysts	51
2.3.3	Preparation of ZrO_2	51
2.3.4	Preparation of Nb_2O_5	52
2.3.5	Preparation of $20\%\text{Cs}_2\text{HPW}_{12}\text{O}_{40}/\text{SiO}_2$	52
2.4	Catalyst characterisation techniques	53
2.4.1	Thermogravimetric analysis (TGA)	53
2.4.2	Inductively coupled plasma atomic emission spectroscopy (ICP-AES)	55
2.4.3	Fourier transform infrared spectroscopy (FTIR)	56
2.4.4	Ultraviolet (UV) spectroscopy	57
2.4.5	Surface area and porosity	58
2.4.6	Powder X-ray diffraction (XRD)	61
2.4.7	Differential scanning calorimetry (DSC)	62
2.4.8	Solid state ^{31}P NMR	64
2.5	Catalyst reaction studies	65
2.5.1	Product analysis	65

2.5.1.1	Gas chromatography (GC)	65
2.5.1.2	GC calibration	68
2.5.2	Reaction studies	76
2.5.2.1	Liquid phase reactions	76
2.5.2.1.1	Heterogeneous versus homogeneous catalysis test	76
2.5.2.1.2	Catalyst reuse	76
2.5.2.2	Gas phase reactions	78
	References	82
3.	Catalyst characterisation	84
3.1	Introduction	84
3.2	Thermogravimetric analysis (TGA)	84
3.3	Surface area and porosity	92
3.4	Infrared spectroscopy	110
3.5	Powder X-ray diffraction	113
3.6	³¹ P MAS NMR	114
3.7	Acidity of HPA catalysts	119
3.7.1	Pulse ammonia adsorption analysis	120
3.7.2	FTIR study of pyridine adsorption	122
3.8	Conclusion	126
	References	128
4.	Liquid phase esterification and transesterification reactions catalysed by heteropoly acids	131
4.1	Introduction	131
4.2	Homogeneously catalysed esterification and transesterification	133
4.2.1	Substrate reactivity	133
4.2.2	Catalyst performance	135
4.2.2.1	Turnover frequency	135
4.2.3	Preliminary kinetic results	138
4.2.3.1	Reaction order	138

4.2.3.2	Rate constants	141
4.3	Heterogeneously catalysed esterification and transesterification	143
4.3.1	Catalyst leaching	143
4.3.2	Catalyst performance	147
4.3.3	Catalyst reuse	156
4.4	Conclusion	157
	References	159
5.	Isopropanol dehydration as test reaction	161
5.1	Introduction	161
5.2	Experimental procedure	165
5.3	Light-off test (T_{50})	166
5.3.1	Effect of calcination temperature	170
5.3.2	Activation energy	170
5.4	Reaction time course	171
5.4.1	Turnover frequency (TOF)	174
5.4.2	Relationship between $\log(\text{TOF})$ and ΔH	175
5.5	Conclusion	176
	References	177
6.	Gas phase isomerisation of α-pinene over heteropoly acid catalysts	179
6.1	Introduction	179
6.2	Isomerisation of α -pinene in gas phase	180
6.2.1	Reaction time course	181
6.2.2	Isomerisation of α -pinene over “standard” HPA catalysts	182
6.2.3	Isomerisation of α -pinene over HPW supported on Nb_2O_5 , ZrO_2 and TiO_2	185
6.2.4	Effect of reaction temperature	189
6.2.5	Effect of calcination temperature	190
6.3	Conclusion	192

References	193
7. Conclusions	194

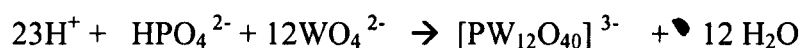
1. Introduction

1.1 Heteropoly acids (HPA)

1.1.1 Introduction to HPA

Heteropolyanions are polyoxometalate anions consisting of nanosized metal-oxygen clusters. These inorganic anions possess unique physicochemical properties, especially their structural mobility and multifunctionality, and are therefore important in several disciplines. Heteropolyanions have a general formula $[X_xM_mO_y]^{q-}$ ($x \leq m$), where M is the addendum atom and X is the heteroatom (also called central atom when located in the centre of the polyanion). The most commonly used addendum atoms are Mo(VI) or W(VI), less frequently V(V) or Nb(V) are used. A broad range of elements can be used as heteroatoms. These include P(V), As(V), Si(IV), Ge(IV), B(III), etc.

These anions are generally prepared by a self-assembly process in an acidic aqueous solution as shown in the following equation [1].



The first heteropoly compound was discovered by Berzelius in 1826 [2]. This was ammonium 12-molybdophosphate. In the next 70 years, heteropoly compounds were intensively investigated and approximately 750 of such compounds were reported [1]. Since then, there have been many proposals for the structure of heteropoly compounds [3-5]. Keggin in 1933 succeeded in determining the structure of $H_3PW_{12}O_{40} \cdot 5H_2O$ by using a powder X-ray diffraction technique [6]. By 1995, the X-ray structures of approximately 180 heteropoly compounds had been reported [1].

1.1.2 Structures of HPA

1.1.2.1 Primary structure

There are different kinds of heteropoly compound structures. The structure of a heteropoly compound molecule itself is called the “primary structure” [7, 8]. In solution, heteropoly anions are usually present as the free units of primary structure, coordinated with solvent molecules and can be protonated. Most heteropolyanions tend to hydrolyse readily at high pH. Protonation and hydrolysis of the primary structure may be major structural concerns in solution catalysis.

1.1.2.1.1 Keggin structure

This structure has been described by Keggin who studied the hydrated tungstophosphoric acid with six water molecules [9]. It is the most popular heteropoly compound structure in catalysis due to its high stability and availability. The Keggin anion has a diameter of approximately 1.2 nm and consists of a central XO_4 tetrahedron (X = heteroatom or central atom) surrounded by twelve MO_6 octahedra (M = addendum atom) as shown in Figure 1.1. The twelve MO_6 octahedra comprise four groups of three edge-shared octahedra. Each group (M_3O_{13}) has a common oxygen vertex connected to the central heteroatom (X). The total assemblage contains 40 close-packed oxygen atoms.

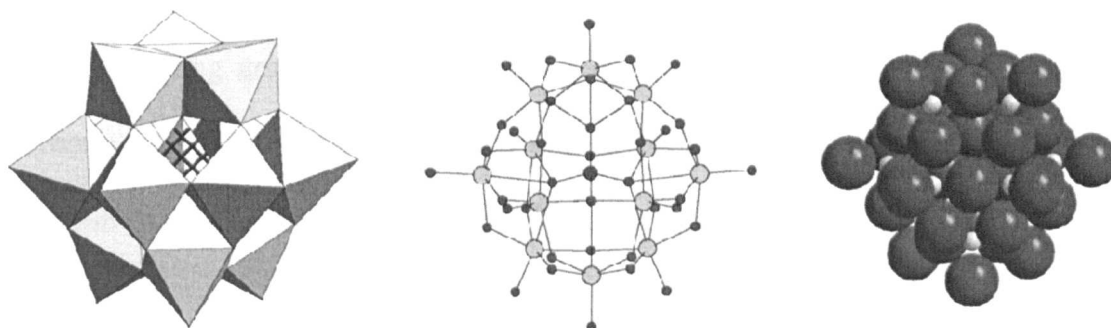


Figure 1.1 The Keggin structure of the $[XM_{12}O_{40}]^{x-8}$ anion (α -isomer): polyhedral (left), ball-and-stick (middle) and space-filling (right) representation [10].

There are four types of oxygen in this structure (Figure 1.2): $X-O_a-(M)_3$, $M-O_b-$ M both connecting two M_3O_{13} units by corner sharing; $M-O_c-M$ connecting two M_3O_{13} units by edge sharing; and O_d-M , where M is the addendum atom and X the heteroatom. These oxygens can be discriminated by ^{17}O NMR and infrared spectroscopic techniques. The $M-O$ and $X-O$ bonds display infrared bands in the range of $600-1100\text{ cm}^{-1}$ [1, 7, 11].

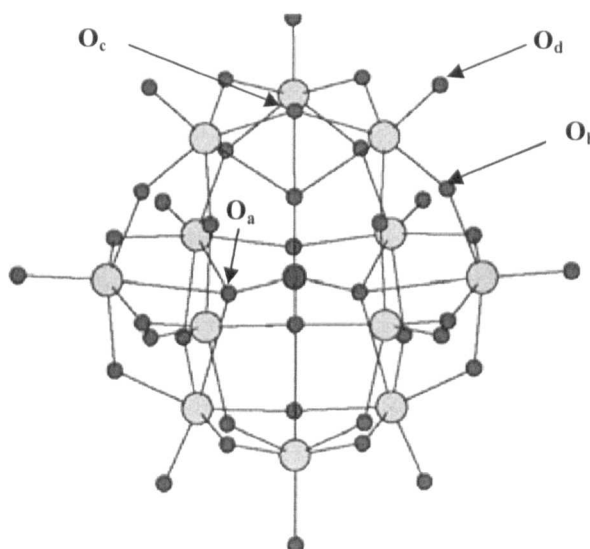


Figure 1.2 Schematic representation of the Keggin unit, $\alpha\text{-XM}_{12}\text{O}_{40}^n$.

There are several isomers of the Keggin structure existing when one or more of the edge-sharing groups of octahedra have been rotated 60° . The structure shown in Figure 1.1 is the α isomer. Rotation of one M_3O_{13} group produces the β -isomer. Rotation of two, three or all four M_3O_{13} groups produces the γ , δ , and ϵ isomers, respectively.

Removal of one or more MO_6 octahedron from the Keggin anion produces lacunary derivatives. Figure 1.3 shows examples of three lacunary derivatives (one monovacant and two trivacant). The two trivacant species correspond to the loss of a corner-shared group of MO_6 octahedra (A-type XM_9) or an edge-shared group (B-type XM_9).

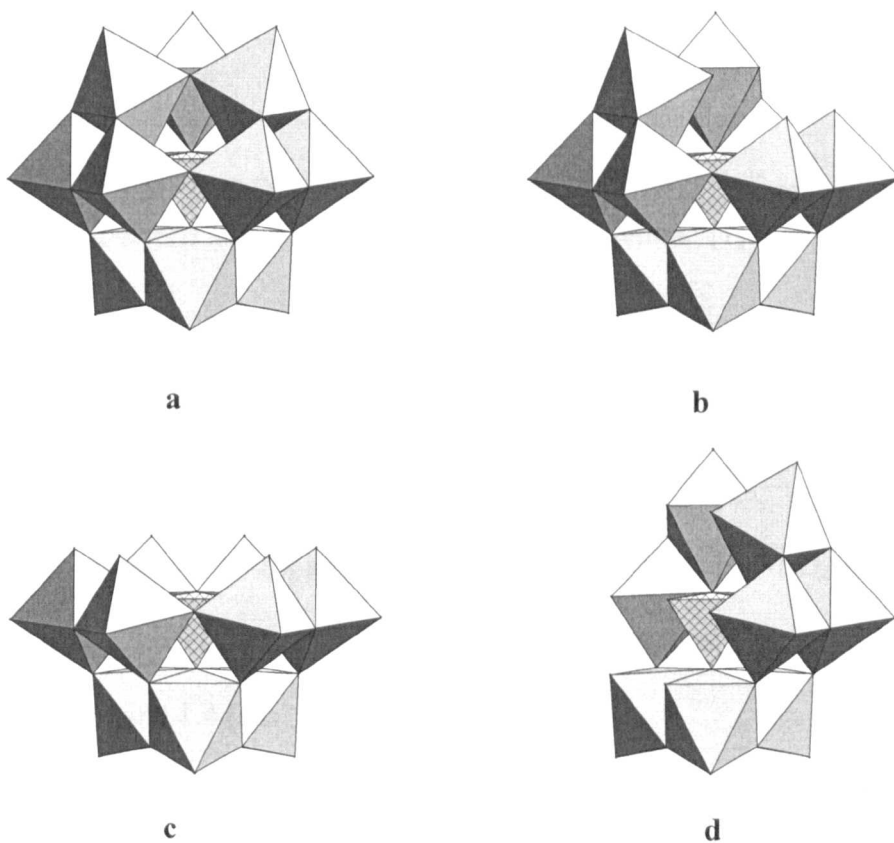


Figure 1.3 The structure of the α -Keggin anion $[XM_{12}O_{40}]^{x-8}$ (a) and its lacunary derivatives: (b) monovacant, (c) trivacant A-(XM_9), and (d) trivacant B-(XM_9)[1].

1.1.2.1.2 Wells-Dawson structure

The Wells-Dawson structure has a general formula $[X_2M_{18}O_{62}]^{2x-16}$ (M= Mo(VI) or W(VI), X= P(V) or As(V)). This structure is an assembly of two trivacant lacunary Keggin species A- XM_9 . Its structure (α isomer) is shown in Figure 1.4 (a).

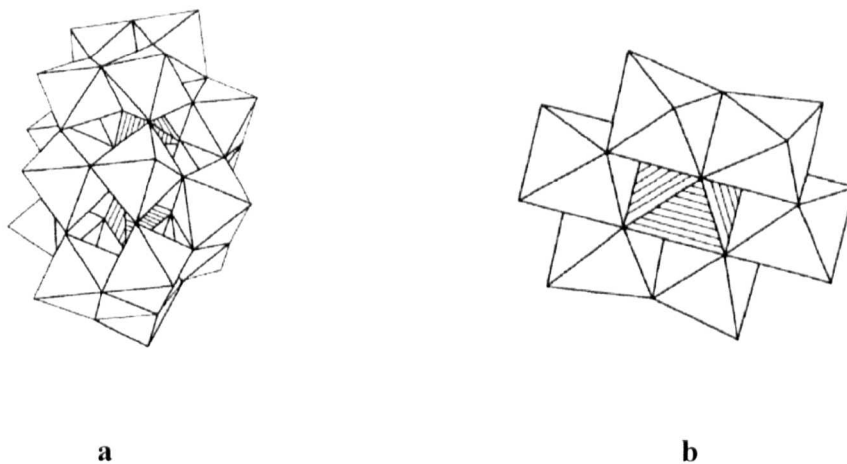


Figure 1.4 (a) The Well-Dawson structure of the $[X_2M_{18}O_{62}]^{2x-16}$ anion (α isomer). (b) The Anderson-Evans structure of the $[Te^{6+}Mo_6O_{24}]^{6-}$ anion. [1].

1.1.2.1.3 Anderson-Evans structure

The Anderson-Evans structure has a general formula $[X M_6O_{24}]^{n-}$ (X = Mn(IV), Ni(IV), Pt(IV), Te(VI), M = Mo(VI), W(VI)) and comprises six edge-shared octahedra as shown in Figure 1.4 (b).

1.1.2.1.4 Dexter-Silverton structure

This is a less common structure $[\text{XM}_{12}\text{O}_{42}]^{x-12}$, where M is Mo^{6+} and X is Ce(IV), U(IV), or Th(IV). In this anion (Figure 1.5), heteroatom (X) is surrounded by 12 oxygen atoms that form an icosahedron as a central polyhedron. The MO_6 octahedra are arranged in face-sharing pairs [1, 11, 12].

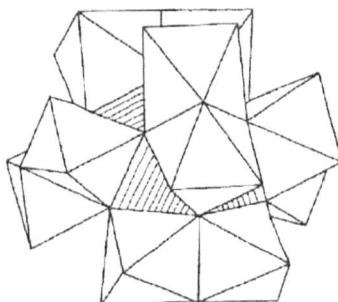


Figure 1.5 The Dexter-Silverton structure of the $[\text{XM}_{12}\text{O}_{42}]^{x-12}$ anion [1].

1.1.2.2 Secondary structure

Heteropoly compounds in the solid state are ionic crystals (sometimes amorphous) consisting of large polyanions (primary structure), counterocations (H^+ , H_3O^+ , H_5O_2^+ , etc), water of crystallisation, and sometimes organic molecules. These structures are called the “secondary structure”. This structure strongly depends on the amount of hydration water [1, 8, 13, 14]. These water molecules are easily removed from the solid by heating. This is a reversible process accompanied by a change in the volume of the crystal cell. For instance, the loss of water brings changes in the anion packing of $\text{H}_3\text{PW}_{12}\text{O}_{40}\cdot n\text{H}_2\text{O}$: $n = 29$ (cubic), $n = 21$ (orthorhombic), $n = 14$ (triclinic), $n = 6$ (cubic).

Protons of crystalline $\text{H}_3\text{PW}_{12}\text{O}_{40}\cdot 6\text{H}_2\text{O}$ are present as hydrated species, H_5O_2^+ , each of which links four neighbouring heteropoly anions by hydrogen bonding to the terminal $\text{W}-\text{O}_d$ oxygen atoms (Figure 1.6b). $\text{Cs}_3\text{PW}_{12}\text{O}_{40}$, in which the Cs^+ ions occupy the sites of H_5O_2^+ ions of $\text{H}_3\text{PW}_{12}\text{O}_{40}$ hexahydrate, has a dense secondary structure and is anhydrous (Figure 1.6c).

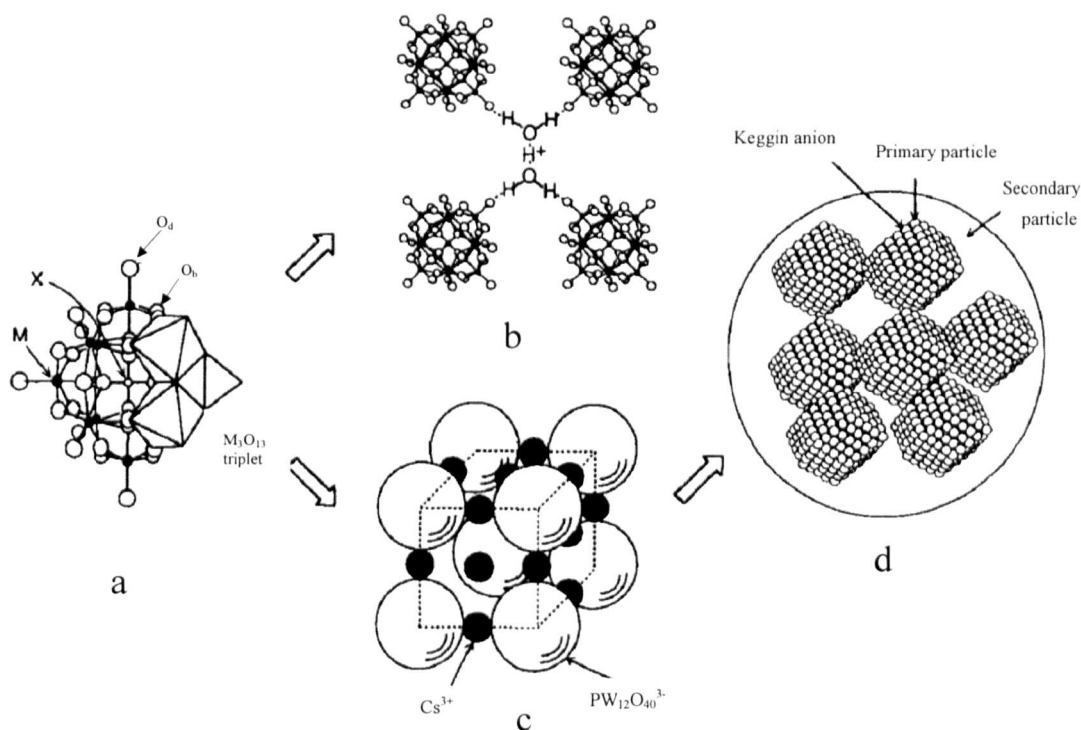


Figure 1.6 Primary, secondary, and tertiary structures of heteropoly compounds. (a) Primary structure (Keggin structure, $\text{XM}_{12}\text{O}_{40}$); (b) secondary structure ($\text{H}_3\text{PW}_{12}\text{O}_{40}\cdot 6\text{H}_2\text{O}$); (c) secondary structure ($\text{Cs}_3\text{PW}_{12}\text{O}_{40}$); (d) tertiary structure [$\text{Cs}_{2.5}\text{H}_{0.5}\text{PW}_{12}\text{O}_{40}$, cubic structure as in (c)][7].

1.1.2.3 Tertiary structure

Besides primary and secondary structures, there is a tertiary structure. The tertiary structure is the structure of solid HPAs as assembled. The sizes of the particles, pore structure, distribution of protons in the particle, etc., are the elements of the tertiary structure and play an important role in heterogeneous catalysis. Figure 1.6 shows primary, secondary, and tertiary structures of heteropoly compounds.

Counteranions greatly affect the tertiary structure of heteropoly compounds [7, 15, 16]. Salts with small cations, such as Li^+ or Na^+ , behave similarly to the acid. They are highly soluble in water and other polar organic solvents and usually have low surface area. In contrast, salts with large cations K^+ , Cs^+ , NH_4^+ are insoluble in water due to the low energy of solvation of large cations and usually have high surface area because of the smaller sizes of the primary particles, giving along with high thermal stability favorable properties for heterogeneous catalysis [17-21].

The surface area and pore structure are closely related. Figure 1.7 shows the surface area as a function of the extent of Na or Cs substitution of $\text{H}_3\text{PW}_{12}\text{O}_{40}$. The surface area decreases monotonically when the Na content increases. On the other hand, the surface area increases significantly when the Cs content, x in $\text{Cs}_x\text{H}_{3-x}\text{PW}_{12}\text{O}_{40}$, changes from $x = 2$ ($1 \text{ m}^2 \text{ g}^{-1}$) to $x = 3$ ($156 \text{ m}^2 \text{ g}^{-1}$), although it decreases only slightly from $x = 0$ ($6 \text{ m}^2 \text{ g}^{-1}$) to $x = 2$. The surface area increases significantly to more than $130 \text{ m}^2 \text{ g}^{-1}$ when the Cs content exceeds 2.5 [7, 21]. According to the TEM observation and nitrogen adsorption measurement [22], $\text{Cs}_{2.5}\text{H}_{0.5}\text{PW}_{12}\text{O}_{40}$ and $\text{Cs}_3\text{PW}_{12}\text{O}_{40}$ consist of very fine particles (8-10 nm in diameter) and therefore, the pores are interparticle, not intracrystalline.

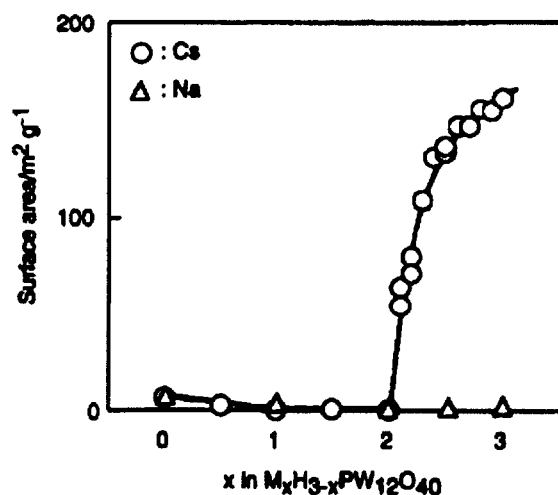


Figure 1.7 Surface areas of Na or Cs acidic salt of $H_3PW_{12}O_{40}$ as a function of the extent of Na or Cs substitution [7].

1.1.3 Stability of heteropoly compounds

1.1.3.1 Stability of heteropoly acids in solution

Stability of heteropoly compounds is an important factor for catalysis. In solutions of heteropoly acids, several species are present of equilibrium, the composition depending on the pH. Figure 1.8 shows the pH range of existence of heteropoly acids in aqueous media. Each heteropoly acid is stable only at pH values lower than the corresponding solid line [7, 23]. Heteropoly acid solutions normally equilibrate quite quickly (in seconds). However, sometimes it can take several months [1, 24].

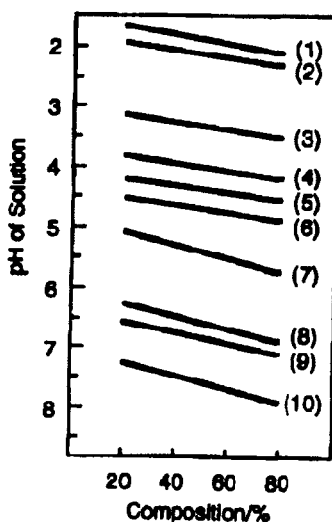


Figure 1.8 Stability of heteropoly acids [23]: (1) $\text{PMo}_{12}\text{O}_{40}^{3-}$, (2) $\text{PW}_{12}\text{O}_{40}^{3-}$, (3) $\text{GeMo}_{12}\text{O}_{40}^{4-}$, (4) $\text{GeW}_{12}\text{O}_{40}^{4-}$, (5) $\text{P}_2\text{W}_{18}\text{O}_{62}^{6-}$, (6) $\text{SiW}_{12}\text{O}_{40}^{4-}$, (7) $\text{PMo}_{11}\text{O}_{39}^{7-}$, (8) $\text{P}_2\text{Mo}_5\text{O}_{23}^{6-}$, (9) $\text{H}_2\text{W}_{12}\text{O}_{40}^{6-}$, (10) $\text{PW}_{11}\text{O}_{39}^{7-}$.

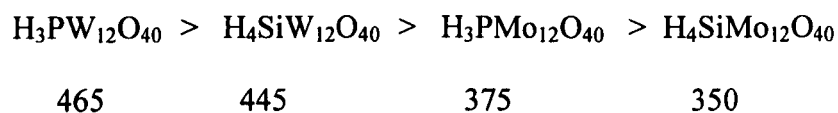
1.1.3.2 Thermal stability

Some solid heteropoly compounds are fairly stable and applicable in reactions at moderately high temperature (300-350°C). However, this stability may not be sufficient for catalyst regeneration, for instance, burning coke that may form on the catalyst surface (500-550°C) [1]. The thermal decomposition of heteropoly compounds to form a mixture of oxides is a complex multistage process [25]. The catalyst activity may be permanently lost at an early stage of decomposition. For example, solid acid catalysts based on tungsten heteropoly acids (e.g. $\text{H}_3\text{PW}_{12}\text{O}_{40}$) possibly lose activity as a result of the loss of protons at the onset of thermal decomposition of the Keggin structure (Table 1.1).

Table 1.1 The onset of thermal decomposition of solid HPAs [1].

HPA	T (°C)	Reference
$\text{H}_3\text{PW}_{12}\text{O}_{40}$	400	[26]
$\text{H}_4\text{SiW}_{12}\text{O}_{40}$	370	[26]
$\text{H}_3\text{PMo}_{12}\text{O}_{40}$	300	[26]
$\text{H}_4\text{SiMo}_{12}\text{O}_{40}$	200	[27]

In general, Keggin-type heteropoly compounds are the most stable among various polyoxometalates. The decomposition temperature (°C) for the most typical Keggin heteropoly acids decreases in the following series [1]:



Heteropoly salts are normally more stable than their parent acids. For example, the acidic cesium salt $\text{Cs}_{2.5}\text{H}_{0.5}\text{PW}_{12}\text{O}_{40}$ is more stable than $\text{H}_3\text{PW}_{12}\text{O}_{40}$; no decomposition of the salt was observed at 500°C [28].

The thermal stability is measured mainly by thermal analytical methods (thermal gravimetric analysis (TGA), differential thermal analysis (DTA), and differential scanning calorimetry (DSC)) as well as in combination with X-ray diffraction, infrared spectroscopy and solid state NMR.

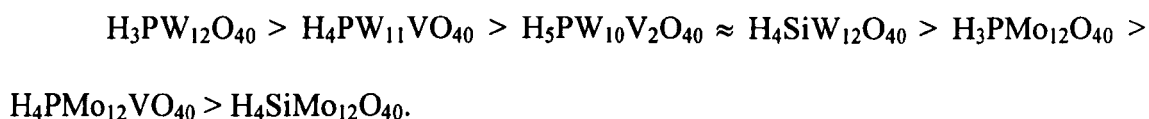
1.1.4 Acid properties of heteropoly compounds

1.1.4.1 Heteropoly acids in solution

In solutions, the acid properties of heteropoly acids are well documented in terms of their dissociation constants and Hammett acidity functions [29]. Heteropoly acids having the Keggin structure $\text{H}_3\text{PW}_{12}\text{O}_{40}$, $\text{H}_4\text{SiW}_{12}\text{O}_{40}$ are strong Brønsted acids. The protons are completely dissociated from the structure in aqueous solutions. Heteropoly acids are much stronger acids than H_2SO_4 , HBr , HCl , HNO_3 , and HClO_4 [1, 7, 30]. The greater acid strength is mainly due to the electrostatic interaction between proton and anion being much weaker in heteropoly acids than mineral acids [7].

Heteropoly acids are soluble in polar solvents such as water, lower alcohols, ketones, ethers and esters. In contrast, they are insoluble in non-polar solvents such as hydrocarbons.

The following order has been reported for the acid strength of Keggin heteropoly acids in polar solvents [1]:

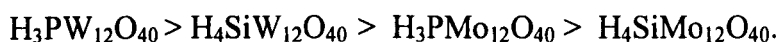


The acid strength decreases when Mo or V replaces W and when the central P atom is replaced by Si. In general, the acidity decreases with an increase in the negative charge of the heteropoly anion, or a decrease in the valence of the central atom (the valence of the central atom decreases in the order P > Ge, Si > B > Co). This order is logical, as the sizes of the polyanions are almost the same; therefore, the interaction between the proton and the polyanion would decrease as the negative charge of polyanion decreases [7].

1.1.4.2 Solid heteropoly acids

Solid HPAs possess purely Brønsted acidity and are stronger acids than the conventional solid acids such as $\text{SiO}_2\text{-Al}_2\text{O}_3$, $\text{H}_3\text{PO}_4/\text{SiO}_2$, and HX and HY zeolites [7, 16, 31]. Thermal desorption of basic molecules reveals the acid properties of solid acids. Okuhara *et al.* [7] compared the acid strength of heteropoly acids and $\text{SiO}_2\text{-Al}_2\text{O}_3$ by thermal desorption of pyridine and found that $\text{H}_3\text{PW}_{12}\text{O}_{40}$ is a very strong acid. Pyridine adsorbed on $\text{SiO}_2\text{-Al}_2\text{O}_3$ is fully desorbed at 300°C, whereas pyridine adsorbed in $\text{H}_3\text{PW}_{12}\text{O}_{40}$ mostly remains on the surface at the same temperature.

The acid strength can also be characterised by the temperature-programmed desorption (TPD) of NH₃ [32-34] and also more accurately by the calorimetry of NH₃ absorption [35-37]. Table 1.2 compares the acid strength of HPA compounds based on the heat of NH₃ adsorption and desorption temperatures of NH₃. The acid strength of crystalline HPAs decreases in the order:



This order is identical to that in polar solvents (section 1.1.4.1). Normally, relative catalytic activities of HPAs are consistent with this order, both in homogeneous and in heterogeneous systems [14, 16, 29]. HPAs, like other strong solid acids, are capable of generating carbocations from adsorbed olefins and arenes [38]. The drawback to the bulk acids is their low surface area (1-5 m² g⁻¹) and low porosity (<0.1 cm³ g⁻¹).

Table 1.2 Acid strength of solid acid catalysts as determined by NH₃ adsorption [7].

Solid acid	Initial heat of NH ₃ adsorption (kJmol ⁻¹)	Desorption temperature of NH ₃ (°C)
H ₃ PW ₁₂ O ₄₀	196	592
H ₄ SiW ₁₂ O ₄₀	185	532
H ₃ PMo ₁₂ O ₄₀	130	463
H ₄ SiMo ₁₂ O ₄₀	100	423

There are two types of protons within HPAs [1]: (i) hydrated protons [H(H₂O)_n]⁺ and (ii) non-hydrated protons. The hydrated protons possess a high mobility and are therefore responsible for the high proton conductivity of crystalline heteropoly acid hydrates. The non-hydrated protons have significantly less mobility and it is thought that they are localised on the peripheral oxygen atoms [29].

In solid HPAs, the protons, hydrated or non-hydrated, participate in the formation of the crystal structure by linking the neighbouring heteropoly anions. The state of protons and their mobility strongly depend on the amount of hydration water in HPA [39, 40]. When the water content decreases, the protons become localised to a large extent. Therefore, the water plays a crucial role in the formation of proton structure and, hence, catalytic features of HPA catalysts.

Keggin anions have three types of outer oxygen atoms as potential protonation centres: terminal oxygens $M=O$ and two types of bridging oxygens $M-O-M$, edge sharing and corner sharing (Figure 1.2). Data obtained by single crystal X-ray diffraction and neutron diffraction techniques [41] confirm that the crystalline hexahydrate structure of $H_3PW_{12}O_{40}\cdot 6H_2O$ contains diaquahydrate protons ($H_5O_2^+$ - $[H_2O...H^+...OH_2]$) that interconnect four neighbouring heteropolyanions within a lattice *via* hydrogen bonding to the terminal $W=O$ oxygen atoms. The same structure was proposed for anhydrous $H_3PW_{12}O_{40}$ and the cesium salt $Cs_3PW_{12}O_{40}$, in which the H^+ or Cs^+ each have four equivalent terminal oxygens as the closest neighbours [41-43]. These structures are shown in Figure 1.9.

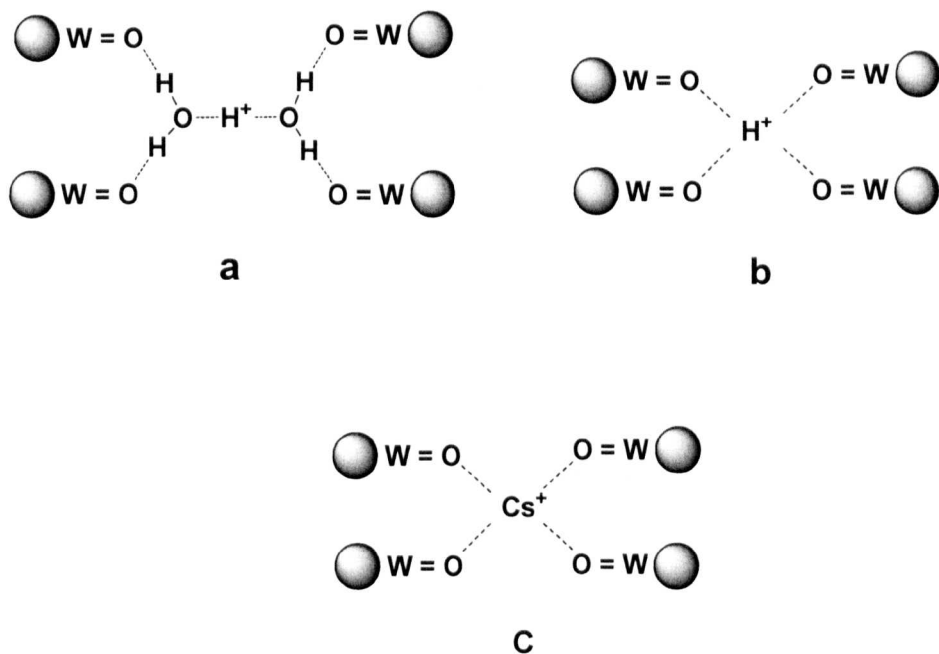


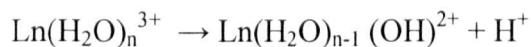
Figure 1.9 Schematic structures: (a) bulk proton sites in crystalline hexahydrate $\text{H}_3\text{PW}_{12}\text{O}_{40}\cdot 6\text{H}_2\text{O}$ (b) bulk proton sites in anhydrous $\text{H}_3\text{PW}_{12}\text{O}_{40}$ and (c) Cs^+ location in $\text{Cs}_3\text{PW}_{12}\text{O}_{40}$ [1].

1.1.4.3 Solid heteropoly salts

The acid properties of heteropoly salts are more complex [8]. They are sensitive to counteranions, constituent elements of polyanions, and tertiary structure.

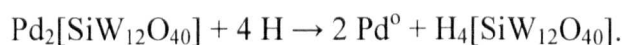
Five mechanisms have been proposed for the generation of acidity in metal salts [1, 7, 8]:

- (i) Proton sites generated by dissociation of coordinated water:



- (ii) Lewis acid sites in salts (metal counteranions, e.g. in $\text{La}^{\text{III}}[\text{PMo}_{12}\text{O}_{40}]$).

- (iii) Proton sites generated by reduction of salts:



- (iv) Proton sites present in the acidic salts (e.g. $\text{Cs}_{2.5}\text{H}_{0.5}[\text{PW}_{12}\text{O}_{40}]$).

(v) Protons generated by partial hydrolysis during the preparation process:



The acidity of salts of HPAs has been characterised by different techniques including adsorption and thermal desorption of basic molecules [44-46] as well as NMR [47, 48].

According to the temperature programmed desorption (TPD) of ammonia and indicator tests, $\text{Cs}_{2.5}\text{H}_{0.5}\text{PW}_{12}\text{O}_{40}$ and $\text{H}_3\text{PW}_{12}\text{O}_{40}$ have similar acid strengths ($H_0 \leq -13.16$) [8]. In the TPD of ammonia, $\text{Cs}_{2.5}\text{H}_{0.5}\text{PW}_{12}\text{O}_{40}$ gave a little broader peak than $\text{H}_3\text{PW}_{12}\text{O}_{40}$, showing a slight inhomogeneity of the acid strength [32]. As the Cs content, x in $\text{Cs}_x\text{H}_{3-x}\text{PW}_{12}\text{O}_{40}$, increased from 0 to 2, the number of surface protons decreased at first due to reducing the surface area (section 1.1.2.3), but significantly increased when the Cs content exceeded 2 and showed the highest surface acidity at $x = 2.5$. When x increased from 2.5 to 3.0, the number of surface protons decreased considerably since the formal concentration of protons became low or zero (Figure 1.10) [7]. The catalytic activity of $\text{Cs}_x\text{H}_{3-x}\text{PW}_{12}\text{O}_{40}$ in many reactions has been found to correlate with their surface acidity [7, 13, 47].

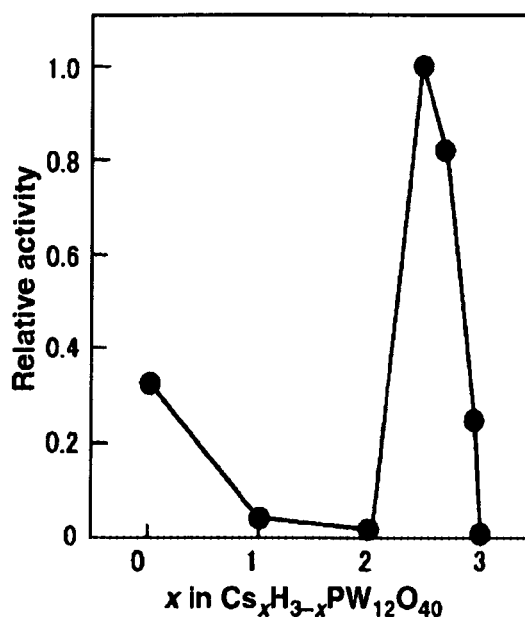


Figure 1.10 The amount of surface protons (surface acidity) as a function of Cs content for Cs_xH_{3-x}PW₁₂O₄₀ [7].

1.1.4.4 Supported heteropoly acids

Bulk Keggin HPAs exhibit high catalytic activity in various reactions. They are thermally stable and easier to synthesise than other HPAs. The major drawbacks of the bulk Keggin-type HPA are their low specific surface areas and high solubility in polar media. These drawbacks can be overcome by dispersing HPAs on high surface area supports. The acidity and catalytic activity of supported HPAs depends on the type of carrier, the HPA loading, condition of pretreatment, etc. Acidic or neutral substances such as SiO₂ [34], active carbon [49, 50], acidic ion-exchange resin [51], etc., are suitable as supports. For metal oxide supports, interaction between the surface and the HPA often degrades the polyanion structure [13]. Basic solids like MgO and Al₂O₃ tend to decompose HPAs as expected from instability of HPAs in aqueous solution at high pH [13, 29, 52]. Generally, strong interactions between HPAs and supports are

observed at low loadings [7]. It has been found that the acid strength of $\text{H}_3\text{PW}_{12}\text{O}_{40}$ decreases when supported on SiO_2 as shown in Figure 1.11 [45, 53, 54].

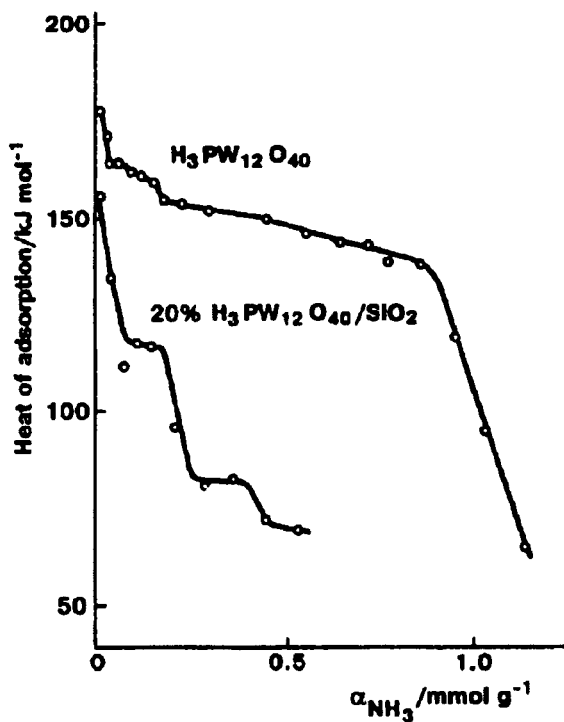


Figure 1.11 Differential heats of adsorption of NH_3 onto $\text{H}_3\text{PW}_{12}\text{O}_{40}$ and 20 wt% $\text{H}_3\text{PW}_{12}\text{O}_{40}/\text{SiO}_2$ measured at 150°C after pre-treatment at $300^\circ\text{C}/10^{-3}\text{ mmHg}$ [45].

1.1.5 Acid catalysis by heteropoly acids

HPAs have a wide range of applications as acid catalysts, including industrial applications. Acid-catalysed reactions by HPAs are carried out in homogeneous or heterogeneous (gas-solid, liquid-solid or biphasic liquid-liquid) systems. Generally, reactions catalysed by HPAs occur by the same mechanisms as with conventional Brønsted acid catalysis. The substrate is protonated by HPA catalyst, followed by the conversion of the ionic intermediate to the product [1]. This can be represented by the equation shown below.



In this equation, S_1 and S_2 are the substrates and P is the product.

1.1.5.1 Homogenous acid catalysis

HPAs catalyse a wide range of reactions in homogeneous systems [1, 7, 8, 14, 30]. Due to their stronger acidity, HPAs have significantly higher catalytic activity than mineral acids. For example, the molar catalytic activity of HPA in organic media is often 100-1000 times higher than that of H_2SO_4 (Table 1.3). This makes it possible to perform the catalytic process at a lower catalyst concentration and/or at a lower temperature [14]. Therefore, HPAs offer strong options for more efficient and cleaner processing compared to the conventional mineral acids. In addition, HPA catalysis lacks side reactions such as sulfonation, chlorination, nitration, etc., which occur with mineral acids. HPAs are also preferable regarding safety: they are stable, relatively non-toxic crystalline substances and easy to handle [1].

Table 1.3 Homogeneous reactions catalysed by heteropoly acids^a [1].

Reaction ^a	Rate ratio ^b	T (°C)
Hydration of isobutene ^c	2-4	40
Hydration of phenylacetylene	100	60
$\text{PhC}(\text{CH}_3)\text{OOH} \rightarrow \text{PhOH} + \text{CH}_3\text{COCH}_3$	1000	25
Olefin + HOAc \rightarrow ester	90	110
Ester \rightarrow olefin + carboxylic acid	100	128
$n\text{THF} + \text{Ac}_2\text{O} \rightarrow \text{AcO}(\text{CH}_2\text{CH}_2\text{CH}_2\text{CH}_2\text{O})_n\text{Ac}$	>1000	50
Styrene + HCHO \rightarrow 1,3-dioxane	50	50

a) Unless otherwise stated, reactions were performed in organic media.

b) HPA/H₂SO₄ (per proton).

c) In aqueous solution.

The relative activity of Keggin HPAs mostly depends on their acid strength. Other properties such as the oxidation potential, which determines the reducibility of HPA by reaction medium, as well as the thermal and hydrolytic stability, are also important.

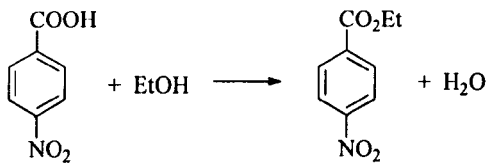
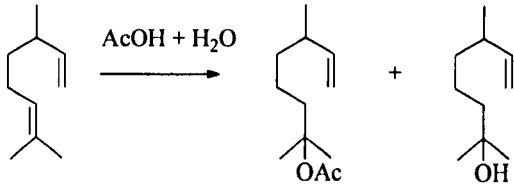
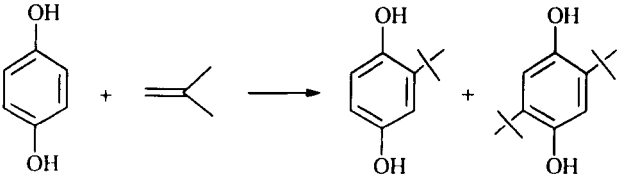
Usually, W-containing HPAs are catalytically preferable as a result of their stronger acidity, higher thermal stability and lower oxidation potential.

The utility of homogeneous HPA catalysis is limited because of difficulty in catalyst recovery and recycling. As HPAs are more costly than mineral acids, the recycling of HPA catalysts is a key issue to their application. There are only a few examples of homogeneous reactions that allow for easy HPA recycling such as the hydration of olefins [14]. In some cases, HPA can be recovered from polar organic solution without neutralization by precipitating with a hydrocarbon solvent. HPA can also be separated from an acidified aqueous solution of its salt with a polar organic solvent.

1.1.5.2 Acid catalysed reactions in biphasic liquid-liquid systems

Biphasic systems consist of two immiscible liquid phases (catalyst phase and product/reactant phase) with intense mass transfer between them. In this system, the separation of products and recovery and recycling of a catalyst are often much easier compared to homogeneous systems. HPAs due to their high solubility in a variety of polar solvents and insolubility in nonpolar solvents are very suitable catalysts for operating under phase-transfer conditions [1, 14]. There are several examples of efficient biphasic processes catalysed by HPA (Table 1.4).

Table 1.4 Biphasic reactions catalysed by heteropoly acids.

Reaction	Reference
$n \text{ (cyclopentane ring with O)} + \text{H}_2\text{O} \longrightarrow \text{HO}-[-(\text{CH}_2)_4\text{-O-}]_n\text{-H}$	[55]
	[56]
	[57]
$3 \text{ RCHO} \longrightarrow \text{R}_2\text{C}(\text{OR})_2$	[58]
	[59]

1.1.5.3 Heterogeneous acid catalysis

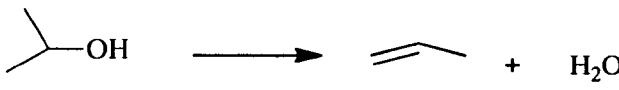
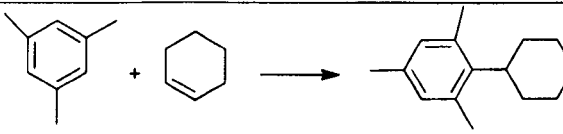
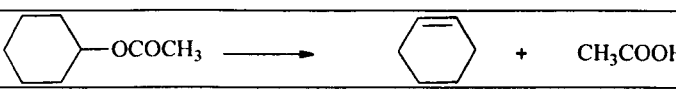
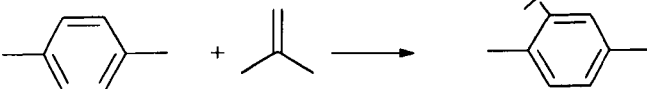
HPAs catalyse a wide range of reactions in heterogeneous systems. In general, the catalytic activity of solid HPAs is higher than that of the conventional solid acid catalysts (e.g., mixed oxides and zeolites). On the other hand, low thermal stability is a serious problem to HPA catalysts (Section 1.1.3.2), restricting reaction temperature and, especially, causing difficulty of regeneration of solid HPA catalysts (decoking) [1, 10, 14].

Acidity, basicity, and pseudoliquid behaviour are the main factors governing the acid catalysis of solid HPAs. The acidic properties are principally controlled by:

- the structure and composition of the heteropoly anion itself;
- the counteranions;
- the dispersion on supports.

The secondary and tertiary structures are also affected by these factors.

Table 1.5 Heterogeneous reactions catalysed by heteropoly acids.

Reaction	Reference
 <chem>CC(C)O >> C=CC + O</chem>	[60]
$\text{CH}_3\text{COOH} + \text{C}_2\text{H}_5\text{OH} \longrightarrow \text{CH}_3\text{COOC}_2\text{H}_5 + \text{H}_2\text{O}$	[61]
 <chem>Cc1cc(C)c(C)cc1 + C1=CCCCC1 >> Cc1cc(C)c(C)cc1C2CCCCC2</chem>	[62]
 <chem>CC(=O)OC1CCCCC1 >> C1=CCCCC1 + CC(=O)O</chem>	[62]
 <chem>C1=CC=CC=C1 + CC(C)=C >> CC(C)(C)C1=CC=CC=C1</chem>	[63]

1.1.5.3.1 Types of heterogeneous catalysis by heteropoly acids

There are three different modes of catalysis by solid HPAs as stated by Misono *et al.* [7, 8, 13] : surface type, bulk type I (pseudo-liquid) and bulk type II (Figure 1.12).

Surface type is a conventional heterogeneous catalysis, whereby the reactions take place on the two-dimensional surface of solid catalysts (on the outer surface and pore walls). In this case, the reaction rate is proportional to the surface area.

Bulk type I catalysis is observed in reactions of polar substrates with bulk solid HPAs and soluble HPA salts (i.e., salts with small cations Li^+ , Na^+ , etc.) at relatively low temperatures. The reactant molecules are absorbed in the interstitial space between polyanions in the ionic crystal and react there. The products come out to the surface and are released to liquid or gas phase. In this case, the solid behaves like a concentrated solution (pseudoliquid phase) and the reaction field becomes three dimensional. The reaction rate is proportional to the volume of the catalyst.

Bulk type II catalysis was found in some oxidation reactions at high temperatures. In spite of the fact that the principal reaction may proceed on the surface, the whole solid bulk take part in redox catalysis due to the rapid migration of redox carriers such as protons and electrons. The reaction rate is proportional to the volume of the catalyst.

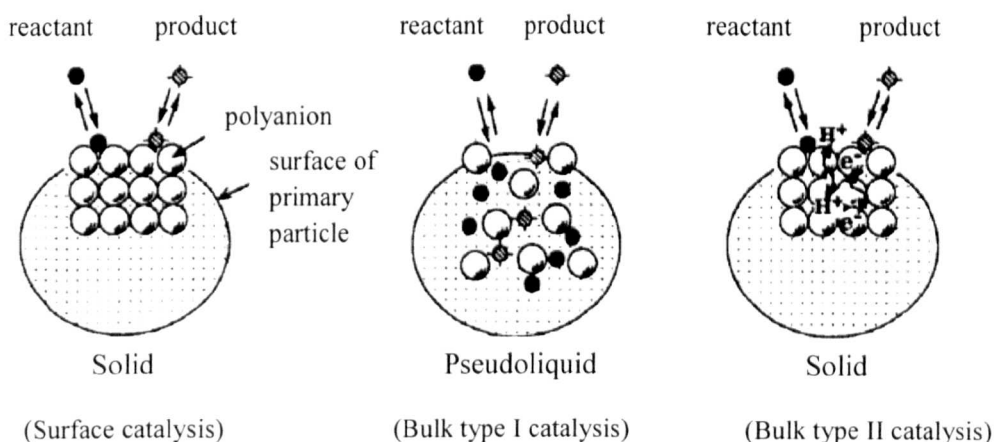


Figure 1.12 The three types of catalysis for solid heteropoly compounds.

1.2 Biodiesel as an alternative fuel

Diesel fuels have a crucial function in the contemporary industrial economy. They are used for the transport of industrial and agricultural goods, in electric generators, locomotives, etc. The high energy demand in the industrialised world and the economic growth in developing countries have been accompanied by a corresponding increase in demand of transport. The pollution problems caused due to the widespread use of fossil fuels has led to the search for alternative fuels. This is aimed at reducing the environmental burden associated with the presently used energy sources.

1.2.1 Alternative diesel fuels

The alternative diesel fuel must be economically competitive, technically acceptable, environmentally friendly and easily available. Among the alternatives, the triglycerides (vegetable oils/ animal fats) and their derivatives are considered as viable alternatives for diesel fuels [64-67]. The use of vegetable oil as alternative fuel dates back to the end of nineteenth century when Rudolf Diesel tested vegetable oil in his engine [68]. However, the engine became adapted for use with fossil fuels since they are much cheaper than vegetable oil.

Vegetable oils are easily available from a variety of sources, and they are renewable. Moreover, the sulfur content of vegetable oils is close to zero and therefore, less damage to the environment caused by sulfuric acid. In addition, vegetable oils take away more carbon dioxide from the atmosphere during their production than is added to it by their later combustion [64]. Thus, it does not increase the carbon dioxide content of the atmosphere as do the fossil fuels which are known to cause global warming. This

alternative diesel fuel can be termed as biodiesel. This fuel is biodegradable and non-toxic and has low emission profiles as compared to petroleum diesel.

The American Society for Testing and Materials (ASTM) defines biodiesel fuel as monoalkyl esters of long chain fatty acids derived from a renewable lipid feedstock, such as vegetable oil or animal fat. “Bio” represents its renewable and biological source in contrast to traditional petroleum-based diesel fuel; “diesel” refers to its use in diesel engines. As an alternative fuel, biodiesel can be used as a substitute or be blended with petroleum-based diesel fuel [65].

The most common way to produce biodiesel is by transesterification of triglycerides (TGs) with low molecular weight alcohols. Figure 1.13 shows that the transesterification of triglyceride with an alcohol to yield a mixture of fatty acid alkyl esters (i.e., biodiesel) and glycerol as a by-product.

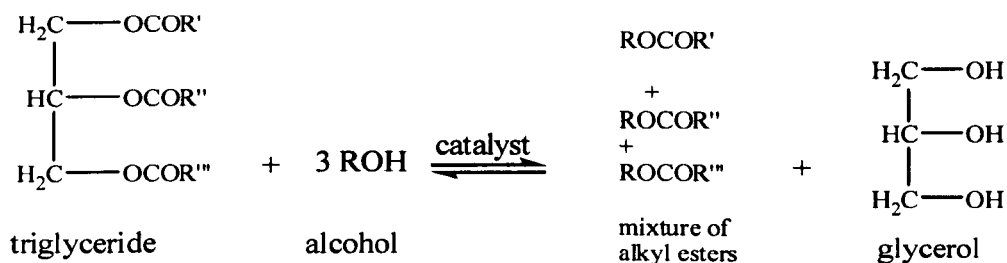


Figure 1.13 Transesterification of vegetable oils.

The overall process is a sequence of three consecutive and reversible reactions, in which di- and monoglycerides are formed as intermediates. The stoichiometric reaction requires 1 mol of a triglyceride and 3 mol of the alcohol. However, an excess of the alcohol is used to increase the yield of the alkyl esters and to allow its phase separation from the glycerol formed. Several factors, including the type of catalyst (alkaline or acid), alcohol/vegetable oil molar ratio, temperature, purity of the reactants

(mainly water content) and free fatty acid content influence the reaction course of the transesterification.

1.2.2 Biodiesel production through transesterification of triglycerides

1.2.2.1 Base catalysts

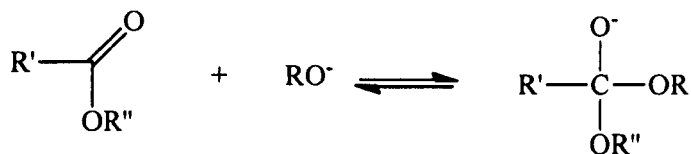
The transesterification reaction requires a catalyst in order to obtain reasonable conversion rates. Currently, most biodiesel is prepared using alkaline catalysts, such as NaOH, KOH, NaOMe and KOMe under mild temperatures (60-80°C) [66-70]. Industrially, NaOH and KOH are preferred owing to their wide availability and low cost.

The mechanism of alkali-catalysed transesterification is described in Figure 1.14. The first step is the nucleophilic attack at the carbonyl group of the triglyceride by the alkoxide to generate a tetrahedral intermediate. In the second step, the tetrahedral intermediate reacts with an alcohol producing the alkoxide ion. In the last step, rearrangement of the tetrahedral intermediate results in an ester and a diglyceride [71].

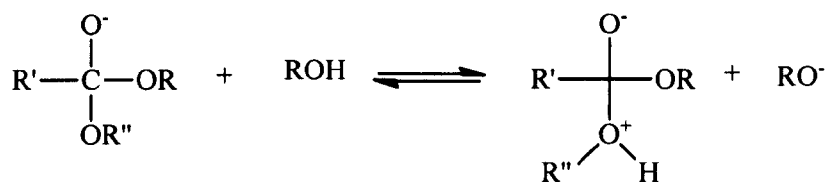
Although transesterification is widely catalysed by base catalysts, this process suffers from serious limitations that lead to high cost of biodiesel production. These limitations include undesirable side reactions such as saponification in the presence of water to yield free fatty acids (FFAs), which creates serious problem of product separation and consequently lowers the ester yield (Equation 1.1 and 1.2) [72, 73]. In fact, even if a water-free alcohol/oil mixture is used, some water is produced in the system by the reaction of the hydroxide with the alcohol (Figure 1.14).



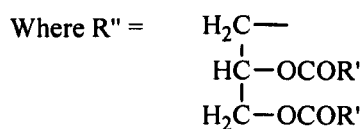
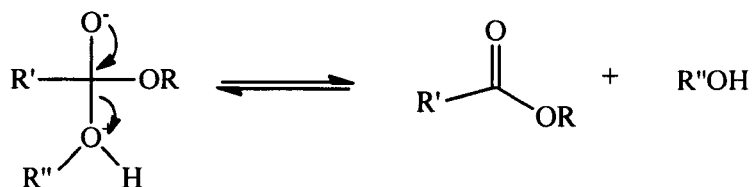
Step. 1.



Step. 2.



Step. 3.



$\text{R}' =$ Carbon chain of fatty acid
 $\text{R} =$ Alkyl group of alcohol

Figure 1.14 Mechanism of base catalysed transesterification.



The cost of traditional biodiesel production depends on two main factors:

- the cost of raw materials;
- the cost of processing (multiple steps).

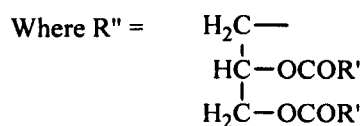
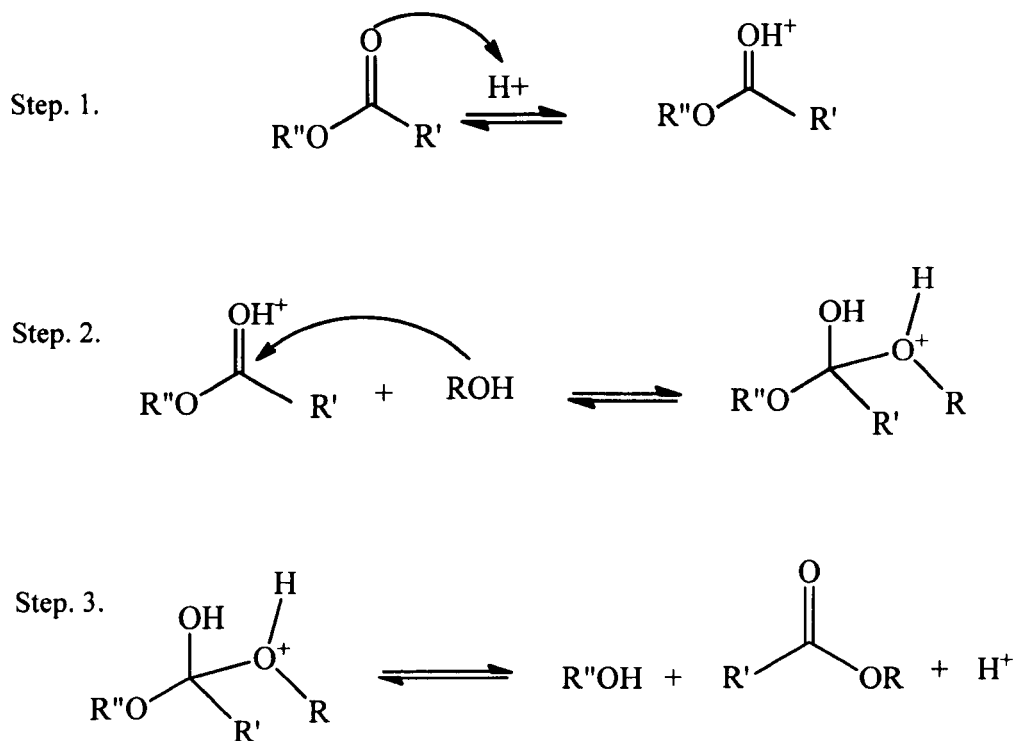
Beside the glycerol produced, waste cooking oils, animal fats or non-edible oils could be used in order to reduce the cost of biodiesel. However, these fats and oils contain a large amount of undesirable components especially FFAs and water. Therefore, FFA concentration in feedstock usually must not exceed 0.5 wt % to avoid soap formation. To control FFA concentration, a pre-esterification step is introduced to reduce the FFAs content in the initial feedstock.

1.2.2.2 Acid catalysts

1.2.2.2.1 Homogeneous acid catalysis

Homogeneous acid catalysts have the potential to replace base catalysts since they do not catalyse the formation of FFAs as well as can catalyse esterification and transesterification simultaneously, thus avoiding the pre-esterification step when using low cost feedstock with high FFA content.

The mechanism of acid catalysed transesterification is shown in Figure 1.15. The first step is the protonation of the carbonyl group by the acid catalyst. Subsequent nucleophilic attack of the alcohol forms a tetrahedral intermediate in the second step. In the last step, there is proton migration and breakdown of the intermediate.



R' = Carbon chain of fatty acid
R = Alkyl group of alcohol

Figure 1.15 Mechanism of acid catalysed transesterification [74].

Sulfuric acid has been the most investigated catalyst. HCl, BF₃, H₃PO₄ [74, 75], AlCl₃, ZnCl₂ [76] and organic sulfonic acid [64] have also been investigated. These catalysts give very high yields in alkyl esters but these reactions are slow. Besides the slow rate, homogeneous acid catalysts require high temperature, high molar ratio of alcohol and oil, difficult separation of the catalyst, and cause corrosion. Solid acid catalysts have a strong potential to replace liquid acids, eliminating corrosion and separation problems.

1.2.2.2.2 Heterogeneous acid catalysis

Although homogeneous catalysts are effective, they lead to serious problems which translate into higher biodiesel production cost. From the economic point of view, processes for the synthesis of biodiesel should be in as few reaction steps as possible and limit the number of separation steps. Solid acid catalysts would be ideal for biodiesel production. Solid acids could be easily removed from the reaction mixture and can catalyse esterification and transesterification simultaneously. On top of that, in particular reaction conditions the acid catalyst can promote the *in-situ* transformation of glycerol into oxygenated-derivatives of interest for the formulation of biodiesel [74, 77, 78]. Nevertheless, not many research studies dealing with transesterification reactions catalysed by solid acids have been reported in the literature compared with esterification reactions. Several recent studies [79-88] and reviews [74, 77, 89-92] have been published in respect to biodiesel production *via* solid acid catalysed transesterification.

Jitputti *et al.* [83] reported the use of sulfated zirconia in the transesterification of crude palm kernel oil and crude coconut oil with methanol. The catalyst showed high catalytic activity but deactivated after first run due to leaching.

Garcia *et al.* [80] compared the sulfated zirconia prepared by calcination of a finely ground mixture of $ZrOCl_2 \cdot 8H_2O$ and $(NH_4)_2SO_4$, with conventional sulfated zirconia in methanolysis of soybean oil. It was found that the preparation method has a dramatic effect on the catalytic activity of these materials. Conventional sulfated zirconia showed a very low catalytic activity whereas the novel material exhibited high conversion of soybean oil. However, a continuous leaching of sulfate groups into the reaction mixture was observed.

Heteropoly acids have been also reported for transesterification reactions [79, 84-88]. Kulkarni *et al.* [84] reported 12-tungstophosphoric acid impregnated on four different supports such as hydrous zirconia, alumina, silica and activated carbon for the transesterification of canola oil containing up to 20 wt% FFAs. All these catalysts exhibit high catalytic activity, though the catalyst prepared from the hydrous zirconia support was the most active catalyst with good stability.

Chai *et al* [85] reported the catalytic activity of $\text{Cs}_{2.5}\text{H}_{0.5}\text{PW}_{12}\text{O}_{40}$ in the transesterification of waste oils. This catalyst displayed significant high catalytic activity, selectivity and stability under mild conditions with comparable catalytic activity of $\text{Cs}_{2.5}\text{H}_{0.5}\text{PW}_{12}\text{O}_{40}$ to that found for conventional homogeneous catalyst such as sodium hydroxide or sulfuric acid.

More recently, Matachowski *et al.* [86] compared the catalytic activity of $\text{Cs}_x\text{H}_{3-x}\text{PW}_{12}\text{O}_{40}$ salts of Cs content ranging from $x = 2$ up to $x = 3$ in the transesterification of triglycerides with methanol in the liquid phase. The results showed the catalytic activity of $\text{Cs}_2\text{HPW}_{12}\text{O}_{40}$ salt was much higher than that of other Cs-salts.

Hamad *et al.* [88] tested $\text{H}_3\text{PW}_{12}\text{O}_{40}/\text{SiO}_2$ and $\text{Cs}_2\text{HPW}_{12}\text{O}_{40}$ in transesterification of rapessed oil with ethanol in mild conditions. It was found that the acid phase of $\text{H}_3\text{PW}_{12}\text{O}_{40}/\text{SiO}_2$ dissolved completely in the reaction medium while the $\text{Cs}_2\text{HPW}_{12}\text{O}_{40}$ presents relative good stability to leaching.

From the above cited work, it can be concluded that there are different acid catalysts which can be used for the transesterification reactions. Supported heteropoly acids are promising catalysts, although they are easily deactivated in the presence of water, leaching in the reaction medium. More effort is needed to overcome these problems.

1.2.3 Biodiesel production through esterification of free fatty acids (FFAs)

One possible way to reduce the cost of biodiesel production is using low-cost lipid feedstock containing high concentrations of FFAs. As discussed above, esterification reaction step is required for reducing the FFA content, typically to below 0.5 wt%; otherwise the saponification of FFAs with basic catalysts will take place. However, this system requires an acid catalyst in the first step and a basic catalyst in the second [77]. A simultaneous esterification and transesterification reaction by acid catalysts is an alternative route to producing biodiesel from low-cost feedstock.

1.2.3.1 Homogeneous acid catalysis

Currently, the esterification of fatty acids with alcohols is driven in the presence of liquid acid catalysts. The mechanism of acid catalysed esterification is shown in Figure 1.16. The first step is protonation of the carbonyl group of the acid followed by nucleophilic attack by the alcohol in the second step. The following steps involve proton transfer from one oxygen atom to another followed by the formation of water and finally the formation of ester and catalyst regeneration [93].

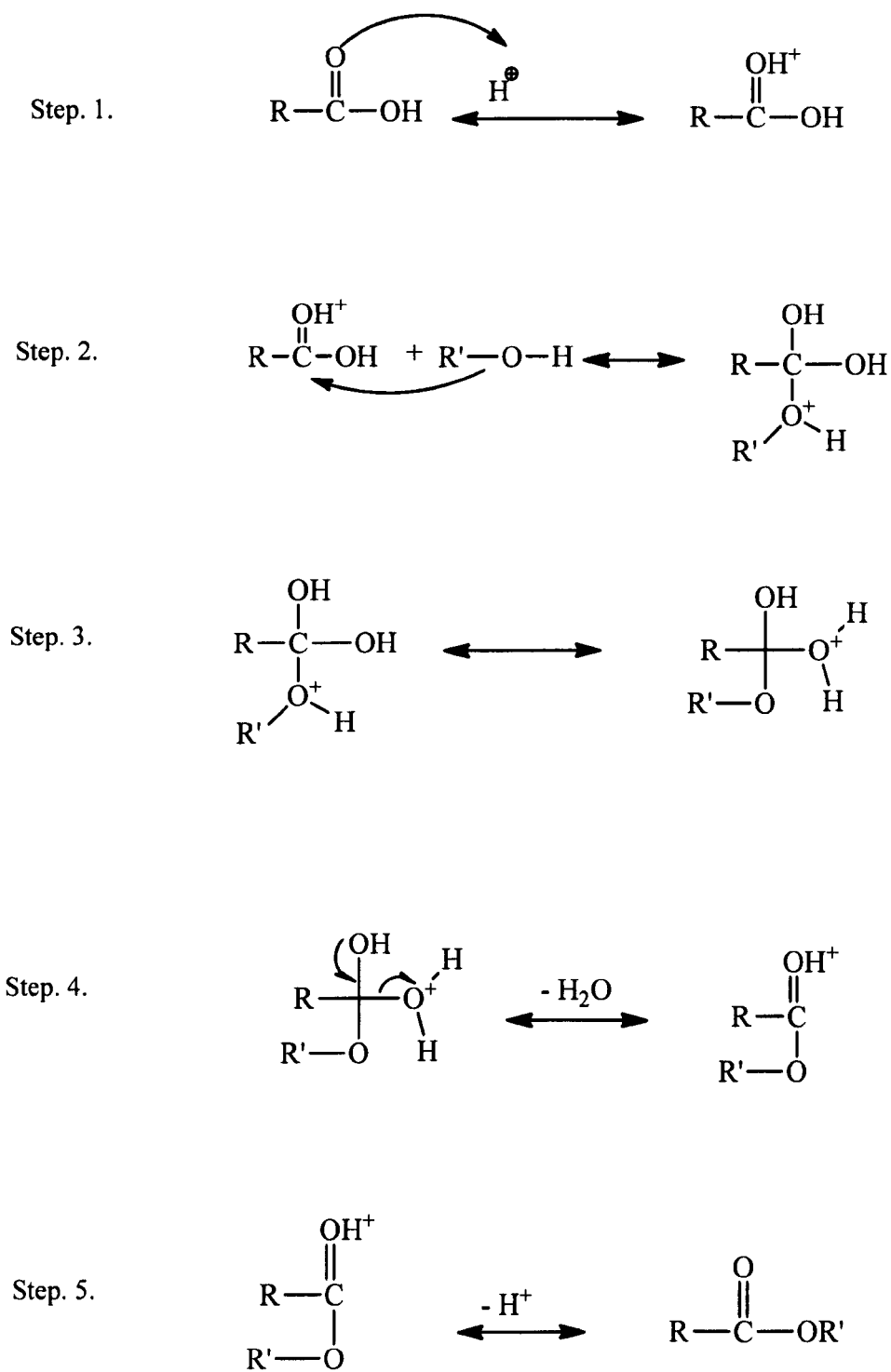


Figure 1.16 Mechanism of acid catalysed esterification.

Sulfuric acid [74, 77, 91] and sulfonic compounds [94] have been the most investigated acid catalysts used for esterification of FFAs. Although these catalysts show high catalytic activity, they contain high sulfur content which is environmentally unacceptable. HCl, HF, H₃PO₄, ClSO₂OH have also been investigated [73, 95].

As mentioned earlier, the liquid acid catalysts suffer from serious limitations such as difficult separation and corrosion. Consequently, solid acid catalysts have a strong potential to replace liquid acids, eliminating corrosion and separation problems.

1.2.3.2 Heterogeneous acid catalysis

Since transesterification and esterification reactions share a common molecular mechanism, acid catalysts showing activity in transesterification also show activity in esterification and vice versa. Hence, most of the solid acid catalysts cited above have also been reported in esterification reactions.

The scientific literature contains a good number of reports about the use of solid acid catalysts for esterification reactions [74, 77]. Ramu *et al.* [96] reported the use of tungsten oxide supported on zirconia in the esterification of palmitic acid with methanol at atmospheric pressure and refluxing conditions. For comparison, different preparation methods (impregnation and co-precipitation) were used. It was found that the catalyst with low WO₃ content impregnated on ZrO₂ showed the highest activity. This catalyst contained the required combination of the tetragonal phase of zirconia and the amorphous WO₃ essential for high activity. The presence of crystalline WO₃ and the monoclinic phase of zirconia appeared to reduce the catalytic activity. Compared with homogenous sulfuric acid, the catalytic activity was found rather low. No reusing test was reported.

Kiss *et al.* [97] compared several solid acids (zeolites, ion-exchange resins, and mixed metal oxides) in the esterification of dodecanoic acid with different alcohols (2-ethylhexanol, 1-propanol, and methanol) at 130–180°C. Zeolites (H-ZSM-5, Y and Beta) displayed poor catalytic activity due to the diffusion limitations of the large fatty acid molecules. Hence, the reaction takes place only on the external surface, which is impractical for an industrial process. Ion-exchange resins (Amberlyst 15 and Nafion-NR50) suffered some deactivation after only 2.0 and 4.5 hours respectively. Sulfated zirconia was used as representative of the metal oxides family and was found a very active catalyst. From the analysis of the reaction media and used catalyst, no leaching of sulfated groups occurred.

Verhoef *et al.* [98] reported MCM-41 supported HPAs ($\text{H}_3\text{PW}_{12}\text{O}_{40}$ and $\text{H}_4\text{SiW}_{12}\text{O}_{40}$) in the liquid-phase esterification of 1-propanol and hexanoic acid and in the gas-phase esterification of acetic acid and 1-butanol. For both reactions MCM-41 supported HPAs showed good activity and were more active than pure HPA. This is probably due to a high dispersion of the HPA on the MCM-41 internal surface. However, water formation during esterification reaction caused HPA migration from the MCM-41 pores to the external surface. This was confirmed by XRD and measuring spent catalyst activities.

Xu *et al.* [79, 99] reported the use of HPA ($\text{H}_3\text{PW}_{12}\text{O}_{40}$) supported on Ta_2O_5 with $\text{H}_3\text{PW}_{12}\text{O}_{40}$ loading from 3.6 to 20.1% in esterification reaction of lauric acid and myristic acid with ethanol. The composite exhibited a large and well-distributed three-dimensionally interconnected pores (3.9–5.0 nm), a high BET surface area (106–127 m^2/g), good porosity (0.44–1.37 cm^3/g), and a homogeneous dispersion of the Keggin unit throughout the composite. $\text{H}_3\text{PW}_{12}\text{O}_{40}/\text{Ta}_2\text{O}_5$ showed high activity and selectivity

under mild conditions. The catalyst was recovered, reactivated, and reused several times.

Recently, Oliveira *et al.* [100] investigated esterification of oleic acid with ethanol by $\text{H}_3\text{PW}_{12}\text{O}_{40}$ supported on zirconia with different loading (5–60 wt%). Based on TON calculation, 20% $\text{H}_3\text{PW}_{12}\text{O}_{40}/\text{ZrO}_2$ is the most active catalyst reaching 88% conversion at 4 h reaction with 1:6 (oleic acid:ethanol) molar ratio and 10 wt% of the catalyst. However, this catalyst showed a leaching of 8 wt% (related to the initial loading), which affects the catalyst reusability.

From the previous studies it can be concluded that heterogeneous acid catalysts, in particular HPAs, are able to carry out the esterification of free fatty acids with short chain alcohols to produce biodiesel. Moreover, these catalysts can effectively catalyse esterification and transesterification simultaneously. However, improvements are still needed to overcome deactivation and leaching problems.

1.3 Isomerisation of α -pinene

Monoterpenes are widely used in pharmaceuticals, cosmetics, flavour and fragrance industries. α -Pinene, one of the important monoterpenes and can be used as starting material for the synthesis of many valuable products via a variety of chemical processes such as isomerisation, epoxidation, hydration and dehydroisomerisation [101]. α -Pinene undergoes isomerisation reaction in the presence of acid catalysts in two parallel pathways: one leading to bicyclic and tricyclic products such as camphene, tricyclene and α -fenchene and the other yielding monocyclic products such as limonene and limonene derived products (Figure 1.17).

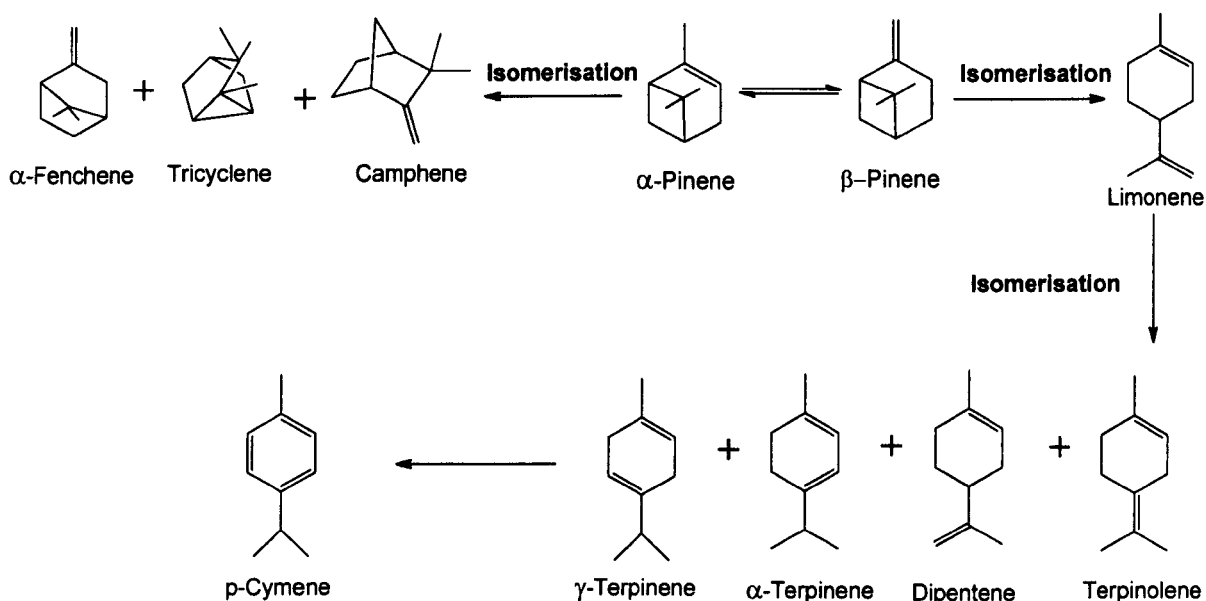


Figure 1.17 Possible products from isomerisation of α -pinene.

Among the various products, camphene and limonene are the most important for their wide application in fragrance and pharmaceutical industries [102]. Limonene is more reactive than camphene; hence, its further disproportionation into different monocyclic terpenes such as menthenes and cymenes may occur. However, the disproportionation is not observed when microporous materials are used as heterogeneous catalysts since it is a bimolecular process that needs space to occur [101].

Isomerisation of α -pinene to camphene and limonene is carried out industrially over treated TiO_2 [101, 103]. Camphene is used as an intermediate in the chemical industry for production of fragrances, acrylates, terpene-phenol resins, and other derivatives [104]. It is also used as a solvent for varnish in the automobile industry and an intermediate for the synthesis of camphor, which is an important product for the pharmaceutical and perfumery industry [105, 106]. Limonene is present in most of the essential oils and widely used as a flavour and fragrance additive in cleaning and

cosmetic products, food, and pharmaceuticals [101]. Since the catalytic performance of the commercial catalyst is low, there is great opportunity to find new catalysts which could exhibit higher activity and selectivity to camphene and/or limonene.

Zeolites and modified clays have been the most investigated catalysts for the isomerisation of α -pinene because of their appropriate acidity and shape selectivity. Lopez *et al.* [107] investigated isomerisation of α -pinene in the liquid phase at 120 °C over dealuminated mordenites and Y-zeolites. Limonene and camphene were the main products observed over zeolites. The maximum yield (68%) of limonene and camphene were obtained over mordenites with a selectivity of camphene/ (limonene + camphene) higher than 54%, while over Y zeolite the formation of undesired compounds was favored. The authors clearly highlighted that the wider pore diameters and larger pore volumes gave higher yields of undesired products.

Akpolat *et al.* [108] investigated the effect of calcination temperature of a natural zeolite (clinoptilolite) on its activity for the isomerisation of α -pinene in the liquid phase at 155 °C. It was found that catalytic activity decreased when the calcination temperature increased. This was explained by disappearance of Brønsted acid sites at high temperatures. Moreover, the selectivity to camphene was independent of the α -pinene conversion level. On the contrary, the selectivity to limonene increased with conversion at conversions lower than 80% and decreased at higher conversion due to secondary reactions of limonene.

Allahverdiev *et al.* [109-111] also studied the catalytic activity of clinoptilolite in the liquid phase using a batch reactor under various conditions (1-20 bar and 100-180 °C). Camphene and limonene were the main products found. Selectivity toward camphene and limonene at particular conversions were independent of temperature and pressure.

Gunduz *et al.* [112-114] studied β -zeolite with different $\text{SiO}_2/\text{Al}_2\text{O}_3$ ratio and various lattice ions (B, Ti, and V) in the isomerisation of α -pinene in the liquid phase using a batch reactor at 100 °C. Mainly camphene, terpinenes, terpinolenes and heavy products were observed. β -zeolite ($\text{SiO}_2/\text{Al}_2\text{O}_3 = 55$) was the most active catalyst (conversion = 99.6%), with selectivity to camphene and terpinenes between 25-28% and 13-21%, respectively. Zeolites containing B, Ti and V as lattice ions showed poor activity.

Modified clays have been also investigated. Yadav *et al.* [115] studied the isomerisation of α -pinene in the liquid phase with natural Indian Montmorillonite pre-treated with sulfuric acid or cation exchange (Ce^{3+} , Fe^{3+} , La^{3+} and Ag^+). They obtained high conversion (>96%) for modified clays with selectivity for camphene ranging from 39 to 49%. It was also found that the selectivity to limonene or terpinene depends on the concentration of sulphuric acid. Ce^{3+} , Fe^{3+} , La^{3+} , Ag^+ exchanged clays showed higher than 90% conversion for α -pinene, while Li^+ , Ca^{2+} , Mg^{2+} exchanged clay showed poor conversion (4-12%). This was explained in terms of surface acidity.

Many other modified clays have been reported for α -pinene isomerisation such as acid-pretreated montmorillonite [103], kaolinitic acid-treated clay [116] and polycation-exchanged clays [117].

Recently, supported HPAs have been tested for this reaction [118-121]. Comelli *et al.* [118] reported the isomerisation of α -pinene over tungstophosphoric acid ($\text{H}_3\text{PW}_{12}\text{O}_{40}$) supported on TiO_2 , SiO_2 and ZrO_2 in the liquid phase at various temperatures (45-130 °C). The activity of these catalysts was in the order: $\text{HPW}/\text{SiO}_2 > \text{HPW}/\text{TiO}_2 > \text{HPW}/\text{ZrO}_2$, which was correlated with the catalyst acidity. It was also found that the selectivity to camphene strongly depends on the reaction temperature. For instance, the selectivity to camphene over HPW/SiO_2 at 45 °C was 50%, while at

80 and 130 °C were 40 and 10% respectively. No results were performed in order to determine the reusability of these catalysts.

More recently, Rocha *et al.* [120] reported the use of $\text{H}_3\text{PW}_{12}\text{O}_{40}$ supported on SiO_2 in the isomerisation of α -pinene in temperature range of 40-120 °C. Camphene and limonene were the main products and accounted ca. 80% of the total products. No leaching of HPW was observed and the catalyst was easily recovered and reused without loss of activity and selectivity.

Many other solid acids have been also studied. These include metal (IV) phosphate polymer [122], Amberlyst-35 [105], silica supported rare earth oxides [123, 124] and porous phosphate heterostructure (PPH) [102].

1.4 Objectives and thesis outline

Recently, heteropoly acids (HPAs) have attracted much interest as “green” catalysts. They are generally revealing higher catalytic activities than conventional acid catalysts, offering significant economic and environmental advantages. The aim of this work is to investigate the homogeneous and heterogeneous catalysis by heteropoly acids for conversion of renewable feedstocks. This includes the preparation, characterisation and testing of a range of acidic solid materials such as bulk HPAs, $\text{Cs}_{2.5}\text{H}_{0.5}\text{PW}_{12}\text{O}_{40}$ and the acidic composites comprising HPW, supported on Nb_2O_5 , ZrO_2 and TiO_2 . The catalyst testing involves esterification of hexanoic acid and transesterification of ethyl propanoate and ethyl hexanoate with methanol modelling biodiesel synthesis, as well as the isomerisation of α -pinene to produce camphene which is an important intermediate in the fragrance and pharmaceutical industries. This

is complemented by the characterisation of catalyst texture and chemical environment of HPA on the catalyst surface by different techniques such as nitrogen adsorption, thermogravimetric analysis (TGA), infrared spectroscopy (IR), X-ray diffraction spectroscopy (XRD), ^{31}P MAS NMR spectroscopy and differential scanning calorimetry (DSC).

In Chapter 1, a brief introduction on heteropoly acids is presented. Literature reviews about biodiesel synthesis by esterification and transesterification reactions, as well as isomerisation of α -pinene are also covered.

In Chapter 2, a brief description of the preparation methods used for the synthesis of catalysts is given. The techniques used for catalyst characterisation along with the liquid and gas phase catalyst reaction testing procedures are also described.

In Chapter 3, the results of catalyst characterisation are described and information about the structure and physicochemical properties of the prepared catalysts is given.

In Chapter 4, the catalytic activity of HPA catalysts is investigated in liquid phase esterification and transesterification reactions in comparison with conventional homogeneous and solid acid catalysts such as H_2SO_4 , Amberlyst-15, zeolites HY and H-Beta. The leaching of HPW in reaction medium is also investigated.

In Chapter 5, isopropanol dehydration is used as a test reaction to characterise the activity of the solid HPA catalysts at the gas-solid interface.

Chapter 6 presents the results of isomerisation of α -pinene in the gas phase over solid HPA catalysts.

Finally, in Chapter 7, the conclusions of the results from the catalytic study and characterisation of the catalysts are presented.

References

- [1] I.V. Kozhevnikov, *Catalysts for Fine Chemicals*. Vol 2. Catalysis by Polyoxometalates, Wiley, Chichester, 2002.
- [2] J.J. Berzelius, *Pogg. Ann. Phys. Chem.* 6 (1826) 369.
- [3] A. Werner, *Ber. Dtsch. Chem. Ges.* 40 (1907) 40.
- [4] A. Miolati, R. Pizzighelli, *J. Prakt. Chem.* 77 (1908) 417.
- [5] L. Pauling, *J. Am. Chem. Soc.* 51 (1929) 2868.
- [6] J.F. Keggin, *Nature*. 131 (1933) 908.
- [7] T. Okuhara, N. Mizuno, M. Misono, *Adv. Catal.* 41 (1996) 113.
- [8] N. Mizuno, M. Misono, *Chem. Rev.* 98 (1998) 199.
- [9] J.F. Keggin, *Pros. Roy. Soc. London. A* 144 (1934).
- [10] I.V. Kozhevnikov, *J. Mol. Catal. A* 262 (2007) 86.
- [11] M.T. Pope, *Heteropoly and Isopoly Oxometalates*, Berlin, 1983.
- [12] D.D. Dexter, J.V. Silverton, *J. Am. Chem. Soc.* 90 (1968) 3589.
- [13] M. Misono, *Chem. Commun. (Cambridge, U. K.)* (2001) 1141.
- [14] I.V. Kozhevnikov, *Chem. Rev.* 98 (1998) 171.
- [15] M. Misono, *Catal. Rev. Sci. Eng.* 30 (1988) 339.
- [16] M. Misono, *Catal. Rev. Sci. Eng.* 29 (1987) 269.
- [17] J.B. Moffat, *J. Mol. Catal.* 52 (1989) 169.
- [18] D.B. Taylor, J.B. Mcmonagle, J.B. Moffat, *J. Colloid Interface Sci.* 108 (1985) 278.
- [19] M.T. Pope, A. Muller, *Angew. Chem. Int. Ed.* 30 (1991) 34.
- [20] S.J. Gregg, R. Stock, *Trans. Faraday Soc.* 53 (1957) 1355.
- [21] S. Tatematsu, T. Hibi, T. Okuhara, M. Misono, *Chem. Lett.* (1984) 865.

- [22] N. Mizuno, M. Misono, *Chem. Lett.* (1987) 967.
- [23] P. Souchay, *Ions Mineraux Condenses*, Masson, Paris, 1969.
- [24] P. Courtin, *Rev. Chim. Mineral.* 8 (1971) 221.
- [25] J.B. Moffat, *Metal-Oxygen Clusters. The Surface and Catalytic Properties of Heteropoly Oxometalates*, Kluwer, New York, 2001.
- [26] V.F. Chuvaev, V.I. Spitsyn, *Dokl. Akad. Nauk. Sssr.* 232 (1977) 1124.
- [27] G.A. Tsigdinos, *Top. Curr. Chem.* 76 (1978) 1.
- [28] K. Na, T. Okuhara, M. Misono, *J. Chem. Soc., Faraday Trans.* 91 (1995) 367-373.
- [29] I.V. Kozhevnikov, *Russ. Chem. Rev.* 56 (1987) 811.
- [30] M.N. Timofeeva, *Appl. Catal. A* 256 (2003) 19.
- [31] M. Misono, *Catal. Rev. Sci. Eng.* 30 (1988) 339.
- [32] T. Okuhara, T. Nishimura, H. Watanabe, M. Misono, *J. Mol. Catal.* 74 (1992) 247.
- [33] C.V. Hidalgo, H. Itoh, T. Hattori, M. Niwa, Y. Murakami, *J. Catal.* 85 (1984) 362.
- [34] Y. Izumi, R. Hasebe, K. Urabe, *J. Catal.* 84 (1983) 402.
- [35] F. Lefebvre, F.X. Liucui, A. Auroux, *J. Mater. Chem.* 4 (1994) 125.
- [36] A. Auroux, M.B. Sayed, J.C. Vedrine, *Thermochim. Acta.* 93 (1985) 557.
- [37] L.C. Josefowicz, H.G. Karge, E. Vasilyeva, J.B. Moffat, *Microporous Mater.* 1 (1993) 313.
- [38] M.N. Timofeeva, A.V. Demidov, A.A. Davydov, I.V. Kozhevnikov, *J. Mol. Catal.* 79 (1993) 21.
- [39] G. Koyano, T. Saito, M. Hashimoto, M. Misono, *Stud. Surf. Sci. Catal.* 130 (2000) 3077.

- [40] C. Paze, S. Bordiga, A. Zecchina, *Langmuir*. 16 (2000) 8139.
- [41] G. Brown, M.-R. Noe-Spirlet, W. Bushing, H. Levy, *Acta Crystallographica, Section B: Structural Science* 33 (1977) 1038.
- [42] I.V. Kozhevnikov, A. Sinnema, R.J.J. Jansen, H. van Bekkum, *Mendeleev Commun.* (1994) 92.
- [43] I.V. Kozhevnikov, A. Sinnema, R.J.J. Jansen, H. van Bekkum, *Catal. Lett.* 27 (1994) 187.
- [44] N. Essayem, R. Frety, G. Coudurier, J.C. Vedrine, *J. Chem. Soc., Faraday Trans.* 93 (1997) 3243.
- [45] G.I. Kapustin, T.R. Brueva, A.L. Klyachko, M.N. Timofeeva, S.M. Kulikov, I.V. Kozhevnikov, *Kinet. Catal.* 31 (1990) 1017.
- [46] R.S. Drago, J.A. Dias, T.O. Maier, *J. Am. Chem. Soc.* 119 (1997) 7702.
- [47] N. Essayem, G. Coudurier, M. Fournier, J.C. Vedrine, *Catal. Lett.* 34 (1995) 223.
- [48] N. Essayem, Y.Y. Tong, H. Jobic, J.C. Vedrine, *Appl. Catal. A* 194 (2000) 109.
- [49] Y. Izumi, K. Urabe, *Chem. Lett.* (1981) 663.
- [50] M.A. Schwegler, H. van Bekkum, *Appl. Catal.* 74 (1991) 191.
- [51] T. Baba, Y. Ono, *Appl. Catal.* 22 (1986) 321.
- [52] T. Matsuda, A. Igarashi, Y. Ogino, *J. Jpn. Pet. Inst.* 23 (1980) 30.
- [53] G.I. Kapustin, T.R. Brueva, *Thermochim. Acta.* 379 (2001) 71.
- [54] B.B. Bardin, R.J. Davis, *Appl. Catal. A* 200 (2000) 219.
- [55] Y. Izumi, K. Matsuo, K. Urabe, *J. Mol. Catal.* 18 (1983) 299-314.
- [56] I.V. Kozhevnikov, *Catal. Rev. Sci. Eng.* 37 (1995) 311.
- [57] I.V. Kozhevnikov, A. Sinnema, A.J.A. van der Weerd, H. van Bekkum, *J. Mol. Catal. A* 120 (1997) 63.

- [58] S. Sato, C. Sakurai, H. Furuta, T. Sodesawa, F. Nozaki, *J. Chem. Soc., Chem. Commun.* (1991) 1327.
- [59] M.N. Timofeeva, I.V. Kozhevnikov, *React. Kinet. Catal. Lett.* 54 (1995) 413.
- [60] N. Hayakawa, T. Okuhara, M. Misono, Y. Yoneda, *Nippon Kagaku Kaishi* (1982) 356.
- [61] R. Thouvenot, M. Fournier, C. Rocchicciolidelcheff, *J. Chem. Soc., Faraday Trans.* 87 (1991) 2829.
- [62] T. Nishimura, T. Okuhara, M. Misono, *Appl. Catal.* 73 (1991) L7.
- [63] H. Soeda, T. Okuhara, M. Misono, *Chem. Lett.* (1994) 909.
- [64] G. Guan, K. Kusakabe, N. Sakurai, K. Moriyama, *Fuel* 88 (2009) 81.
- [65] Y. Zhang, M.A. Dube, D.D. McLean, M. Kates, *Bioresour. Technol.* 89 (2003) 1.
- [66] A. Srivastava, R. Prasad, *Renewable Sustainable Energy Rev.* 4 (2000) 111.
- [67] L.C. Meher, D.V. Sagar, S.N. Naik, *Renewable Sustainable Energy Rev.* 10 (2006) 248.
- [68] E.G. Shay, *Biomass Bioenergy* 4 (1993) 227.
- [69] B.K. Barnwal, M.P. Sharma, *Renewable Sustainable Energy Rev.* 9 (2005) 363.
- [70] J.M. Marchetti, V.U. Miguel, A.F. Errazu, *Fuel* 86 (2007) 906.
- [71] U. Schuchardt, R. Sercheli, R.M. Vargas, *J. Braz. Chem. Soc.* 9 (1998) 199.
- [72] F.R. Ma, M.A. Hanna, *Bioresour. Technol.* 70 (1999) 1.
- [73] J.M. Marchetti, A.F. Errazu, *Biomass Bioenergy* 32 (2008) 892.
- [74] E. Lotero, Y.J. Liu, D.E. Lopez, K. Suwannakarn, D.A. Bruce, J.G. Goodwin, *Ind. Eng. Chem. Res.* 44 (2005) 5353.
- [75] K.S. Liu, *J. Am. Oil Chem. Soc.* 71 (1994) 1179.
- [76] N.U. Soriano, R. Venditti, D.S. Argyropoulos, *Fuel* 88 (2009) 560.

- [77] J.A. Melero, J. Iglesias, G. Morales, *Green Chem.* 11 (2009) 1285.
- [78] A.H. West, D. Posarac, N. Ellis, *Bioresour. Technol.* 99 (2008) 6587.
- [79] L.L. Xu, Y.H. Wang, X. Yang, X.D. Yu, Y.H. Guo, J.H. Clark, *Green Chem.* 10 (2008) 746.
- [80] C.M. Garcia, S. Teixeira, L.L. Marciniuk, U. Schuchardt, *Bioresour. Technol.* 99 (2008) 6608.
- [81] A. Zieba, L. Matachowski, J. Gurgul, E. Bielanska, A. Drelinkiewicz, *J. Mol. Catal. A* 316 (2010) 30.
- [82] L.L. Xu, W. Li, J.L. Hu, K.X. Li, X. Yang, F.Y. Ma, Y.N. Guo, X.D. Yu, Y.H. Guo, *J. Mater. Chem.* 19 (2009) 8571.
- [83] J. Jitputti, B. Kitiyanan, P. Rangsunvigit, K. Bunyakiat, L. Attanatho, P. Jenvanitpanjakul, *Chem. Eng. J. (Lausanne)*. 116 (2006) 61.
- [84] M.G. Kulkarni, R. Gopinath, L.C. Meher, A.K. Dalai, *Green Chem.* 8 (2006) 1056.
- [85] F. Chai, F.H. Cao, F.Y. Zhai, Y. Chen, X.H. Wang, Z.M. Su, *Adv. Synth. Catal.* 349 (2007) 1057.
- [86] L. Matachowski, A. Zieba, M. Zembala, A. Drelinkiewicz, *Catal. Lett.* 133 (2009) 49.
- [87] A. Zieba, L. Matachowski, E. Lalik, A. Drelinkiewicz, *Catal. Lett.* 127 (2009) 183.
- [88] B. Hamad, R.O.L. de Souza, G. Sapaly, M.G.C. Rocha, P.G.P. de Oliveira, W.A. Gonzalez, E.A. Sales, N. Essayem, *Catal. Commun.* 10 (2008) 92.
- [89] S. Lestari, P. Maki-Arvela, J. Beltramini, G.Q.M. Lu, D.Y. Murzin, *ChemSusChem.* 2 (2009) 1109.
- [90] A.P. Vyas, J.L. Verma, N. Subrahmanyam, *Fuel* 89 (2010) 1.

- [91] J.M. Marchetti, V.U. Miguel, A.F. Errazu, *Renewable Sustainable Energy Rev.* 11 (2007) 1300.
- [92] A. Sivasamy, K.Y. Cheah, P. Fornasiero, F. Kemausuor, S. Zinoviev, S. Miertus, *Chemosuschem.* 2 (2009) 278.
- [93] L. C. H. HART, H. D. HART, *Organic Chemistry A Short Course*, 12th ed., 2007.
- [94] L. Canoira, M. Rodriguez-Gamero, E. Querol, R. Alcantara, M. Lapuerta, F. Oliva, *Ind. Eng. Chem. Res.* 47 (2008) 7997.
- [95] S.S. Dash, K.M. Parida, *J. Mol. Catal. A* 266 (2007) 88.
- [96] S. Ramu, N. Lingaiah, B.L.A.P. Devi, R.B.N. Prasad, I. Suryanarayana, P.S.S. Prasad, *Appl. Catal. A.* 276 (2004) 163.
- [97] A.A. Kiss, A.C. Dimian, G. Rothenberg, *Adv. Synth. Catal.* 348 (2006) 75.
- [98] M.J. Verhoef, P.J. Kooyman, J.A. Peters, H. van Bekkum, *Microporous Mesoporous Mater.* 27 (1999) 365.
- [99] L.L. Xu, X. Yang, X.D. Yu, Y.H. Guo, Maynurdader, *Catal. Commun.* 9 (2008) 1607.
- [100] C.F. Oliveira, L.M. Dezaneti, F.A.C. Garcia, J.L. de Macedo, J.A. Dias, S.C.L. Dias, K.S.P. Alvim, *Appl. Catal. A* 372 (2010) 153.
- [101] A. Corma, S. Iborra, A. Velty, *Chem. Rev.* 107 (2007) 2411.
- [102] Y. Li, C. Wang, H. Chen, W.M. Hua, Y.H. Yue, Z. Gao, *Catal. Lett.* 131 (2009) 560.
- [103] N. Besun, F. Ozkan, G. Gunduz, *Appl. Catal. A* 224 (2002) 285.
- [104] W.E. Erman, *Chemistry of the Monoterpenes. an Encyclopedic Handbook*, New York 1985.

- [105] O. Chimal-Valencia, A. Robau-Sanchez, V. Collins-Martinez, A. Aguilar-Elguezabal, *Bioresour. Technol.* 93 (2004) 119.
- [106] S. Findik, G. Gunduz, *J. Am. Oil Chem. Soc.* 74 (1997) 1145.
- [107] C.M. Lopez, F.J. Machado, K. Rodriguez, B. Mendez, M. Hasegawa, S. Pekerar, *Appl. Catal. A* 173 (1998) 75.
- [108] O. Akpolat, G. Gunduz, F. Ozkan, N. Besun, *Appl. Catal. A* 265 (2004) 11.
- [109] A.I. Allahverdiev, G. Gunduz, D.Y. Murzin, *Ind. Eng. Chem. Res.* 37 (1998) 2373.
- [110] A.I. Allahverdiev, S. Irandoust, D.Y. Murzin, *J. Catal.* 185 (1999) 352.
- [111] A.I. Allahverdiev, S. Irandoust, B. Andersson, D.Y. Murzin, *Appl. Catal. A* 198 (2000) 197.
- [112] G. Gunduz, R. Dimitrova, S. Yilmaz, L. Dimitrov, *Appl. Catal. A* 282 (2005) 61.
- [113] G. Gunduz, R. Dimitrova, S. Yilmaz, L. Dimitrov, M. Spassova, *J. Mol. Catal. A* 225 (2005) 253.
- [114] R. Dimitrova, G. Gunduz, M. Spassova, *J. Mol. Catal. A* 243 (2006) 17.
- [115] M.K. Yadav, C.D. Chudasama, R.V. Jasra, *J. Mol. Catal. A* 216 (2004) 51.
- [116] C. Volzone, O. Masini, N.A. Comelli, L.M. Grzona, E.N. Ponzi, M.I. Ponzi, *Mater. Chem. Phys.* 93 (2005) 296.
- [117] C. Breen, *Appl. Clay Sci.* 15 (1999) 187.
- [118] N.A. Comelli, L.M. Grzona, O. Masini, E.N. Ponzi, M.I. Ponzi, *J. Chil. Chem. Soc.* 49 (2004) 245.
- [119] O. Masini, L. Grzona, N. Comelli, E. Ponzi, M. Ponzi, *J. Chil. Chem. Soc.* 48 (2003) 101.

- [120] K.A.D. Rocha, P.A. Robles-Dutenhefner, I.V. Kozhevnikov, E.V. Gusevskaya, *Appl. Catal. A* 352 (2009) 188.
- [121] A.D. Newman, A.F. Lee, K. Wilson, N.A. Young, *Catal. Lett.* 102 (2005) 45.
- [122] M.Conceicao Cruz Costa, Robert A. W. Johnstone, David Whittaker, *J. Mol. Catal. A* 104 (1996) 251.
- [123] T. Yamamoto, T. Tanaka, T. Funabiki, S. Yoshida, *J. Phys. Chem. B.* 102 (1998) 5830.
- [124] T. Yamamoto, T. Matsuyama, T. Tanaka, T. Funabiki, S. Yoshida, *J. Mol. Catal. A* 155 (2000) 43.

2. Experimental

2.1 Introduction

This chapter consists of three parts. In the first part, a description of the preparation of catalysts based on heteropoly compounds is given. In the second part, the techniques used to characterise them are described in detail. Finally, the third part provides the experimental set up and the reaction procedure.

2.2 Chemicals and solvents

The organic and inorganic chemicals and catalysts used were purchased from Aldrich[®] unless stated otherwise and used as supplied without further purification. Ethyl propionate (99.0%), ethyl hexanoate (99.0%), hexanoic acid (99.5%), methanol (>99.9%), isopropanol (99.5%) and α -pinene (98.0%) are used as reactants; decane (99.0%) and dodecane (99.0%) as GC standards; cesium carbonate (99.9%), $\text{H}_3\text{PW}_{12}\text{O}_{40}$ (HPW) (>99.9%), Nb_2O_5 (>99.5%), ZrO_2 (>99.0%), TiO_2 (>98.0%), ammonia solution (>30%), ethanol (99.9%), $\text{ZrOCl}_2 \cdot 8\text{H}_2\text{O}$ (98.0%), silica Aerosil 300 (S_{BET} , $300 \text{ m}^2\text{g}^{-1}$) and NbCl_5 (99%) for catalyst preparation, Amberlyst-15, Zeolite H β , Zeolite H-Y, HPW, $\text{H}_4\text{SiW}_{12}\text{O}_{40}$ (HSiW) (>99.9%), $\text{H}_3\text{PMo}_{12}\text{O}_{40}$ (HPMo) (>99.9%) and H_2SO_4 (>98.0%) as commercial catalysts for comparison.

2.3 Catalyst preparation

2.3.1 Preparation of $\text{Cs}_{2.5}\text{H}_{0.5}\text{PW}_{12}\text{O}_{40}$

The acidic salt $\text{Cs}_{2.5}\text{H}_{0.5}\text{PW}_{12}\text{O}_{40}$ was prepared by adding dropwise the required amount of aqueous caesium carbonate (0.47 M) to an aqueous solution of $\text{H}_3\text{PW}_{12}\text{O}_{40}$

(0.75 M) at room temperature with stirring [1]. The precipitate obtained was aged in aqueous mixture for 48 h at room temperature and dried using a rotary evaporator at 45°C /25 Torr. This was followed by drying in an oven at 150°C/0.5 Torr for 1.5 h.

2.3.2 Preparation of supported HPW catalysts

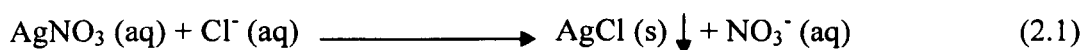
Supported 15 wt% HPW catalysts were prepared by wet impregnation of the HPW from aqueous solution onto Nb₂O₅, ZrO₂, TiO₂ and SiO₂. Some of the oxides used as supports were commercial samples from Aldrich with a rather low surface area of 1-8 m²/g. In addition, Nb₂O₅ and ZrO₂ possessing large surface areas were prepared in the lab (see below). For impregnation, an aqueous solution of HPW (1.5 g) was mixed with 8.5 g of oxide support to form a slurry with a minimal amount of aqueous phase. The slurry was then aged for 24 h with stirring either at room temperature or 100 °C, followed by drying in a rotary evaporator. Finally, the catalyst was calcined in air at a temperature from 100 to 500 °C for 3 h.

A supported 15 wt% HPW/SiO₂ was prepared by wet impregnation of 8.5 g Aerosil 300 silica (300 m²/g) in 60-80 ml aqueous solution of HPW [2]. The mixture was stirred overnight at room temperature, followed by drying in a rotary evaporator. Finally, the catalyst was dried at 150°C/0.5 Torr for 1.5 h.

2.3.3 Preparation of ZrO₂

ZrO₂ with a surface area of 162 m²/g was prepared by adding aqueous ammonium hydroxide (25%) dropwise to an aqueous solution of ZrOCl₂.8H₂O at room temperature with intense stirring until a pH of 10 was reached. The hydrogel was aged with stirring for 24 hours and then filtered through a Buchner funnel. The white precipitate was

washed with distilled water many times to remove chloride ions. The filtrate was tested by adding a small amount of AgNO₃ solution. In the presence of chloride ions the filtrate turned turbid due to the formation of AgCl.



This test was carried out together with a blank test, where distilled water was used instead of the filtrate. The white precipitate was washed with distilled water until the filtrate was clear ($[\text{Cl}^-] < 10^{-8}$ mol/l) [3] in washing. Finally the precipitate was dried in an oven at 100°C for 24 hours.

2.3.4 Preparation of Nb₂O₅

Nb₂O₅ with a surface area of 287 m²/g was prepared as described in the literature [4]. NbCl₅ powder (5 g) was dissolved in 10 ml of ethanol and slowly added to 200 ml of 0.3 M NH₃ aqueous solution to afford a white precipitate of niobic acid Nb₂O₅.nH₂O. The precipitate was washed with distilled water until chloride free (AgNO₃). The niobic acid was dried in an oven at 100 °C for 24 h.

2.3.5 Preparation of 20%Cs₂HPW₁₂O₄₀/SiO₂

Preparation was carried out via two steps. First, Aerosil 300 (4 g) was impregnated with caesium carbonate by stirring with 50 ml of aqueous solution of Cs₂CO₃ (0.104 g, 0.32 mmol) at room temperature for 3 h, followed by drying in an oven at 100°C overnight and calcination at 300°C for 3 h in air. In the second step, the

silica-supported Cs_2CO_3 was treated with a stoichiometric amount of $\text{H}_3\text{PW}_{12}\text{O}_{40}$ (0.32 mmol) in methanol (50 ml) at room temperature for 24 h, followed by drying, first in an oven at 100°C overnight, then at $150^\circ\text{C}/0.5$ Torr for 1 h.

2.4 Catalyst characterisation techniques

2.4.1 Thermogravimetric analysis (TGA)

Most chemical compounds decompose and lose some weight when heated. TGA monitors the change in weight of substance as a function of temperature or time as the sample is subjected to a controlled temperature program. The TGA is used to rank materials in order of their thermal stability by comparing their loss of weight versus temperature. Other TGA applications include the determination of moisture and coke percentage as well as the oxidation temperature of samples [5]. A derivative thermogravimetric weight loss curve (DTG) can be used to show the point at which the weight loss becomes most apparent. TGA consists of an extremely sensitive pan balance (generally platinum) and an accurate draft-free furnace. A schematic diagram of a TGA apparatus is seen in Figure 2.1. In this study, thermogravimetric analysis was mainly used to measure the percentage by mass of physisorbed water in materials in order for the correct amount of reactants to be used in the catalyst synthesis. A Perkin Elmer TGA 7 instrument was used to perform the thermogravimetric experiments using a heating rate of 20°C per minute to raise the temperature from room temperature to 700°C , under nitrogen gas flow. Figure 2.2 is an example of a typical TGA curve for $\text{H}_3\text{PW}_{12}\text{O}_{40}$.

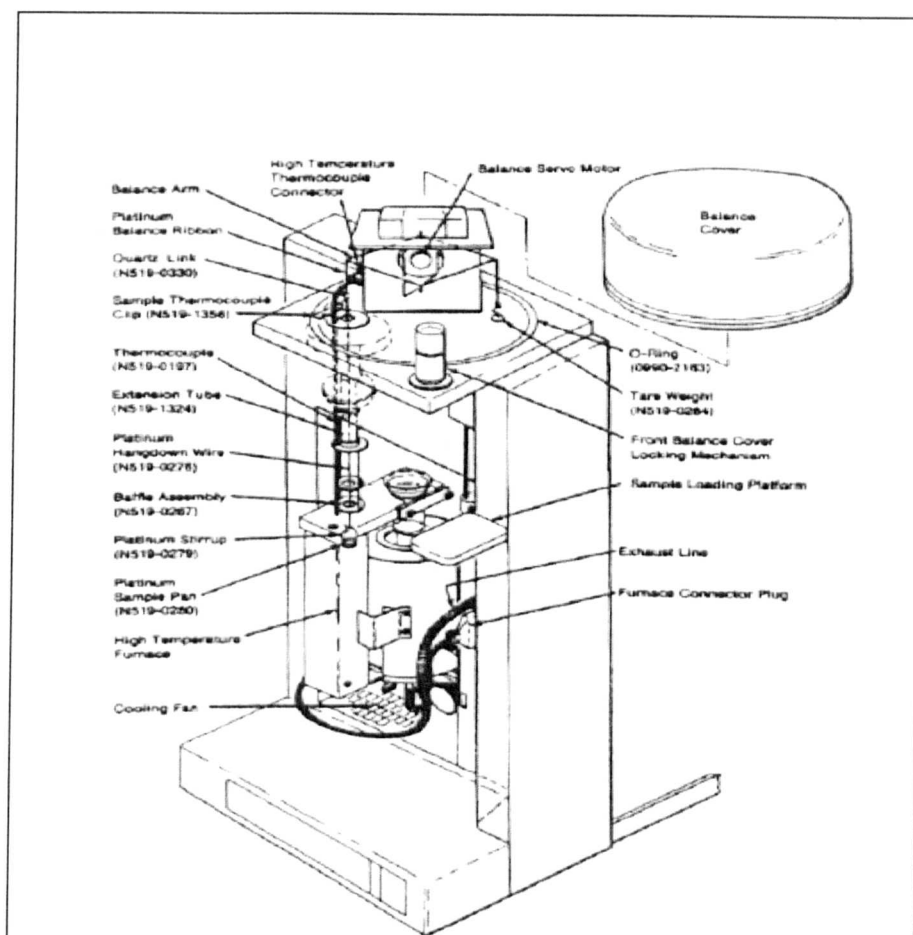


Figure 2.1 Schematic diagram of TGA [6].

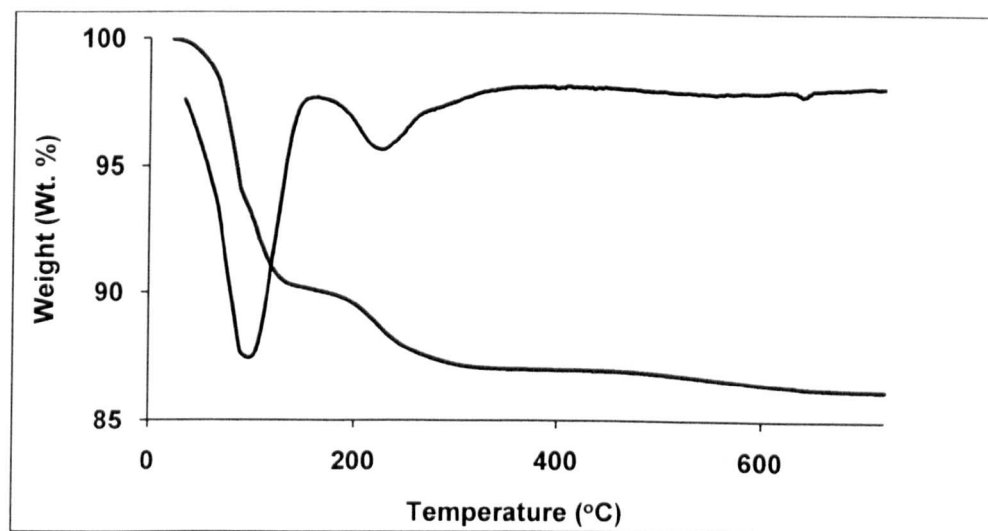


Figure 2.2 Thermogravimetric analysis of $\text{H}_3\text{PW}_{12}\text{O}_{40}$.

2.4.2 Inductively coupled plasma atomic emission spectroscopy (ICP-AES)

At high temperature ($\sim 6000\text{K}$), gases such as argon form a plasma – that is a gas containing a high proportion of ions and free electrons [7, 8]. There are two types of plasma sources: the direct current plasma (DCP) or the inductively coupled plasma (ICP). ICP is an analytical technique used for the detection of trace metals in samples. The main objective of ICP is to get elements to emit characteristic wavelengths of specific light which can then be measured.

The ICP apparatus consists of three concentric tubes, usually made of silica, shown in Figure 2.3. These tubes are the outer tube, the inner tube, and the central tube; together they comprise the torch of the ICP.

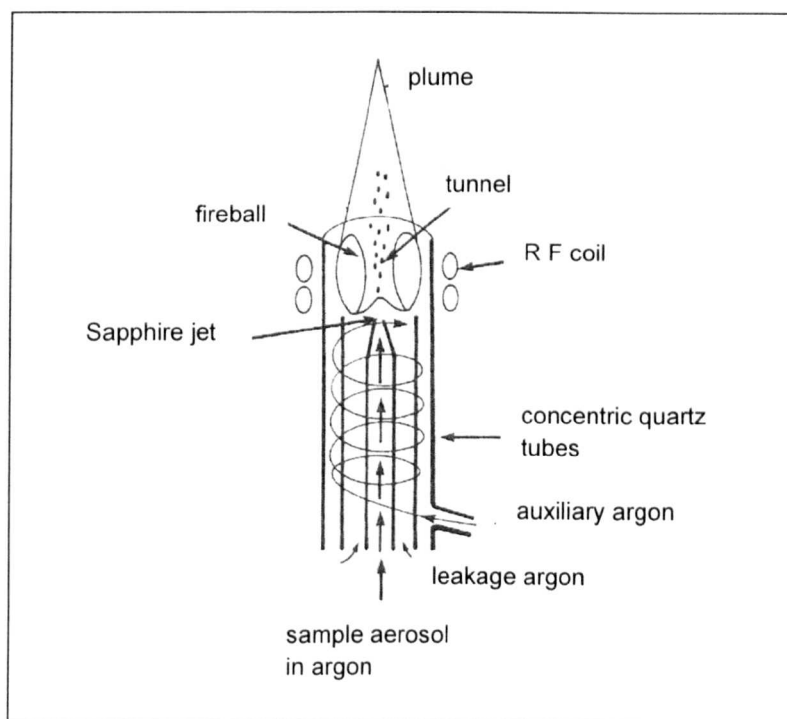


Figure 2.3 An ICP torch.

The elements to be analysed should be dissolved in solution. An aqueous solution is preferred over an organic solution, as organic solutions require special pre-treatment prior to injection into the ICP. On the other hand, solid samples may block the instrumentation. The light emitted by the atoms of an element in the ICP must be converted to an electrical signal that can be measured quantitatively.

Often, ICP instruments are linked with other analytical instruments, such as Atomic Emission Spectroscopy (AES) and Mass spectroscopy (MS). ICP-MS provides valuable information about samples that contain several isotopes of metallic elements. ICP-AES takes advantage of the complementary sensitivities of each technique to specific elements.

ICP was performed by S. Apter within the Department of Chemistry, at the University of Liverpool using a Spectro Ciros CCD Inductively Coupled Plasma (ICP) source, linked to an Atomic Emission Spectroscopy (AES).

2.4.3 Fourier transform infrared spectroscopy (FTIR)

Infrared spectroscopy is an important method for obtaining information about the structural framework of materials [7-9]. Most IR spectrometers operate on the double-beam principle, with one beam passing through the sample and the other through a reference cell.

In this study, Diffuse Reflectance Infrared Fourier Transform (DRIFT) spectroscopy was used to examine the state of HPW on Nb₂O₅, ZrO₂ and TiO₂ in comparison with SiO₂ as well as to determine the nature of acid sites (Brønsted and Lewis) by adsorption of pyridine. Samples for analysis were prepared by first drying a small amount of the sample under vacuum at 150 °C for 1 h. Then 5 mg of the catalyst

was mixed with 45 mg of dried KBr (10 wt %) and ground thoroughly to create a diffusely scattering matrix that lowers absorption and hence increases the throughput of the beam, enhancing the resolution for analysis. The measurements were performed using a Nicolet Model Nexus FTIR-Raman spectrometer at room temperature under N₂ atmosphere to prevent interference by the gaseous environment in the chamber. The spectrum was taken in the region between 4000 and 400 cm⁻¹ after 256 scans.

2.4.4 Ultraviolet (UV) spectroscopy

The ultraviolet (UV) and visible region of the electromagnetic spectrum covers the wavelength range from 100 nm to 800 nm. The region between 100 to 200 nm is difficult to measure. Most analytical measurements are made in the UV region (200-400 nm) and visible region (400-800 nm).

In this work, UV spectroscopy was used for measuring the concentration of H₃PW₁₂O₄₀ in solution. The amount of H₃PW₁₂O₄₀ in 1 N H₂SO₄ aqueous solution was measured with a VARIAN Cary 50 UV spectrophotometer in a 1 cm quartz cuvette at a wavelength of 267 nm. The UV spectrum of the PW₁₂O₄₀³⁻ anion in aqueous solution is shown in Figure 2.4.

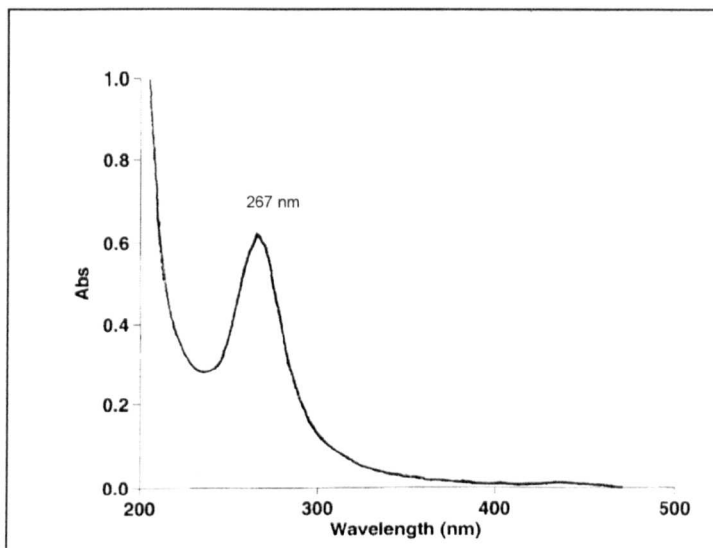


Figure 2.4 UV spectrum for aqueous solution of $\text{H}_3\text{PW}_{12}\text{O}_{40}$ in 1 N H_2SO_4 .

2.4.5 Surface area and porosity

Adsorption measurements have a wide range of uses and applications. The most important use is determining the surface area and porosity of catalysts. The activity of a catalyst is accurately expressed as the rate per unit area of active surface. On this basis, comparisons between different catalysts are made. Thus, catalysts with a high surface area are preferred. However, as it is difficult to use very fine powder, the solution is to make the material porous. The total surface areas of porous solids are much higher than the area of the external surface as a result of the contribution of the pore walls. Typically heterogeneous catalysts have a specific surface area between 1 and 1000 m^2/g , while their external surface area is in the range of 0.01-10 m^2/g [10, 11].

Substances are divided into three groups according to their pore size: microporous (<2 nm), mesoporous (2-50 nm) and macroporous (>50 nm). The physical adsorption of inert gases such as nitrogen is used to determine the surface area [10-14]. Several equations have been used to calculate surface area. However, the Brunauer-Emmett-Teller (BET) equation developed in 1938 is the most widely used for this purpose [15].

$$\frac{P}{V(P_0-P)} = \frac{1}{V_m C} + \frac{C-1}{V_m C} \frac{P}{P_0} \quad (2.2)$$

In this equation, V_m is the volume of gas required to form a monolayer on the adsorbent, V is the volume of gas adsorbed at pressure P , P_0 is the saturated vapor pressure at the test temperature (77 K) and C is a constant, which is a measure of the change in the heat of adsorption between the first and second adsorbed layers. Therefore, a plot of $P/V (P_0-P)$ versus P/P_0 gives a straight line with the slope $(C - 1)/V_m C$ and the intercept $1/V_m C$. Consequently, the value of V_m can be calculated, which is then converted to the area of the surface (S):

$$S = V_m \times \frac{N_A}{V_A} \times A \quad (2.3)$$

where A is the area of the nitrogen molecule (0.162 nm^2), N_A is the Avogadro number ($6.022 \times 10^{23} \text{ mol}^{-1}$) and V_A is the molar volume of N_2 (22.4 l/mol at standard conditions). The specific surface area is calculated by dividing the area obtained by the weight of the catalyst used in the measurement. It should be noted that equation 2.2 is only valid when P/P_0 is between 0.05 and 0.30 (i.e. where a linear relationship exists) [13].

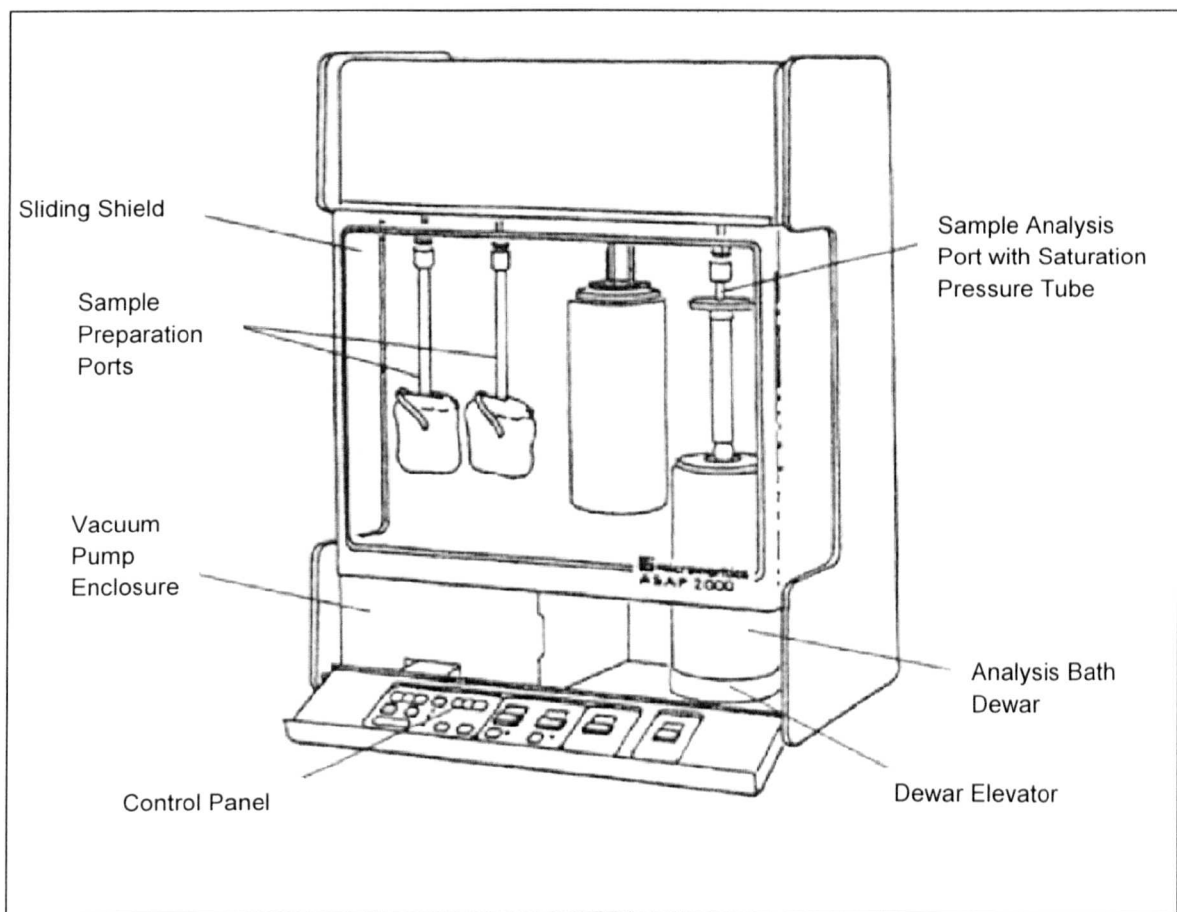


Figure 2.5 Micromeritics ASAP 2000 adsorption apparatus [6].

Surface area measurement of the catalysts was carried out on a Micromeritics ASAP 2000 adsorption apparatus (Figure 2.5). Before the measurement, the samples were evacuated at 150 °C for 1-2 h. Typically, 0.15-0.30 g sample was packed into the sample tube and pretreated on the Micromeritics ASAP 2000 at 250°C to reach a vacuum of 8 μ mHg. Once outgassed, the samples were allowed to cool to room temperature, and the sample tube immersed in liquid nitrogen. The gas pressure was allowed to reach equilibrium before a series of successive nitrogen doses (\approx 55) were performed in order to obtain sufficient information to plot an adsorption isotherm.

2.4.6 Powder X-ray diffraction (XRD)

X-rays are electromagnetic radiation with a wavelength of the order of 10^{-10} m (1 Å). They are suitable for probing the structural arrangement of atoms and molecules because their wavelength is comparable to the size of atoms [16]. The energetic x-rays can go through deep into the materials and provide information about the bulk structure.

X-rays interact with electrons in atoms. When x-ray photons collide with electrons, some photons from the incident beam will be reflected with the angle of reflection equal to the angle of incidence as shown in Figure 2.6. The directions in which X-rays are scattered depend on several factors, expressed in Bragg's law (Equation 2.4).

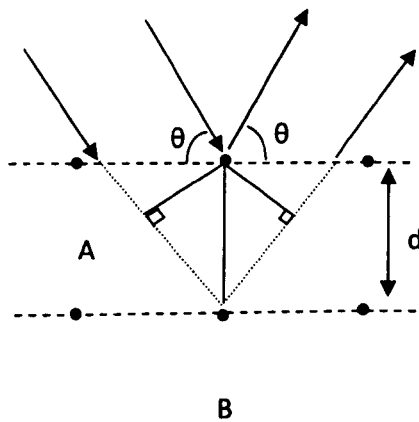


Figure 2.6 Schematic representation of Bragg's law.

$$n\lambda = 2d\sin\theta \quad (2.4)$$

where n is the order of the reflection (an integer value), λ the incident X-ray wavelength, d is the lattice planar spacing and θ is the diffraction angle.

Powder X-ray diffraction (XRD) spectra of catalysts were recorded on a PANalytical Xpert diffractometer with a monochromatic Cu K_{α} radiation ($\lambda=1.54 \text{ \AA}$). Typically, the powdered sample was placed on a sample holder and exposed to X-ray radiation at room temperature. The pattern was recorded in the range of 2θ between 10 and 70° , and attributed using the JCPDS database.

2.4.7 Differential scanning calorimetry (DSC)

Differential scanning calorimetry is one of the most important techniques for acidity characterisation [17-19]. The determination of the number of acid sites and the distribution of their strength was carried out by ammonia pulse chemisorption method using a Setaram TGA-DSC 111 analyser.

The DSC 111 (Figure 2.7) is built around two open refractory tubes crossing the heating furnace. The detection unit, designed according to the Calvet principle, is placed in the medium part of the tubes (i.e. since the cylindrical sample crucible is completely surrounded by the detector, all heat exchange is evaluated and hence gives very accurate measurements). The calorimetric block is fixed on a vertical stand, and a symmetrical balance is sat above. The suspensions of the balance are brought into line with the axis of each experimental tube. The crucibles, hooked at the ends of the suspensions, are driven in the detection zone of the DSC by sliding the balance [17].

In this study, the fresh samples were pre-treated under a flow of dry helium (30 ml/min) at 300°C for one hour (rate 5°C/min) to remove all the water. The temperature was then lowered to 100°C. After stabilisation of the sample weight at 100°C (about 2 h), the analysis was performed by successive injections of ammonia carried by flow of helium. Sufficient time (20 min) was allowed after each injection for the ammonia to be absorbed and equilibrium to be reached. Weight gain and corresponding heat of adsorption were recorded.

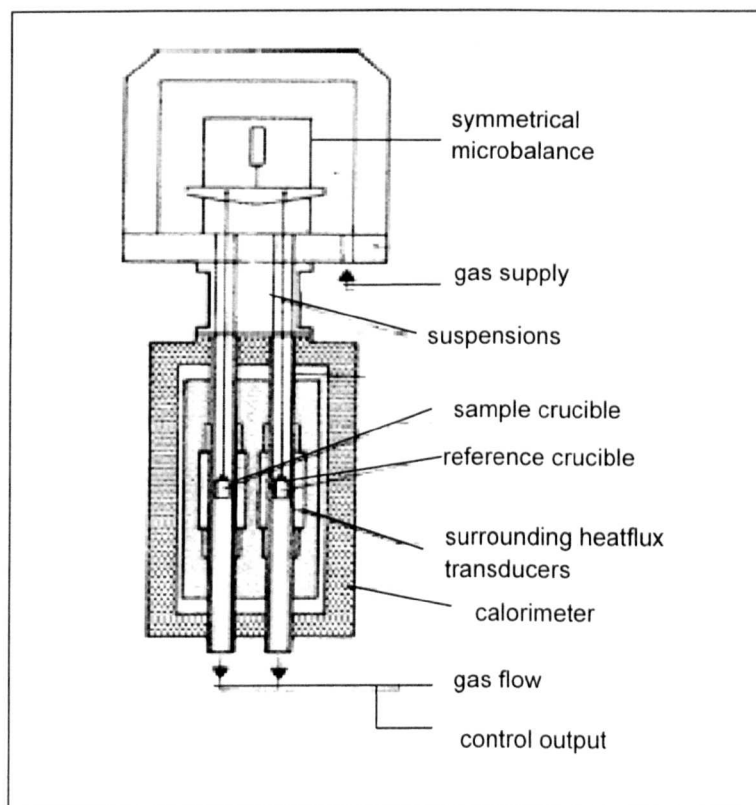


Figure 2.7 TG-DSC schematic cross section [17].

2.4.8 Solid state ^{31}P NMR

NMR spectroscopy is a fundamental technique for structural elucidation [9, 20, 21]. It is used for the study of the properties of molecules containing magnetic nuclei. When applied external magnetic field B_0 , the net field effective at a nucleus is $B_{\text{eff}} = B_0(1-\sigma)$, where σ is the shielding constant. Thus, chemically different nuclei, even those in the same element as long as they are in different parts in the molecule come to resonance at different frequency. The different resonance frequency for each chemically distinct nucleus is identified in a NMR spectrum with the term chemical shift. The chemical shift of a nucleus is the difference between its resonance frequency and that of a reference standard.

Magic-angle spinning (MAS) is well-known technique in solid-state NMR. It is used to overcome some problems such as very broad resonances and long relaxation time. MAS-NMR spectroscopy is a powerful method to investigate the primary structure of heteropoly compounds. ^{31}P nuclei studies give an opportunity to investigate on the environment in which the central atom is situated in the Keggin unit and the hydration state of the heteropoly compound.

^{31}P MAS NMR spectra were recorded* at 9.4 T using a Bruker DSX-400 spectrometer with an MAS triple resonance probe-head using zirconia rotor 4 mm in diameter at 161.9 MHz with an MAS rate of 10 kHz. The ^{31}P $\pi/2$ pulse length was 3.5 μs with a recycle delay of 30 s and 3000 scans. A ^1H TPPM (two-pulse phase modulation) decoupling pulse length of 5.5 μs with RF field strength of 45.45 kHz was used. The position of the ^{31}P resonances was quoted in ppm from external aqueous 85% H_3PO_4 .

* NMR measurements were kindly done by P. V. Wiper in the Department of Chemistry.

2.5 Catalyst reaction studies

2.5.1 Product analysis

Gas chromatography was used for product separation and quantitative analysis of the gas-phase and liquid-phase catalyst reactions.

2.5.1.1 Gas chromatography (GC)

Gas chromatography (GC) is a type of partition technique in which the mobile phase is a carrier gas, usually an inert gas, and the stationary phase is a microscopic layer of liquid on an inert solid support, inside glass or metal tubing, called a column. Gas chromatography is used in many applications in research laboratories, industry and so on. One of the major applications of gas chromatography is in finding legal evidence of the presence of illicit materials. In addition, gas chromatography analyses the content of a chemical product, for example in assuring the quality of products in the chemical industry; or measuring toxic substances in soil, air or water.

A gas chromatograph (Figure 2.8) consists of (i) a source of carrier gas with a flow rate controller which can be fixed at a desired magnitude within the range provided; (ii) an inlet that can be heated (25 to 500°C); (iii) a column in a thermostatted air bath (25 to 400°C); (iv) a detector suitable for vapour-phase samples. To vaporise the solutes of interest and maintain them in the gas phase the temperature must be high. The carrier gas must be chemically inert. Normally used gases include helium, nitrogen, argon or hydrogen to prevent the degradation of the column. The choice of carrier gas is often dependent upon the type of detector which is used. The carrier gas system also contains a molecular sieve to remove water and other impurities. The inlet and detector

are generally kept at a temperature approximately 10% (in °C) above that of the column to speed up the volatilisation of the sample and to avoid condensation [22].

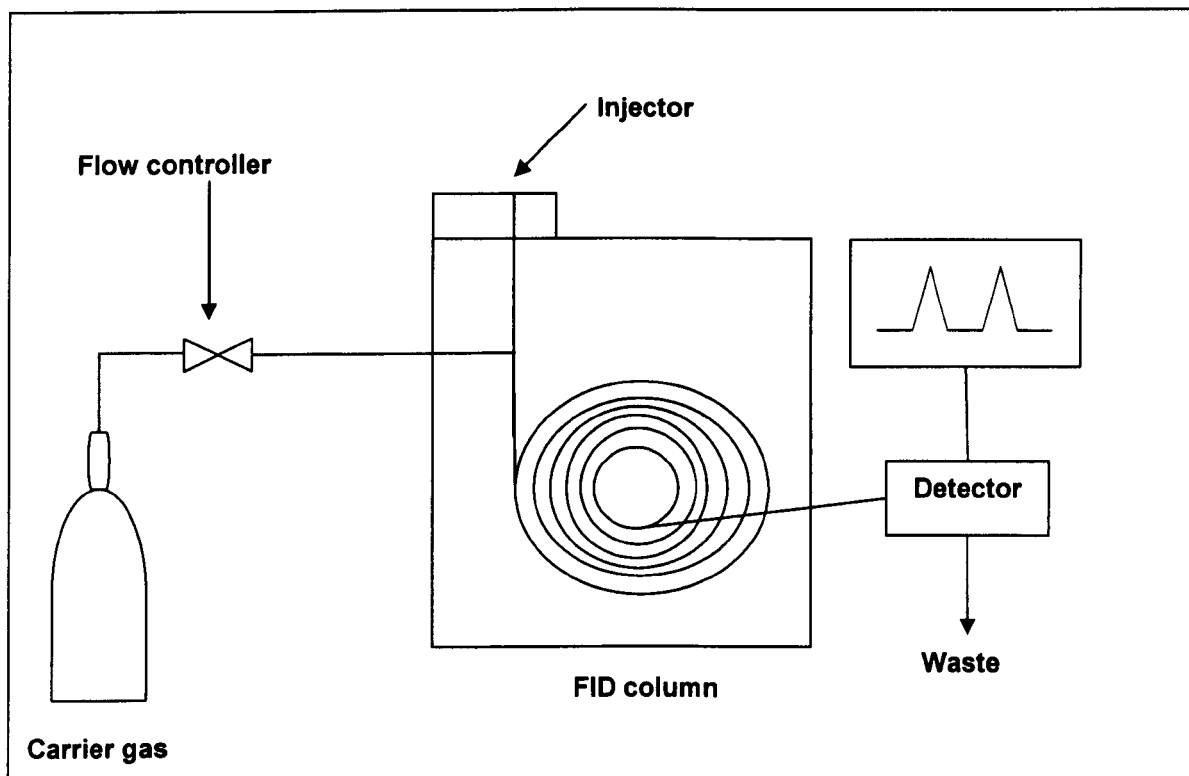


Figure 2.8 Schematic representation of gas chromatography.

Liquid-phase reactions (esterification and transesterification) were monitored by a Varian CP-3380 gas chromatograph equipped with a BP1 capillary non-polar column (25 m length, 0.32 mm internal diameter, 0.5 μm film thickness). The helium carrier gas flow rate was 2 ml/min. Nitrogen was used as the make-up gas at a flow rate of 30 ml/min. The split ratio and split vent flow were 20 and 40 ml/min respectively. The

injector and detector temperatures were set at 250 and 300°C respectively. The heating programme of the column is shown in Figure 2.9, giving a total GC run time of 15 min.

For gas phase reactions (α -pinene isomerisation and isopropanol dehydration), the effluent from the reactor was analysed using a Varian Star 3400 CX gas chromatograph equipped with a 30 m \times 0.25 mm \times 0.25 μ m ZB-1701 capillary column and a flame ionisation detector. The detector and injector temperature was set at 250°C. The heating program of the column for α -pinene isomerisation and isopropanol dehydration are shown in Figure 2.10 and 2.11 respectively, giving a total GC run time of 15 and 10 min respectively.

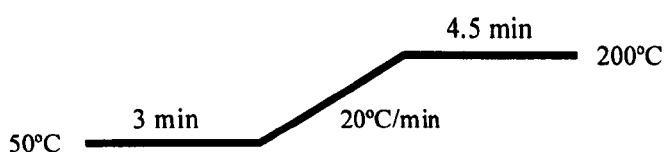


Figure 2.9 Temperature programme used for liquid-phase esterification and transesterification.

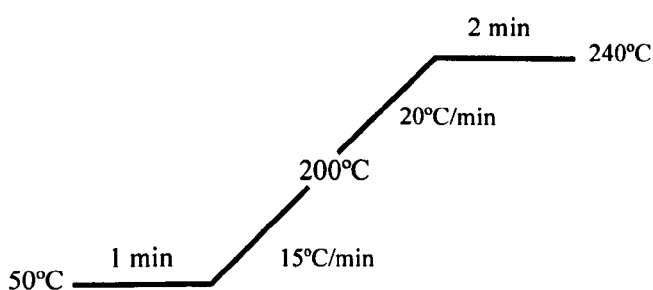


Figure 2.10 Temperature programme used for gas-phase α -pinene isomerisation.

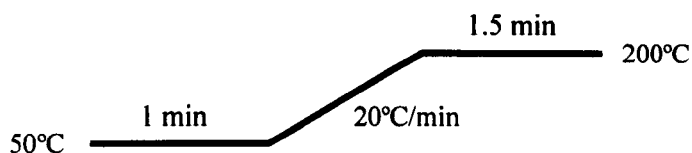


Figure 2.11 Temperature programme used for gas-phase isopropanol dehydration.

2.5.1.2 GC calibration

The liquid reactants and potential products of the reactions were calibrated using the internal standard method. A series of solutions, each with a different amount of analyte and a constant amount of the internal standard were diluted in a solvent. The ratio of the concentrations (moles) of analysed compound M and the internal standard M_0 were plotted against the ratio of area counts of the corresponding peaks, S and S_0 respectively (Equation 2.5). The gradient produced is the calibration factor K .

$$\frac{M}{M_0} = K \times \frac{S}{S_0} \quad (2.5)$$

The molecular weights, boiling points, retention times and calibration factors for the compound involved in the esterification and transesterification reactions are given in Table 2.1. The conditions of the GC analysis are shown in Figure 2.9. A typical GC

trace for the transesterification of ethyl propionate is shown in Figure 2.12. The calibration plots (Equation 2.5) for this system are shown in Figure 2.13-2.18. The calibrations were done in the same concentration ranges as those employed in the reactions.

Table 2.1 Molecular weights, boiling points, GC retention times and calibration factors for compounds involved in esterification and transesterification reactions.

Compound	Molecular weight (g/mol)	Boiling point (°C)	Retention time (min)	Calibration factor (K)	Standard
ethyl propionate	102.1	99	4.9-5.0	3.03	n-decane
methyl propionate	88.1	79	4.0	3.97	n-decane
ethyl hexanoate	144.2	166	9.0-9.1	1.64	n-decane
methyl hexanoate	130.2	148	8.0-8.1	1.82	n-decane
methyl hexanoate	130.2	148	8.0-8.1	2.28	n-dodecane
hexanoic acid	116.2	202	9.1-9.7	2.89	n-dodecane
methanol	32.0	65	2.8-2.9	-	-
ethanol	46.1	78	3.0	-	-
n-decane	142.3	174	9.2	-	-
n-dodecane	170.3	216	11.3	-	-

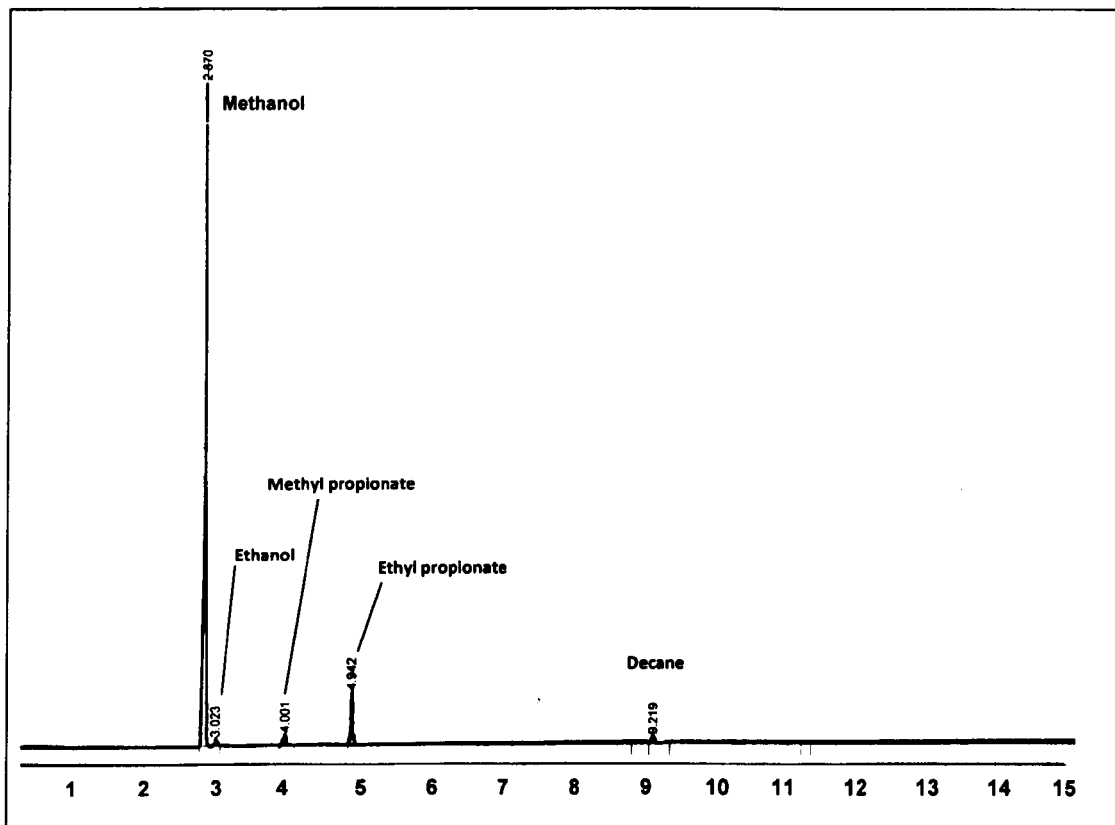


Figure 2.12 GC chromatogram for the liquid phase conversion of ethyl propionate.

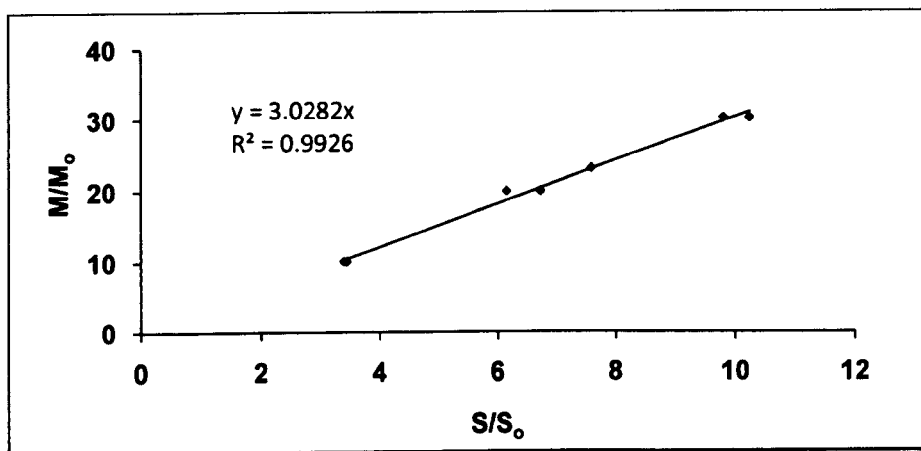


Figure 2.13 Calibration of ethyl propionate with n-decane as a standard.

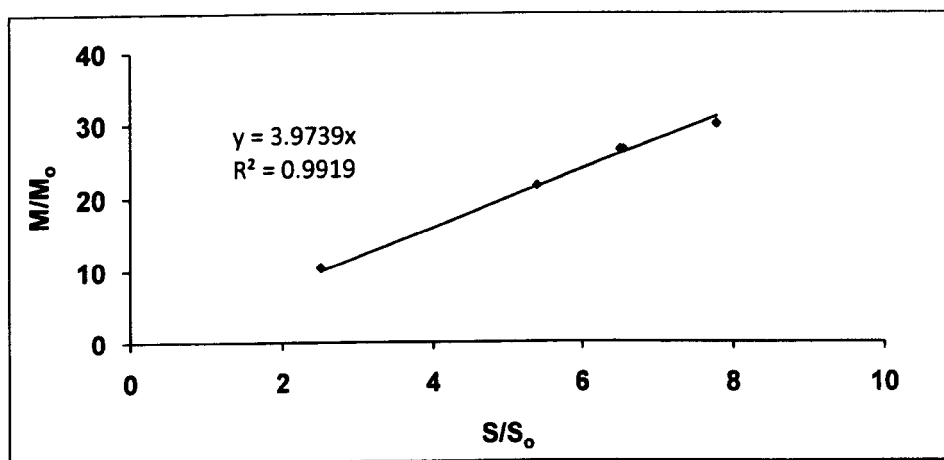


Figure 2.14 Calibration of methyl propionate with n-decane as a standard.

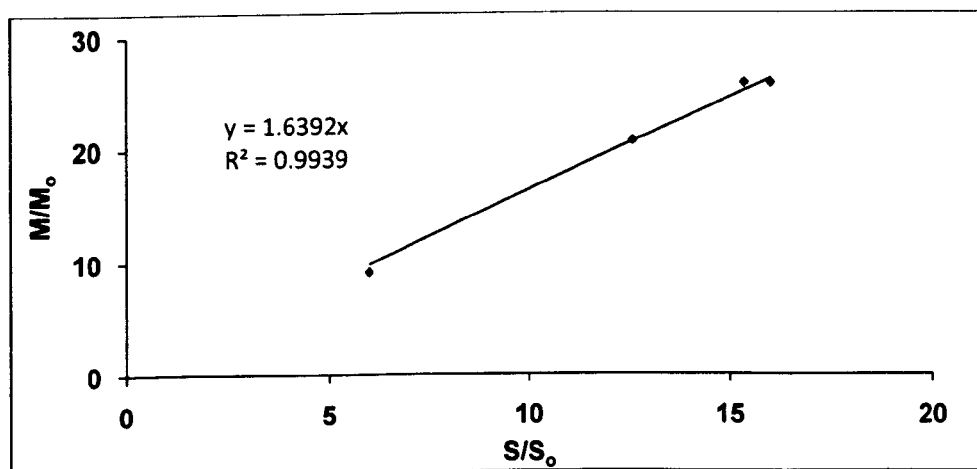


Figure 2.15 Calibration of ethyl hexanoate with n-decane as a standard.

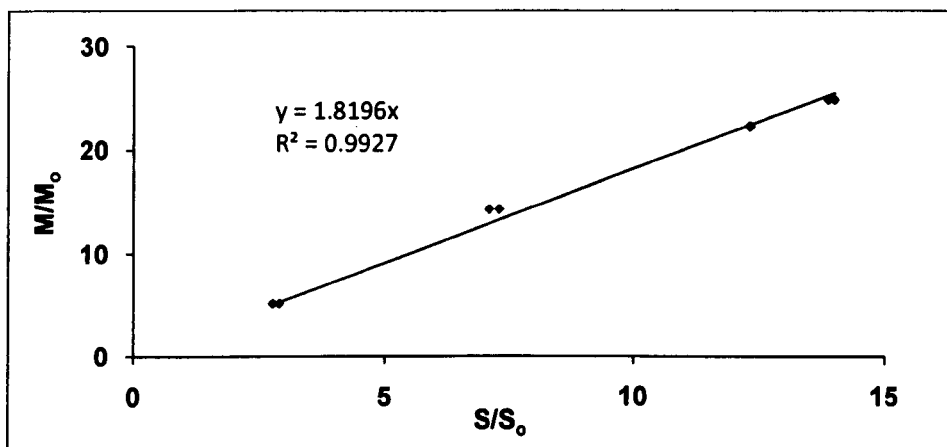


Figure 2.16 Calibration of methyl hexanoate with n-decane as a standard.

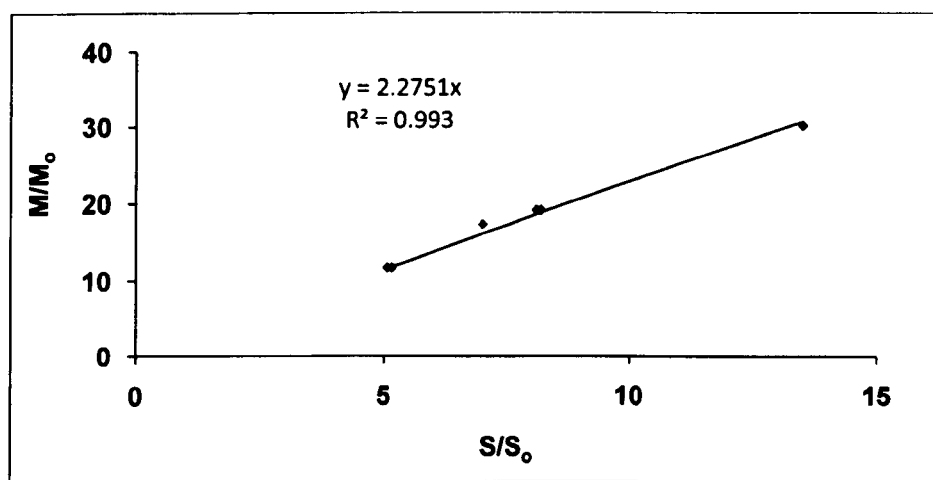


Figure 2.17 Calibration of methyl hexanoate with n-dodecane as a standard.

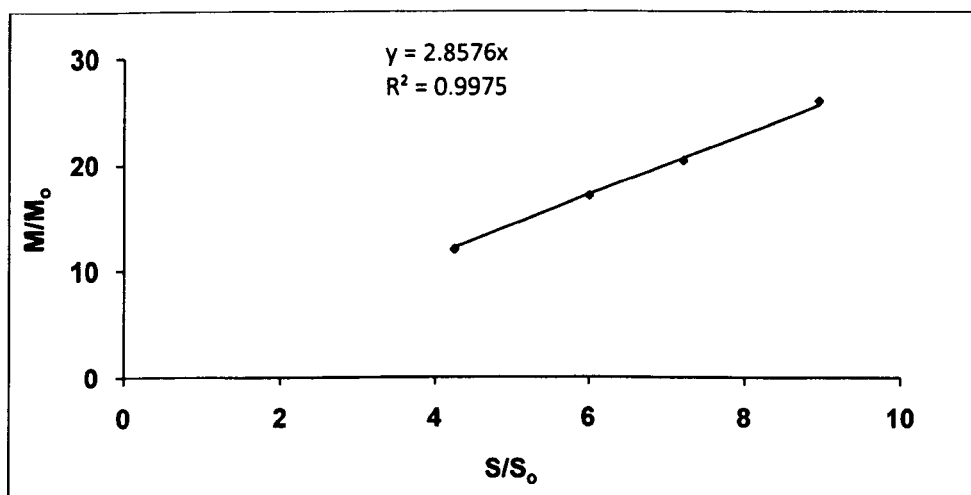


Figure 2.18 Calibration of hexanoic acid with n-dodecane as a standard.

The calibration data for the isomerisation of α -pinene are given in Table 2.2. The calibration factors were assumed to be the same for all monoterpene products. The conditions of the GC analysis are shown in Figure 2.10. A typical GC trace for the isomerisation of α -pinene is shown in Figure 2.19.

Table 2.2 GC retention times and calibration factors (K) for compounds involved in isomerisation of α -pinene.

Compound	Molecular weight (g/mol)	Boiling point ($^{\circ}$ C)	Retention time (min)	Calibration factor (K)
α -pinene	136.24	156	3.88	1.00
camphene	136.24	159	4.10	1.00
p-cymene	134.22	177	5.41	1.00
terpinolene	136.24	184	5.77	1.00
limonene	136.24	176	5.04	1.00
β -pinene	136.24	164	4.46	1.00
β -terpinene	136.24	174	4.95	1.00

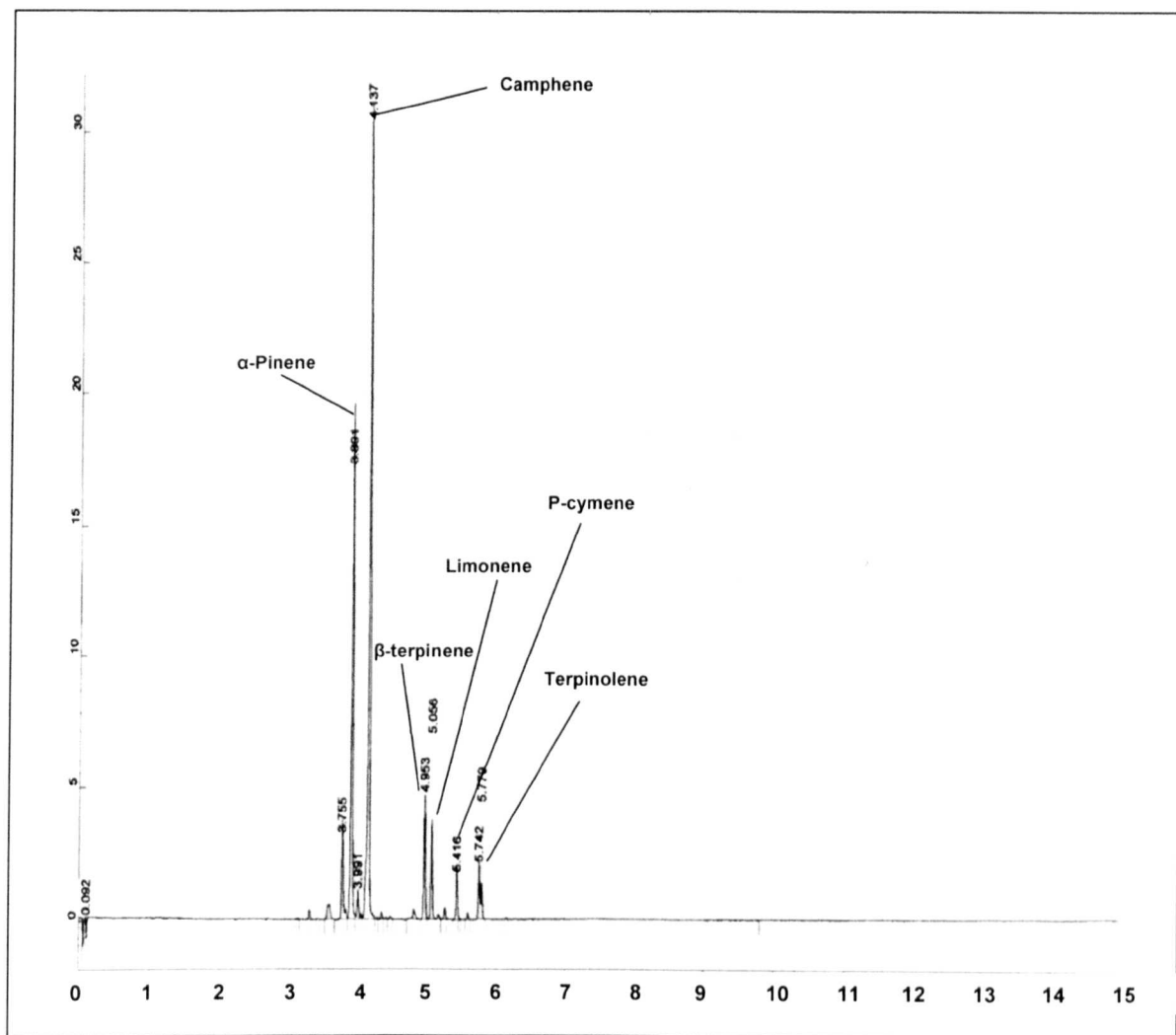


Figure 2.19 GC chromatogram for the gas- phase conversion of α -pinene.

The molecular weights, boiling points and retention times for the dehydration of isopropanol are given in Table 2.3. The conditions of the GC analysis are shown in Figure 2.11. A typical GC trace for the dehydration of isopropanol is shown in Figure 2.20.

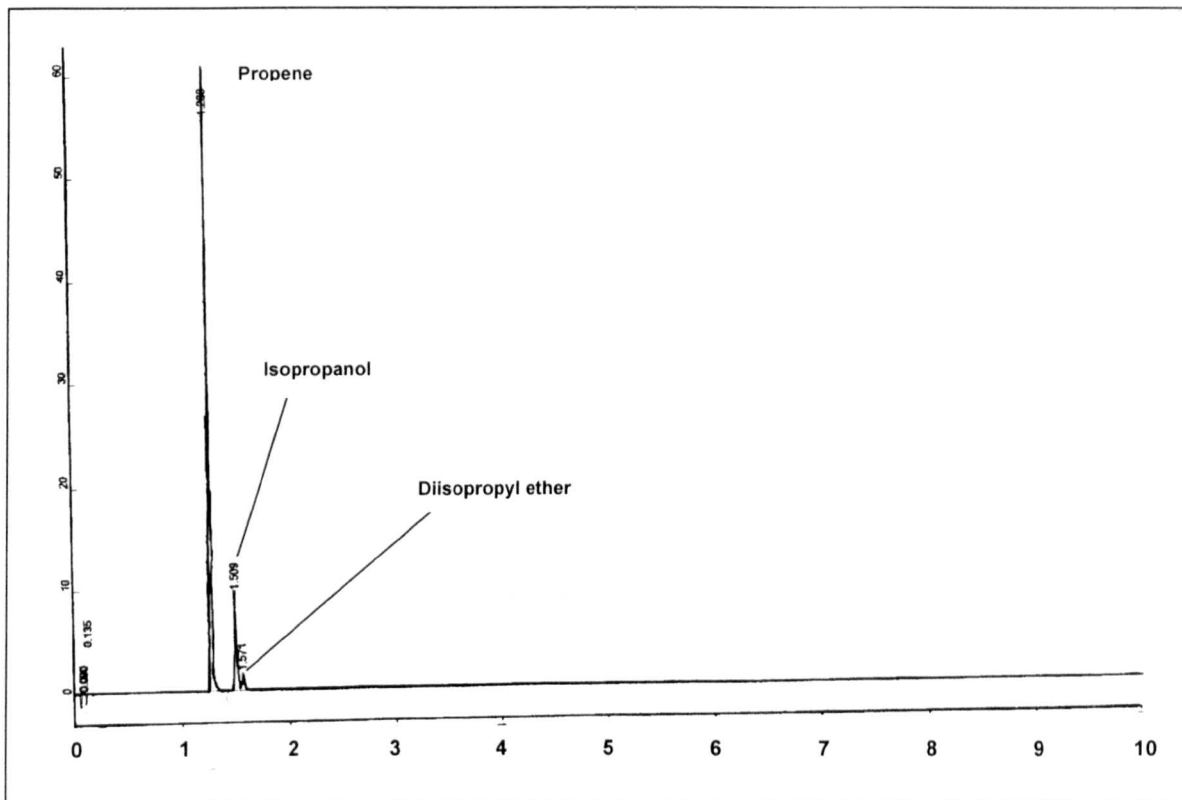


Figure 2.20 GC chromatogram for the gas- phase conversion of isopropanol.

Table 2.3 GC retention times for compounds involved in dehydration of isopropanol.

Compound	Molecular weight (g/mol)	Boiling point (°C)	Retention time (min)
isopropanol	60.10	82	1.51
propene	42.08	-47	1.28
diisopropyl ether	102.18	-60	1.57

2.5.2 Reaction studies

2.5.2.1 Liquid phase reactions

The liquid-phase esterification and transesterification reactions were carried out in a 25 ml glass reactor (round-bottom two-neck flask) equipped with a condenser and a magnetic stirrer at 60°C under atmospheric pressure (Figure 2.21). The total weight of reaction mixture (ester or acid + methanol) was 10.0 g. n-Decane or n-dodecane (1 wt%) was added as a GC internal standard. 0.1 g catalyst was added to reaction mixture unless otherwise stated. The reaction was carried out for 6 h. To monitor the reaction, 0.1 ml samples of the reaction mixture were taken periodically, at ½ h, 1 h, 2 h and 6 h. The samples were diluted with methanol and then separated from the catalyst by centrifugation. The samples were analysed by gas chromatography (a Varian CP-3380 gas chromatograph) equipped with a BP1 capillary non-polar column (25 m× 0.32 mm×0.5 µm).

2.5.2.1.1 Heterogeneous versus homogeneous catalysis test

The test for leaching of HPW from the surface of the support was carried out to check the contribution of homogeneous catalysis. This test includes centrifuging of the reacting mixture to separate the solid catalyst, followed by analysing the reactivity of the clear supernatant.

2.5.2.1.2 Catalyst reuse

Catalyst reuse studies were carried out on a scale up to 50 g of the initial reaction mixture. After each run, the catalyst was filtered off and, prior to reuse, treated at 150 °C/0.5 Torr for 1.5 h.

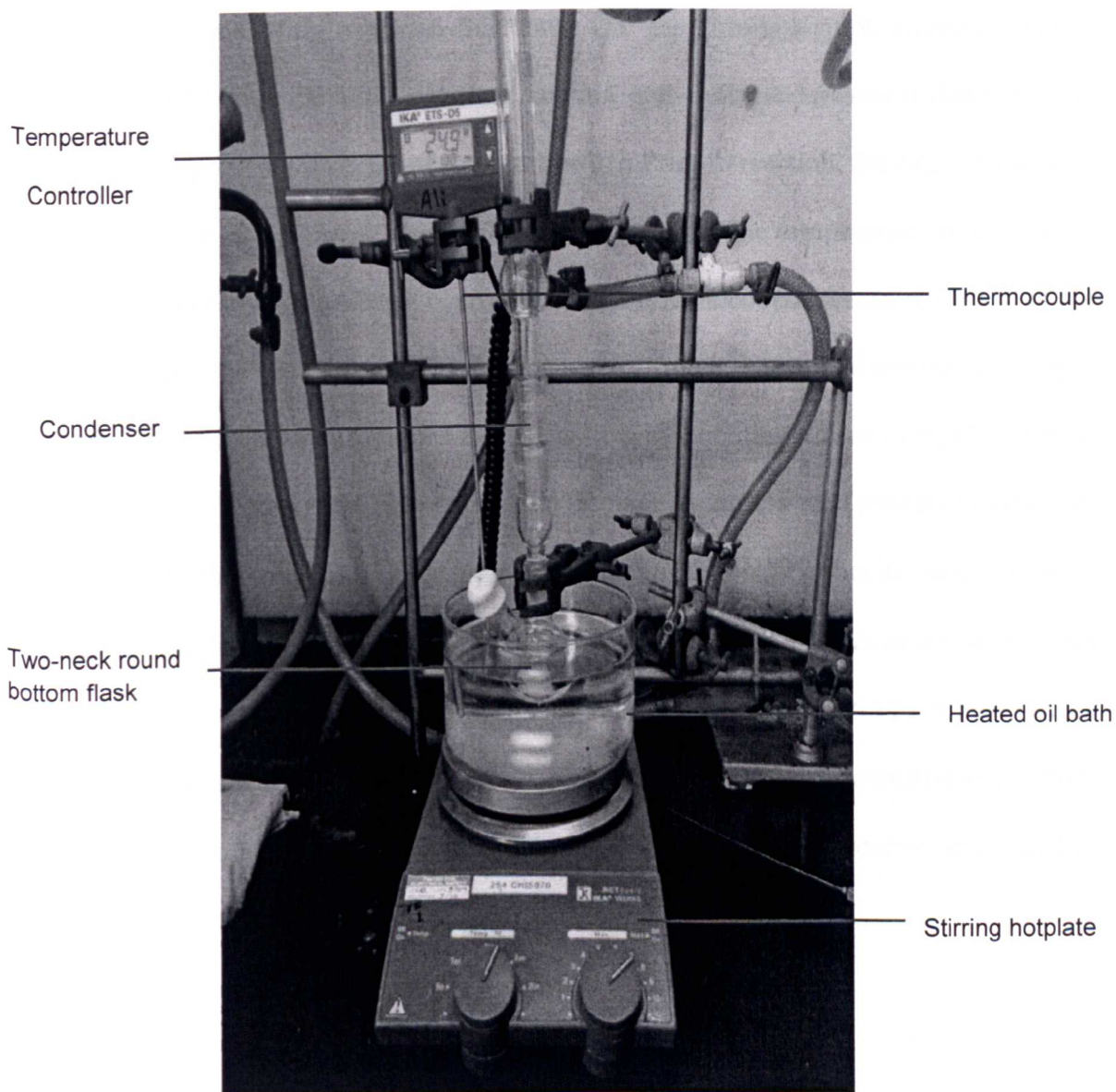


Figure 2.21 Reactor for esterification and transesterification reactions.

2.5.2.2 Gas phase reactions

The catalytic tests were performed under atmospheric pressure in a Pyrex glass fixed-bed microreactor (28 cm in length and 0.9 cm internal diameter) with on-line GC product analysis using a Varian Star 3400 CX gas chromatograph equipped with a 30×0.25×0.25 mm ZB-1701 capillary column and a flame ionisation detector. The reactor was packed with 0.1 g of catalyst powder. Prior to reaction, the catalyst was pre-treated in situ in a nitrogen flow (20 mL/min) for 1 h. The temperature in the reactor was controlled by a Eurotherm controller using a thermocouple placed at the top of the catalyst bed. The gas feed was fed into the reactor from the top. The reactant (isopropyl alcohol or α -pinene) was supplied to the gas flow by bubbling a flow of N₂ (20 ml/min, controlled by Brooks mass flow controller) through a stainless steel saturator containing the reactant (isopropyl alcohol or α -pinene), which was kept at a specific temperature to maintain the chosen vapour pressure (Table 2.4). All gas lines were made of stainless steel. The downstream lines and sampling valves were heated at 175 °C to prevent reactant and product condensation. At regular time intervals, the downstream gas flow was analysed by on-line GC. Figure 2.22 shows a diagram of the reactor setup used in the gas-phase reactions.

Table 2.4 The partial vapour pressure of α -pinene and isopropyl alcohol at saturation temperatures used in experiments (calculated from reference book [23]).

Reactant	Temperature ($^{\circ}\text{C}$)	Partial vapour pressure (kPa)
α -pinene	50	2.00
isopropyl alcohol	25	5.52

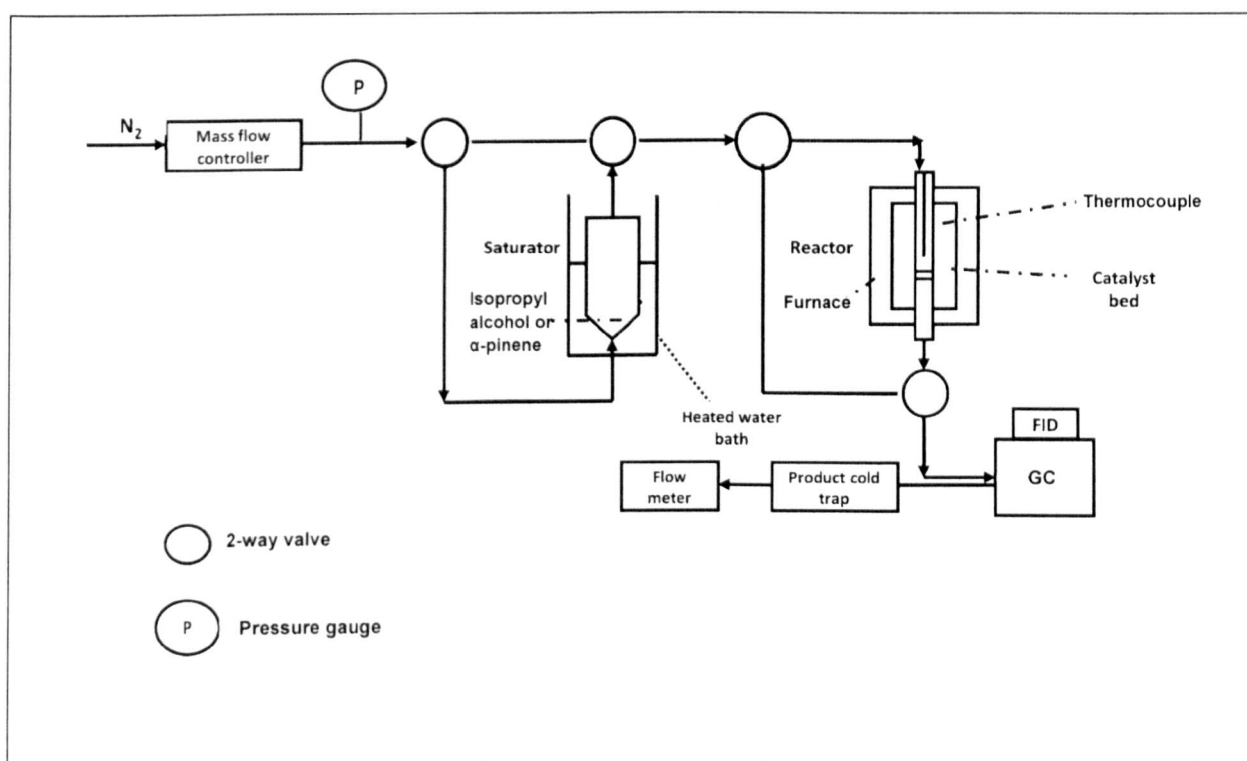


Figure 2.22 A diagram of the reactor setup used in the gas-phase reactions.

The product yields (Y_p), total conversion (X) and the selectivity of a particular product ($S_{p,s}$) was calculated using equations (2.6)-(2.8) respectively.

$$Y_p = \frac{S_p \times K_g \times A}{S_r + (\sum S_p \times K_g \times A)} \times 100 \quad (2.6)$$

$$X = \sum Y_p \quad (2.7)$$

$$S_{p,s} = \frac{Y_p}{X} \times 100 \quad (2.8)$$

In equation (2.6), S_r is the peak area of unreacted substrate, S_p is the peak area of product, K_g is the calibration factor of the product relative to the substrate (α -pinene or isopropyl alcohol), A is the stoichiometry factor of the product relative to the substrate and $(\sum S_p \times K_g \times A)$ is the summation for all reaction products. For the reaction studied, $A=1$.

The reaction activation energy, E_a , for isopropanol dehydration was measured under differential conditions using 0.1 g catalyst samples. In differential conditions (conversion less than 10%) the reaction rate becomes approximately linearly proportional to the change in conversion. Therefore, the activation energy can be calculated directly from the incremental change in conversion [24, 25].

The activation energy was calculated using the Arrhenius equation (Equation 2.9). Where k is the reaction rate constant, A is the pre-exponential factor, E_a is the activation energy, R is the gas constant and T is the absolute temperature. A plot of $\ln k$ against $1/T$ gives a straight line, from which the activation energy can be determined.

$$k = Ae^{-\frac{E_a}{RT}} \quad (2.9)$$

$$\ln k = \ln A - \frac{E_a}{RT} \quad (2.10)$$

References

- [1] M.O.Y. Izumia, M. Kitagawaa, M. Yoshidaa, *Microporous Mater.* 5 (1995) 255.
- [2] E.F. Kozhevnikova, I.V. Kozhevnikov, *J. Catal.* 224 (2004) 164.
- [3] T.L. Stuchinskaya, M. Musawir, E.F. Kozhevnikova, I.V. Kozhevnikov, *J. Catal.* 231 (2005) 41.
- [4] N. Uekawa, T. Kudo, F. Mori, Y.J. Wu, K. Kakegawa, *J. Colloid Interface Sci.* 264 (2003) 378.
- [5] P. Patnaik, *Dean's Analytical Chemistry Handbook*, 2nd ed., 2004.
- [6] A.A. Mirzaei, PhD thesis, University of Liverpool, 1998.
- [7] D. Kealey, P.J. Haines, *Analytical Chemistry*, 1st ed., 2002.
- [8] F.W. Fifield, *Principles and Practice of Analytical Chemistry* 5th ed., 2000.
- [9] L.M. Harwood, C.J. Moody, J.M. Percy, *Experimental Organic Chemistry: Standard and Microscale*, Blackwell Science, 2001.
- [10] G.C. Bond, *Heterogeneous Catalysis*, 2nd ed., 1987.
- [11] G. Leofanti, M. Padovan, G. Tozzola, B. Venturelli, *Catal. Today* 41 (1998) 207.
- [12] J.M. Thomas, W.J. Thomas, *Principles and Practice of Heterogeneous Catalysis*, VCH, 1997.
- [13] G. Attard, C. Barnes, *Surfaces*, Oxford University Press, 1998.
- [14] M. Bowker, *The Basis and Application of Heterogeneous Catalysis*, Oxford University Press, 1998.
- [15] S. Brunauer, P.H. Emmet, E. Teller, *J. Am. Chem. Soc.* 60 (1938) 309.
- [16] P. Atkins, J. Paula, *Atkins' Physical Chemistry*, 7th ed., Oxford, 2002.
- [17] P. Leparlouer, J. Mercier, B. Jalon, *Thermochim. Acta* 103 (1986) 21.
- [18] F. Lefebvre, F.X. Liucai, A. Auroux, *J. Mater. Chem.* 4 (1994) 125.

- [19] V. Rakic, V. Dondur, U. Mioc, D. Jovanovic, *Top. Catal.* 19 (2002) 241.
- [20] D.D. Laws, H.M.L. Bitter, A. Jerschow, *Angew. Chem. Int. Ed.* 41 (2002) 3096.
- [21] J. Klinowski, *Chem. Rev.* 91 (1991) 1459.
- [22] G.D. Chistian, J.E. Oreeilly, *Instrumental Analysis*, 2nd ed., 1986.
- [23] D.R. Lide, *Handbook of Chemistry and Physics*, 84th ed., CRC press, 2003-2004.
- [24] C. Perego, S. Peratello, *Catal. Today* 52 (1999) 133.
- [25] H. Purnama, T. Ressler, R.E. Jentoft, H. Soerijanto, R. Schlogl, R. Schomacker, *Appl. Catal. A* 259 (2004) 83.

3. Catalyst characterisation

3.1 Introduction

In this chapter, the results of catalyst characterisation will be presented and discussed. Catalyst texture including surface area, pore diameter and pore volume, the state of heteropoly acids on the catalyst surface, catalyst crystallinity, and the nature and the strength of acid sites were investigated using different techniques: nitrogen adsorption, IR (infrared spectroscopy), XRD (X-ray diffraction), ^{31}P MAS NMR spectroscopy and DSC (differential scanning calorimetry).

3.2 Thermogravimetric analysis (TGA)

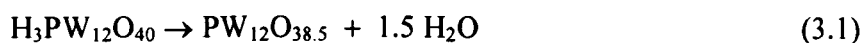
The thermogravimetric experiments were carried out using a Perkin Elmer TGA 7 instrument with a heating rate of 20 °C per minute to raise the temperature from room temperature to 700 °C, under nitrogen gas flow.

The TGA results are summarised in Table 3.1. The TG analysis (TGA) and derivative TG (DTG) results for bulk HPAs (HPW, HSiW and HPMo), supported catalysts, Nb_2O_5 , ZrO_2 and TiO_2 support, and CsPW are shown in Figure 3.1 – 3.10.

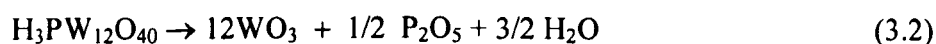
Table 3.1 Summary of TGA results.

Sample	Temperature range, °C	Weight loss %	Number of H ₂ O molecules
H ₃ PW ₁₂ O ₄₀	30 - 150	9.80	17.40
	150 - 300	3.30	5.40
	300 - 600	0.90	1.50
H ₄ SiW ₁₂ O ₄₀	30 - 150	1.00	17.70
	150 - 300	3.50	5.80
	300 - 600	1.00	1.90
H ₃ PMo ₁₂ O ₄₀	30 - 150	12.30	4.20
	150 - 300	2.30	2.40
	300 - 600	1.40	1.40
CS _{2.5} H _{0.5} PW ₁₂ O ₄₀	30 - 150	2.10	3.40
	150 - 300	0.80	1.44
	300 - 600	0.14	0.25
15% HPW/Nb ₂ O ₅	30 - 150	2.66	
	150 - 300	4.57	
	300 - 600	0.77	
15% HPW/ZrO ₂	30 - 150	4.50	
	150 - 300	5.45	
	300 - 600	2.45	
15% HPW/TiO ₂	30 - 150	1.00	
	150 - 300	0.55	
	300 - 600	0.35	
Nb ₂ O ₅	30 - 150	1.36	0.20
	150 - 300	5.49	0.86
	300 - 600	1.35	0.20
ZrO ₂	30 - 150	2.70	0.15
	150 - 300	4.60	0.26
	300 - 600	2.00	0.11
TiO ₂	30 - 150	0.73	0.03
	150 - 300	0.31	0.01
	300 - 600	0.82	0.04

The thermal behaviour of HPA catalysts has been investigated by other researchers previously [1-6]. Figure 3.1 shows the TGA analysis for $\text{H}_3\text{PW}_{12}\text{O}_{40}$ hydrate. Three main peaks can be observed: (i) a peak at a temperature below 100°C corresponding to the loss of physisorbed water (a variable amount depending on the number of hydration waters in the sample); (ii) a peak in the temperature range of $150 - 280^\circ\text{C}$ centred at about 220°C attributed to the loss of ca. six H_2O molecules per Keggin unit, corresponding to the dehydration of a relatively stable hexahydrate $\text{H}_3\text{PW}_{12}\text{O}_{40}\cdot 6\text{H}_2\text{O}$ in which the waters are hydrogen-bonded to the acidic protons; and (iii) a peak in the range of $370 - 600^\circ\text{C}$ centred at about 470°C due to the loss all acidic protons to evolve 1.5 water molecules per Keggin unit. This water is suggested to form as a result of the extraction of oxygen from the anion by the protons, apparently without collapse of the Keggin structure of the anion but with some rearrangement of its secondary structure (Equation 3.1), as indicated by the XRD data [3].



Decomposition of $\text{H}_3\text{PW}_{12}\text{O}_{40}$ to its constituent oxides WO_3 and P_2O_5 occurred above 550°C [3]:



It is known that $\text{H}_4\text{SiW}_{12}\text{O}_{40}$ and $\text{H}_3\text{PMo}_{12}\text{O}_{40}$ are less stable than $\text{H}_3\text{PW}_{12}\text{O}_{40}$ [1-3]. Our data (Figures 3.2-3.3) showed good agreement with data reported in literature.

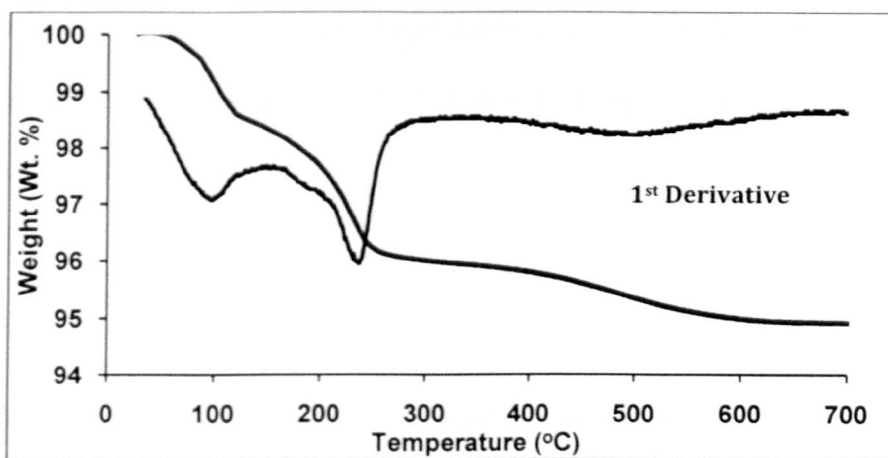


Figure 3.1 TGA analysis of $H_3PW_{12}O_{40}$ hydrate.

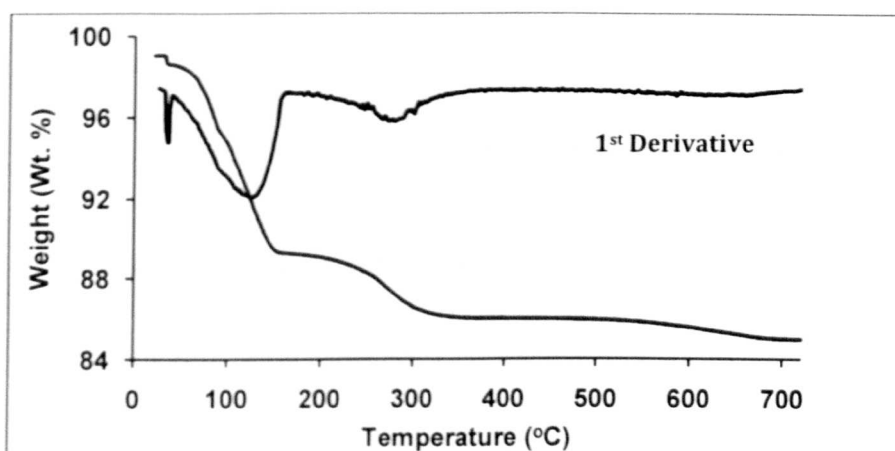


Figure 3.2 TGA analysis of $H_4SiW_{12}O_{40}$.

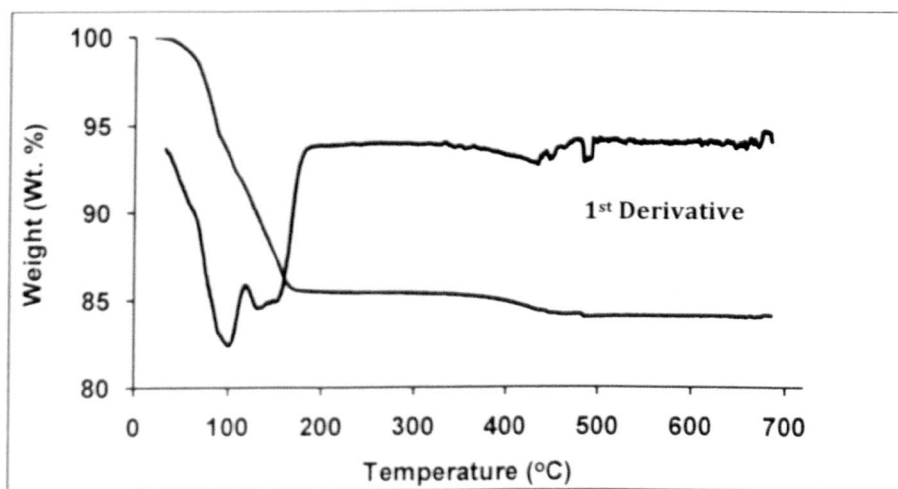
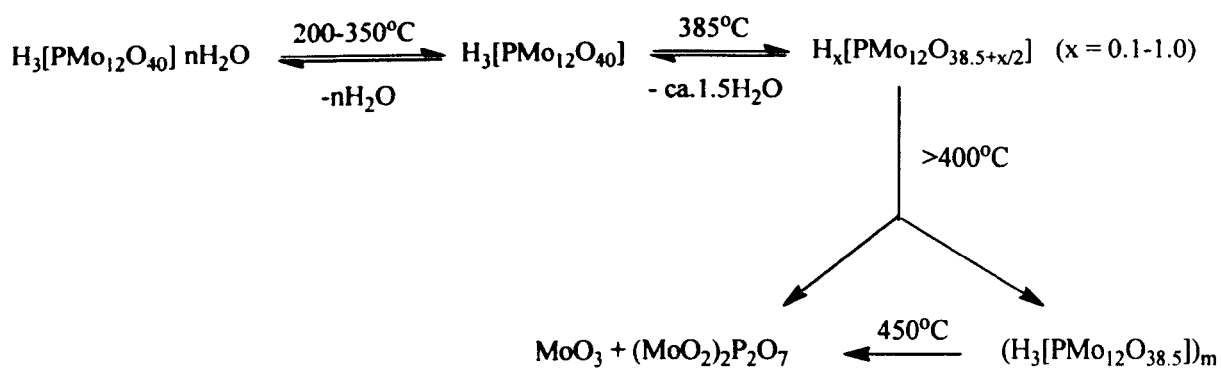


Figure 3.3 TGA analysis of $H_3PMo_{12}O_{40}$.

It has been found that the thermal decomposition of $\text{H}_3\text{PMo}_{12}\text{O}_{40}$ occurs in several steps as shown in Scheme 3.1 [7], first two steps being reversible while the third is irreversible and occurs at 450°C .



Scheme 3.1 Thermal decomposition of $\text{H}_3\text{PMo}_{12}\text{O}_{40}$ [1].

The acidic Cs^+ salt, $\text{Cs}_2.5\text{H}_{0.5}\text{PW}_{12}\text{O}_{40}$, has been found thermally stable up to 600°C and insoluble in polar solvents [1, 8]. Figure 3.4 shows the thermal analysis of $\text{Cs}_2.5\text{H}_{0.5}\text{PW}_{12}\text{O}_{40}$. The loss in weight of 3 % up to a temperature of 300°C , corresponds to the removal of physisorbed water and/or dehydrated crystalline water as reported by Essayem *et al.* [9]. The second weight loss of 0.14 % was observed about 550°C attributed to the deprotonation step and corresponds to 0.25 H_2O molecules per Keggin unit.

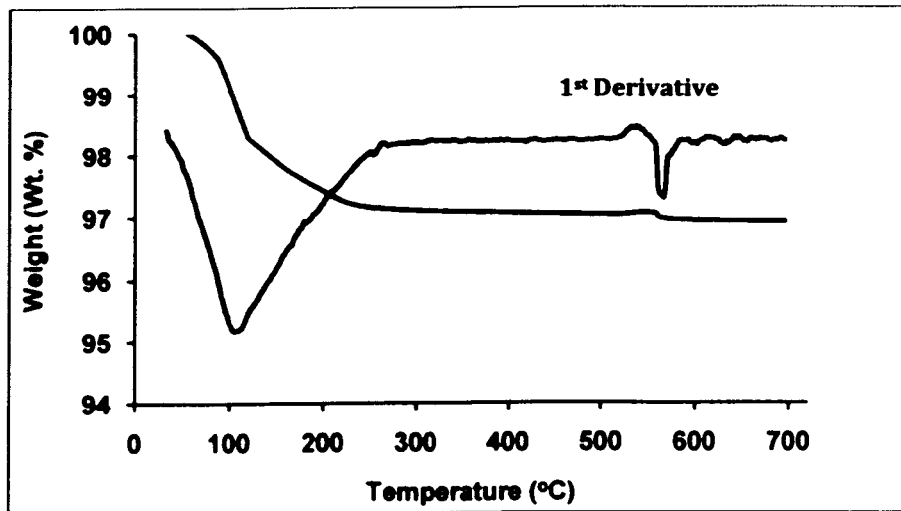


Figure 3.4 TGA analysis of $\text{Cs}_{2.5}\text{H}_{0.5}\text{PW}_{12}\text{O}_{40}$.

The TGA results for HPA supported catalysts along with Nb_2O_5 , ZrO_2 and TiO_2 supports are shown in Figure 3.5–3.10. The most significant weight loss in these catalysts was found at temperatures below 300°C , which corresponds to the removal of adsorbed water and/or dehydrated crystalline water. These results are close to those reported in the literature [10, 11]. Catalyst dehydration proceeds via two steps or more for the HPW supported on Nb_2O_5 and ZrO_2 but in a single step for HPW supported on TiO_2 . It should be noted that Nb_2O_5 and ZrO_2 were prepared in the lab as described in Sections 2.3.3-2.3.4 while TiO_2 was supplied by Aldrich[®]. Therefore, Nb_2O_5 and ZrO_2 accommodate a large amount of water during preparation stage.

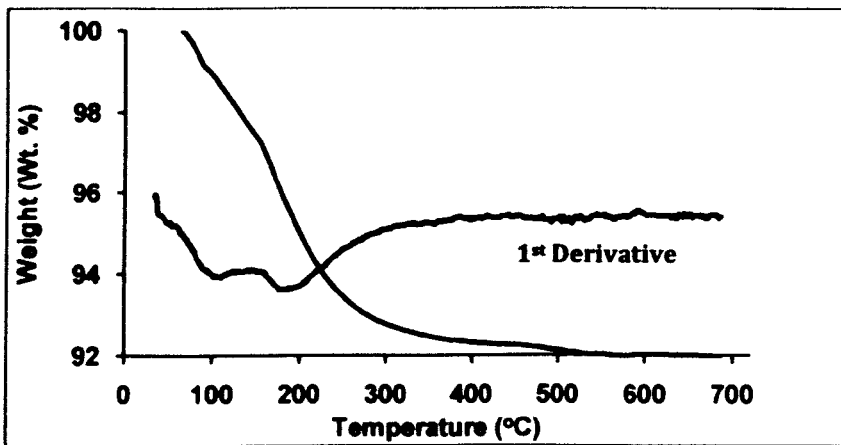


Figure 3.5 TGA analysis of 15%HPW/Nb₂O₅.

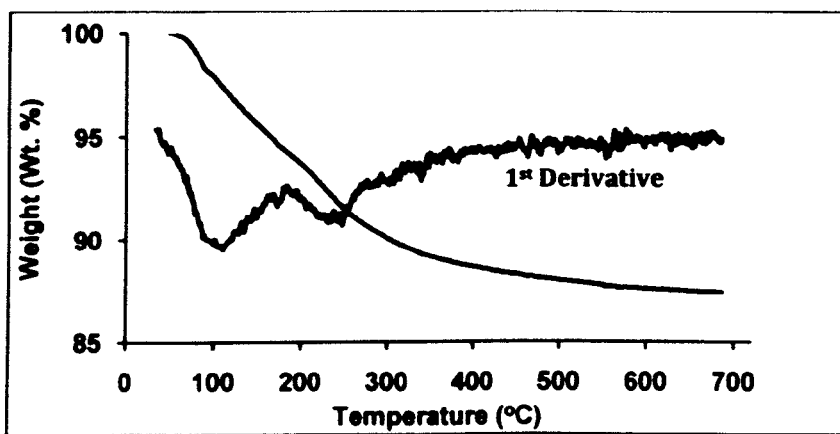


Figure 3.6 TGA analysis of 15%HPW/ZrO₂.

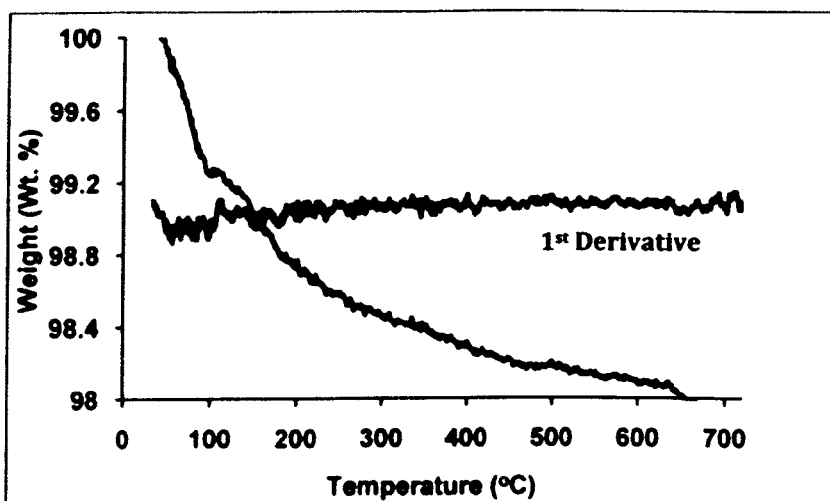


Figure 3.7 TGA analysis of 15%HPW/TiO₂.

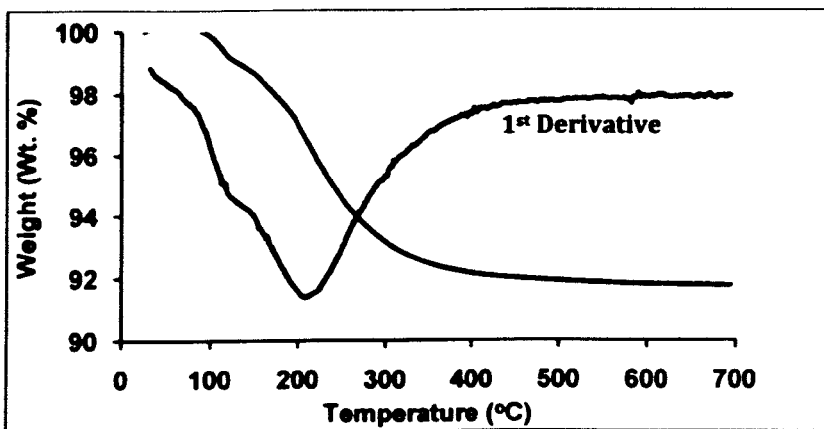


Figure 3.8 TGA analysis of $\text{Nb}_2\text{O}_5 \cdot x\text{H}_2\text{O}$.

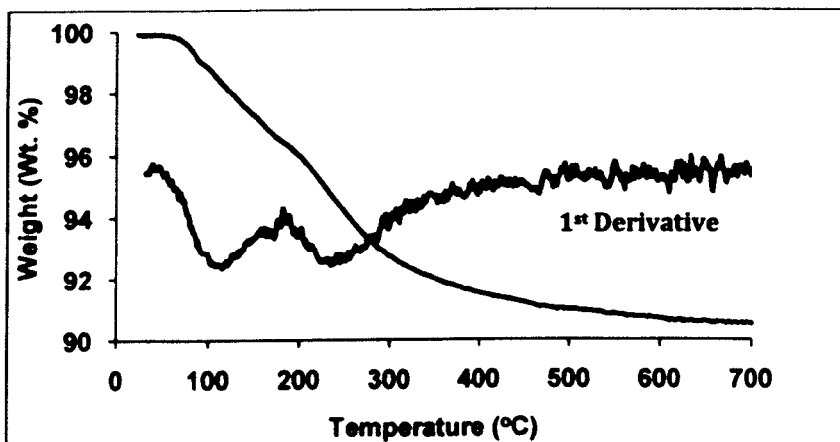


Figure 3.9 TGA analysis of $\text{ZrO}_2 \cdot x\text{H}_2\text{O}$.

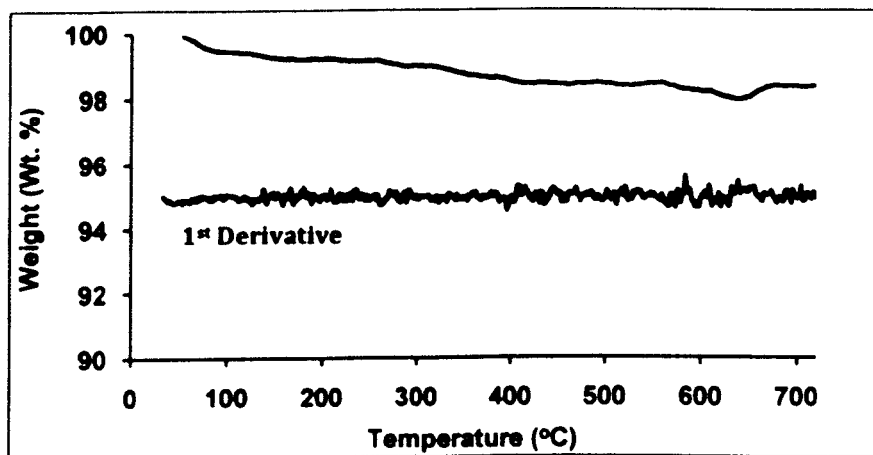


Figure 3.10 TGA analysis of TiO_2 .

3.3 Surface area and porosity

Nitrogen adsorption technique at 77 K has been widely used to determine catalyst surface area and porosity. A plot of the volume of N₂ adsorbed against its relative pressure gives the nitrogen adsorption isotherm. The shape of the isotherm depends on the porous texture of individual solids. According to the IUPAC classification, there are six types of isotherm. Four types, however, are generally found in catalyst characterisation (Figure 3.11) [12-15]. Type I, II, IV, and VI isotherms are representative of microporous, macroporous, mesoporous and uniform ultramicroporous solids respectively.

On macroporous solids (type II), the formation of monolayer of adsorbed molecules occurs at a low relative pressure, whereas multilayer formation takes place at a high relative pressure. The thickness of adsorbate increases gradually with increasing pressure until condensation has been reached.

On mesoporous solids (type IV), similar behaviour to macroporous solids is observed at a low relative pressure. At high relative pressure, the formation of adsorption multilayer occurs until condensation takes place. The pressure of condensation depends on the pore size, the larger the size, the higher the condensation pressure. As mesopores are filled, the adsorption continues on the external surface. Most catalysts belong to this class of solid [16].

On microporous solids (Type I), a strong interaction between the pore walls and adsorbate occurs. Therefore, the adsorption takes place at very low relative pressures. A higher pressure favoured by interaction between adsorbed molecules required to complete filling of pores. After the micropores have been filled, the adsorption continues on the

external surface as is the case with mesopores. Active carbons and zeolites are typical examples of this type.

Type VI (uniform ultramicroporous solids) has only been included recently, with the advent of well-defined single crystal substrates, where such behaviour was observed. Each step in the isotherm corresponds to the completion of the first, second, etc., monolayers [17].

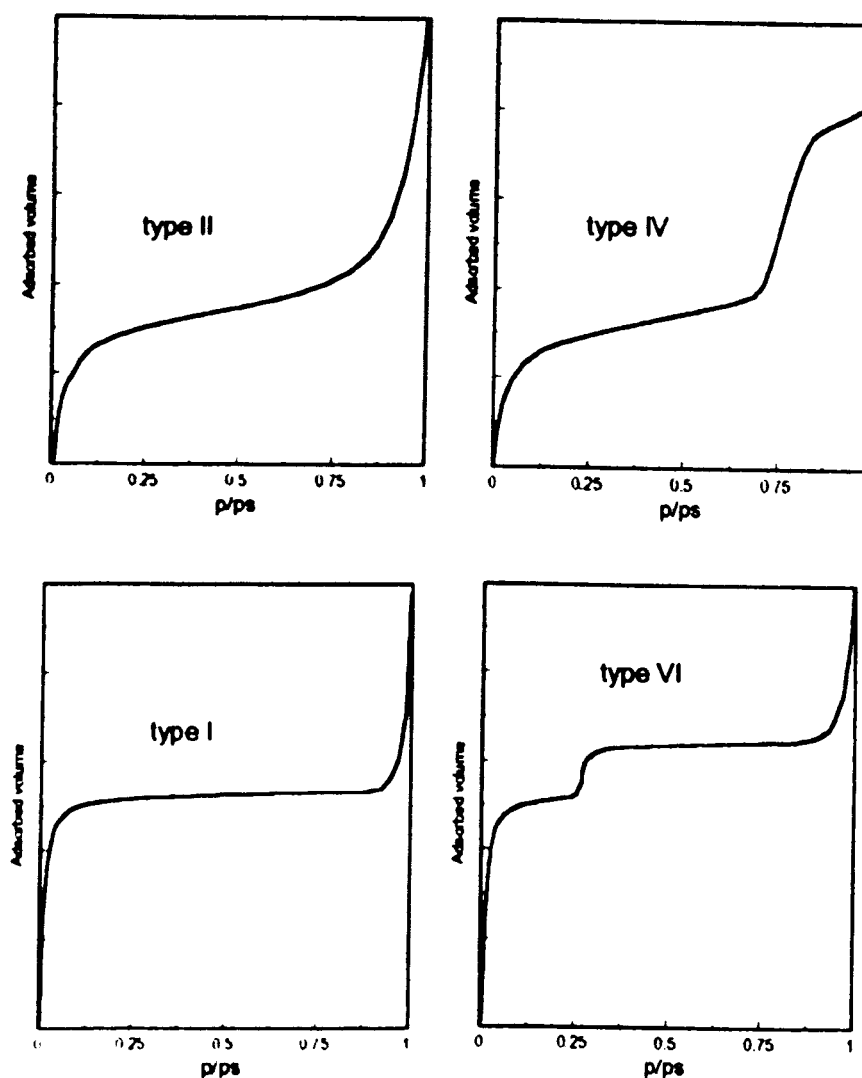


Figure 3.11 The four types of adsorption isotherm found with the N₂ adsorption [16].

When saturation is reached, desorption of adsorbate occurs in the opposite process to that of adsorption. However, on mesoporous solids, evaporation usually takes place at a pressure lower than that of capillary condensation giving a hysteresis loop. Figure 3.12 shows the four hysteresis types that have been classified by IUPAC [16].

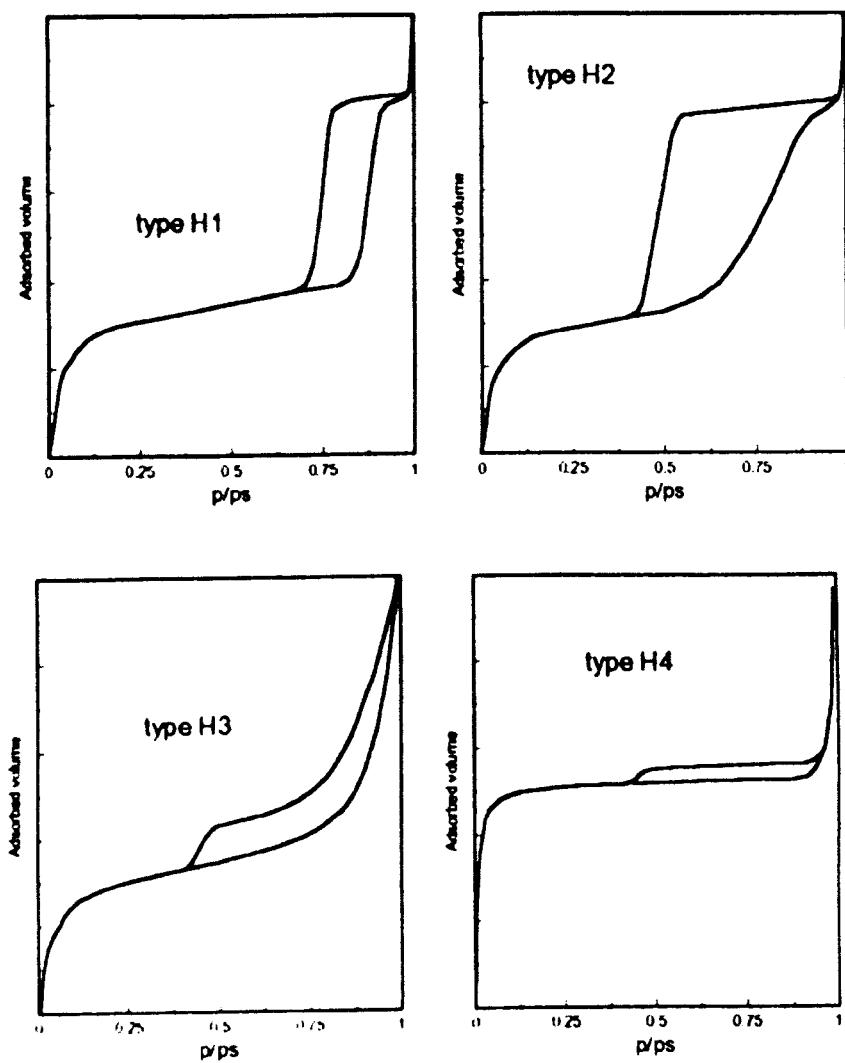


Figure 3.12 The four hysteresis types usually observed with N_2 adsorption [16].

Types H1 and H2 hysteresis isotherms are shown when the solids consist of particles crossed by nearly cylindrical channels or made by aggregates (consolidated) or agglomerates (unconsolidated) that are spheroidal in shape. Type H1 samples have pores with uniform size and shape, while type H2 samples have pores of non-uniform size and shape. These hystereses are owing to different size of pore mouth and pore body (e.g. ink-bottle shaped pores) and/or a different behaviour in adsorption and desorption in near cylindrical pores. Most mesoporous catalysts show Type H1 and H2 hysteresis adsorption isotherms [16].

Types H3 and H4 hysteresis isotherms are found when the solids consist of aggregates or agglomerates of particles forming slit shaped pores (plates or edged particles similar to cubes), with non-uniform and uniform size and/or shape, respectively. These hystereses are due to the different behaviour in adsorption and desorption. Active carbon and zeolites are examples of this class.

An absence of adsorption isotherm hysteresis indicates that the solids possessing blind cylindrical, cone-shaped and/or wedge shaped pores. However, as catalyst pores are usually irregular, only solids with a much reduced hysteresis loop will be observed.

Closure of a hysteresis loop in nitrogen adsorption generally occurs at a relative pressure of 0.42 owing to liquid adsorbate properties and irrespective of the adsorbent or the pore size distribution.

The general procedure for the measurement of surface area and porosity is described in Section 2.4.5. The total surface area of the catalysts was calculated using the Brunauer-Emmett-Teller (BET) method [18]. The pore size distribution and the total pore volumes were both determined using the Barrett, Joyner and Halenda (BJH) method [19].

The texture (surface area, pore diameter and pore volume) of bulk Keggin HPAs is well documented in the literature [1, 2, 20]. Supported HPW catalysts and $\text{Cs}_{2.5}\text{PW}_{12}\text{O}_{40}$ have also been thoroughly characterised ([1, 2, 20] and references therein). In our supported catalysts, 15 wt% HPW loading with monolayer coverage will occupy an area of $\sim 45 \text{ m}^2/\text{g}$, assuming a footprint of the HPW molecule of 144 \AA^2 [1, 2]. The catalysts with surface areas larger $45 \text{ m}^2/\text{g}$ should have an HPW coverage less than monolayer and *vice versa*.

The texture for HPA catalysts and catalyst supports used in this study, with relation to their preparation conditions such as aging and calcination temperature is shown in Tables 3.2a and 3.2b. All the catalysts were mesoporous materials with average pore diameters of 22 – 230 Å. Table 3.2a shows the texture for bulk HPW, $\text{Cs}_{2.5}\text{PW}_{12}\text{O}_{40}$ and HPA supported on commercial oxides. The texture of bulk HPW and $\text{Cs}_{2.5}\text{PW}_{12}\text{O}_{40}$ is in agreement with the literature [21, 22]. Nb_2O_5 , ZrO_2 and TiO_2 supplied by Aldrich® have very low surface area ($1\text{--}8 \text{ m}^2/\text{g}$) (Table 3.2a, entries 5–7). Consequently, HPA supported on these oxides have rather low surface area (Table 3.2a, entries 8–13). Changing the aging temperature from room temperature to $100 \text{ }^\circ\text{C}$ did not affect the texture of supported HPW catalysts.

Table 3.2b shows the texture for HPA supported on in-house made Nb_2O_5 and ZrO_2 as well as commercial TiO_2 . These possess relatively high surface area. The pure oxides Nb_2O_5 and ZrO_2 (Table 3.2b, entries 1–2) were prepared in order to obtain supported catalysts with high surface area. For HPA catalysts supported on Nb_2O_5 and ZrO_2 , the surface area reduced upon HPA loading. Also, it reduced significantly with increasing the calcination temperature. In contrast, the surface area of TiO_2 -supported

catalysts practically did not change. In terms of pore diameter, titania based catalysts possessed larger pores and zirconia based ones smaller pores, with niobia catalysts in between. Increasing the calcination temperature increased the pore diameter of supported HPA.

Table 3.2a Catalyst texture from nitrogen adsorption.

	Catalyst	Aging ^a (°C)	Calcination ^b (°C)	S _{BET} (m ² /g)	Pore diameter ^c (Å)	Pore volume ^d (cm ³ /g)
1	H ₃ PW ₁₂ O ₄₀			2	81	0.040
2	Cs _{2.5} H _{0.5} PW ₁₂ O ₄₀ ^e	rt	150	111	24	0.067
3	20%Cs ₂ HPW ₁₂ O ₄₀ /SiO ₂	rt	150	185	191	0.880
4	15%HPW/SiO ₂	rt	150	229	204	1.170
5	Nb ₂ O ₅			1	48	0.001
6	ZrO ₂			3	53	0.005
7	TiO ₂			8	75	0.015
8	15%HPW/Nb ₂ O ₅	rt	500	2	95	0.005
9	15%HPW/Nb ₂ O ₅	100	500	2	111	0.005
10	15%HPW/ZrO ₂	rt	500	3	56	0.004
11	15%HPW/ZrO ₂	100	500	2	47	0.002
12	15%HPW/TiO ₂	rt	500	9	76	0.017
13	15%HPW/TiO ₂	100	500	9	79	0.017

a) Aging of aqueous slurry for 24 h at room temperature (rt) or 100 °C.

b) Calcination in air for 3 h.

c) Average BET pore diameter.

d) Single point total pore volume.

e) Cs_{2.5}H_{0.5}PW₁₂O₄₀ was aged for 48 h and calcined at 150 °C/0.5 torr for 1.5 h.

Table 3.2b Catalyst texture from nitrogen adsorption.

	Catalyst	Aging ^a (°C)	Calcination ^b (°C)	S _{BET} (m ² /g)	Pore diameter ^c (Å)	Pore volume ^d (cm ³ /g)
1	Nb ₂ O ₅			287	46	0.330
2	ZrO ₂			162	23	0.091
3	TiO ₂ ^e			44	90	0.100
4	15%HPW/Nb ₂ O ₅	rt	100	193	48	0.230
5	15%HPW/Nb ₂ O ₅	rt	300	166	52	0.220
6	15%HPW/Nb ₂ O ₅	rt	500	96	80	0.190
7	15%HPW/ZrO ₂	rt	100	176	22	0.095
8	15%HPW/ZrO ₂	rt	200	155	23	0.083
9	15%HPW/ZrO ₂	rt	300	121	24	0.070
10	15%HPW/ZrO ₂	rt	500	54	56	0.075
11	15%HPW/TiO ₂ ^e	rt	100	49	174	0.212
12	15%HPW/TiO ₂ ^e	rt	200	51	144	0.185
13	15%HPW/TiO ₂ ^e	rt	300	41	154	0.160
14	15%HPW/TiO ₂ ^e	rt	400	44	163	0.173
15	15%HPW/TiO ₂ ^e	rt	500	40	230	0.230

- a) Aging of aqueous slurry for 24 h at room temperature (rt).
b) Calcination in air for 3 h.
c) Average BET pore diameter.
d) Single point total pore volume.
e) Commercial catalyst support (from Aldrich®).

The nitrogen adsorption-desorption isotherm for bulk HPW is shown in Figure 3.13. The isotherm has a type II which is usually observed for nonporous materials [12]. This is in agreement with results reported by Misono *et al.* [22, 23]. $\text{Cs}_{2.5}\text{H}_{0.5}\text{PW}_{12}\text{O}_{40}$ exhibits a type IV isotherm which is found in mesoporous materials (Figure 3.14) [16]. The isotherm has a type H2 hysteresis loop indicating the presence of mesoporous solids, which are of a non-uniform shape [17]. It can be seen from the pore size distribution obtained by the BJH method (Figure 3.15) that a sharp peak appeared at about 40 Å diameter. These results are in agreement with the previous studies [22-24]. Figures 3.16 and 3.17 show isotherms of silica supported HPW and $\text{Cs}_2\text{H}_1\text{PW}_{12}\text{O}_{40}$. In both cases type IV with a hysteresis loop (type H3) are observed indicating the presence of non-uniform size and/or shape mesopores.

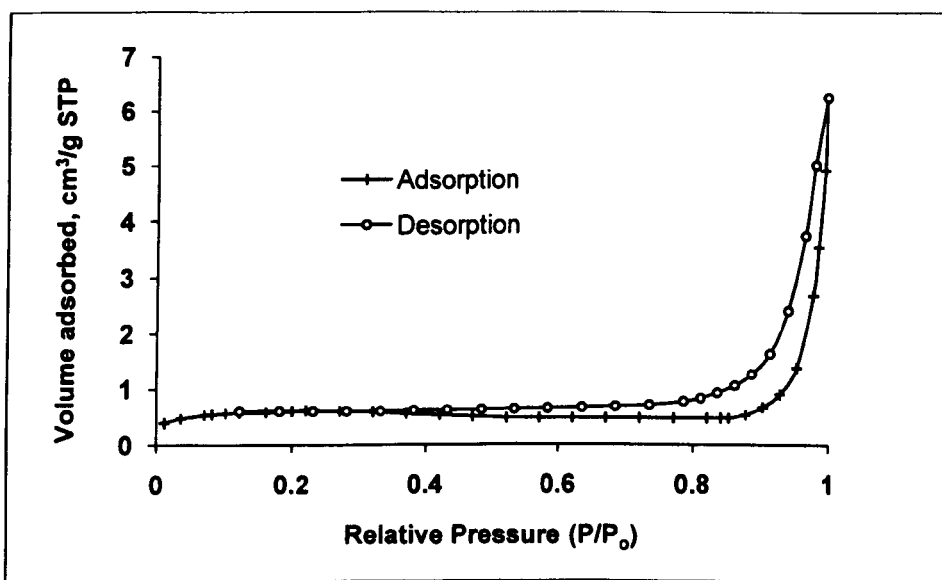


Figure 3.13 N_2 adsorption isotherm for bulk HPW.

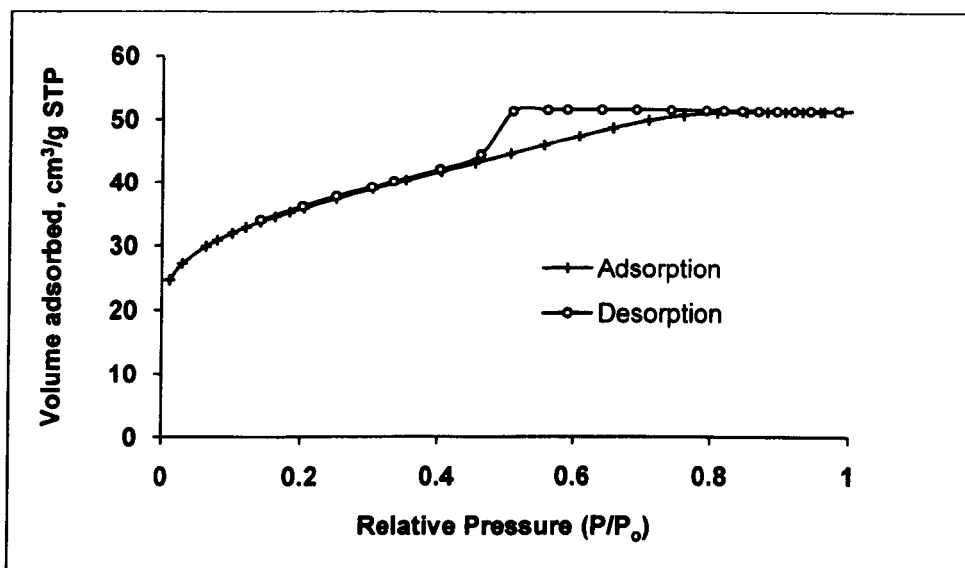


Figure 3.14 N₂ adsorption isotherm for Cs_{2.5}H_{0.5}PW₁₂O₄₀.

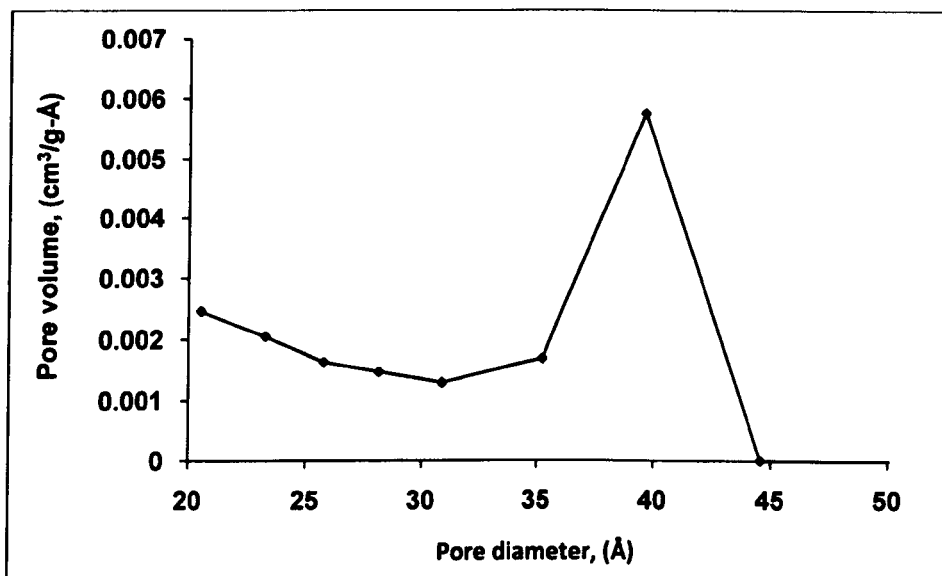


Figure 3.15 Distribution of pore volume as a function of pore diameter for Cs_{2.5}H_{0.5}PW₁₂O₄₀.

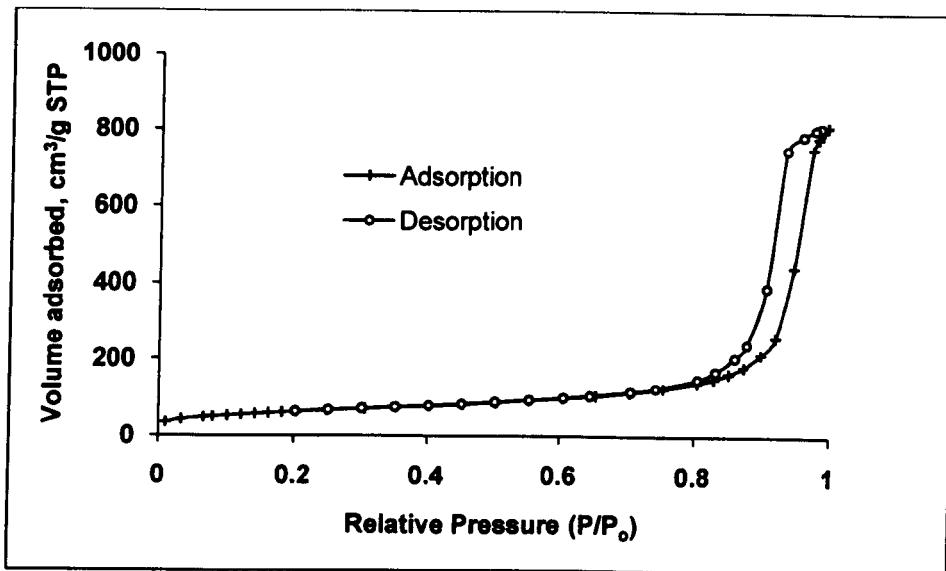


Figure 3.16 N₂ adsorption isotherm for 15%HPW/SiO₂.

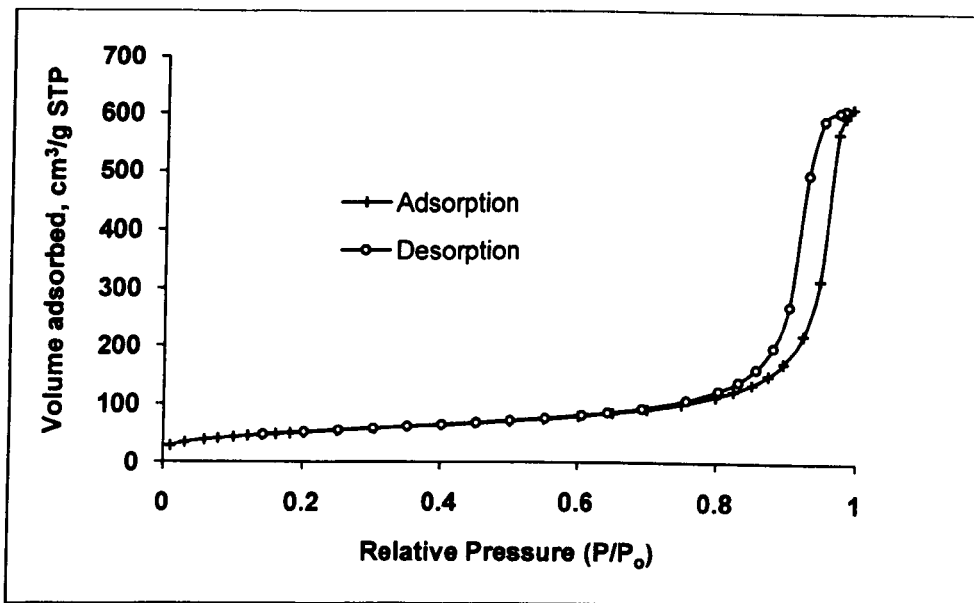


Figure 3.17 N₂ adsorption isotherm for 20%Cs₂H₁PW₁₂O₄₀/SiO₂.

All HPW supported on N_2O_5 oxide possess large surface area along with N_2O_5 oxide itself their adsorption isotherms were type IV characteristic of mesoporous materials (Figures 3.18 - 3.20). All these isotherms possess a H2 type hysteresis loop, an indication of a non-uniform size and/or shape mesopores. Mesopores of 39 Å in diameter were found in the pore size distribution for these catalysts which is presented in Figure 3.21. If these pores were wider, type II isotherms would be observed [17], and this is clearly seen for 15%HPW/ Nb_2O_5 -500, which possesses a low surface area (Figures 3.22). This type of isotherm is characteristic of nonporous or macroporous materials (>50 nm) [16, 17]. However, a hysteresis loop (type H3) is observed, indicating the presence of mesopores. Figure 3.23 shows the pore size distribution for this catalyst.

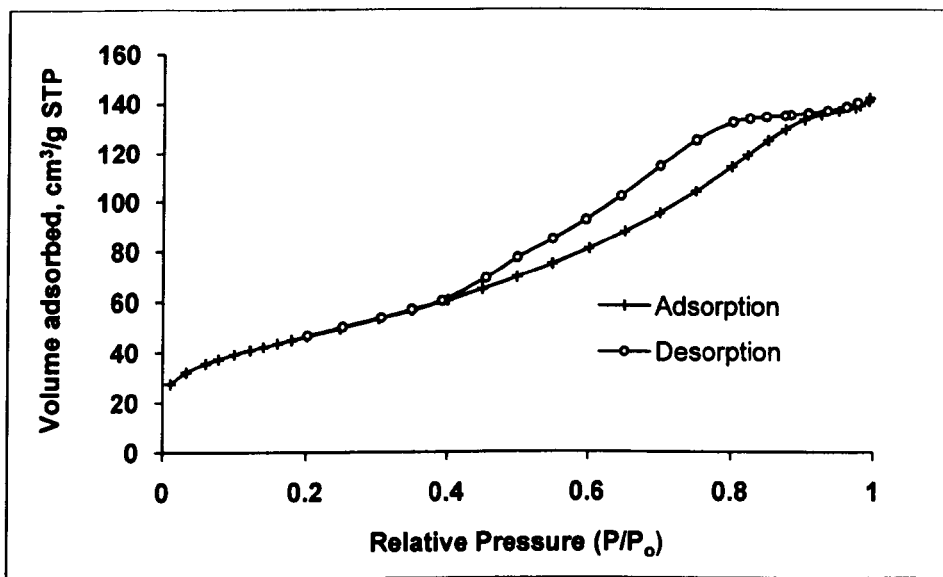


Figure 3.18 N_2 adsorption isotherm for 15%HPW/ Nb_2O_5 -300 (Table 3.2b, entry 5).

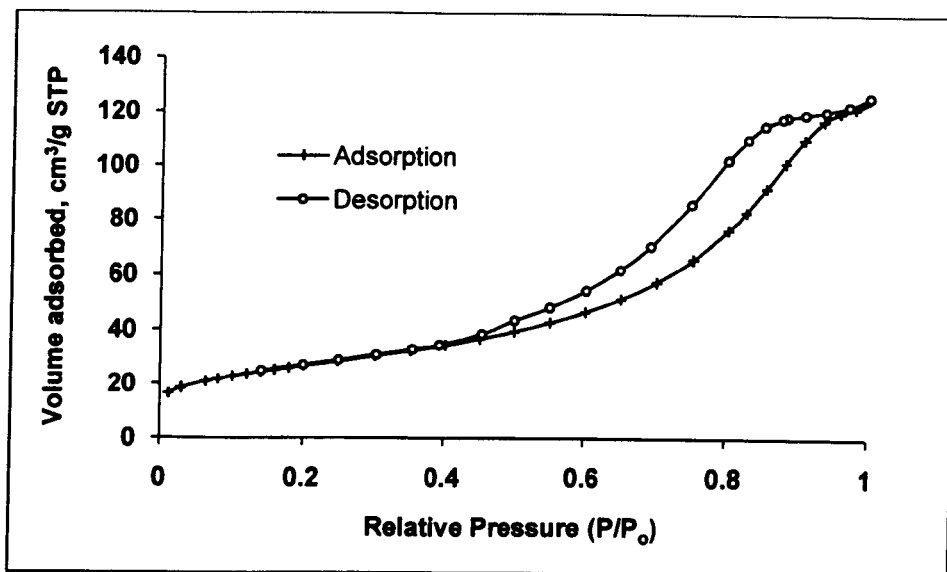


Figure 3.19 N₂ adsorption isotherm for 15%HPW/Nb₂O₅-500 (Table 3.2b, entry 6).

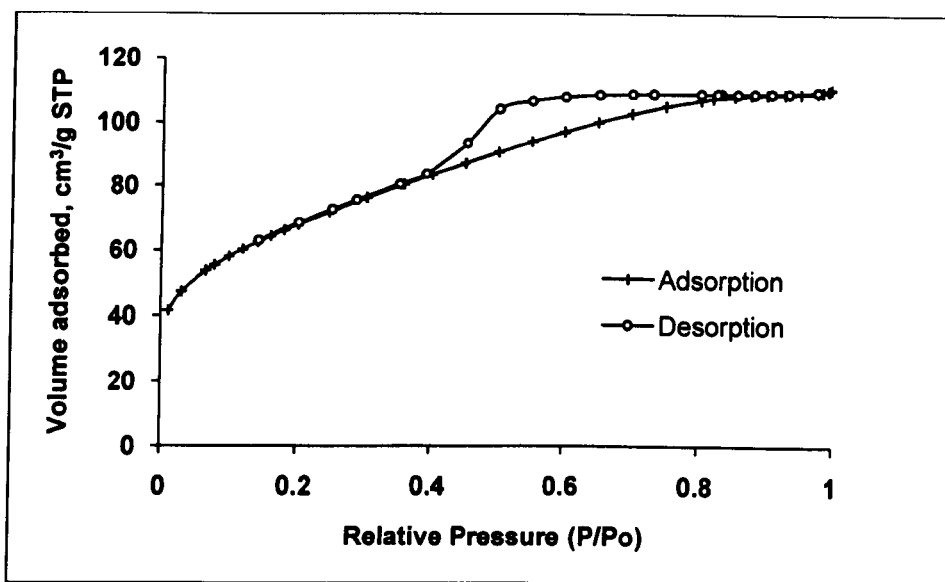


Figure 3.20 N₂ adsorption isotherm for Nb₂O₅ (Table 3.2b, entry 1).

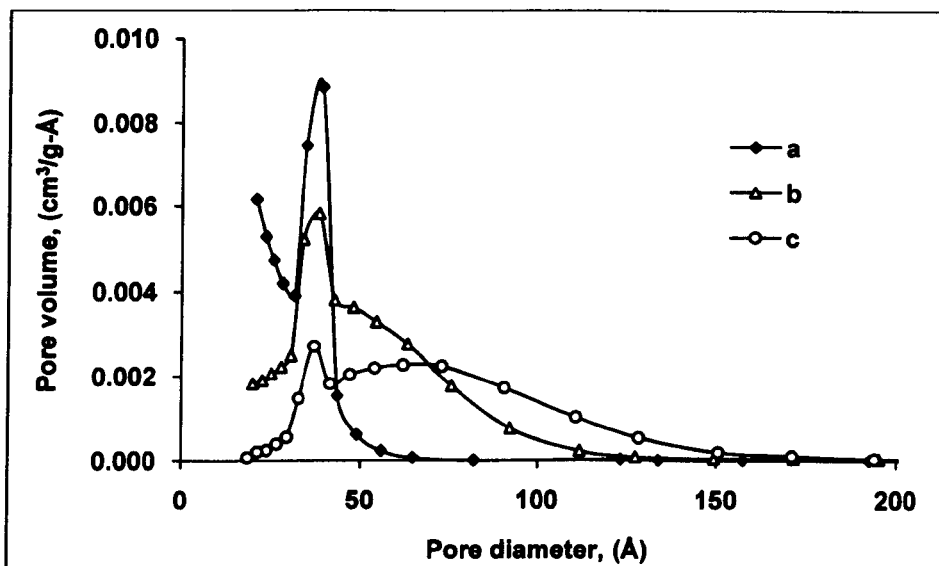


Figure 3.21 Distribution of pore volume as a function of pore diameter for (a) Nb_2O_5 , (b) 15%HPW/ Nb_2O_5 -300 and (c) 15%HPW/ Nb_2O_5 -500.

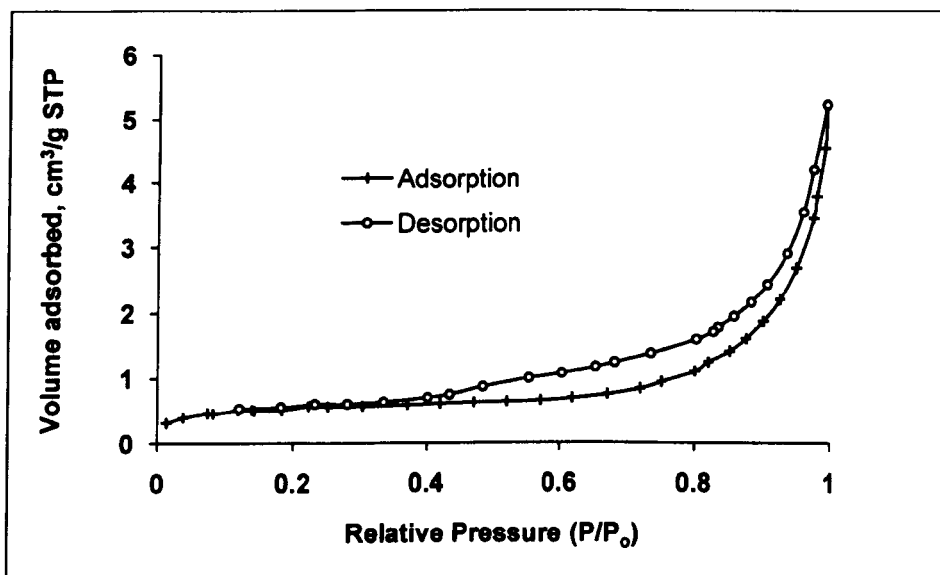


Figure 3.22 N_2 adsorption isotherm for 15%HPW/ Nb_2O_5 -500 (Table 3.2a, entry 9).

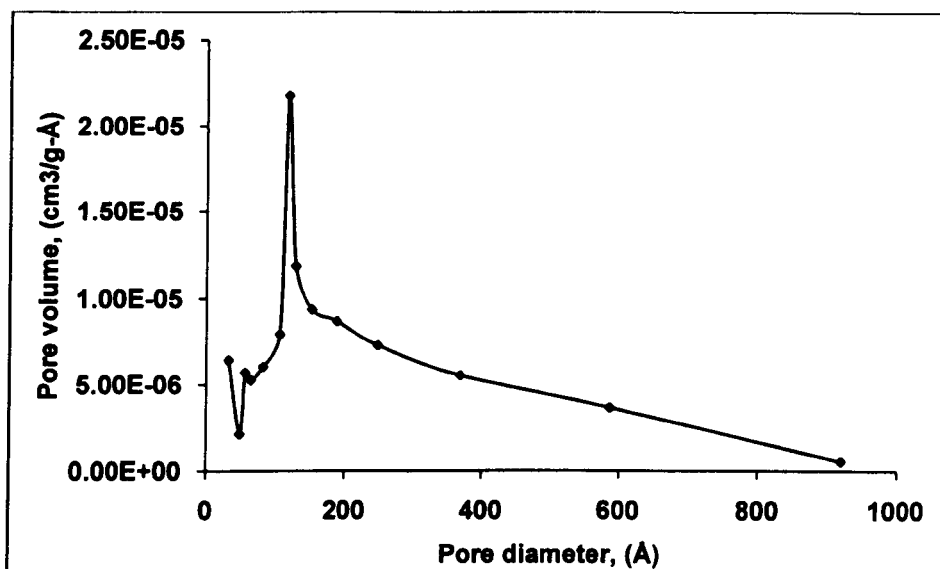


Figure 3.23 Distribution of pore volume as a function of pore diameter for 15%HPW/Nb₂O₅-500 (Table 3.2a, entry 9).

The adsorption isotherm for 15%HPW/ZrO₂-300 possessing large surface area is shown in Figure 3.24. It is similar to that of ZrO₂ (Figure 3.25) and both are type I with H3 hysteresis loop indicating the presence of nonuniform micro/mesoporous structures. The BJH pore size distribution (Figure 3.27) for pores >19 Å also refer to a microporous distribution because the highest volume of adsorbate is physisorbed into micropores close to the lowest detectable range (~20 Å). There is also a significant but smaller distribution of mesopores, close to 34 Å in diameter. The average pore diameter was calculated at 23-24 Å. Increasing calcination temperature to 500 °C leading pores to be wider (Figure 3.27) and hence a type IV isotherm with a hysteresis loop type H2 was observed as shown in Figure 3.26. A peak relating to pores approximately 40 Å in diameter is clearly shown in the pore size distribution shown in Figure 3.27. There is a broad distribution of pore sizes,

ranging from 43 Å to 115 Å in size in the mid mesopore range. The average pore diameter was calculated to be 56 Å.

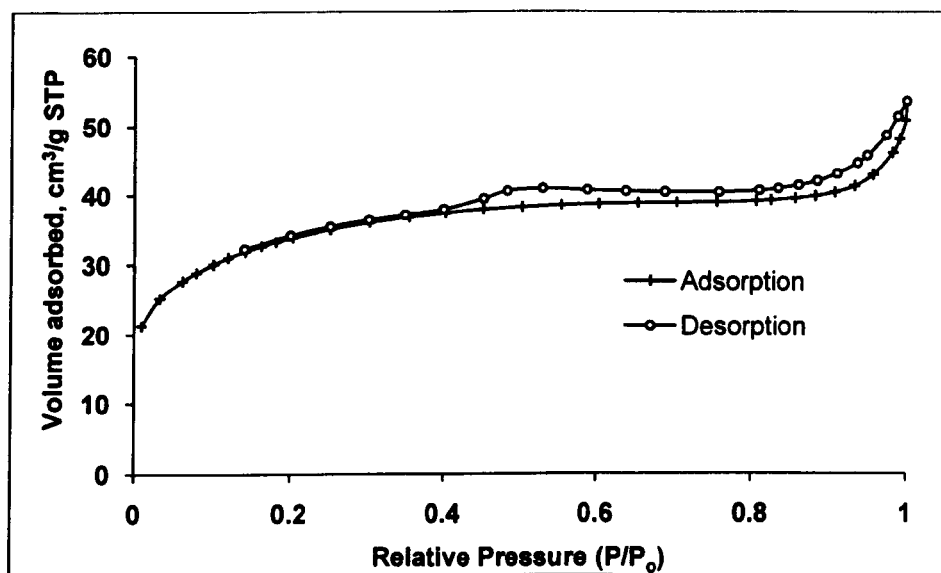


Figure 3.24 N₂ adsorption isotherm for 15%HPW/ZrO₂-300 (Table 3.2b, entry 9).

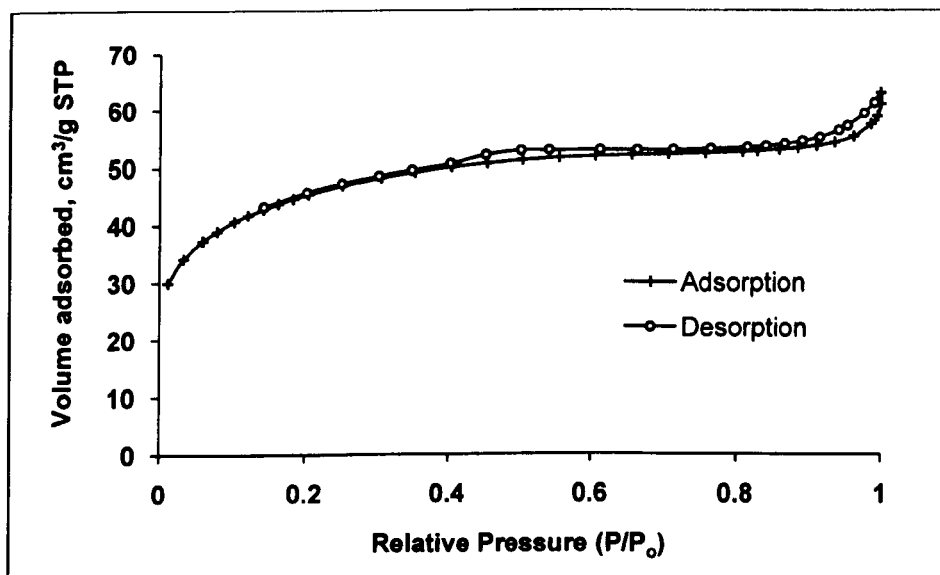


Figure 3.25 N₂ adsorption isotherm for ZrO₂ (Table 3.2b, entry 2).

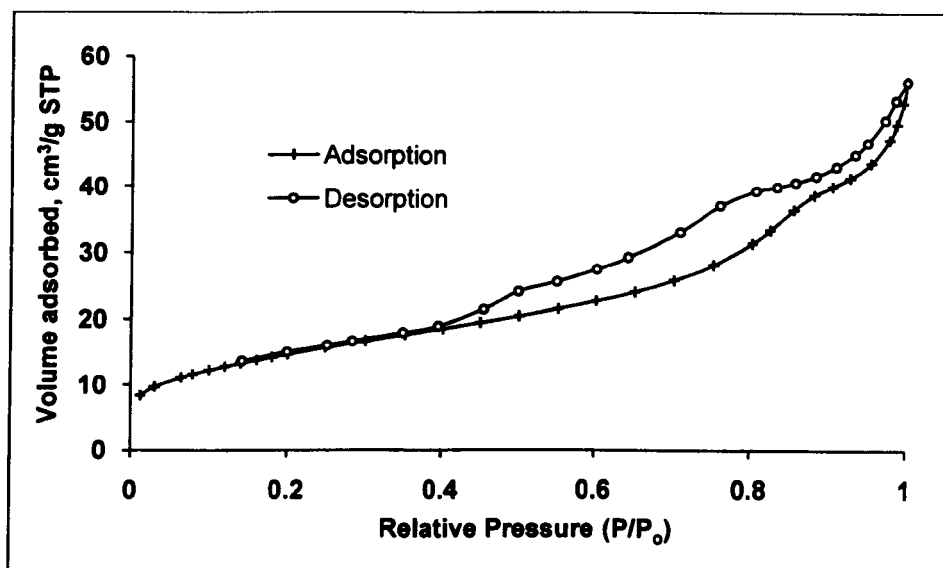


Figure 3.26 N₂ adsorption isotherm for 15%HPW/ZrO₂-500 (Table 3.2b, entry 10).

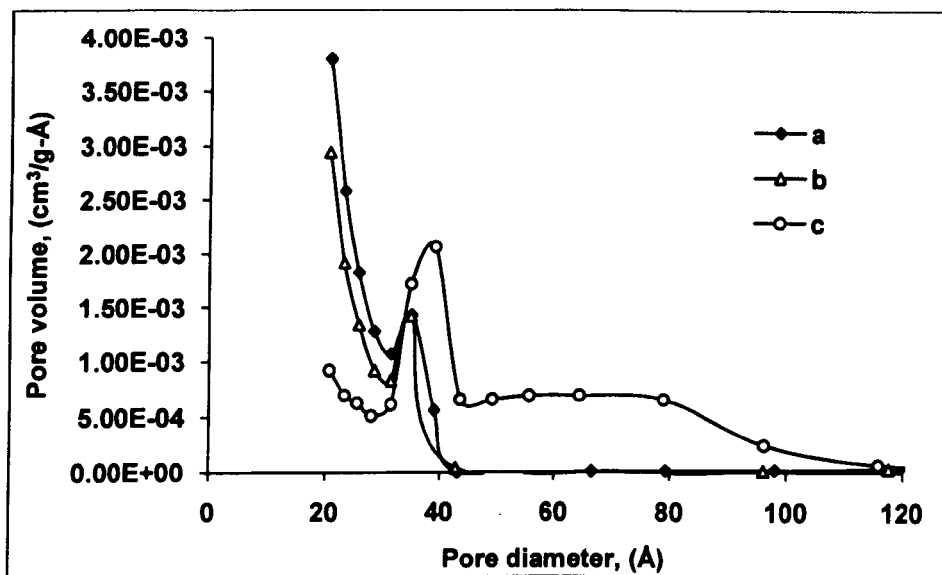


Figure 3.27 Distribution of pore volume as a function of pore diameter for (a) ZrO₂, (b) 15%HPW/ZrO₂-300 and (c) 15%HPW/ZrO₂-500 (Table 3.2b, entries 2, 9, 10).

Analysis of HPW supported on TiO_2 resulted in type II isotherms, regardless of oxide type or calcination temperatures. The isotherm for 15%HPW/ TiO_2 -500 is shown in Figure 3.28 as an example. Although this type of isotherm is characteristic of nonporous or macroporous materials, a small hysteresis loop (type H3) was observed. This indicates the presence of mesopores. The BJH pore size distribution for HPW supported on TiO_2 was extremely broad in the large mesopore range of 50-1300 Å (Figures 3.29 and 3.30). The BJH average pore diameter was calculated between 75 and 230 Å.

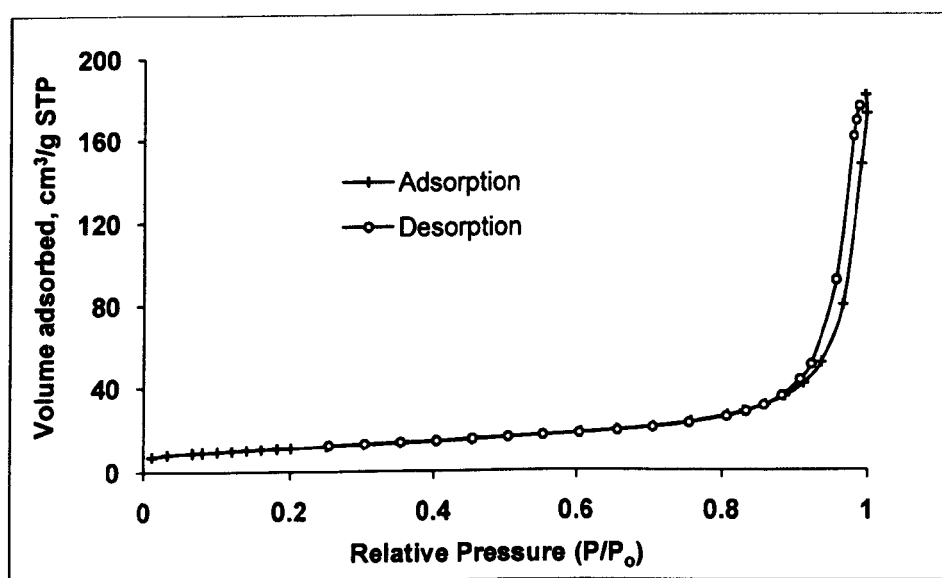


Figure 3.28 N_2 adsorption isotherm for 15%HPW/ TiO_2 -500 (Table 3.2b, entry 15).

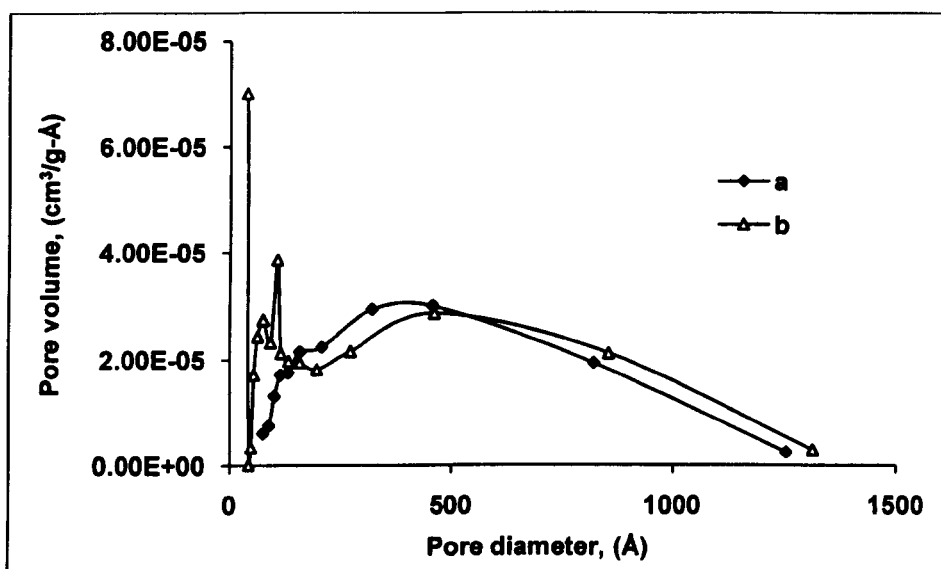


Figure 3.29 Distribution of pore volume as a function of pore diameter for (a) TiO₂ and (b) 15%HPW/TiO₂-500 (Table 3.2a, entries 7, 12).

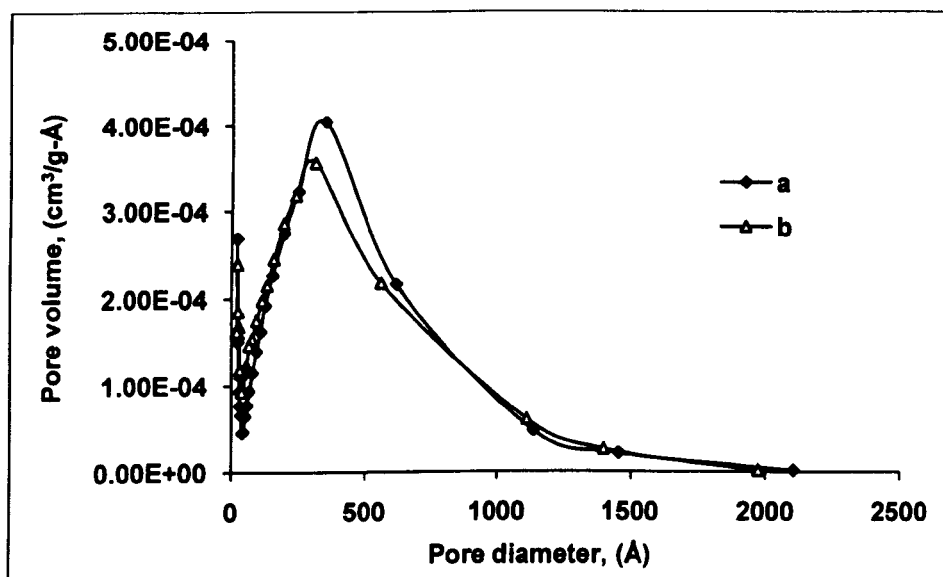


Figure 3.30 Distribution of pore volume as a function of pore diameter for (a) 15%HPW/TiO₂-300 and (b) 15%HPW/TiO₂-500 (Table 3.2b, entries 13, 15).

3.4 Infrared spectroscopy

The state of $\text{H}_3\text{PW}_{12}\text{O}_{40}$ on the surface of Nb_2O_5 , ZrO_2 and TiO_2 has been studied by various techniques such as XRD, FTIR, ^{31}P MAS NMR and others [3, 11, 25-30]. Okumura *et al.* reported that $\text{H}_3\text{PW}_{12}\text{O}_{40}$, that forms in the $\text{H}_3\text{PO}_4 - \text{WO}_3 - \text{Nb}_2\text{O}_5$ system, partially decomposes upon calcination at 500°C [11, 25]. Recently, Srilatha *et al.* [29] found decomposition of HPA in 25%HPW/ Nb_2O_5 catalyst between $400 - 500^\circ\text{C}$, with profound loss of catalyst activity in esterification of fatty acids. In 20%HPW/ TiO_2 calcined at 700°C , both fragmented and intact HPA have been found [28]. In HPW/ ZrO_2 calcined at 750°C , the HPA has been claimed to be stabilised by ZrO_2 , if its loading does not exceed a monolayer (15 wt%) [26]. However, in earlier study, $\text{H}_3\text{PW}_{12}\text{O}_{40}$ on ZrO_2 had been found to decompose above 500°C [30]. Sawant *et al.* [27] found that $\text{H}_3\text{PW}_{12}\text{O}_{40}$ is present on the mixed support $\text{ZrO}_2 - \text{MCM-41}$ even after calcination at 850°C . This should be treated with caution, however, since these calcination temperatures are higher than the temperature of decomposition of bulk $\text{H}_3\text{PW}_{12}\text{O}_{40}$.

Infrared spectroscopy has been used to characterise heteropoly acids [2, 3]. The majority of the characteristic infrared active bands of the Keggin anion are found in the fingerprint region between 1200 and 500 cm^{-1} [2, 3]. Choi *et al.* [8] reported characteristic IR bands of bulk HPW calcined at 300°C at 1080 cm^{-1} (P-O in the central tetrahedron), 984 cm^{-1} (terminal W=O), 897 and 812 cm^{-1} (W-O-W) associated with the asymmetric vibrations in the Keggin polyanion.

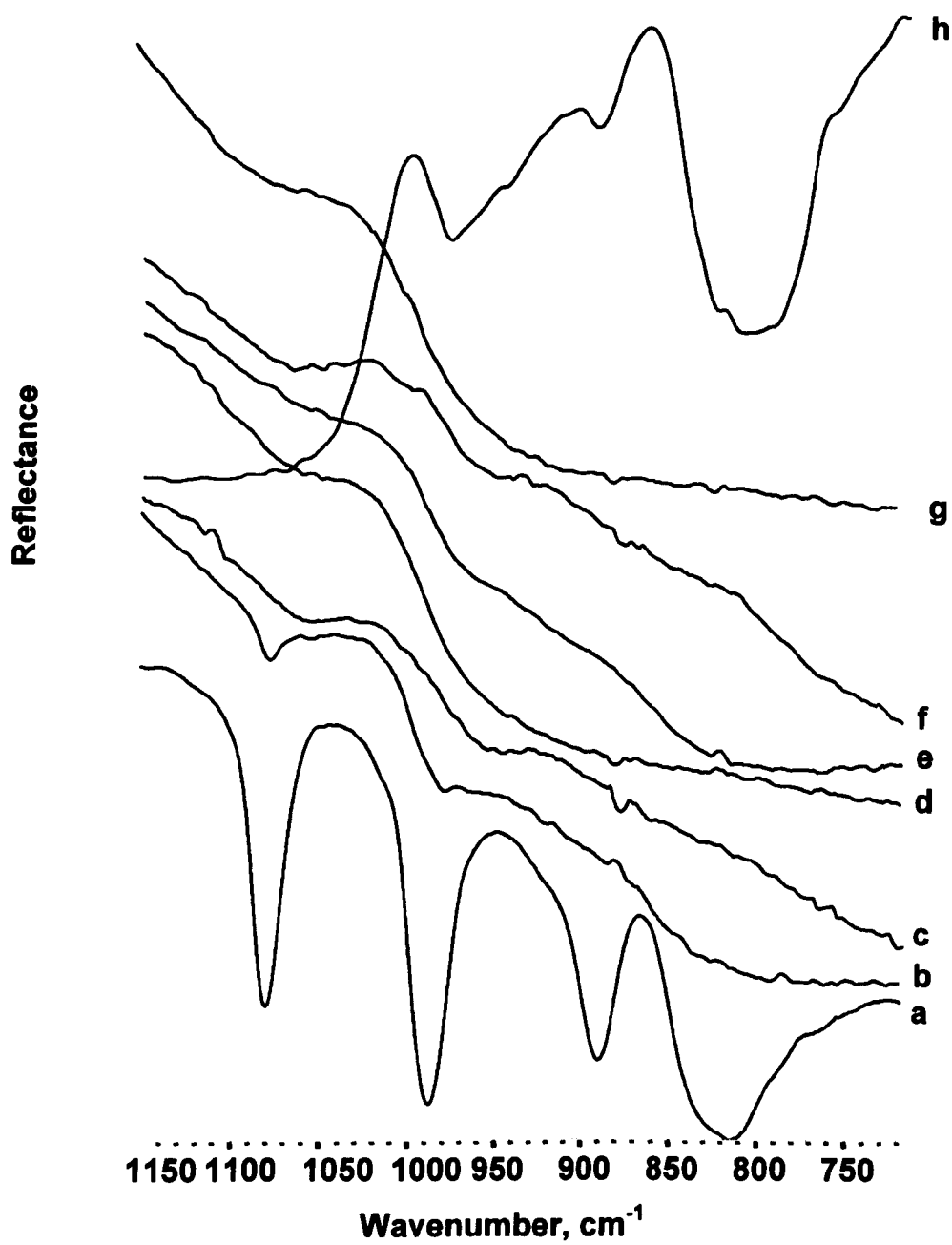


Figure 3.31 DRIFT spectra of (a) Bulk HPW, (b) 15%HPW/TiO₂-300, (c) 15%HPW/ZrO₂-300, (d) 15%HPW/Nb₂O₅-300, (e) 15%HPW/TiO₂-500, (f) 15%HPW/ZrO₂-500, (g) 15%HPW/Nb₂O₅-500 and (h) 15%HPW/SiO₂-300.

The experimental procedure for our infrared measurements is described in Section 2.4.3. We examined the state of HPA on Nb₂O₅, ZrO₂ and TiO₂ in comparison with SiO₂. The spectra were measured using 10% catalyst mixtures with KBr. All samples contained the same amount of HPA and support.

Figure 3.31 displays the IR spectra of the catalysts in the range of 750 – 1150 cm⁻¹. A 15:85 w/w mechanical mixture of bulk HPA and ZrO₂ (both calcined separately at 300°C in air prior to mixing) exhibited four infrared bands characteristic of the Keggin structure (a): 1080, 983, 890 and 812 cm⁻¹ [2, 3, 8]. This spectrum shows that the HPA was not affected by ZrO₂ in this sample.

Spectra (b) – (d), (h) represent supported HPA catalysts calcined at 300°C. At this temperature, HPA should remain intact [1, 2]. In fact, the 15%HPA/TiO₂-300 catalyst clearly exhibited the Keggin unit vibrations at 1080 (P-O) and 983 cm⁻¹ (W=O) (spectrum (b)) but their intensity was much weaker compared to those in spectrum (a). However, no vibrations of the bridging W-O-W groups appeared in this spectrum. This is probably because the bridging O atoms in HPA, having a higher negative charge than the terminal ones, interact stronger with support causing restriction of W-O-W vibrations. On the contrary, HPA/ZrO₂-300 and HPA/Nb₂O₅-300 did not show any Keggin unit bands (spectra (c), (d)). This may be explained by strong HPA/support interaction. The HPW/SiO₂ catalyst is known to be stable at 300°C and beyond, with weak HPA/support interaction [1-3]. In spectrum (h) for 15%HPA/SiO₂-300, silica exhibited strong infrared bands at 1100 and 806 cm⁻¹ and a weak shoulder band at 984 cm⁻¹. The strong bands from silica masked the HPA vibrations at 1080 and 812 cm⁻¹, but the vibrations at 983 (W=O) and 890 (W-O-W) appeared at their normal positions.

IR spectra (e) – (g) for HPA supported on Nb₂O₅, ZrO₂ and TiO₂ after calcination at 500°C show no Keggin unit bands, the spectra being similar to those for the pure oxide supports. This could be the result of HPA decomposition and/or strong HPA/support interaction.

From these results, it can be inferred that the HPA/support interaction increases in the series: SiO₂ < TiO₂ < Nb₂O₅, ZrO₂, in which the acid strength of the corresponding supported HPA catalysts decreases (see Section 3.7.1 and Chapter 5).

3.5 Powder X-ray diffraction

Figure 3.32 shows XRD patterns for bulk and supported H₃PW₁₂O₄₀ catalysts as well as for catalyst supports. The XRD diffraction patterns are obtained using the experimental procedure described in Section 2.4.6.

The supports used for catalyst preparation were in-house made amorphous Nb₂O₅ and ZrO₂ hydrous oxides and commercial anatase TiO₂. The supported HPA catalysts on Nb₂O₅ and ZrO₂ calcined at 300°C were amorphous. After calcination at 500°C, they became crystalline, exhibiting the patterns of the corresponding oxide supports: hexagonal Nb₂O₅ and a mixture of tetragonal and monoclinic ZrO₂ for 15%HPW/Nb₂O₅ and 15%HPW/ZrO₂, respectively. 15%HPW/TiO₂ after calcination at 300 and 500 °C exhibited the pattern of anatase TiO₂. No crystalline phase of H₃PW₁₂O₄₀ was observed in these catalysts, which indicates a high dispersion of HPA on the catalyst surface. Whenever comparison is possible, our XRD data are close to those obtained by other researchers [26, 29, 31-33].

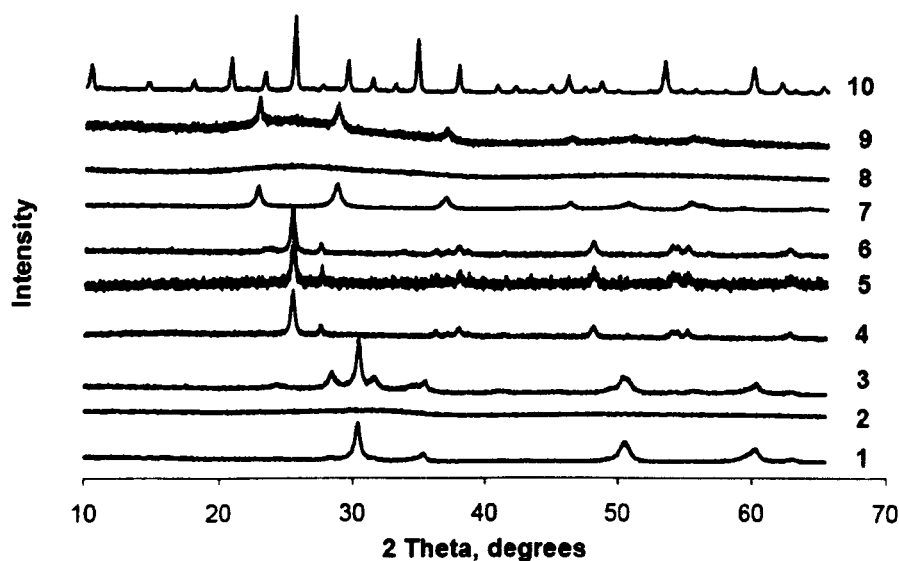


Figure 3.32 XRD patterns (Cu K α radiation) for: (1) ZrO₂-500, (2) 15%HPW/ZrO₂-300, (3) 15% HPW/ZrO₂-500, (4) TiO₂-500, (5) 15% HPW/TiO₂-300, (6) 15% HPW/TiO₂-500, (7) Nb₂O₅-500, (8) 15% HPW/Nb₂O₅-300, (9) 15% HPW/Nb₂O₅-500, (10) Bulk HPW.

3.6 ³¹P MAS NMR

This is one of the most useful characterisation techniques to investigate phosphorus environment in heteropoly acids [4, 26, 34-39]. The chemical shift of nuclei provides important information concerning the structure, composition, and electronic states of heteropoly compounds. Several factors determine the chemical shift of nuclei. These include hydration number, addenda metal ion, support, etc. Misono *et al.* [4, 38] studied the ³¹P chemical shifts of HPW with a variety of hydration states. As can be seen in Figure 3.33, the chemical shift is greatly dependent on water content in HPW.

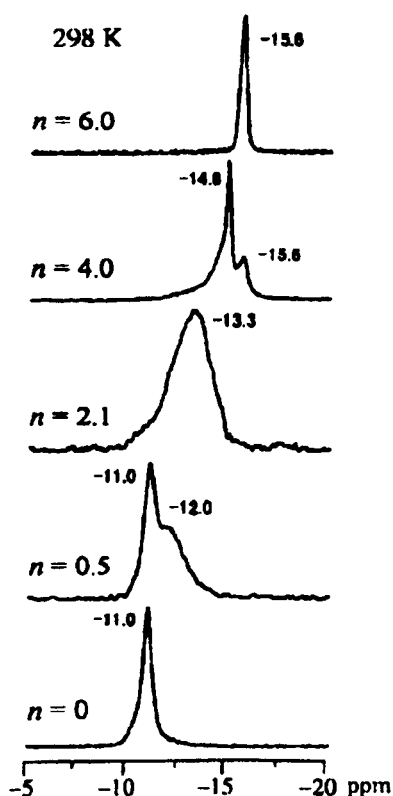


Figure 3.33 ^{31}P NMR spectra of $\text{H}_3\text{PW}_{12}\text{O}_{40} \cdot n\text{H}_2\text{O}$ with a variety of hydration states ($0 \leq n \leq 6$) measured at 25°C [4].

For supported HPW, solid-state ^{31}P MAS NMR has shown a single peak at ca. -15 ppm which corresponds to the Keggin HPW. In some cases, additional peaks are observed which were ascribed to the strong interactions between heteropoly acid and support and/or decomposition of HPW, depending on nature of the support, loading percentage and calcination temperature [39-42].

Figures 3.34-3.37 show the ^{31}P MAS NMR spectra for bulk and supported HPW catalysts pre-treated at 300°C and 500°C for 3 h in air. The well-documented bulk and SiO_2 -supported HPW can be considered as reference systems for the assessment of the state of HPW in supported catalysts.

Bulk HPW calcined at 300°C (Figure 3.34), which should retain the Keggin structure, exhibits a sharp resonance at -15.3 ppm characteristic of the HPW Keggin unit [1, 2, 4]. However, two extra peaks are observed at -3.7 and -11.6 ppm indicating some decomposition of the HPW. This was probably due to a relatively long pre-treatment time (3 h). In contrast, the bulk HPW calcined at 500°C shows no signal at ~ -15 ppm, which points to decomposition of the Keggin structure, as expected.

The silica-supported HPA calcined at 300°C, like the corresponding bulk HPA, is expected to be stable. This is confirmed by the strong peak of the Keggin unit at -15.7 ppm, with some decomposition fragments also present like in the bulk HPA (peaks at -11.7 and 3.1 ppm).

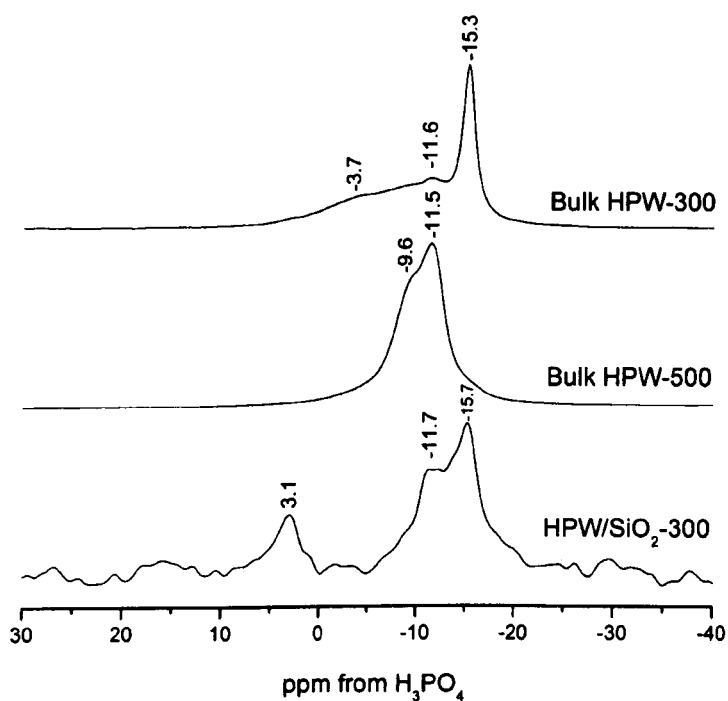


Figure 3.34 ³¹P MAS NMR of bulk and silica supported HPW catalysts calcined at 300 °C or 500 °C for 3 h in air.

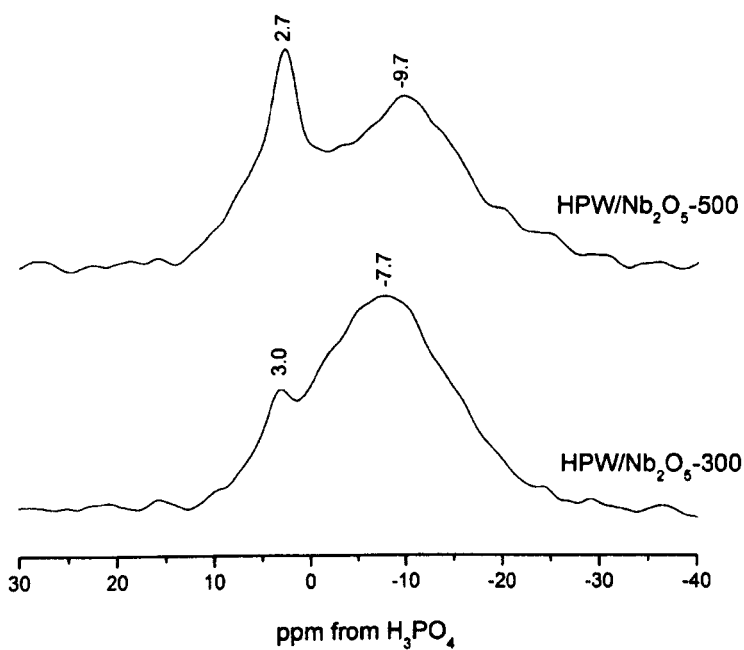


Figure 3.35 ^{31}P MAS NMR of 15% HPW/ Nb_2O_5 catalysts calcined at 300 °C or 500 °C for 3 h in air.

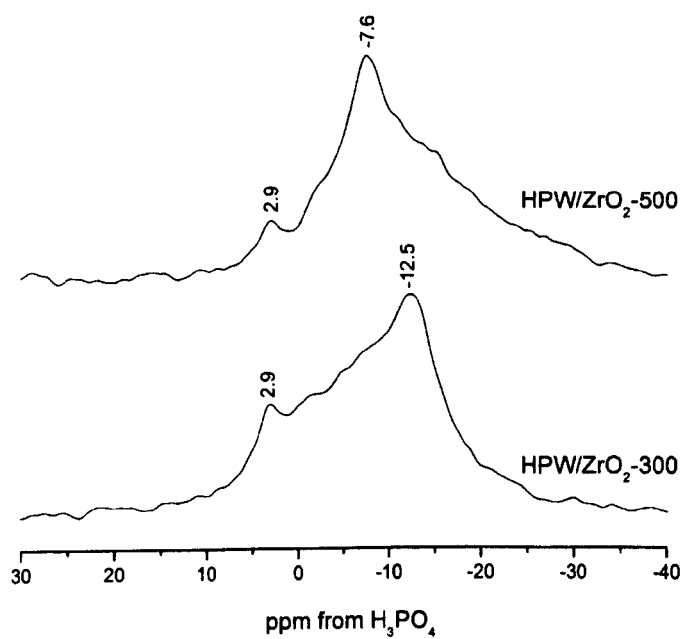


Figure 3.36 ^{31}P MAS NMR of 15% HPW/ ZrO_2 catalysts calcined at 300 °C or 500 °C for 3 h in air.

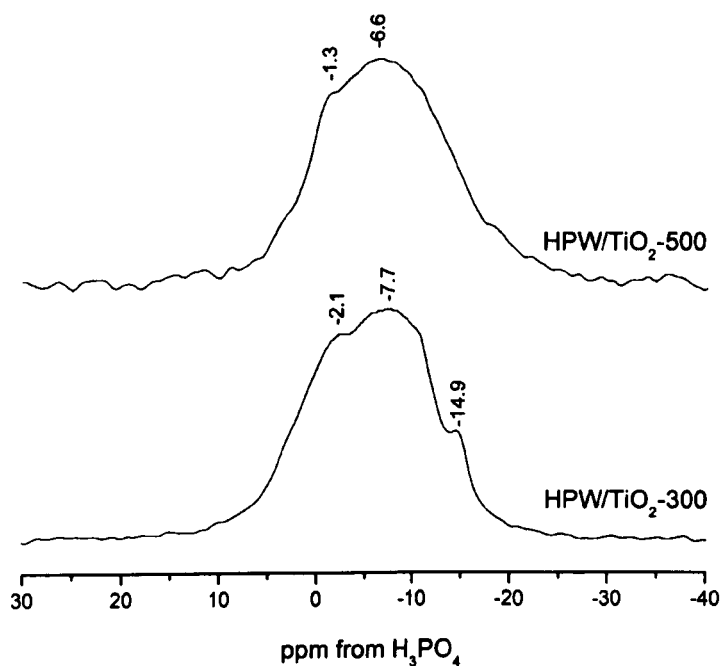


Figure 3.37 ^{31}P MAS NMR of 15% HPW/TiO₂ catalysts calcined at 300 °C or 500 °C for 3 h in air.

The HPA catalysts supported on TiO₂, ZrO₂ and Nb₂O₅ showed different ^{31}P environments (Figures 3.35-3.37). Only the HPA/TiO₂-300 catalyst, calcined at 300°C, exhibited the presence of a small number of Keggin species (peak at -14.9 ppm). This is in agreement with the DRIFT spectrum (Figure 3.31), which also showed the presence of Keggin species in this catalyst. HPA/TiO₂-300 and HPA/TiO₂-500 display a very broad signal centred at about -7.7 ppm, except no Keggin species could be seen in for the latter material. Neither HPA/ZrO₂ nor HPA/Nb₂O₅ exhibited any Keggin species in their ^{31}P MAS NMR spectra, also very broad and quite featureless ones.

Although it is difficult to attribute these ^{31}P NMR spectra to any particular species, some suggestions regarding the state of HPW on the surface of TiO_2 , ZrO_2 and Nb_2O_5 could be made. The broad signals observed indicate strong interaction between finely dispersed HPW and support. It is conceivable that the catalysts calcined at 300°C mainly contain various distorted Keggin species that are different (regarding ^{31}P NMR) from those in bulk and SiO_2 -supported HPW. The catalysts calcined at 500°C , besides the distorted Keggin species, appear to contain a number of decomposition fragments represented by the ^{31}P NMR peaks at 2.7 – 3.1 ppm and (-7.6) – (-12.5) ppm. In summary, both ^{31}P NMR and DRIFT spectroscopy (Section 3.4) indicate that HPA/support interaction increases in the order of supports: $\text{SiO}_2 < \text{TiO}_2 < \text{Nb}_2\text{O}_5, \text{ZrO}_2$. This can be thought to cause the decrease in acid strength of supported HPA catalysts, as found by NH_3 adsorption calorimetry (Section 3.7.1).

3.7 Acidity of HPA catalysts

In this section, we aim to characterise the acidity of bulk and supported HPA using various techniques: differential scanning calorimetry (DSC) of NH_3 adsorption in a gas-solid system to determine the strength of acid sites and Fourier transform infrared spectroscopy (FTIR) to determine the nature of acid sites (Brønsted and Lewis) by adsorption of pyridine. The experimental procedures for these measurements are described in Section 2.4.7 and 2.4.3 respectively.

3.7.1 Pulse ammonia adsorption analysis

The strength of acid sites in the catalysts was characterised by measuring the enthalpy of ammonia adsorption at the gas-solid system. This technique does not discriminate between Brønsted and Lewis acid sites. The values of ΔH for the catalysts are given in Table 3.3. Figure 3.38 shows the determination of the initial enthalpy of NH_3 adsorption, ΔH , for $\text{H}_3\text{PW}_{12}\text{O}_{40}$, $\text{Cs}_{2.5}\text{H}_{0.5}\text{PW}_{12}\text{O}_{40}$ and 15%HPW/ ZrO_2 -500. Our ΔH values for the well-documented bulk $\text{H}_3\text{PW}_{12}\text{O}_{40}$ and $\text{Cs}_{2.5}\text{H}_{0.5}\text{PW}_{12}\text{O}_{40}$ are in excellent agreement with those reported previously by Okuhara [20]. For the catalysts pre-treated at 300°C , the acid strength decreases in the order: $\text{H}_3\text{PW}_{12}\text{O}_{40} > \text{Cs}_{2.5}\text{H}_{0.5}\text{PW}_{12}\text{O}_{40} > 20\%\text{Cs}_2\text{HPW}_{12}\text{O}_{40}/\text{SiO}_2 > 15\%\text{HPW}/\text{SiO}_2 > 15\%\text{HPW}/\text{TiO}_2 \gg 15\%\text{HPW}/\text{Nb}_2\text{O}_5 > 15\%\text{HPW}/\text{ZrO}_2$. This shows that the catalysts comprising HPA supported on Nb_2O_5 , ZrO_2 and TiO_2 possess weaker acid sites than the “standard” HPA catalysts (i.e. $\text{H}_3\text{PW}_{12}\text{O}_{40}$, $\text{Cs}_{2.5}\text{H}_{0.5}\text{PW}_{12}\text{O}_{40}$ and 15%HPW/ SiO_2). Their ΔH values are in the range from -121 to -143 kJ/mol, which is similar to that for acidic zeolites [43].

The catalyst acid strength decreases in the order of supports: $\text{SiO}_2 > \text{TiO}_2 \gg \text{Nb}_2\text{O}_5 > \text{ZrO}_2$, which indicates increasing interaction between the HPA and oxide support in that order. The latter is also supported by infrared spectroscopy (Section 3.4) and ^{31}P NMR (Section 3.6).

Table 3.3 Initial enthalpies of ammonia adsorption at 100 °C.

	Catalyst	Calcination temperature (°C)	-ΔH (kJ/mol)
1	H ₃ PW ₁₂ O ₄₀	300	195
2	Cs _{2.5} H _{0.5} PW ₁₂ O ₄₀	300	164
3	20%Cs ₂ H ₁ PW ₁₂ O ₄₀ /SiO ₂	300	160
4	15% H ₃ PW ₁₂ O ₄₀ /SiO ₂	300	154
5	15% H ₃ PW ₁₂ O ₄₀ /Nb ₂ O ₅	500	121
6	15% H ₃ PW ₁₂ O ₄₀ /Nb ₂ O ₅	300	132
7	15% H ₃ PW ₁₂ O ₄₀ /ZrO ₂	500	129
8	15% H ₃ PW ₁₂ O ₄₀ /ZrO ₂	300	121
9	15% H ₃ PW ₁₂ O ₄₀ /TiO ₂	500	130
10	15% H ₃ PW ₁₂ O ₄₀ /TiO ₂	300	143

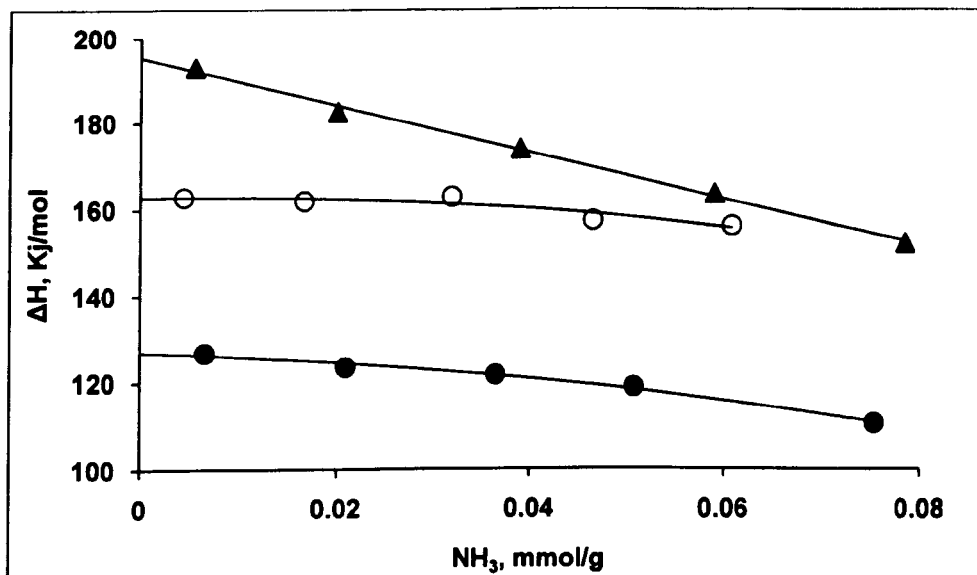


Figure 3.38 The plot of enthalpy of NH₃ adsorption versus NH₃ uptake for (●) 15%HPW/ZrO₂-500, (○) C_{2.5}H_{0.5}PW₁₂O₄₀ and (▲) H₃PW₁₂O₄₀.

3.7.2 FTIR study of pyridine adsorption

Adsorption of pyridine on the surface of solid acids is one of the most commonly used methods for the characterisation of surface acidity [26, 44]. The use of IR spectroscopy to detect adsorbed pyridine allows us to discriminate between different acid sites. The pyridinium ion displays a vibration at 1540 cm^{-1} indicating the presence of Brønsted acid sites. On the other hand, coordinately bonded pyridine shows a band at 1450 cm^{-1} which is characteristic of Lewis acid sites.

Bulk $\text{H}_3\text{PW}_{12}\text{O}_{40}$ and $\text{Cs}_{2.5}\text{H}_{0.5}\text{PW}_{12}\text{O}_{40}$ pre-treated at temperatures below 300°C are known to possess strong Brønsted acid sites [1, 2]. From the DRIFT spectra of adsorbed pyridine (Figures 3.39 – 3.41), all HPA catalysts supported on Nb_2O_5 , ZrO_2 and TiO_2 possessed both Brønsted and Lewis acid sites, as confirmed by strong IR bands at 1540 and 1450 cm^{-1} , respectively. This is consistent with the previous studies [25-28]. In agreement with the literature [45], all pure oxides Nb_2O_5 , ZrO_2 and TiO_2 were found to exhibit Lewis acid sites. Nb_2O_5 and ZrO_2 also displayed Brønsted acid sites capable of protonating pyridine (Figure 3.39 – 3.41). Table 3.4 shows the relative number of Brønsted and Lewis acid sites, B/L, in the catalysts and supports. As expected, the B/L value was higher in supported HPA catalysts than in the corresponding oxide supports. The relative number of Brønsted acid sites decreased with increasing calcination temperature due to catalyst dehydration. In ZrO_2 , however, the number of Brønsted sites capable of protonating pyridine increased with increasing the calcination temperature. From these results, it can be concluded that Lewis acid sites in our HPA/ Nb_2O_5 , HPA/ ZrO_2 and HPA/ TiO_2 catalysts were mainly originated from the oxide supports, and Brønsted acid sites were provided by the HPA and in the case of Nb_2O_5 and ZrO_2 also by support.

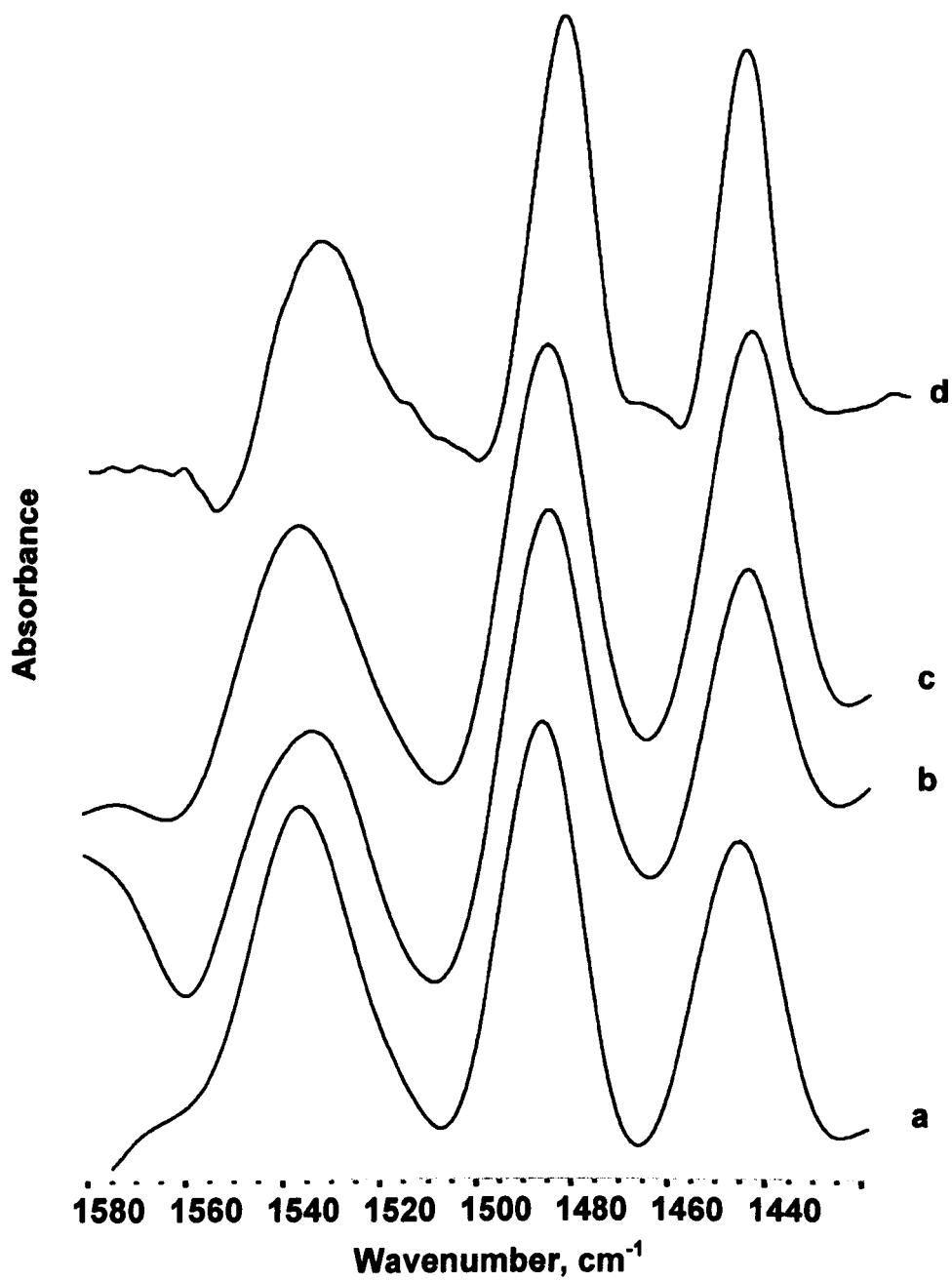


Figure 3.39 DRIFT spectra of pyridine adsorbed on (a) 15% HPW/Nb₂O₅-500, (b) 15% HPW/Nb₂O₅-300, (c) Nb₂O₅-500 and (d) Nb₂O₅-300.

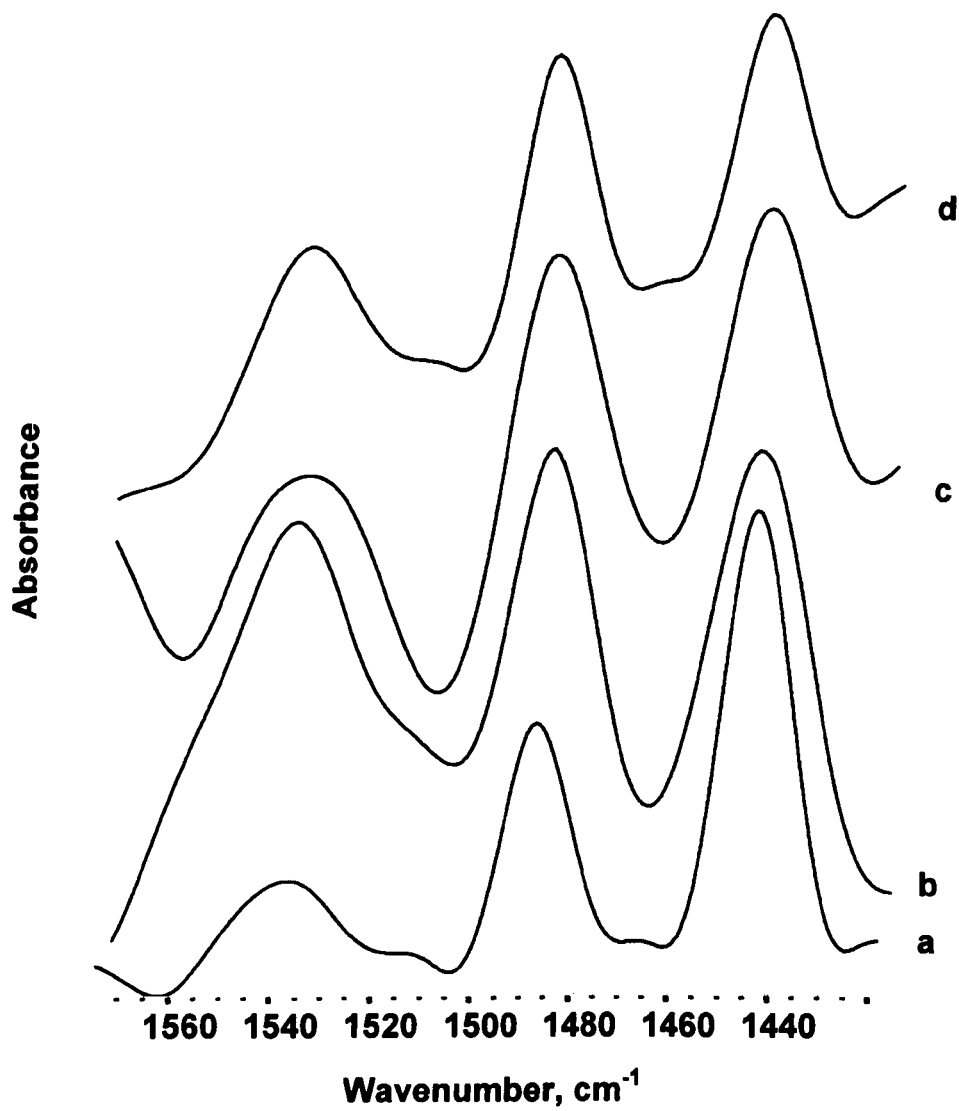


Figure 3.40 DRIFT spectra of pyridine adsorbed on (a) ZrO_2 -300, (b) 15%HPW/ ZrO_2 -300, (c) ZrO_2 -500 and (d) 15%HPW/ ZrO_2 -500.

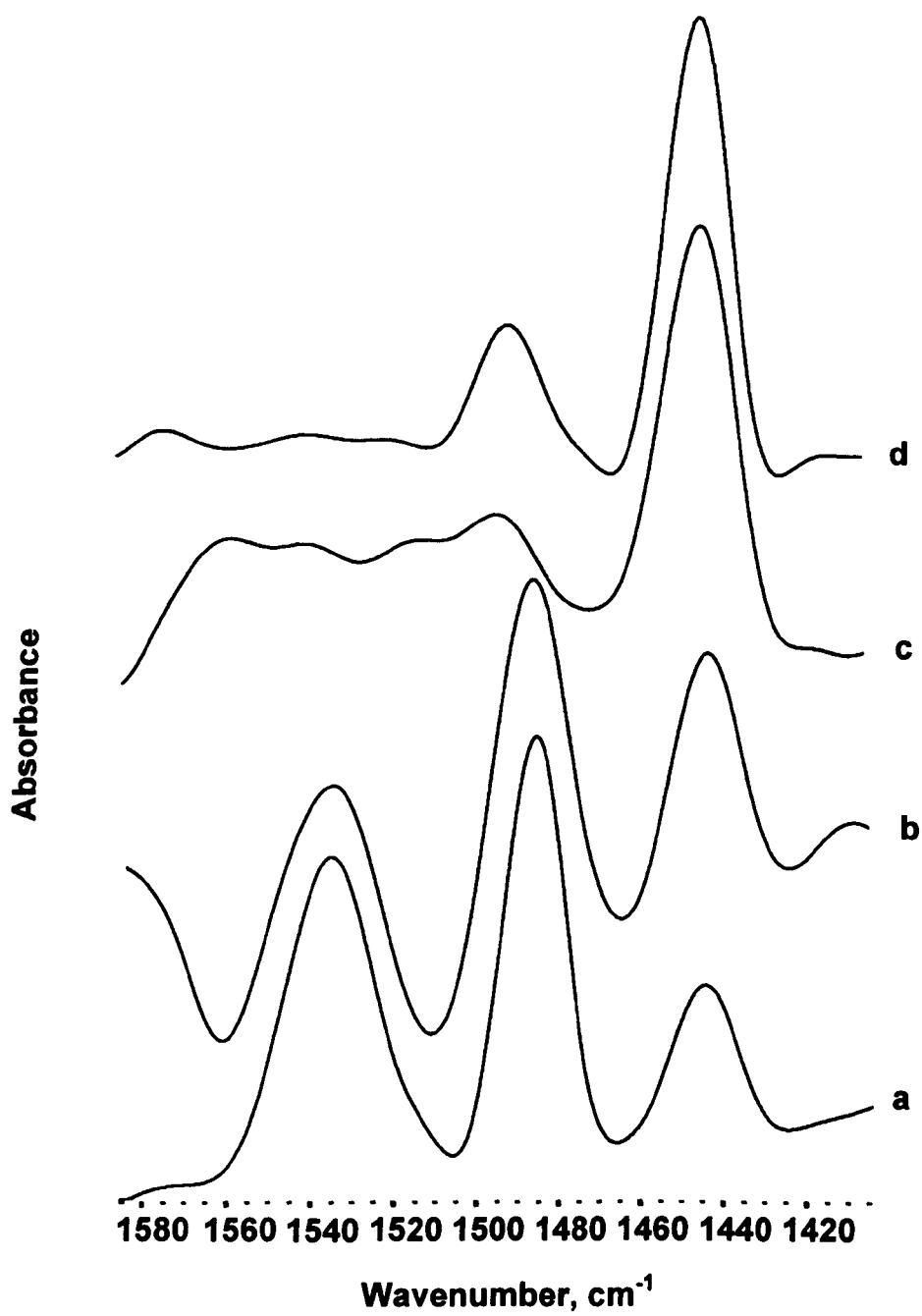


Figure 3.41 DRIFT spectra of pyridine adsorbed on (a) 15%HPW/TiO₂-300, (b) 15%HPW/TiO₂-500, (c) TiO₂-300 and (d) TiO₂-500.

Table 3.4 Brønsted (B) versus Lewis (L) acidity of catalysts from DRIFTS of adsorbed pyridine.

	Catalyst	B/L ^a
1	TiO ₂ -300	0.04
2	TiO ₂ -500	0.04
3	15% HPW/TiO ₂ -300	2.82
4	15% HPW/TiO ₂ -500	1.53
5	Nb ₂ O ₅ -300	1.32
6	Nb ₂ O ₅ -500	0.99
7	15% H ₃ PW/Nb ₂ O ₅ -300	1.42
8	15% H ₃ PW/Nb ₂ O ₅ -500	1.25
9	ZrO ₂ -300	0.32
10	ZrO ₂ -500	0.98
11	15% HPW/ZrO ₂ -300	1.42
12	15% HPW/ZrO ₂ -500	1.07

a) The ratio of intensities of the DRIFTS peaks at 1540 cm⁻¹ and 1450 cm⁻¹.

3.8 Conclusion

The texture of catalysts was characterised by N₂ physisorption. All the catalysts under study were mesoporous materials with average pore diameters of 22 – 230 Å. Changing the aging temperature did not affect the texture of supported HPW catalysts, while the surface area decreased significantly after increasing the calcination temperature. The XRD measurements showed that HPA supported on Nb₂O₅ and ZrO₂ calcined at 300°C were amorphous. After calcination at 500°C, they became crystalline, exhibiting the

patterns of the corresponding oxide supports. HPA supported on TiO₂ calcined at 300 and 500 °C exhibited the pattern of anatase TiO₂. The state of HPA on Nb₂O₅, ZrO₂ and TiO₂ was investigated by FT-IR and ³¹P MAS NMR using well-documented bulk and silica-supported HPA as reference materials. After calcination at 300 °C, only 15%HPA/TiO₂ catalyst exhibited Keggin species (vibrations at 1080 and 983 cm⁻¹, and ³¹P NMR peak at -14.9 ppm). After calcination at 500 °C, none of the catalysts under study showed any Keggin species, which is explained by HPA decomposition and/or strong HPA/support interaction. The catalysts comprising HPW supported on Nb₂O₅, ZrO₂ and TiO₂ were found to possess both Brønsted and Lewis acid sites. The Brønsted/ Lewis site ratio (B/L) was higher in supported HPA catalysts than in the corresponding oxide supports. The relative number of Brønsted acid sites decreased with increasing calcination temperature due to catalyst dehydration. From ammonia adsorption calorimetry, their acid sites were weaker than those in HPW and CsPW.

References

- [1] I.V. Kozhevnikov, *Catalysts for Fine Chemicals. Vol 2. Catalysis by Polyoxometalates*, Wiley, Chichester, 2002.
- [2] T. Okuhara, N. Mizuno, M. Misono, *Adv. Catal.* 41 (1996) 113.
- [3] J.B. Moffat, *Metal-Oxygen Clusters. The Surface and Catalytic Properties of Heteropoly Oxometalates*, Kluwer, New York, 2001.
- [4] M. Misono, *Chem. Comm.* (2001) 1141.
- [5] B.W.L. Southward, J.S. Vaughan, C.T. O'Connor, *J. Catal.* 153 (1995) 293.
- [6] P.A. Jalil, M. Faiz, N. Tabet, N.M. Hamdan, Z. Hussain, *J. Catal.* 217 (2003) 292.
- [7] V.M. Bondareva, T.V. Andrushkevich, R.I. Maksimovskaya, L.M. Plyasova, A.V. Ziborov, G.S. Litvak, L.G. Detusheva, *Kinet. Catal.* 35 (1994) 114.
- [8] S.M. Choi, Y. Wang, Z.M. Nie, J. Liu, C.H.F. Peden, *Catal. Today* 55 (2000) 117.
- [9] N. Essayem, G. Coudurier, M. Fournier, J.C. Vedrine, *Catal. Lett.* 34 (1995) 223.
- [10] N.A. Comelli, L.M. Grzona, O. Masini, E.N. Ponzi, M.I. Ponzi, *J. Chil. Chem. Soc.* 49 (2004) 245.
- [11] K. Okumura, K. Yamashita, K. Yamada, M. Niwa, *J. Catal.* 245 (2007) 75.
- [12] S.J. Gregg, K.S.W. Sing, *Adsorption, Surface Area and Porosity*, Academic Press, London, 1982.
- [13] K.K. Unger, J. Roquerol, K.S.W. Sing, H.K. (Eds.), *Characterization of Porous Solids*, Elsevier, Amsterdam, 1988.
- [14] F. Rodriguez-Reinoso, J. Roquerol, K.S.W. Sing, K.K.U. (Eds.), *Characterization of Porous Solids II*, Elsevier, Amsterdam, 1991.

- [15] J. Roquerol, F. Rodriguez-Reinoso, K.S.W. Sing, K.K.U. (Eds.), *Characterization of Porous Solids III*, Elsevier, Amsterdam, 1994.
- [16] G. Leofanti, M. Padovan, G. Tozzola, B. Venturelli, *Catal. Today* 41 (1998) 207.
- [17] G. Attard, C. Barnes, *Surfaces*, Oxford University Press, 1998.
- [18] S. Brunauer, P.H. Emmet, E. Teller, *J. Am. Chem. Soc.* 60 (1938) 309.
- [19] E.P. Barrett, L.G. Joyner, P.P. Halenda, *J. Am. Chem. Soc.* 73 (1951) 373.
- [20] T. Okuhara, *Chem. Rev.* 102 (2002) 3641.
- [21] Y. Izumi, M. One, M. Kitagawa, M. Yoshida, K. Urabe, *Microporous Mater.* 5 (1995) 255.
- [22] T. Okuhara, H. Watanabe, T. Nishimura, K. Inumaru, M. Misono, *Chem. Mater.* 12 (2000) 2230.
- [23] N. Mizuno, M. Misono, *Chem. Rev.* 98 (1998) 199.
- [24] T. Nakato, Y. Toyoshi, M. Kimura, T. Okuhara, *Catal. Today* 52 (1999) 23.
- [25] K. Okumura, K. Yamashita, M. Hirano, M. Niwa, *J. Catal.* 234 (2005) 300.
- [26] B.M. Devassy, F. Lefebvre, S.B. Halligudi, *J. Catal.* 231 (2005) 1.
- [27] D.P. Sawant, A. Vinu, F. Lefebvre, S.B. Halligudi, *J. Mol. Catal. A* 262 (2007) 98.
- [28] S.M. Kumbar, G.V. Shanbhag, F. Lefebvre, S.B. Halligudi, *J. Mol. Catal. A* 256 (2006) 324.
- [29] K. Srilatha, N. Lingaiah, B.L.A.P. Devi, R.B.N. Prasad, S. Venkateswar, P.S.S. Prasad, *Appl. Catal. A* 365 (2009) 28.
- [30] E. Lopez-Salinas, J.G. Hernandez-Cortez, I. Schifter, E. Torres-Garcia, J. Navarrete, A. Gutierrez-Carrillo, T. Lopez, P.P. Lottici, D. Bersani, *Appl. Catal. A* 193 (2000) 215.

- [31] M.G. Kulkarni, R. Gopinath, L.C. Meher, A.K. Dalai, *Green Chem.* 8 (2006) 1056.
- [32] N. Yamamoto, S. Sato, R. Takahashi, K. Inui, *J. Mol. Catal. A* 243 (2006) 52.
- [33] D.E. Lopez, K. Suwannakarn, D.A. Bruce, J.G. Goodwin, *J. Catal.* 247 (2007) 43.
- [34] C.J. Dillon, J.H. Holles, R.J. Davis, J.A. Labinger, M.E. Davis, *J. Catal.* 218 (2003) 54.
- [35] I.V. Kozhevnikov, A. Sinnema, R.J.J. Jansen, H. Vanbekkum, *Catal. Lett.* 27 (1994) 187.
- [36] I.V. Kozhevnikov, S. Holmes, M.R.H. Siddiqui, *Appl. Catal. A* 214 (2001) 47.
- [37] A. Ghanbari-Siahkali, A. Philippou, J. Dwyer, M.W. Anderson, *Appl. Catal. A* 192 (2000) 57.
- [38] S. Uchida, K. Inumaru, M. Misono, *J. Phys. Chem. B* 104 (2000) 8108.
- [39] I.V. Kozhevnikov, *Catal. Rev. Sci. Eng.* 37 (1995) 311.
- [40] S. Udayakumar, S. Ajaikumar, A. Pandurangan, *Appl. Catal. A* 302 (2006) 86.
- [41] V.M. Mastikhin, *Colloids and Surfaces a-Physicochemical and Engineering Aspects.* 78 (1993) 143.
- [42] E. Caliman, J.A. Dias, S.C.L. Dias, A.G.S. Prado, *Catal. Today* 107-08 (2005) 816.
- [43] M. Brandle, J. Sauer, *J. Am. Chem. Soc.* 120 (1998) 1556.
- [44] B.H. Davis, R.A. Keogh, S. Alerasool, D.J. Zalewski, D.E. Day, P.K. Doolin, *J. Catal.* 183 (1999) 45.
- [45] K. Tanabe, M. Misono, Y. Ono, H. Hattori, *New Solid Acids and Bases: Their Catalytic Properties*, Kodansha, Tokyo, 1989.

4. Liquid phase esterification and transesterification reactions catalysed by heteropoly acids

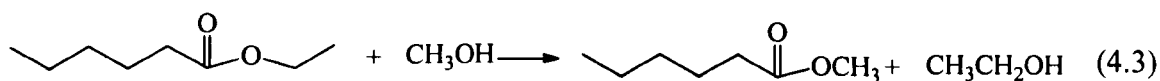
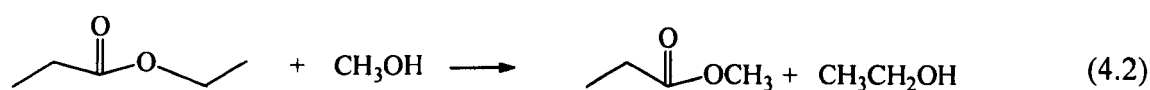
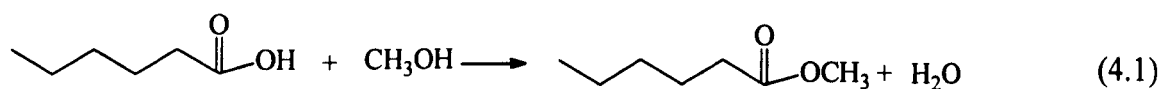
4.1 Introduction

Esterification and transesterification reactions have attracted much interest recently in connection with the development of new synthetic routes to fuels and chemicals based on renewable feedstocks [1, 2]. In particular, the synthesis of biodiesel via transesterification of triglycerides – vegetable oils and fats – with methanol has been investigated in detail [1-5]. Commercial production of biodiesel employs homogeneous alkali catalysts. However, these catalysts are sensitive to water and suffer from poisoning by fatty acids that are present in the feedstock. On the other hand, usage of homogeneous acid catalysts suffers from serious limitations such as difficult separation and corrosion. Therefore, solid acid catalysts could potentially overcome these drawbacks [3-5].

Heteropoly acids (HPAs) possess very strong Brønsted acidity, being stronger than conventional acids such as H_2SO_4 , $\text{Al}_2\text{O}_3\text{-SiO}_2$, zeolites, acidic resins, etc. [6-8]. Hence HPAs frequently exhibit superior catalytic activity in acid-catalysed reactions, including esterification and transesterification, in homogeneous and heterogeneous systems [6-8]. Several reports demonstrating efficient homogeneous and heterogeneous catalysis by HPAs in biodiesel synthesis have been published recently [9-13].

In this Chapter, the results of our study into the esterification of hexanoic acid and transesterification of ethyl propanoate and ethyl hexanoate with methanol catalysed by a range of HPAs in homogeneous and heterogeneous liquid-phase systems are presented and discussed. The HPA catalysts include $\text{H}_3\text{PW}_{12}\text{O}_{40}$ (HPW), $\text{H}_4\text{SiW}_{12}\text{O}_{40}$ (HSiW), $\text{H}_3\text{PMo}_{12}\text{O}_{40}$ (HPMo), $\text{Cs}_{2.5}\text{H}_{0.5}\text{PW}_{12}\text{O}_{40}$ (CsPW), HPW supported on Nb_2O_5 , ZrO_2 , and TiO_2 . The catalytic activity of these materials was investigated in comparison with conventional homogeneous and solid acid catalysts such as H_2SO_4 , Amberlyst-15, zeolites HY and H-Beta. The leaching of HPW into the reaction medium was also investigated.

The reactions were carried out in a 25 ml glass reactor (round-bottom two-neck flask) equipped with a condenser and a magnetic stirrer at 60°C under atmospheric pressure at a substrate/methanol molar ratio of 1:20. Unless otherwise stated, the catalyst weight was always constant (0.10 g). The products were analysed by gas chromatography (refer to Section 2.4.2 for more details). The reactions occurred with 100% selectivity in accordance with equations (4.1) – (4.3), with no by-products observed.

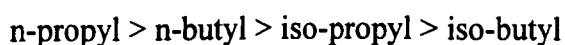


4.2 Homogeneously catalysed esterification and transesterification

Keggin type HPA (HPW, HSiW and HPMo) along with H₂SO₄ were tested as the catalysts for the esterification and transesterification reactions. The substrate reactivity and catalytic performance of the catalysts was studied. Turnover frequency (TOF), reaction order and rate constants were calculated.

4.2.1 Substrate reactivity

Esterification and transesterification reactions share a common molecular mechanism [14] (see Sections 1.2.2.2 and 1.2.3.1). However, the rate of esterification is much higher than the rate of transesterification [15]. In addition, due to steric effects, the rate of reaction in both esterification and transesterification decreases with increasing the length of acid alkyl chain. Ingold [14] reported the esterification of RCO₂H by ethanol catalysed by HCl (Table 4.1) and demonstrated that steric effects affect the reaction rate. On the other hand, Kirumakki *et al.* [16] reported the esterification of alcohols with acetic acid. The conversion was found to decrease in the order of alcohols:



In the esterification and transesterification reactions studied, hexanoic acid was the most reactive substrate followed by ethyl propanoate and ethyl hexanoate. Figure 4.1 shows the reaction conversion for different catalysts after 1 hour of reaction. The esterification of hexanoic acid occurred even without catalyst to a small extent (Table 4.2, entry 1) due to catalysis by the hexanoic acid itself. In contrast, the less reactive ethyl propanoate and hexanoate showed no spontaneous reaction (Table 4.3, entry 1 and Table 4.4, entry 1).

R	Me	Et	<i>i</i> -Pr	<i>t</i> -Bu
rate	1	0.83	0.27	0.025
R	CH ₃	CH ₂ Ph	CHPh ₂	CPh ₃
rate	1	0.56	0.015	0.000

Table 4.1 Relative rates of acid-catalysed esterification of RCO₂H with ethanol catalysed by HCl at 14.5 °C [14].

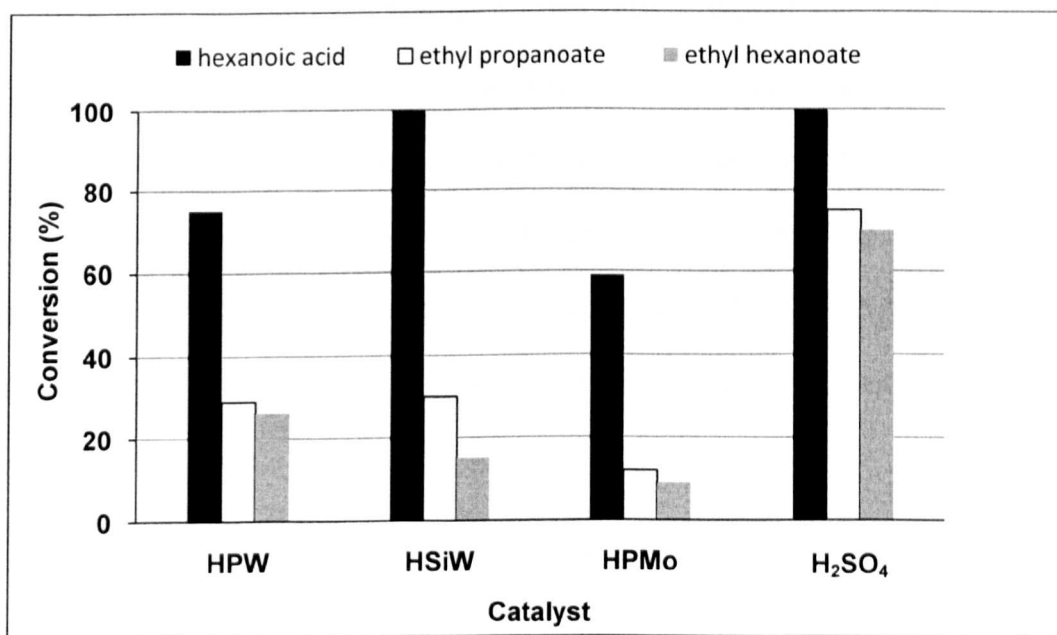


Figure 4.1 Substrate reactivity after 1 hour of reaction.

4.2.2 Catalyst performance

The results of HPA-catalysed homogeneous esterification of hexanoic acid (Equation 4.1) and transesterification of ethyl propanoate (Equation 4.2) and ethyl hexanoate (Equation 4.3) with methanol are given in Table 4.2, 4.3 and 4.4 respectively. For comparison, these reactions were also performed with sulfuric acid under the same conditions. Unless otherwise stated, the catalyst weight was always the same (0.10 g), except for HPW where a 15% catalyst charge (0.015 g) was also tested for comparison with 15% HPW supported catalysts.

Heteropoly acids, HPW, HSiW and HPMo exhibited high catalytic activities in these reactions. In terms of turnover frequency (TOF), per proton, HPAs were much more active than H_2SO_4 , namely: $\text{HPW} > \text{HSiW} > \text{HPMo} > \text{H}_2\text{SO}_4$. This order exactly follows the order of acid strength for these acids [7, 8]. However, as per unit catalyst weight, sulphuric acid was the most active catalyst: $\text{H}_2\text{SO}_4 > \text{HPW} \approx \text{HSiW} > \text{HPMo}$. This order reflects the number of protons per unit catalyst weight. (Note that the HPAs have 30 times larger molecular weight than H_2SO_4). Usually, in non-polar solvents, differentiating the effect of a strong acid, HPAs are more active than H_2SO_4 as based on both TOF and catalyst weight [7, 8]. However, in methanol, a levelling solvent similar to water, the difference in acid strength between HPAs and H_2SO_4 is not large enough to offset the larger proton density of H_2SO_4 , resulting in the higher activity of H_2SO_4 on the catalyst weight basis.

4.2.2.1 Turnover frequency

The turnover frequency (TOF) is an important quantity used for comparing catalyst efficiency [17]. The TOF was calculated as the number of moles of product

formed per mole of protons in the catalyst and per reaction time (Equation (4.4)). The TOF values are given in Tables 4.2-4.4 and Tables 4.7-4.9.

$$\text{TOF} = \frac{\text{moles of product}}{(\text{moles of H}^+ \text{ in catalyst}) \times (\text{time})} \quad (4.4)$$

It should be noted that some TOF values were obtained from large substrate conversion, hence are not under strict kinetic control. These should be taken as an approximate measure of catalyst activity. More accurate comparison of catalyst activities can be based on rate constants (Section 4.2.3).

Table 4.2 Homogeneous esterification of hexanoic acid with methanol (60 °C, 0.10 g catalyst, 10.0 g reaction mixture, 1:20 substrate/MeOH molar ratio).

Catalyst	Conversion (%)				TOF ^a (h ⁻¹)
	0.5 h	1 h	2 h	6 h	
Blank	0	0	0	2.5	0
HPW	58.1	74.8	100	100	147
HPW (15%) ^b	19.1	32.0	48.5	81.7	323
HSiW	69.3	100	100	100	131
HPMo	35.1	58.8	79.0	98.9	57
H ₂ SO ₄	100	100	100	100	>13
H ₂ SO ₄ ^c	69.0	87.7	99.5	100	45

- a) Turnover frequency for 0.5 h reaction time.
b) 0.015 g HPW corresponding to its amount (15%) in supported catalysts.
c) 0.02 g catalyst.

Table 4.3 Homogeneous transesterification of ethyl propanoate with methanol (60 °C, 0.10 g catalyst, 10.0 g reaction mixture, 1:20 substrate/MeOH molar ratio).

Catalyst	Conversion (%)				TOF ^a (h ⁻¹)
	0.5 h	1 h	2 h	6 h	
Blank	0	0	0	0	0
HPW	18.3	28.9	46.8	83.6	59
HPW (15%) ^b	2.7	5.7	10.8	26.9	59
HSiW ^c	17.7	30.3	51.1	79.0	43
HPMo	5.9	11.8	21.5	47.6	12
H ₂ SO ₄	55.0	74.5	82.3	100	9

a) Turnover frequency for 0.5 h reaction time.

b) 0.015 g HPW corresponding to its amount (15%) in supported catalysts.

Table 4.4 Homogeneous transesterification of ethyl hexanoate with methanol (60 °C, 0.10 g catalyst, 10.0 g reaction mixture, 1:20 substrate/MeOH molar ratio).

Catalyst	Conversion (%)				TOF ^a (h ⁻¹)
	0.5 h	1 h	2 h	6 h	
Blank	0	0	0	0	0
HPW	9.3	25.7	42.3	77.1	23
HPW (15%) ^b	1.5	3.2	6.1	18.2	25
HSiW	11.8	15.2	48.1	86.2	22
HPMo	3.9	6.0	15.0	29.8	6
H ₂ SO ₄	38.4	69.9	93.2	100	5

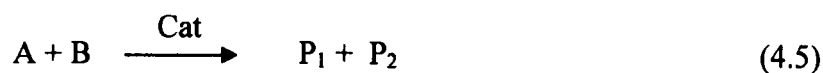
a) Turnover frequency for 0.5 h reaction time.

b) 0.015 g HPW corresponding to its amount (15%) in supported catalysts.

4.2.3 Preliminary kinetic results

4.2.3.1 Reaction order

In homogeneous systems, it was attempted to fit the data to a simple first order kinetic equation. Consider the acid-catalysed reaction



where A is the substrate (hexanoic acid, ethyl propanoate or ethyl hexanoate), B is methanol, P₁ and P₂ are the products and Cat is the catalyst. From the mechanism discussed in Sections 1.2.3.2 and 1.2.4.1, the rate law may be expected to be:

$$r = - \frac{d[A]}{dt} = k[\text{Cat}][A][B] \quad (4.6)$$

$$= k_1 [A][B] \quad (4.7)$$

where $k_1 = k[\text{Cat}]$, and k and k_1 are the corresponding rate constants.

Since the reactions were carried out under pseudo-first-order conditions with a 20-fold excess of methanol, the rate equation reduces to a simpler form (4.8):

$$r = - \frac{d[A]}{dt} = k_2 [A] \quad (4.8)$$

where $k_2 = k_1[B]$ is the pseudo-first-order rate constant.

The integrated form of equation (4.8) is:

$$\ln[A] = -k_2 t + \ln [A]_o \quad (4.9)$$

or
$$\ln[1 - x] = -k_2 t \quad (4.10)$$

where x is the conversion of A. In accordance with equation (4.10), a plot of $\ln [1-x]$ against t gives a straight line with a slope of $-k_2$.

The first order kinetic plots for homogeneous esterification of hexanoic acid and transesterification of ethyl propanoate and ethyl hexanoate with 20-fold excess methanol are given in Figure 4.2-4.4, respectively. These results show that the reactions under study are indeed first-order in the substrate.

The reaction order in HPA is also close to 1, judging from the results for the two concentrations of HPW tested. Thus the ratio of first-order rate constants for ethyl hexanoate transesterification with 0.10 g HPW and 0.015 g HPW is 6.8 (Figure 4.4) which equals the ratio of HPW concentrations (6.7). This is in agreement with equation (4.8).

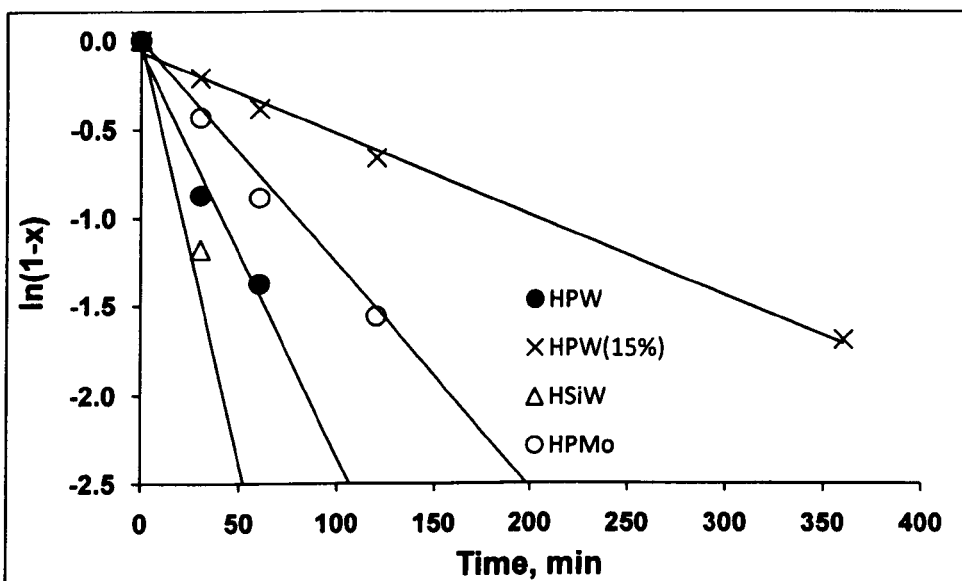


Figure 4.2 First order kinetic plot for homogeneous esterification of hexanoic acid with methanol (X is hexanoic acid conversion).

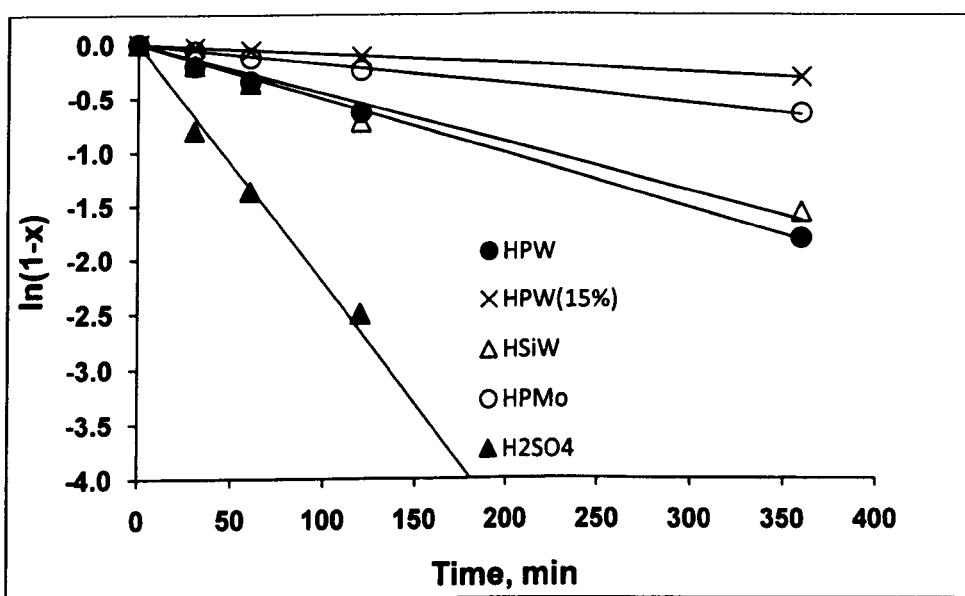


Figure 4.3 First order kinetic plot for homogeneous transesterification of ethyl propanoate with methanol (X is ester conversion).

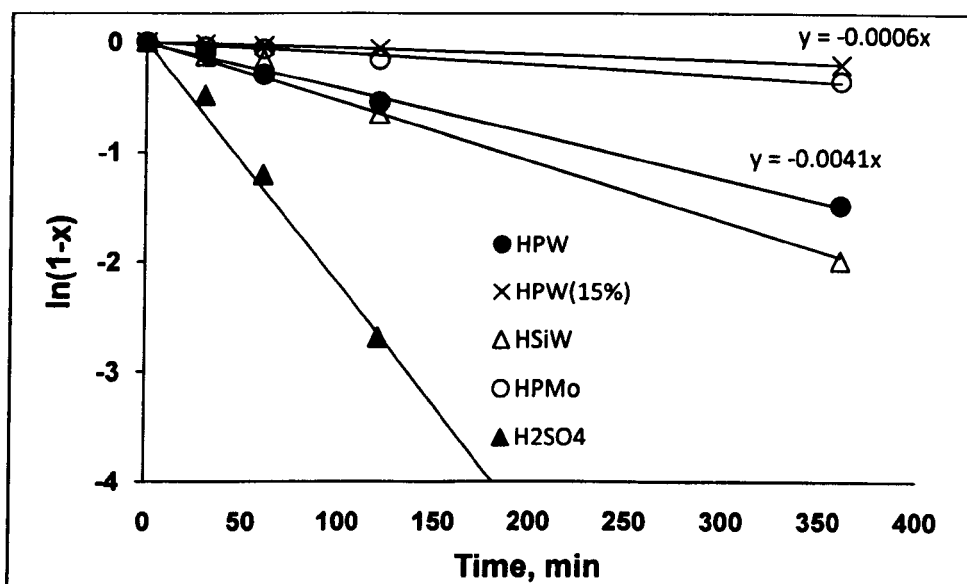


Figure 4.4 First order kinetic plot for homogeneous transesterification of ethyl hexanoate with methanol (X is ester conversion).

4.2.3.2 Rate constants

The catalytic activity of an acid catalyst is related to its acid strength by the Brønsted law [18]. This relation can be given in terms of rate constant (k) and acid dissociation constant (K_a):

$$\log k = \alpha \log K_a + C \quad (4.11)$$

where α is the Brønsted slope (typically $0 < \alpha < 1$) and C is a constant.

Heteropoly acids such as $H_3PW_{12}O_{40}$, $H_4SiW_{12}O_{40}$ and $H_3PMo_{12}O_{40}$ are strong, fully dissociated acids in aqueous solution [8, 19]. Stepwise dissociation is not observable due to the levelling effect of the solvent. On the other hand, HPAs are more stable in non-aqueous media than in water. The first two protons in $H_3PW_{12}O_{40}$ are fully dissociated and the third only partly in ethanol and acetone. The weaker acids

$H_4SiW_{12}O_{40}$ and $H_3PMo_{12}O_{40}$ are fully dissociated in the first step and partly in the second. Table 4.5 shows dissociation constant, pK_a , for HPAs as well as for sulfuric acid in acetone. The pK_a values of acids in lower alcohols are very similar to those in acetone [8].

For bulk HPA catalysts under study, the pseudo-first-order rate constants k_2 for transesterification reactions were calculated from equation (4.10) as shown in Figures 4.3 and 4.4, and presented in Table 4.5. Consequently, the third-order rate constants k were calculated (Table 4.5). The k values were calculated per moles of catalysts rather than per mole of H^+ , since the concentration of free protons in solution is unknown. The k values ($mol^{-2}L^2min^{-1}$) decrease with decreasing the catalyst acid strength: $HPW \geq HSiW > HPMo > H_2SO_4$. This is in line with the pK_1 values except for HPMo. This HPA, possessing higher oxidation potential than HPW and HSiW, often reduces in organic media, losing its acidity [19]. Hence it shows a lower catalytic activity than that expected from its acid strength [19].

Table 4.5 Rate constants of ester transesterification and dissociation constants of HPAs.

	pK_1^a	ethyl propanoate		ethyl hexanoate	
		$k_2^b (min^{-1})$	$k^c (mol^{-2}L^2min^{-1})$	$k_2^b (min^{-1})$	$k^c (mol^{-2}L^2min^{-1})$
HPW	1.6	0.005	0.092	0.004	0.073
HSiW	2.0	0.004	0.081	0.005	0.096
HPMo	2.0	0.002	0.021	0.001	0.011
H_2SO_4	6.6	0.022	0.014	0.022	0.001

- Dissociation constants of HPAs in acetone at 25 °C.
- Pseudo-first-order rate constants.
- Third order rate constants per mole of catalyst.

4.3 Heterogeneously catalysed esterification and transesterification

In this section of the chapter we investigate the activity of CsPW and supported HPAs in comparison with conventional solid acids such as Amberlyst-15, zeolites HY and H-Beta. Leaching of $\text{PW}_{12}\text{O}_{40}^{3-}$ anions in reaction medium was also investigated.

4.3.1 Catalyst leaching

Solid heteropoly acids, in particular those of the Keggin structure are strong Brønsted acids. These acids are stronger than conventional solid acids such as mixed oxides and zeolites. The disadvantage of bulk HPAs such as their low surface area can be overcome by dispersing HPAs on high surface area supports. However, in the liquid-phase reactions, leaching of HPA from the carrier to the reaction medium could be occurring. The stability of HPAs with Keggin-type structure in aqueous solutions has been extensively studied [7, 8, 20-22] and found to be directly related to the pH. For example, in aqueous solutions of $\text{H}_3\text{PW}_{12}\text{O}_{40}$, the $\text{PW}_{12}\text{O}_{40}^{3-}$ anion has a limited stability range; at pH 1.5-2 [6], it is reversibly and quickly transformed into the lacunary species $\text{PW}_{11}\text{O}_{39}^{7-}$. The lacunary anion is stable until pH~8, above which further degradation occurs to give the trivacant lacunary species $\text{PW}_9\text{O}_{34}^{9-}$ [8].

In this work, the leaching of the $\text{PW}_{12}\text{O}_{40}^{3-}$ heteropoly anions from CsPW and supported HPW catalysts in methanol and water was evaluated by refluxing catalyst samples (0.1 g) in methanol or water (10 g) for 2-6 h at 60 and 100 °C respectively, followed by separating supernatant by centrifugation. The supernatant was diluted with 1 N H_2SO_4 to adjust the pH to 1. The concentration of $\text{PW}_{12}\text{O}_{40}^{3-}$ was measured by UV-vis spectroscopy (Varian Cary 50 spectrophotometer) in a 1 cm quartz cuvette at a wavelength of 267 nm corresponding to the maximum of the $\text{PW}_{12}\text{O}_{40}^{3-}$ absorption

band [23] (Figure 4.5). This band has been assigned to the oxygen-metal charge-transfer band of the tungstophosphate anions [24].

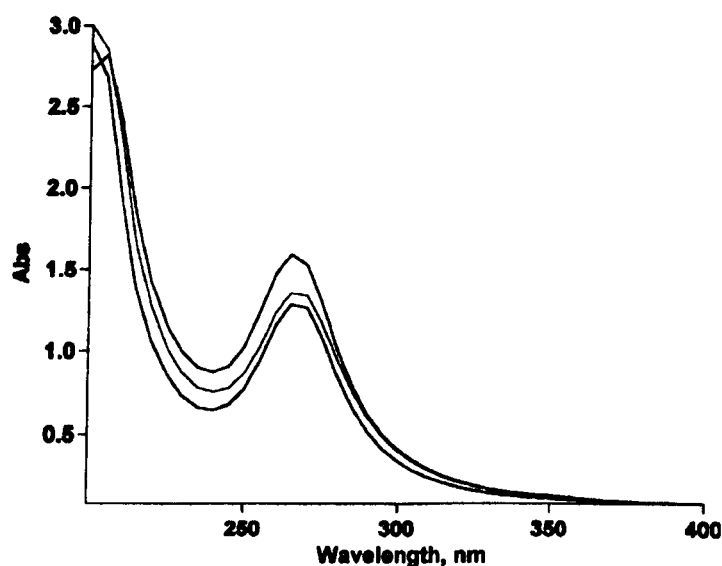


Figure 4.5 UV-vis spectra of $\text{PW}_{12}\text{O}_{40}^{3-}$ in aqueous solution at pH 1. From top to bottom: standard solution of 0.02 M $\text{H}_3\text{PW}_{12}\text{O}_{40}$; 0.015 M $\text{PW}_{12}\text{O}_{40}^{3-}$ leached from 15%HPW/ Nb_2O_5 in methanol; 0.014 M $\text{PW}_{12}\text{O}_{40}^{3-}$ leached from CsPW in water.

The results of leaching HPW in methanol and water are shown in Table 4.6. The leaching in water ranged from 3.7 – 25%, and, as expected, was larger than that in methanol (0.5 – 19%) due to the higher reflux temperature and greater solubilisation power of water. In methanol, the leaching after 6 h was found to be practically the same as after 2 h. In addition, the leaching for 15%HPW/ Nb_2O_5 calcined at 100, 300 and 500 °C was measured in methanol after 1 h, and it was found similar to that after 2 and 6 h. This shows that HPW leaching in refluxing methanol reached equilibrium in less than 1 h.

CsPW was found to be the most stable catalyst towards leaching, losing 2.7% $\text{PW}_{12}\text{O}_{40}^{3-}$ in methanol and 3.7% in water upon reflux. The value in water is in agreement with that reported previously by Okuhara [23].

For the supported HPW catalysts, aging and calcination temperature as well as support surface area caused a profound effect on the HPW leaching. Increasing the aging temperature from room temperature to 100 °C at a constant calcination temperature of 500 °C, greatly stabilised the catalysts regardless of the support used (cf. entries 2 and 3, 7 and 8, 13 and 14). As expected, the leaching decreased with increasing the calcination temperature. The surface area of support caused a dramatic effect on HPW leaching: the larger the surface area, the smaller the leaching (cf. entries 2 and 6 for HPW/ Nb_2O_5 and 7 and 12 for HPW/ ZrO_2).

Table 4.6 Catalyst characterisation.

Entry	Catalyst	Aging ^a (°C)	Calcination ^b (°C)	S _{BET} (m ² /g)	Leaching on reflux ^c (%)		
					MeOH 2 h	MeOH 6 h	H ₂ O 2 h
1	Cs _{2.5} H _{0.5} PW ₁₂ O ₄₀ ^d	rt	150	111	2.7	2.7	3.7
2	15%HPW/Nb ₂ O ₅ ^e	rt	500	2	19.0	18.2	22.9
3	15%HPW/Nb ₂ O ₅ ^e	100	500	2	6.4	5.9	
4	15%HPW/Nb ₂ O ₅ ^f	rt	100	193	4.5	5.9	25.6
5	15%HPW/Nb ₂ O ₅ ^f	rt	300	166	6.0	6.2	10.3
6	15%HPW/Nb ₂ O ₅ ^f	rt	500	96	3.3	3.9	4.4
7	15%HPW/ZrO ₂ ^e	rt	500	3	10.6	16.6	23.4
8	15%HPW/ZrO ₂ ^e	100	500	2	3.2	2.2	19.3
9	15%HPW/ZrO ₂ ^f	rt	100	176		18.6	
10	15%HPW/ZrO ₂ ^f	rt	200	149		17.9	
11	15%HPW/ZrO ₂ ^f	rt	300	121		6.4	
12	15%HPW/ZrO ₂ ^f	rt	500	54		0.5	
13	15%HPW/TiO ₂ ^e	rt	500	9	17.5	17.6	
14	15%HPW/TiO ₂ ^e	100	500	9	4.4	4.6	25.1
15	15%HPW/TiO ₂ ^e	rt	100	49		18.6	
16	15%HPW/TiO ₂ ^e	rt	200	51		17.9	
17	15%HPW/TiO ₂ ^e	rt	300	41		17.8	
18	15%HPW/TiO ₂ ^e	rt	400	44		17.7	
19	15%HPW/TiO ₂ ^e	rt	500	40		12.9	

a) Aging of aqueous slurry for 24 h at room temperature (rt) or 100 °C.

b) Calcination in air for 3 h.

c) Percentage of PW₁₂O₄₀⁻³ heteropoly anions leached into solution.

d) CsPW was aged for 48 h and calcined at 150 °C/0.5 torr for 1.5 h.

e) Commercial catalyst support (from Aldrich).

f) In-house made catalyst support.

4.3.2 Catalyst performance

Tables 4.7, 4.8 and 4.9 show our results for the esterification and transesterification of respectively hexanoic acid, ethyl propanoate and ethyl hexanoate with methanol in the presence of solid acid catalysts based on HPW, including bulk CsPW and HPW (15 wt%) supported on Nb₂O₅, ZrO₂ and TiO₂. Figures in round brackets after catalyst names refer to the entries in Table 4.6 for catalyst characterisation. For comparison, the results for conventional solid acid catalysts such as acidic resin Amberlyst-15, zeolite H-Beta and zeolite HY are shown in bottom entries. In all cases, the reaction conditions were the same as that for the homogeneous reactions above, with the catalyst amount of 0.1 g. The supported 15% HPW catalysts can be compared to the homogeneous “HPW (15%)” catalyst – both contained the same amount of HPW. The bulk CsPW and the homogeneous “HPW (15%)” contained almost the same amount of protons, hence are comparable as well.

In terms of per unit catalyst weight, all the solid acid catalysts tested in reactions (4.1)-(4.3) were less active than the homogeneous catalysts detailed above, with their activity falling in the order: H₂SO₄ > HPW ≈ HSiW > HPMo > Amberlyst-15 ≥ CsPW > supported HPW > HY, H-Beta. Regarding the TOF, reflecting the catalyst acid strength, the solid HPA catalysts were superior to H₂SO₄ and the conventional solid acid catalysts: HPW ≈ CsPW > supported HPW > H₂SO₄ > HY, H-Beta > Amberlyst-15. From the TOF values, the bulk CsPW was about as active as the homogeneous HPW. It should be noted that the TOF values for supported HPW may not truly represent their activity due to HPW leaching and a contribution of homogeneous catalysis.

Table 4.7 Esterification of hexanoic acid with methanol (60 °C, 0.10 g catalyst, 10.0 g reaction mixture, 1:20 substrate/MeOH molar ratio).

Entry	Catalyst ^a	Conversion (%)				Catalyst leaching (%)	TOF ^b (h ⁻¹)
		0.5 h	1 h	2 h	6 h		
1	CsPW (1)	7.1	12.2	22.4	41.3	2.7	223
2	CsPW ^c (1)	8.2	15.4	27.4	56.3	2.7	273
3	15%HPW/Nb ₂ O ₅ (2)	3.5	8.2	16.4	33.3	18.2	71
4	15%HPW/Nb ₂ O ₅ ^c (2)	5.2	9.3	16.5	39.4	18.2	71
5	15%HPW/Nb ₂ O ₅ (3)	0	1.5	1.5	3.5	5.9	7
6	15%HPW/Nb ₂ O ₅ (4)	0	3.3	6.1	16.2	5.9	26
7	15%HPW/Nb ₂ O ₅ (5)	0	1.2	2.4	6.3	6.2	10
8	15%HPW/Nb ₂ O ₅ (6)	0	0.7	1.2	3.3	3.9	5
9	15%HPW/ZrO ₂ (7)	0	2.1	4.6	16.2	16.6	20
10	15%HPW/ZrO ₂ (8)	0	0	2.1	6.5	2.2	9
11	15%HPW/ZrO ₂ (9)	9.1	16.3	27.1	53.2	18.6	117
12	15%HPW/ZrO ₂ (11)	2.4	4.5	8.3	20.5	6.4	36
13	15%HPW/ZrO ₂ (12)	0	1.6	2.5	7.1	0.5	11
14	15%HPW/TiO ₂ (13)	2.5	6.5	16.3	51.2	17.6	71
15	15%HPW/TiO ₂ (14)	0	0.0	2.6	10.5	4.6	11
16	15%HPW/TiO ₂ (18)	2.3	6.2	14.3	46.0	17.7	62
17	15%HPW/TiO ₂ (19)	2.1	4.3	9.0	27.2	12.9	39
18	Amberlyst-15	8.2	16.3	27.1	59.1		4
19	Zeolite H-Beta ^d	4.5	7.8	14.7	33.5		25
20	Zeolite HY ^d	2.4	4.1	7.8	16.8		4

- a) In round brackets are entries in Table 4.6 to reference catalyst characterisation.
b) Turnover frequency for 2 h reaction time assuming that all acid protons are equally active. For CsPW, TOF is for the surface protons calculated assuming a cross section of 144 Å² for HPW.
c) The catalyst was pre-refluxed in MeOH for 2 h prior to adding hexanoic acid.
d) Calcined in air at 500 °C for 3 h.

Table 4.8 Transesterification of ethyl propionate with methanol (60 °C, 0.10 g catalyst, 10.0 g reaction mixture, 1:20 substrate/MeOH molar ratio).

Entry	Catalyst ^a	Conversion (%)				Catalyst leaching (%)	TOF ^b (h ⁻¹)
		0.5 h	1 h	2 h	6 h		
1	CsPW (1)	0	3.2	6.3	15.4	2.7	68
2	15%HPW/Nb ₂ O ₅ (2)	0	0	0	6.2	18.2	11
3	15%HPW/Nb ₂ O ₅ (3)	0	0	0	0	5.9	0
4	15%HPW/Nb ₂ O ₅ (4)	0	0	0	0	5.9	0
5	15%HPW/Nb ₂ O ₅ (5)	0	0	0	0	6.2	0
6	15%HPW/Nb ₂ O ₅ (6)	0	0	0	0	3.9	0
7	15%HPW/ZrO ₂ (7)	0	0	0	0	16.6	0
8	15%HPW/ZrO ₂ (8)	0	0	0	0	2.2	0
9	15%HPW/ZrO ₂ (9)	0	1.5	2.9	8.3	18.6	15
10	15%HPW/ZrO ₂ (11)	0	0	0	1.5	6.4	3
11	15%HPW/ZrO ₂ (12)	0	0	0	0	0.5	0
12	15%HPW/TiO ₂ (13)	0	0	0	6.5	17.6	12
13	15%HPW/TiO ₂ (14)	0	0	0	0	4.6	0
14	15%HPW/TiO ₂ (18)	0	0	0	3.9	17.7	7
15	15%HPW/TiO ₂ (19)	0	0	0	2.9	12.9	5
16	Amberlyst-15	0	0	9.3	21.6		1
17	Zeolite H-Beta ^c	0	0	0	3.2		2
18	Zeolite HY ^c	0	3.3	6.0	15.3		3

- a) In round brackets are entries in Table 4.6 to reference catalyst characterisation.
b) Turnover frequency for 6 h reaction time assuming that all acid protons are equally active. For CsPW, TOF is for the surface protons calculated assuming a cross section of 144 Å² for HPW.
c) Calcined in air at 500 °C for 3 h.

Table 4.9 Transesterification of ethyl hexanoate with methanol (60 °C, 0.10 g catalyst, 10.0 g reaction mixture, 1:20 substrate/MeOH molar ratio).

Entry	Catalyst ^a	Conversion (%)				Catalyst leaching (%)	TOF ^b (h ⁻¹)
		0.5 h	1 h	2 h	6 h		
1	CsPW (1)	0	1.6	2.6	7.7	2.7	25
2	15%HPW/Nb ₂ O ₅ (2)	0	0	0	4.3	18.2	6
3	15%HPW/Nb ₂ O ₅ (3)	0	0	0	0	5.9	0
4	15%HPW/ZrO ₂ (7)	0	0	0	0	16.6	0
5	15%HPW/ZrO ₂ (8)	0	0	0	0	2.2	0
6	15%HPW/TiO ₂ (13)	0	0	1.1	5.2	17.6	7
7	15%HPW/TiO ₂ (14)	0	0	0	0	4.6	0
8	15%HPW/TiO ₂ (16)	0	1.3	2.5	7.2	17.9	10
9	15%HPW/TiO ₂ (18)	0	0	0	2.0	17.7	3
10	Amberlyst-15	0	1.3	3.0	7.8		0.4
11	Zeolite H-Beta ^c	0	0	0	2.6		1.5
12	Zeolite HY ^c	0	0	1.2	3.1		0.5

- a) In round brackets are entries in Table 4.6 to reference catalyst characterisation.
b) Turnover frequency for 6 h reaction time assuming that all acid protons are equally active. For CsPW, TOF is for the surface protons calculated assuming a cross section of 144 Å² for HPW.
c) Calcined in air at 500 °C for 3 h.

Based on the TOF values, the relative reactivity of hexanoic acid, ethyl propanoate and ethyl hexanoate is approximately 10:3:1 for the catalysts such as HPW, CsPW and Amberlyst-15, i.e. the transesterification of esters slows down with increasing the length of acid alkyl chain in agreement with literature [14, 16]

An induction period of 0.5-2 h was often observed for the solid acid catalysts, especially in ester transesterification (Table 4.8-4.9). The reason for this could be that a certain change in catalyst texture as well as in the local environment of acid sites is

required for effective catalysis to occur. This may be similar to acid resin swelling in liquid-phase catalytic reactions [25].

Interestingly, pre-refluxing CsPW and HPW/Nb₂O₅ in methanol for 2 h increased their activity in hexanoic acid esterification as shown in Figure 4.6 and 4.7 respectively.

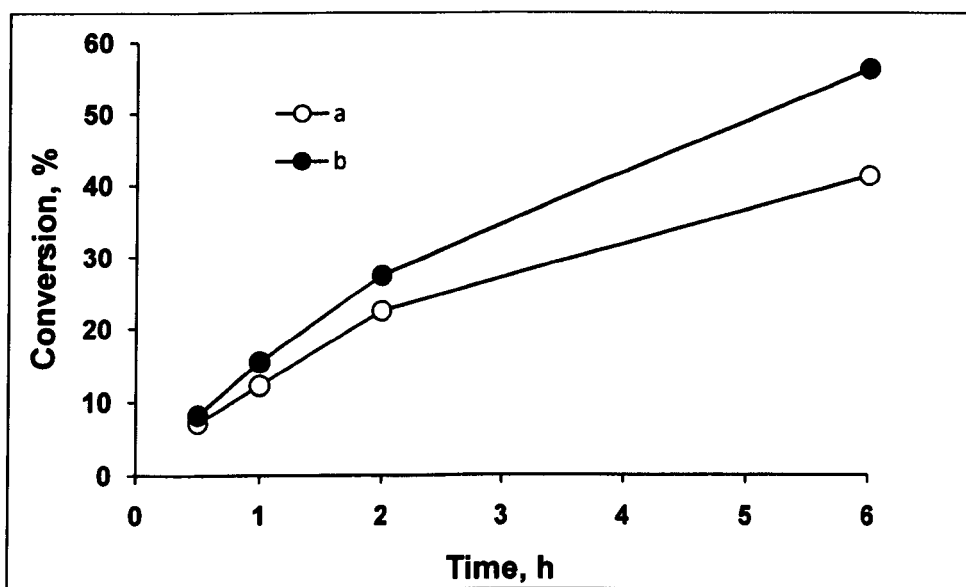


Figure 4.6 Esterification of hexanoic acid with MeOH in the presence of: (a) CsPW; (b) pre-refluxing CsPW in methanol for 2 h (Table 4.7, entries 1, 2).

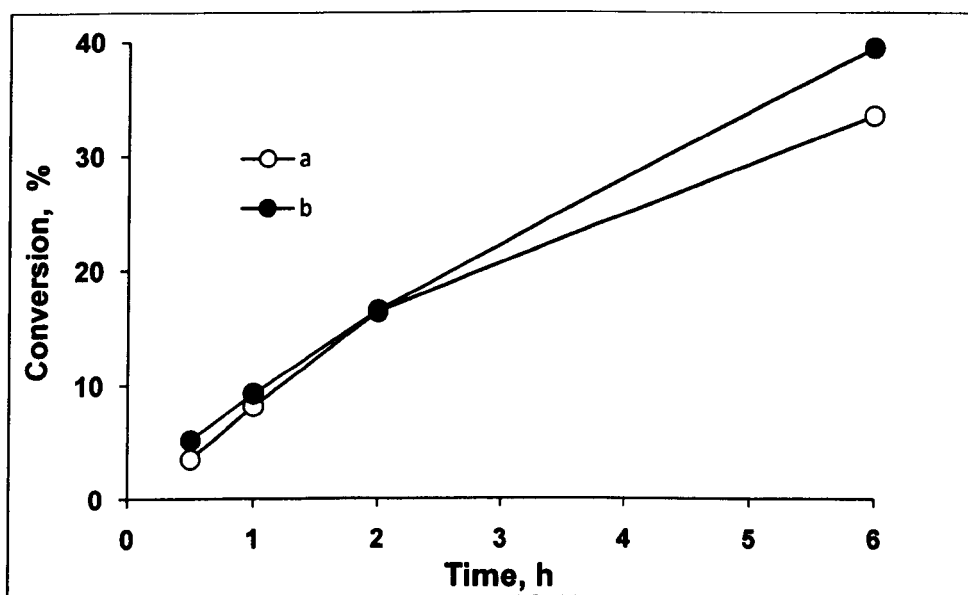


Figure 4.7 Esterification of hexanoic acid with MeOH in the presence of: (a) HPW/Nb₂O₅; (b) pre-refluxing HPW/Nb₂O₅ in methanol for 2 h (Table 4.7, entries 3, 4).

Given the catalyst leaching in methanol (Section 4.3.1), reactions (4.1)-(4.3) could, to some extent, be homogeneously catalysed by the leached HPW. Tables 4.7-4.9 show the leaching of HPW from the catalysts in methanol together with the catalyst activities in reactions (4.1)-(4.3). What becomes apparent is a clear relation between the activity of supported HPW catalysts and their leaching: the larger the leaching, the higher the activity. Figure 4.8 illustrates the effect of the calcination temperature of HPW/ZrO₂ on leaching of HPW and the catalyst activity.

The catalysts comprising HPW supported on Nb₂O₅, ZrO₂ and TiO₂ that are stable to leaching showed practically no activity. This indicates a significant contribution of homogeneous catalysis by the leached HPW for such catalysts. In contrast, the bulk CsPW heteropoly salt exhibited high catalytic activity despite its very low leaching, suggesting true heterogeneous catalysis in this case.

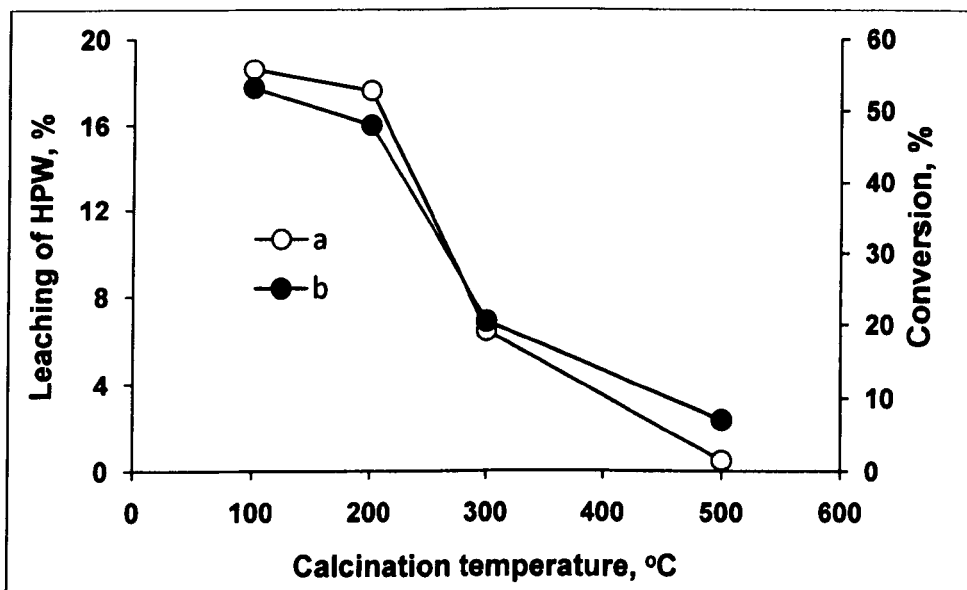


Figure 4.8 Effect of calcination temperature of HPW/ZrO₂ on: (a) leaching of HPW after reflux in MeOH for 6 h (b) conversion of hexanoic acid at 6 h (Table 4.7, entries 11, 12 and 13).

To gain an insight into the nature of catalysis in reactions (4.1)-(4.3), we estimated the role of homogeneous and heterogeneous routes in some reaction systems using the following method. After 1 h of reaction time – the time sufficient for leaching equilibrium to be reached (Section 4.3.1) – the catalyst was quickly filtered off from warm reaction mixture and the supernatant allowed reacting on. This test showed that CsPW, which leached only 2.7% HPW, exhibited practically no contribution of homogeneous catalysis in esterification of hexanoic acid (Figure 4.9) and transesterification of ethyl propanoate (Figure 4.10).

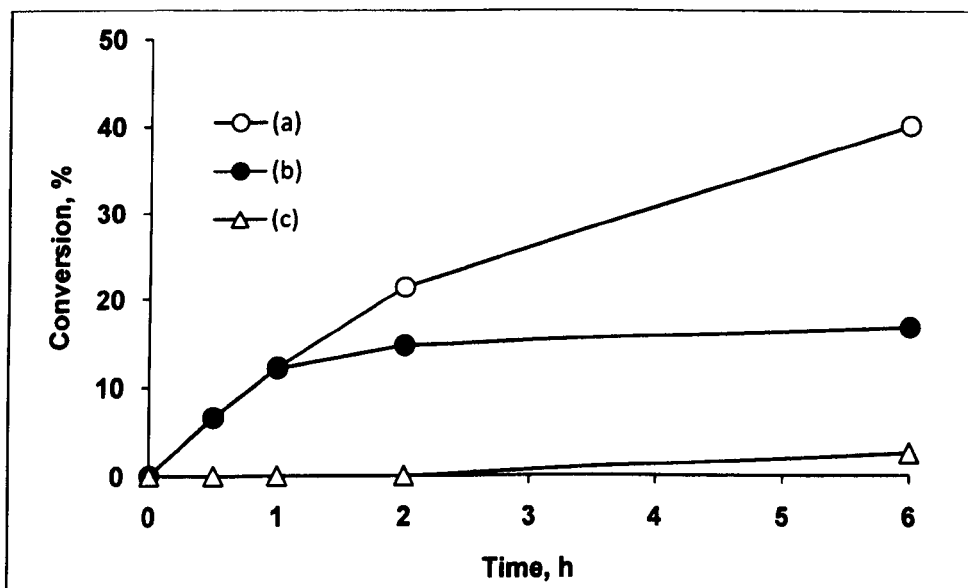


Figure 4.9 Esterification of hexanoic acid with MeOH in the presence of CsPW: (a) catalyst present all along; (b) catalyst removed after 1 h; (c) blank reaction in the absence of catalyst.

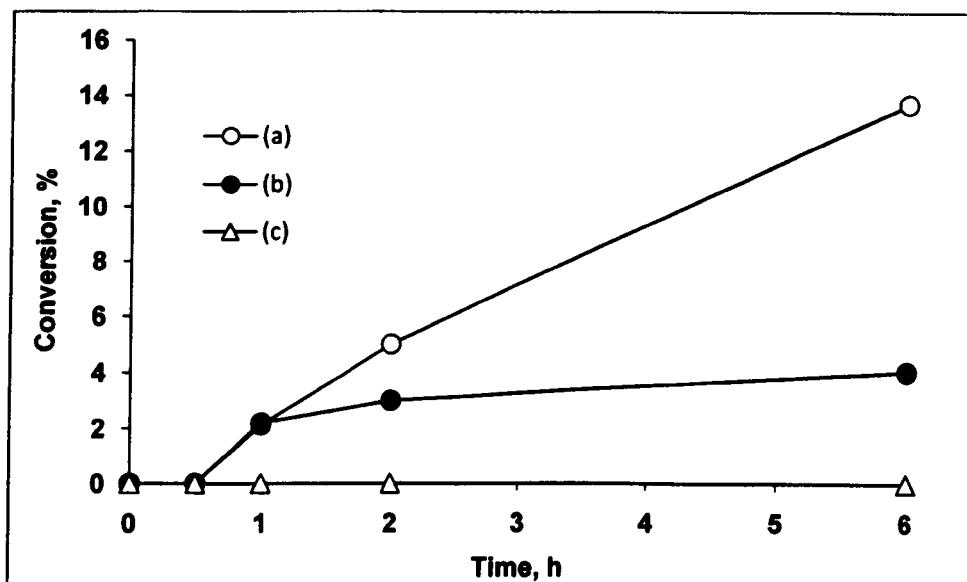


Figure 4.10 Transesterification of ethyl propionate with MeOH in the presence of CsPW: (a) catalyst present all along; (b) catalyst removed after 1 h; (c) blank reaction in the absence of catalyst.

Likewise, 15%HPW/Nb₂O₅, with a low leaching of 5.9% and a relatively low activity, showed no homogeneous contribution in hexanoic acid esterification (Figure 4.11). In contrast, a strongly leaching (18.2%) and more active sample of 15%HPW/Nb₂O₅ gave a 32% contribution of homogeneous catalysis in this reaction (Figure 4.12). It appears that low-leaching catalysts release partially degraded HPW species into methanol solution, with a weak acidity, hence low catalytic activity. On the other hand, strongly-leaching catalysts probably release intact HPW molecules that are active homogeneous catalysts.

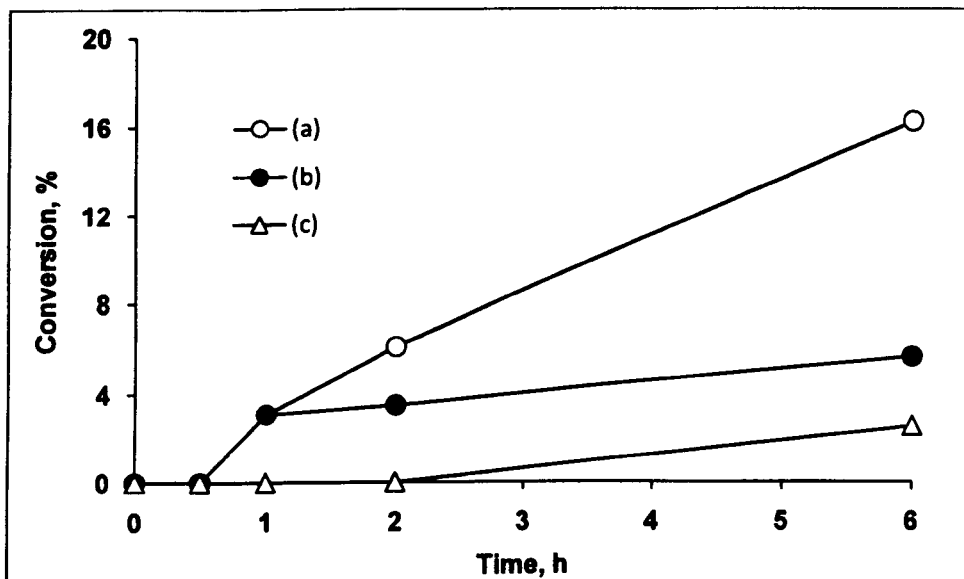


Figure 4.11 Esterification of hexanoic acid with MeOH in the presence of 15%HPW/Nb₂O₅ (Table 4.6, entry 4): (a) catalyst present all along; (b) catalyst removed after 1 h; (c) blank reaction in the absence of catalyst.

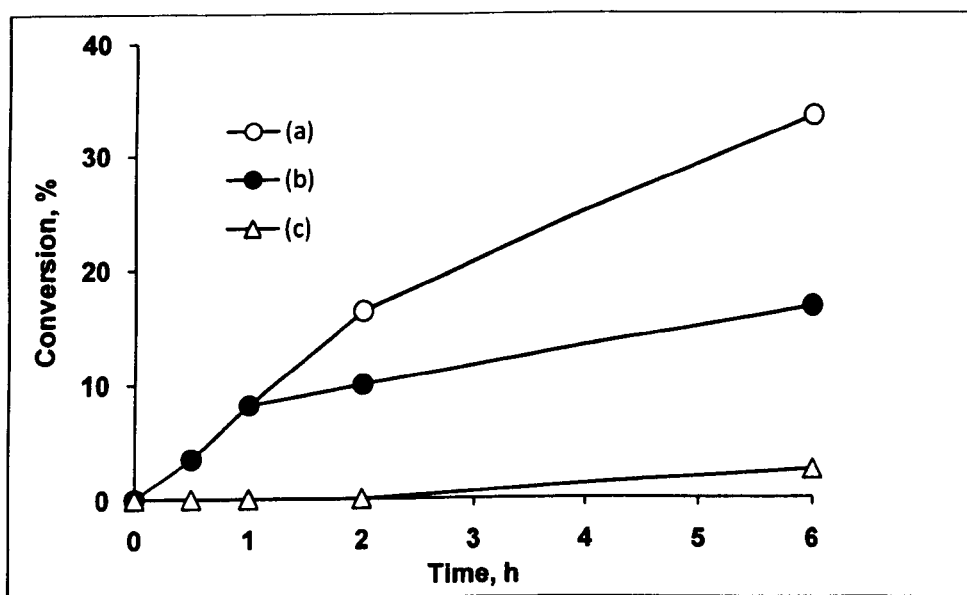


Figure 4.12 Esterification of hexanoic acid with MeOH in the presence of 15%HPW/Nb₂O₅ (Table 4.6, entry 2): (a) catalyst present all along; (b) catalyst removed after 1 h; (c) blank reaction in the absence of catalyst.

4.3.3 Catalyst reuse

Catalyst reuse was attempted for hexanoic acid esterification by CsPW and HPW/Nb₂O₅. After the first run, the catalyst was separated by centrifugation and, prior to reuse, treated at 150 °C/0.5 Torr for 1.5 h. In the second run, the CsPW showed 84% of its initial activity (Figure 4.13). The loss of activity may be due to the leaching and a loss of the catalyst (fine powder) in separation. HPW/Nb₂O₅ showed 68% of its initial activity (Figure 4.14). The decline of activity in the second run can be attributed to the leaching of HPW.

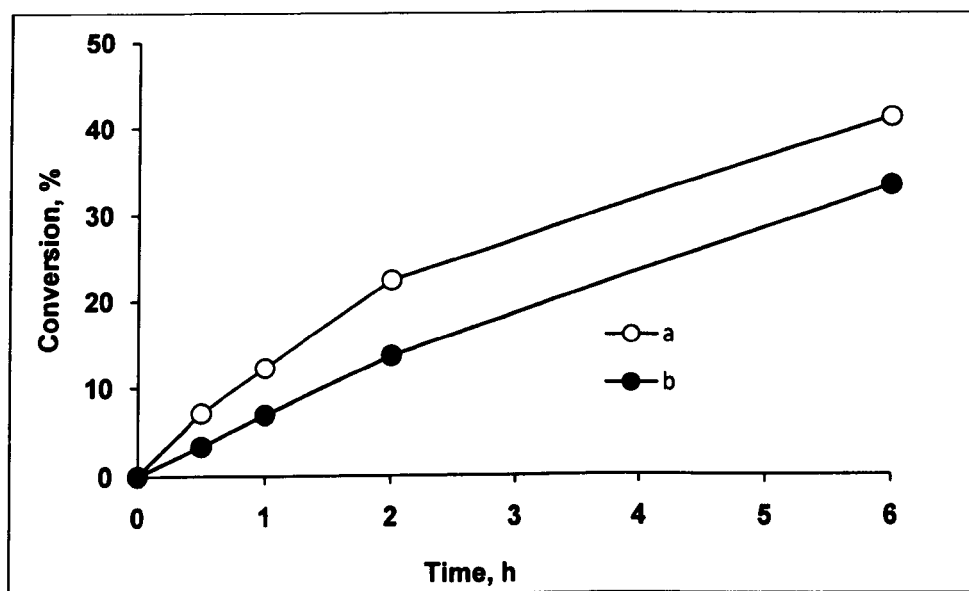


Figure 4.13 Catalyst reuse in esterification of hexanoic acid with MeOH in the presence of CsPW: (a) first run; (b) second run.

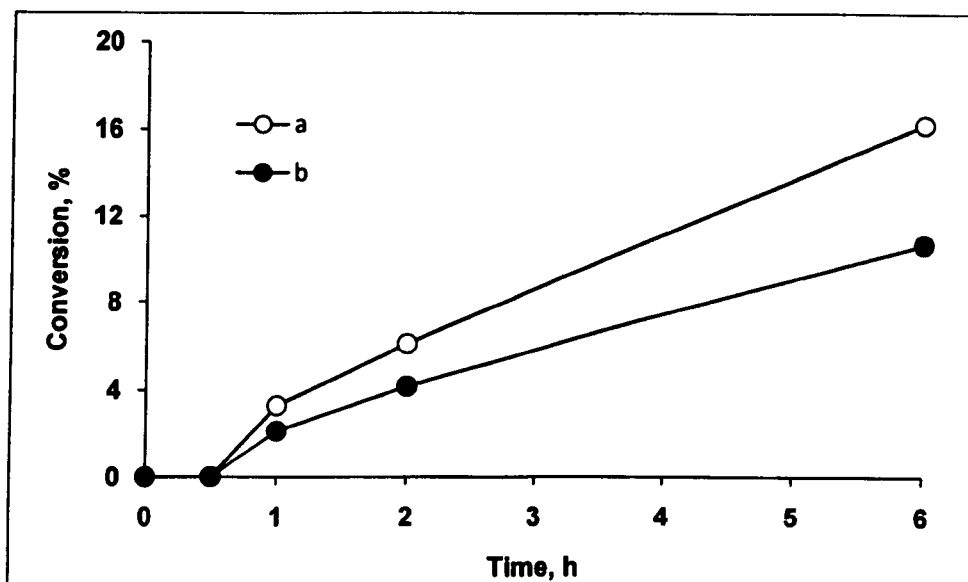


Figure 4.14 Catalyst reuse in esterification of hexanoic acid with MeOH in the presence of HPW/Nb₂O₅ (Table 4.6, entry 4); (a) first run; (b) second run.

4.4 Conclusion

Tungsten heteropoly acids are active catalysts for the transesterification and esterification reactions studied. Their intrinsic catalytic activity (TOF) both in homogeneous and heterogeneous systems is higher than that of the conventional acid catalysts such as H₂SO₄, Amberlyst-15, HY and H-Beta, in line with the acid strength of these catalysts: H₃PW₁₂O₄₀ ≈ Cs_{2.5}H_{0.5}PW₁₂O₄₀ > H₄SiW₁₂O₄₀ > H₃PMo₁₂O₄₀ > 15%H₃PW₁₂O₄₀/Nb₂O₅, 15%H₃PW₁₂O₄₀/ZrO₂, 15%H₃PW₁₂O₄₀/TiO₂ > H₂SO₄ > HY, H-Beta > Amberlyst-15. Regarding the activity per unit catalyst weight, sulfuric acid is superior to H₃PW₁₂O₄₀, H₃PMo₁₂O₄₀ and H₄SiW₁₂O₄₀ in homogeneous systems and Amberlyst-15 is slightly better than Cs_{2.5}H_{0.5}PW₁₂O₄₀ in heterogeneous systems. The supported HPW catalysts suffer from leaching and exhibit significant contribution of

homogeneous catalysis by the leached HPA. The leaching can be reduced by a more severe catalyst pre-treatment, albeit at the expense of catalyst activity. Homogeneous acid catalysts, although more active, pose a threat to the environment which makes solid acid catalysts attractive.

From the results obtained, Amberlyst-15, which is stable below 120 °C [25], appears to be the catalyst of choice under relatively mild reaction conditions. $\text{Cs}_{2.5}\text{H}_{0.5}\text{PW}_{12}\text{O}_{40}$, which has higher thermal stability than Amberlyst-15 and is sufficiently stable to leaching, could compete under more forcing reaction conditions that may be needed in order to enhance the rather slow acid-catalysed transesterification and esterification reactions. Recently developed by Rohm and Haas sulfonated macroporous acidic resin Amberlyst 70 based on halogenated styrene/divinylbenzene co-polymer, which is thermally stable up to 190 °C [26], could be a promising catalyst for transesterification and esterification reactions at higher temperatures.

References

- [1] A.J. Ragauskas, C.K. Williams, B.H. Davison, G. Britovsek, J. Cairney, C.A. Eckert, W.J. Frederick, J.P. Hallett, D.J. Leak, C.L. Liotta, J.R. Mielenz, R. Murphy, R. Templer, T. Tschaplinski, *Science* 311 (2006) 484.
- [2] A. Corma, S. Iborra, A. Velty, *Chem. Rev.* 107 (2007) 2411.
- [3] A. Srivastava, R. Prasad, *Renewable Sustainable Energy Rev.* 4 (2000) 111.
- [4] J.A. Melero, J. Iglesias, G. Morales, *Green Chem.* 11 (2009) 1285.
- [5] A.P. Vyas, J.L. Verma, N. Subrahmanyam, *Fuel* 89 (2010) 1.
- [6] T. Okuhara, N. Mizuno, M. Misono, *Adv. Catal.* 41 (1996) 113.
- [7] I.V. Kozhevnikov, *Chem. Rev.* 98 (1998) 171.
- [8] I.V. Kozhevnikov, *Catalysts for Fine Chemicals. Vol 2. Catalysis by Polyoxometalates*, Wiley, Chichester, 2002.
- [9] A. Zieba, L. Matachowski, J. Gurgul, E. Bielanska, A. Drelinkiewicz, *J. Mol. Catal. A* 316 (2010) 30.
- [10] A. Zieba, L. Matachowski, E. Lalik, A. Drelinkiewicz, *Catal. Lett.* 127 (2009) 183.
- [11] L. Matachowski, A. Zieba, M. Zembala, A. Drelinkiewicz, *Catal. Lett.* 133 (2009) 49.
- [12] L.L. Xu, W. Li, J.L. Hu, K.X. Li, X. Yang, F.Y. Ma, Y.N. Guo, X.D. Yu, Y.H. Guo, *J. Mater. Chem.* 19 (2009) 8571.
- [13] L.L. Xu, Y.H. Wang, X. Yang, X.D. Yu, Y.H. Guo, J.H. Clark, *Green Chem.* 10 (2008) 746.
- [14] C.K. Ingold, *Structure and Mechanism in Organic Chemistry*, G. Bell and Sons Ltd, London, 1953.

- [15] Y.S. Lien, L.S. Hsieh, J.C.S. Wu, *Ind. Eng. Chem. Res.* 49 (2010) 2118.
- [16] S.R. Kirumakki, N. Nagaraju, K.V. Chary, *Appl. Catal. A* 299 (2006) 185.
- [17] G. Rothenberg, *Catalysis concepts and green applications*, Wiley-VCH, 2008.
- [18] R.P. Bell, *The Proton in Chemistry*, 2nd ed., Cornell University Press, Ithaca, NY, 1973.
- [19] I.V. Kozhevnikov, *Russ. Chem. Rev.* 56 (1987) 811.
- [20] M.T. Pope, *Heteropoly and Isopoly Oxometalates*, Berlin, 1983.
- [21] D.L. Kepert, J.H. Kyle, *J. Chem. Soc., Dalton Trans.* (1978) 137.
- [22] D.L. Kepert, J.H. Kyle, *J. Chem. Soc., Dalton Trans.* (1978) 1781.
- [23] T. Okuhara, *Chem. Rev.* 102 (2002) 3641.
- [24] K. Nomiya, Y. Sugie, K. Amimoto, M. Miwa, *Polyhedron*. 6 (1987) 519.
- [25] M.A. Harmer, Q. Sun, *Appl. Catal. A* 221 (2001) 45.
- [26] <http://www.amberlyst.com/sac.htm>.

5. Isopropanol dehydration as test reaction

5.1 Introduction

Isopropanol undergoes dehydration to propene and in some cases diisopropyl ether over acidic sites (Figure 5.1) and dehydrogenation to acetone over basic or redox sites (Figure 5.2) [1-5]. Several factors determine the selectivity of dehydration/dehydrogenation of isopropanol: surface structure, reaction temperature, the oxidant or inert atmosphere and pretreatment conditions of the catalyst [3, 6].

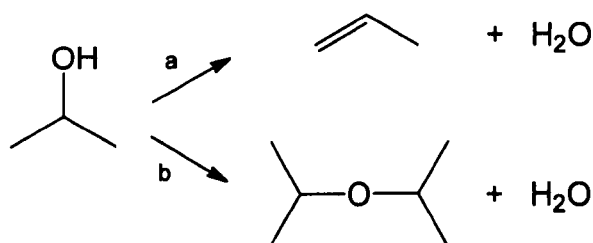


Figure 5.1 Isopropanol dehydration forming (a) propene and (b) diisopropyl ether.

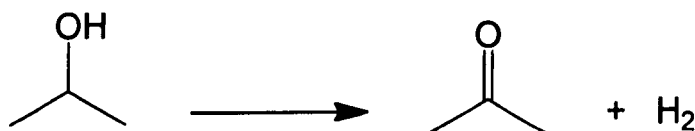


Figure 5.2 Isopropanol dehydrogenation forming acetone.

Most primary and secondary alcohols react via the E_2 mechanism, while tertiary alcohols react via a two-step E_1 mechanism as a result of the higher stability of the carbenium ion. The E_1 mechanism requires strong acid sites and leads to olefin formation, while the E_2 mechanism, which occurs over both acid and base sites, leads to ether formation as well as olefins [7]. Alcohol dehydration can also occur via the E_{1cB} mechanism through a carbanion intermediate on very basic solids which possess acid and base sites with imbalanced strength [3]. The dehydrogenation via the E_{1cB} mechanism involving the intermediate carbanion gives the ketone which is formed by the abstraction of the α -hydrogen [8]. Figure 5.3 illustrates the different reaction mechanisms for isopropanol decomposition which can occur on acid and basic solids.

The mechanism proposed for propene formation shown in Figure 5.4 involves either surface Brønsted acid sites or Lewis acid sites, leading to hydrogen bonded or coordinated isopropanol species, respectively, followed by a concerted mechanism involving a hydrogen atom of a methyl group.

The mechanisms proposed for diisopropyl ether formation are shown in Figure 5.5. Isopropyl ether is formed by an intermolecular dehydration which requires acidic OH groups.

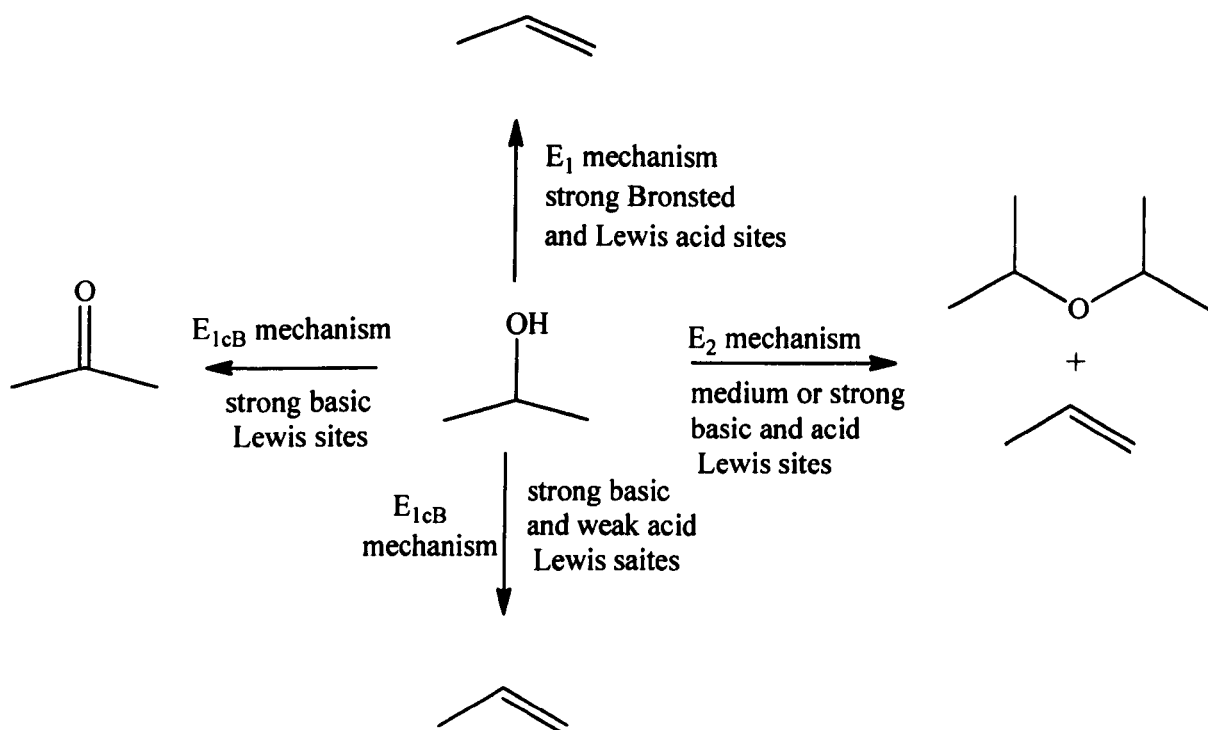


Figure 5.3 Reaction mechanisms of isopropanol decomposition on acid and basic catalysts leading to dehydration products (propene, diisopropyl ether) and to dehydrogenation product (acetone) [3].

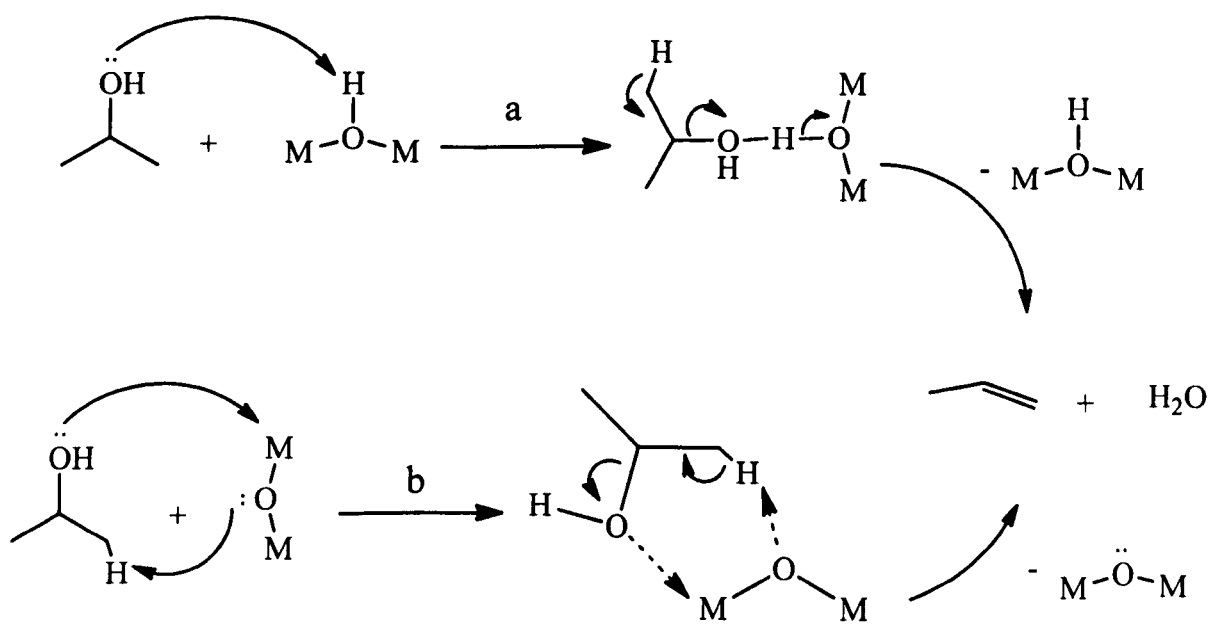


Figure 5.4 Proposed mechanisms for propene formation: (a) involving surface Brønsted acid sites and (b) involving surface Lewis acid sites [4].

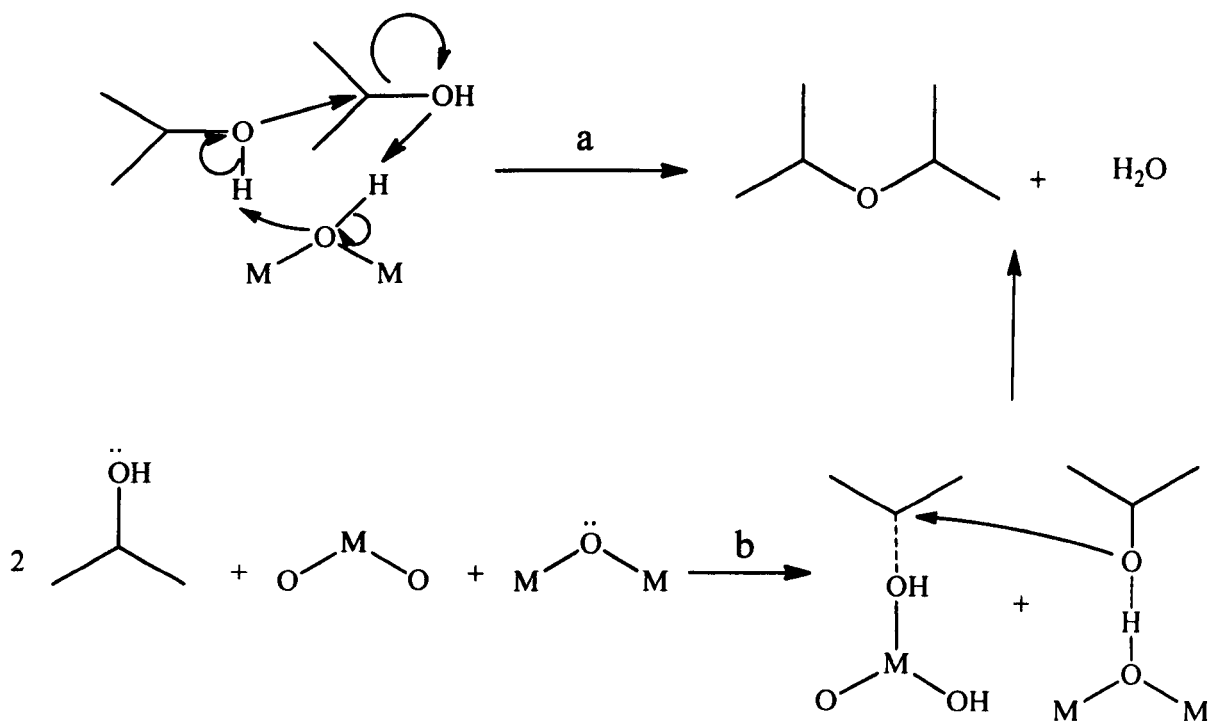


Figure 5.5 Proposed mechanisms for ether formation (a) involving surface Brønsted acid sites and (b) involving surface Lewis acid sites [4, 6].

The dehydration of isopropanol has been widely used for probing the acidity of catalysts through their catalytic activity [1]. The standard enthalpies of propene and diisopropyl ether formation are 50.8 and -15.8 kJ/mol respectively for the gas-phase dehydration. As a result, propene formation has higher activation energy than ether formation, and propene selectivity increases with increasing the reaction temperature, making it the main product at higher temperatures [3]. Isopropanol dehydration does not discriminate between Brønsted and Lewis acid sites. It should be noted that strong Lewis acid sites can be affected by the water produced in this reaction, turning them into Brønsted acid sites. Therefore, isopropanol dehydration is more suitable for probing relatively strong Brønsted acid sites, which makes it appropriate for probing

HPA catalysts. Bulk and supported $\text{H}_3\text{PW}_{12}\text{O}_{40}$ have been tested in isopropanol dehydration [9-11]. Okuhara *et al.* [9] studied in detail the dehydration of isopropanol over solid HPAs in order to prove the bulk type I (pseudoliquid phase) mechanism. $\text{H}_3\text{PW}_{12}\text{O}_{40}$ was found to be much more active for the dehydration of isopropanol than $\text{SiO}_2\text{-Al}_2\text{O}_3$ (by a factor of about 30 per weight and about 2000 per surface area) at 125°C . The activities of HPAs decrease in the order: $\text{H}_3\text{PW}_{12}\text{O}_{40} > \text{H}_4\text{SiW}_{12}\text{O}_{40} > \text{H}_5\text{PW}_{10}\text{V}_2\text{O}_{40} > \text{H}_3\text{PMo}_{12}\text{O}_{40} > \text{H}_5\text{PMo}_{10}\text{V}_2\text{O}_{40} \approx \text{H}_4\text{SiMo}_{12}\text{O}_{40}$, which is in line with their acid-strength. A detailed study of kinetics and mechanism of 2-butanol dehydration over supported HPA catalysts has been published recently [12].

The aim of the work in this chapter is to study the isopropanol dehydration in the gas phase as test reaction over solid HPA catalysts. The catalysts under study are both the “standard” HPA catalysts, such as $\text{H}_3\text{PW}_{12}\text{O}_{40}$ (HPW), HPW/ SiO_2 and $\text{Cs}_{2.5}\text{H}_{0.5}\text{PW}_{12}\text{O}_{40}$, and the acidic composites comprising $\text{H}_3\text{PW}_{12}\text{O}_{40}$, supported on Nb_2O_5 , ZrO_2 and TiO_2 . Hereafter, the calcination temperature is noted in the catalyst formulation as, for example, 15%HPW/ Nb_2O_5 -300 and 15%HPW/ Nb_2O_5 -500.

5.2 Experimental procedure

The experimental procedure is explained in detail in Section 2.5.2.2, but briefly summarised here for clarity. Isopropanol dehydration was carried out in the gas phase under atmospheric pressure in a Pyrex fixed-bed downflow reactor fitted with an on-line gas chromatograph. The gas flow containing isopropanol (5.52 kPa) and nitrogen as a carrier gas entered the reactor at the top at a flow rate of 20 ml/min. Isopropanol was supplied into the gas flow by passing nitrogen through a saturator, which was kept at a constant temperature (25°C) to maintain the chosen reactant pressure. The reactor

was packed with 0.1 g catalyst powder. Prior to reaction, the catalysts were pre-treated in situ at 300°C in a nitrogen flow (20 ml/min) for 1 h. At regular time intervals, the downstream gas flow was analysed by the on-line GC. In light-off tests, the temperature dependent conversion of isopropanol was measured in a temperature range from 80°C up to the point where 100% conversion was observed. From these results, the temperature of 50% conversion, T_{50} , was obtained and the apparent activation energy of reaction, E_a , was calculated at isopropanol conversion < 10%.

5.3 Light-off test (T_{50})

Table 5.1 shows our results on catalyst activity in isopropanol dehydration. The activity was characterised per unit catalyst weight by measuring the temperatures of 50% conversion, T_{50} , in light-off tests. Examples of such test are shown in Figures 5.6-5.9. The light-off tests rank the catalyst activity regarding the values of T_{50} as follows: $H_3PW_{12}O_{40} \approx Cs_{2.5}H_{0.5}PW_{12}O_{40} \approx 15\%HPW/SiO_2 \approx 20\%Cs_2HPW_{12}O_{40}/SiO_2 > 15\%HPW/TiO_2 \gg 15\%HPW/Nb_2O_5 > 15\%HPW/ZrO_2 \gg Nb_2O_5 \gg TiO_2 > ZrO_2$. This order is in agreement with the order of catalyst acid strength determined by NH_3 adsorption calorimetry (Table 5.1) (see Section 3.7.1). The “standard” HPA catalysts (i.e. HPW, CsPW and 15%HPW/SiO₂) possess higher activity per catalyst weight than the catalysts comprising HPA supported Nb₂O₅, ZrO₂ and TiO₂, in line with the catalyst acid strength. Supported HPA catalysts are much more active, as expected, than the corresponding oxide supports, so the supports make only minor (Nb₂O₅) or no contribution (ZrO₂ and TiO₂) to the activity of these catalysts.

Table 5.1 Isopropanol dehydration (0.1 g catalyst, 5.5 vol.% isopropanol in N₂, 20 ml/min flow rate).^a

	Catalyst	S _{BET} ^b (m ² /g)	T ₅₀ ^c (°C)	S ^d (%)	E ^e (kJ/mol)	-ΔH ^f (kJ/mol)
1	H ₃ PW ₁₂ O ₄₀	2	104	93	90	195
2	Cs _{2.5} H _{0.5} PW ₁₂ O ₄₀	111	100	91	68	164
3	20%Cs ₂ H ₁ PW ₁₂ O ₄₀ /SiO ₂	185	105	93	67	160
4	15% HPW/SiO ₂	229	103	89	86	154
5	15% HPW/Nb ₂ O ₅ -500	96	165	97	72	121
6	15% HPW/Nb ₂ O ₅ -300	166	155	92	71	132
7	15% HPW/ZrO ₂ -500	54	170	93	63	129
8	15% HPW/ZrO ₂ -300	121	168	98	59	121
9	15% HPW/TiO ₂ -500	40	137	89	81	130
10	15% HPW/TiO ₂ -300	41	110	91	90	143
11	Nb ₂ O ₅ -500		200	99	64	
12	ZrO ₂ -500		310	100	43	
13	TiO ₂ -500		285	100	41	

- a) Prior to reaction the catalysts were pre-treated in situ at 300 °C for 1 h in N₂ (20 ml/min).
- b) BET surface area.
- c) Temperature corresponding to 50% isopropanol conversion from light-off tests in a temperature range from 80 °C up to the point where 100% isopropanol conversion was observed.
- d) Propene selectivity at T₅₀; the only other product was diisopropyl ether.
- e) Apparent activation energy determined from light-off tests at isopropanol conversion < 10%.
- f) Initial enthalpy of ammonia adsorption at 100 °C.

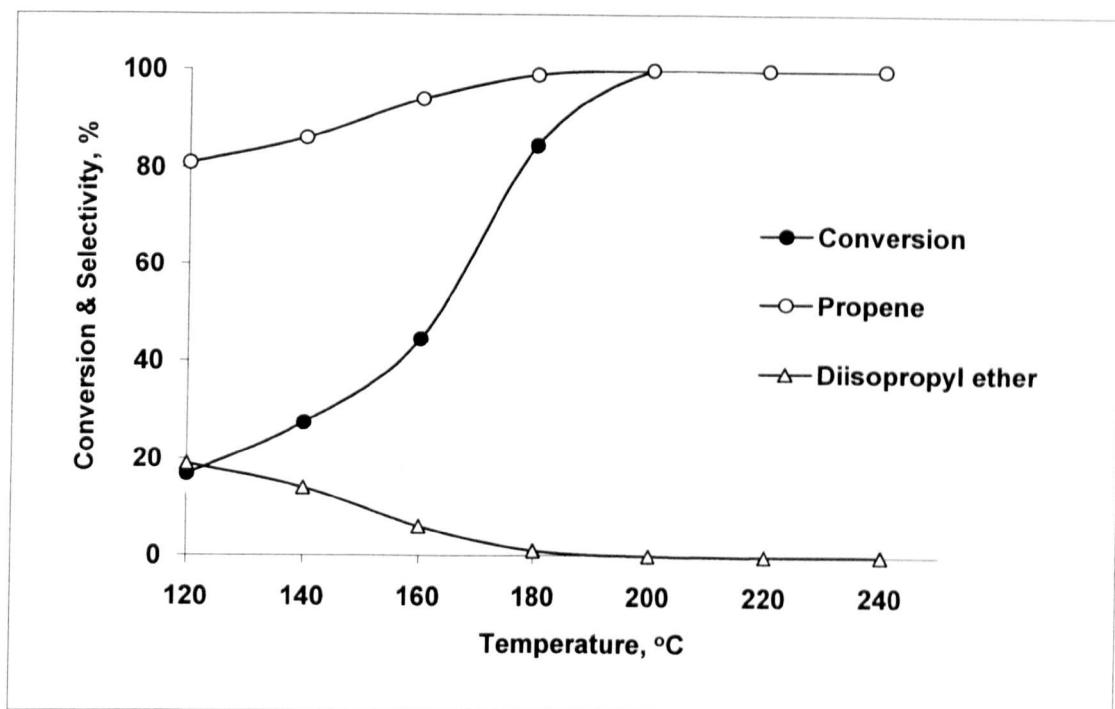


Figure 5.6 Isopropanol dehydration over 15%HPW/Nb₂O₅-500.

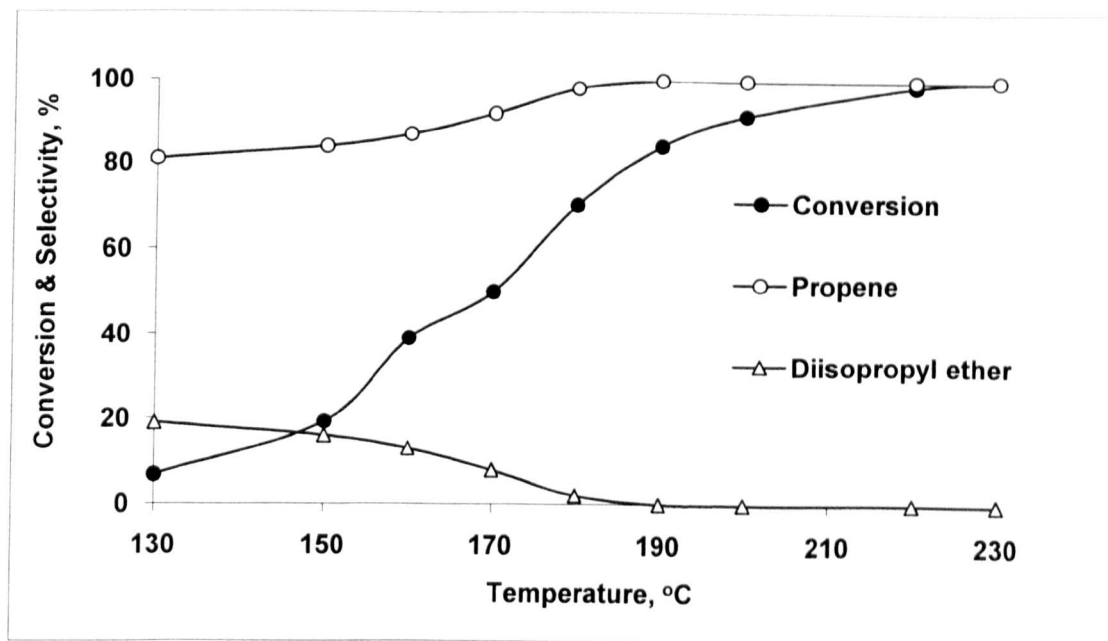


Figure 5.7 Isopropanol dehydration over 15%HPW/ZrO₂-500.

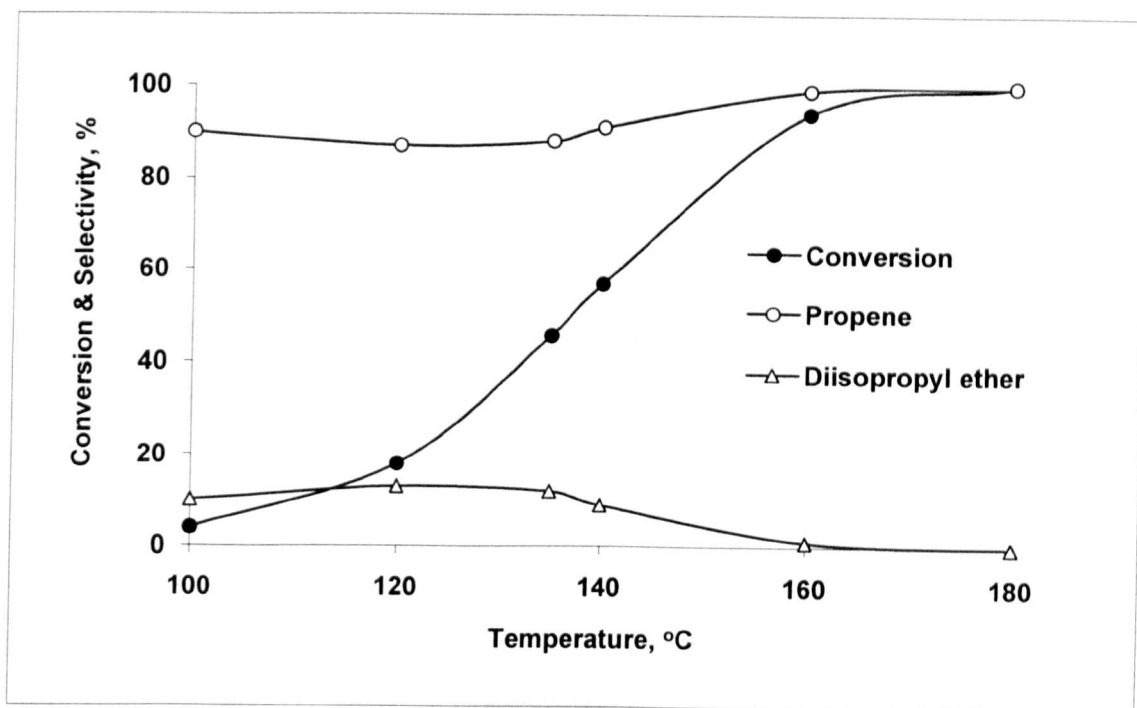


Figure 5.8 Isopropanol dehydration over 15%HPW/TiO₂-500.

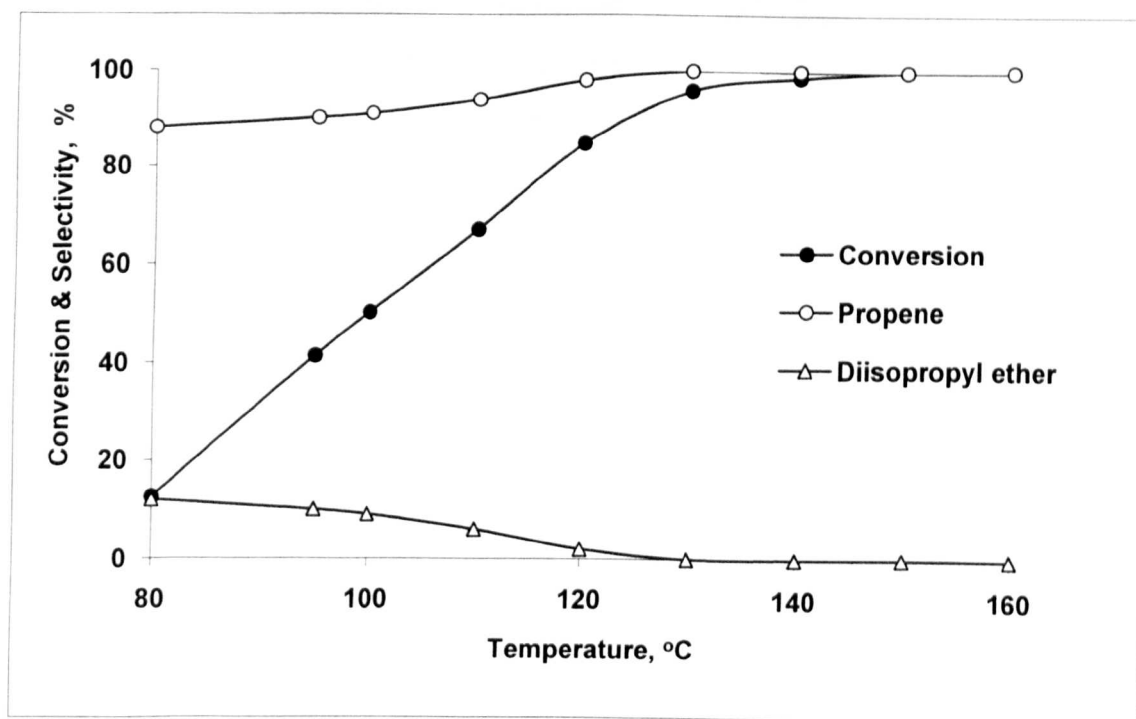


Figure 5.9 Isopropanol dehydration over Cs_{2.5}H_{0.5}PW₁₂O₄₀.

5.3.1 Effect of calcination temperature

The activity of supported catalysts decreases with increasing calcination temperature from 300 to 500°C (Table 5.1, Figure 5.10) in line with the catalyst acid strength (Table 5.1). For example, T_{50} for 15%HPW/ Nb_2O_5 calcined at 300 and 500 °C is 155 and 165 °C respectively. This can be explained by the loss of proton sites due to catalyst dehydration and the decrease in surface area.

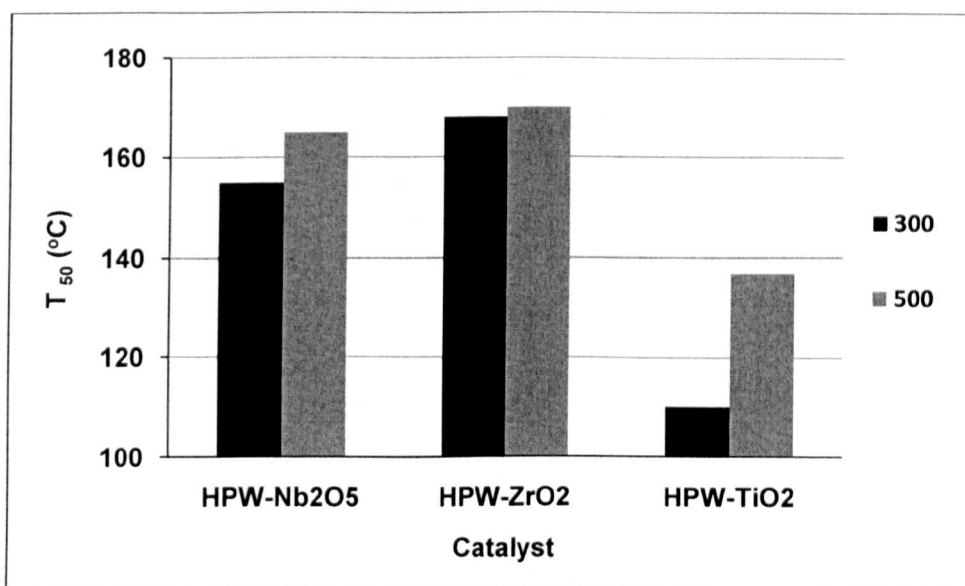


Figure 5.10 Effect of catalyst calcination temperature on T_{50} for supported HPW catalysts.

5.3.2 Activation energy

The reaction activation energy, E_a , for isopropanol dehydration was calculated from the light-off tests under differential conditions. In differential conditions (conversion less than 10%) the reaction rate becomes approximately linearly proportional to the change in conversion. Therefore the reaction rate can be calculated

directly from the incremental change in conversion [13, 14]. Apparent activation energy of less than 20 kJ/mol indicates the possibility of internal diffusion limitations [13]. The apparent activation energies for HPA catalysts were in the range of 59 – 90 kJ/mol (Table 5.1). This suggests that the reaction with all the catalysts studied occurred in the chemical regime without diffusion limitations.

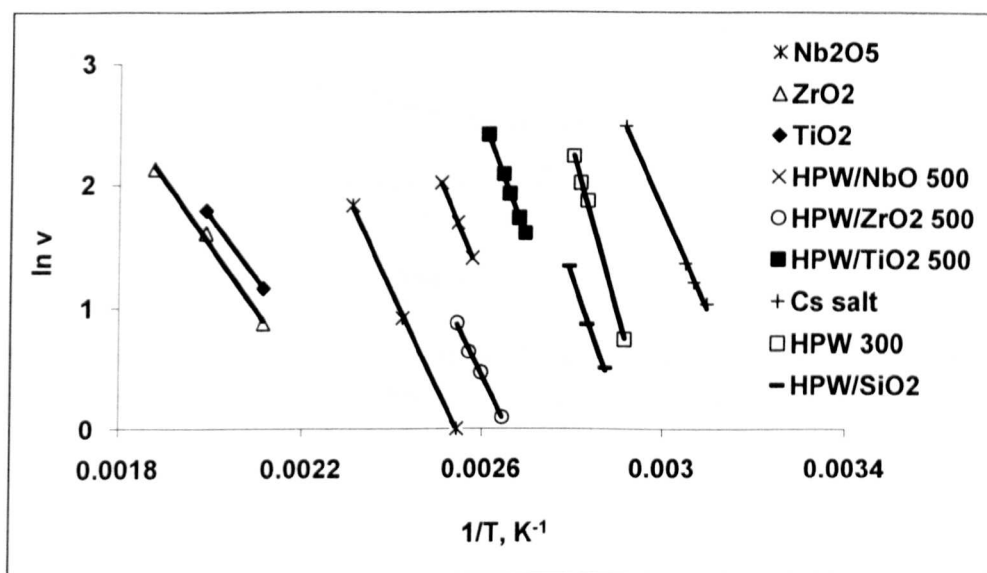


Fig. 5.11 Arrhenius plot for the calculation of the activation energy for isopropanol dehydration over different catalysts.

5.4 Reaction time course

The values of isopropanol conversion at a constant temperature of 120°C are presented in Figures 5.12a and 5.12b and in Table 5.2. Typically, the reaction reached steady state in less than 1 h and proceeded without catalyst deactivation for at least 4 h on stream. The values of isopropanol conversion at 120 °C closely follow the corresponding values of T_{50} . Propene was the major reaction product both at T_{50} and

120°C (Tables 5.1 and 5.2) and its selectivity increased with increasing the temperature in agreement with literature [3].

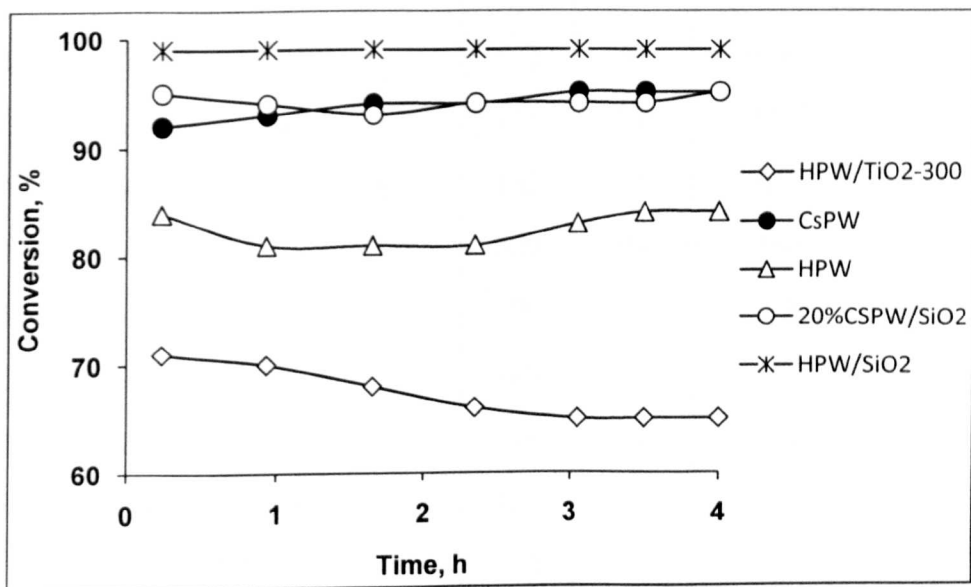


Figure 5.12a Time course for isopropanol dehydration (120 °C, 0.1 g catalyst, 2 h time on stream, 5.5 vol.% isopropanol in N₂, 20 ml/min flow rate).

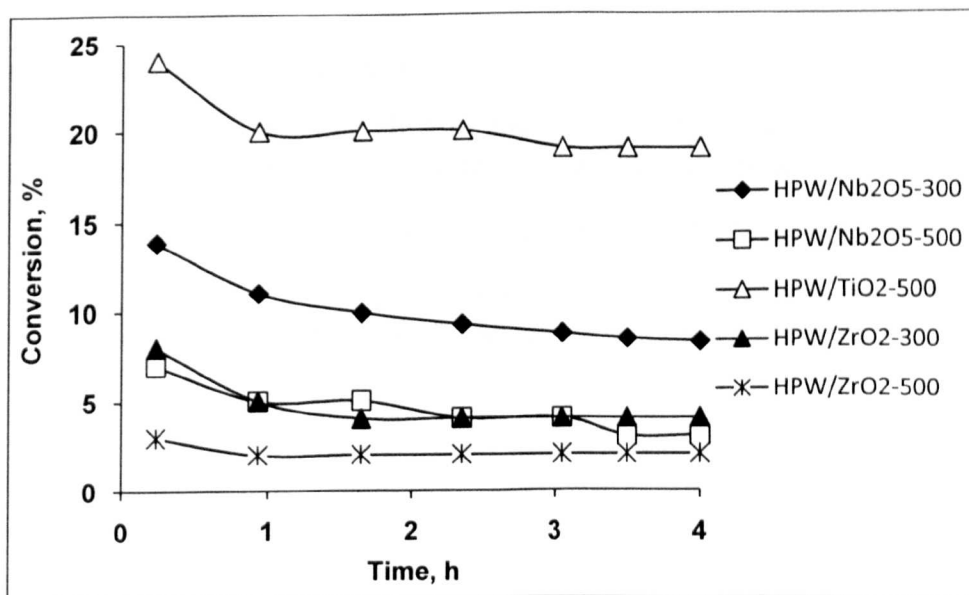


Figure 5.12b Time course for isopropanol dehydration (120 °C, 0.1 g catalyst, 2 h time on stream, 5.5 vol.% isopropanol in N₂, 20 ml/min flow rate).

Table 5.2 Isopropanol dehydration^a (120 °C, 0.1 g catalyst, 2 h time on stream, 5.5 vol.% isopropanol in N₂, 20 ml/min flow rate).

	Catalyst	S _{BET} ^b (m ² /g)	X ^c (%)	TOF ^d (h ⁻¹)	S ^e (%)
1	H ₃ PW ₁₂ O ₄₀	2	81	3500 ^f	98
2	Cs _{2.5} H _{0.5} PW ₁₂ O ₄₀	111	94	430 ^f	99
3	20%Cs ₂ H ₁ PW ₁₂ O ₄₀ /SiO ₂	185	94	430	99
4	15% HPW/SiO ₂	229	99	190	99
5	15% HPW/Nb ₂ O ₅ -500	96	4	8	84
6	15% HPW/Nb ₂ O ₅ -300	166	9	17	84
7	15% HPW/ZrO ₂ -500	54	2	4	100
8	15% HPW/ZrO ₂ -300	121	5	10	100
9	15% HPW/TiO ₂ -500	40	19	36	83
10	15% HPW/TiO ₂ -300	41	67	130	93

- a) Prior to reaction the catalysts were pre-treated in situ at 300 °C for 1 h in N₂ (20 ml/min).
- b) BET surface area.
- c) Isopropanol conversion at 120 °C.
- d) Turnover frequency per one HPA proton site at 120 °C and 2 h time on stream, assuming that all HPA protons are equally available for reaction.
- e) Propene selectivity at 120 °C; the only other product was diisopropyl ether.
- f) Turnover frequency per one surface proton site estimated assuming a Keggin anion cross section of 144 Å² and using the surface area for fresh catalysts.

5.4.1 Turnover frequency (TOF)

Turnover frequency (TOF) is a more accurate measure of catalyst activity, which is directly related to the strength of acid sites. Table 5.2 displays the TOF values for the catalysts under study at 120°C which were calculated from the corresponding values of isopropanol conversion per proton site. The number of proton sites available for reaction was worked out as follows. For supported HPA and $\text{Cs}_2\text{HPW}_{12}\text{O}_{40}$, all protons were assumed to be equally available for reaction due to a monolayer surface coverage ($\sim 45 \text{ m}^2/\text{g}$). For bulk $\text{Cs}_{2.5}\text{H}_{0.5}\text{PW}_{12}\text{O}_{40}$, which has been suggested to catalyse isopropanol dehydration via the surface type mechanism [9, 15] (see Section 1.1.5.3.1), only surface protons were taken into account. Their number was calculated assuming a Keggin unit cross section of 144 \AA^2 [9, 15] and a surface area of $111 \text{ m}^2/\text{g}$ for the fresh catalyst (Table 5.2). The TOF values thus obtained should be regarded as an approximation. The true values may be higher because the number of accessible proton sites on the surface could be smaller than the stoichiometric number of protons used in our calculations. In case of bulk HPW the situation was less clear. It has been suggested to catalyse isopropanol dehydration via the bulk type mechanism [9]. It seemed unlikely, however, that isopropanol molecules would penetrate deep in the bulk of HPA crystals at 120°C. Such reaction would be almost inevitably diffusion-hindered [16], which is not consistent with the high activation energy for the dehydration over bulk HPA (Table 5.1). Assuming that all HPA protons were available for reaction (bulk type catalysis) gave a TOF value of 23 h^{-1} , which is obviously too small. From the HPA acid strength, this value might be expected to be higher than that for $\text{Cs}_{2.5}\text{H}_{0.5}\text{PW}_{12}\text{O}_{40}$ (430 h^{-1}). If only the surface protons were active (surface type catalysis), the TOF would increase to 3500 h^{-1} , as estimated from the above Keggin unit cross section and the surface area of $2.0 \text{ m}^2/\text{g}$ for the fresh HPA catalyst (Table 5.2). It is, therefore,

conceivable that only protons in a few top layers of solid $\text{H}_3\text{PW}_{12}\text{O}_{40}$ participated in catalysis rather than all the protons in the HPA bulk.

It should be noted that the TOF values for the “standard” HPA catalysts were calculated from high isopropanol conversions (Table 5.2) and, therefore, were not under strict kinetic control. The true values may be higher under differential conditions. This, however, will not affect the general outcome of our work.

5.4.2 Relationship between log (TOF) and ΔH

Figure 5.13 shows a Brønsted type relationship between the catalytic activity of HPA catalysts in isopropanol dehydration, log (TOF), and their enthalpy of NH_3 adsorption, ΔH . This is a fairly good linear plot. The plot becomes even better if only the catalysts calcined at 300°C are included (Figure 5.13, inset). The point for bulk $\text{H}_3\text{PW}_{12}\text{O}_{40}$, calculated assuming the surface type catalysis, fits this plot well, which supports the suggested mechanism. This relationship shows that isopropanol dehydration and NH_3 adsorption calorimetry give consistent results regarding the acidity of HPA catalysts. Recently, Macht *et al.* [12] displayed similar relationship between the rate constants for 2-butanol dehydration over silica-supported HPA catalysts in the gas phase and the deprotonation energies of HPA calculated by density functional theory (DFT).

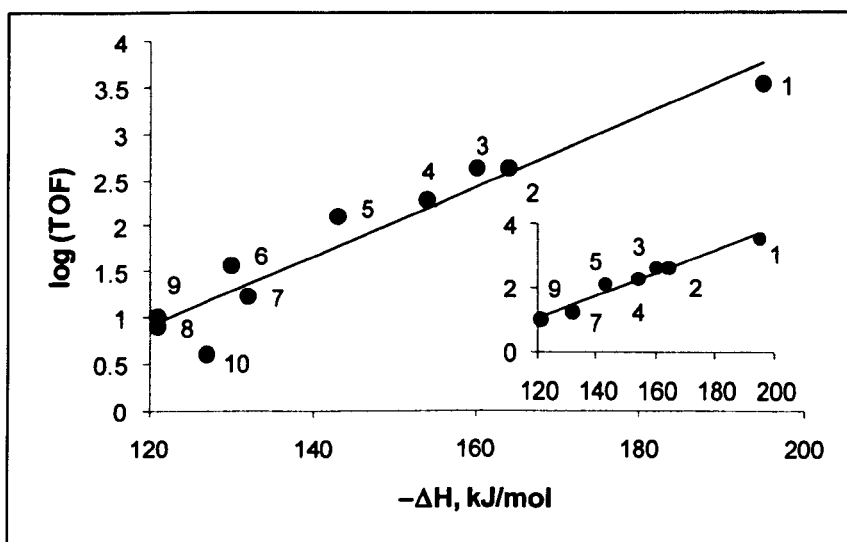


Figure 5.13 Relationship between log (TOF) and ΔH . Inset shows the catalysts calcined at 300°C. (1) $H_3PW_{12}O_{40}$, (2) $Cs_{2.5}H_{0.5}PW_{12}O_{40}$, (3) 20% $Cs_2HPW_{12}O_{40}/SiO_2$, (4) 15% HPW/ SiO_2 , (5) 15% HPW/ TiO_2 -300, (6) 15% HPW/ TiO_2 -500, (7) 15% HPW/ Nb_2O_5 -300, (8) 15% HPW/ Nb_2O_5 -500, (9) 15% HPW/ ZrO_2 -300, (10) 15% HPW/ ZrO_2 -500.

5.5 Conclusion

Solid acid catalysts comprising 15 wt% $H_3PW_{12}O_{40}$ heteropoly acid (HPA) supported on TiO_2 , ZrO_2 and Nb_2O_5 were characterised regarding their acid properties using isopropanol dehydration as a test reaction. These catalysts have been compared with “standard” HPA catalysts such as bulk and silica-supported $H_3PW_{12}O_{40}$ and $Cs_{2.5}H_{0.5}PW_{12}O_{40}$. The catalytic activity (turnover frequency) in gas-phase isopropanol dehydration decreases in the order: $H_3PW_{12}O_{40} > Cs_{2.5}H_{0.5}PW_{12}O_{40} > 15\%H_3PW_{12}O_{40}/SiO_2 > 15\%H_3PW_{12}O_{40}/TiO_2 \gg 15\%H_3PW_{12}O_{40}/Nb_2O_5 > 15\%H_3PW_{12}O_{40}/ZrO_2$, which is in line with the acid strength determined by NH_3 adsorption calorimetry.

References

- [1] K. Tanabe, M. Misono, Y. Ono, H.H. (Eds.), *New Solid Acids and Bases: Their Catalytic Properties*, Kodansha, Tokyo, 1989.
- [2] A. Ouqour, G. Coudurier, J.C. Vedrine, *J. Chem. Soc., Faraday Trans. 89* (1993) 3151.
- [3] A. Gervasini, J. Fenyvesi, A. Auroux, *Catal. Lett.* 43 (1997) 219.
- [4] D. Haffad, A. Chambellan, J.C. Lavalley, *J. Mol. Catal. A* 168 (2001) 153.
- [5] W. Turek, J. Haber, A. Krowiak, *Appl. Surf. Sci.* 252 (2005) 823.
- [6] S.R. deMiguel, A.C. Martinez, A.A. Castro, O.A. Scelza, *J. Chem. Technol. Biotechnol.* 65 (1996) 131.
- [7] Padmanab.Vr, F.J. Eastburn, *J. Catal.* 24 (1972) 88.
- [8] K.C. Waugh, M. Bowker, R.W. Petts, HD. Vandervell, J. OMalley, *Appl. Catal.* 25 (1986) 121.
- [9] T. Okuhara, N. Mizuno, M. Misono, *Adv. Catal.* 41 (1996) 113.
- [10] E. Lopez-Salinas, J.G. Hernandez-Cortez, I. Schifter, E. Torres-Garcia, J. Navarrete, A. Gutierrez-Carrillo, T. Lopez, P.P. Lottici, D. Bersani, *Appl. Catal. A* 193 (2000) 215.
- [11] L.R. Pizzio, C.V. Caceres, M.N. Blanco, *Appl. Catal. A* 167 (1998) 283.
- [12] J. Macht, R.T. Carr, E. Iglesia, *J. Catal.* 264 (2009) 54.
- [13] C. Perego, S. Peratello, *Catal. Today* 52 (1999) 133.
- [14] H. Purnama, T. Ressler, R.E. Jentoft, H. Soerijanto, R. Schlogl, R. Schomacker, *Appl. Catal. A* 259 (2004) 83.
- [15] I.V. Kozhevnikov, *Catalysts for Fine Chemicals. Vol 2. Catalysis by Polyoxometalates*, Wiley, Chichester, 2002.

- [16] J.B. Moffat, *Metal-Oxygen Clusters. The Surface and Catalytic Properties of Heteropoly Oxometalates*, Kluwer, New York, 2001.

6. Gas phase isomerisation of α -pinene over heteropoly acid catalysts

6.1 Introduction

The isomerisation of α -pinene in the presence of acid catalysts has been widely studied [1]. It produces, on one hand, camphene and tricyclene, and on the other hand, limonene and limonene derived products (see Section 1.3). Commercially, α -pinene isomerisation is carried out in the liquid-phase over an acid-treated TiO_2 catalyst. The drawback to this process is its low rate and poor selectivity, hence there is a demand for new catalysts exhibiting higher activity and selectivity and a continuous process [1].

The aim of the work in this chapter is to study the isomerisation of α -pinene in the gas phase over solid HPA catalysts. The catalysts under study are both the “standard” HPA catalysts, such as $\text{H}_3\text{PW}_{12}\text{O}_{40}$ (HPW), HPW/SiO_2 and $\text{Cs}_{2.5}\text{H}_{0.5}\text{PW}_{12}\text{O}_{40}$, and the acidic composites comprising $\text{H}_3\text{PW}_{12}\text{O}_{40}$, supported on Nb_2O_5 , ZrO_2 and TiO_2 . Hereafter, the calcination temperature is noted in the catalyst formulation as, for example, 15%HPW/ Nb_2O_5 -300 and 15%HPW/ Nb_2O_5 -500.

The characterisation of catalysts studied is given in Table 6.1. This includes parameters such as surface area, pore diameter and pore volume (Section 3.3) and initial enthalpy of ammonia adsorption (Section 3.7.1).

Table 6.1 Catalyst characterisation.

Catalyst	$S_{\text{BET}}^{\text{a}}$ (m^2/g)	Pore diameter ^b (Å)	Pore volume ^c (cm^3/g)	$-\Delta H^{\text{d}}$ (kJ/mol)
$\text{H}_3\text{PW}_{12}\text{O}_{40}$	2	81	0.04	195
$\text{Cs}_{2.5}\text{H}_{0.5}\text{PW}_{12}\text{O}_{40}$	111	24	0.07	164
15%HPW/ SiO_2	229	204	1.17	154
15%HPW/ Nb_2O_5 -300	166	52	0.22	132
15%HPW/ Nb_2O_5 -500	96	80	0.19	121
15%HPW/ ZrO_2 -300	121	24	0.07	121
15%HPW/ ZrO_2 -500	54	56	0.08	129
15%HPW/ TiO_2 -300	41	154	0.16	143
15%HPW/ TiO_2 -500	40	230	0.23	130

- BET surface area.
- Average BET pore diameter.
- Single point total pore volume.
- Initial enthalpy of ammonia adsorption at 100 °C.

6.2 Isomerisation of α -pinene in gas phase

The procedure for gas-phase isomerisation of α -pinene reactions is described in depth within Section 2.5.2.2. It is similar to that used for isopropanol dehydration which is described in Section 5.2, and is shown here for purposes of clarity. A 0.1 g catalyst was set in place on a thin layer of glass wool within a Pyrex glass reactor. All catalysts were pretreated at a temperature of 300 °C with a flow of N_2 for a period of 1 h. A N_2 flow rate of 20 mL/min was used for all reactions in this chapter, flowing through α -pinene saturator set at a temperature of 50 °C. The downstream gas flow was analysed by the on-line GC. The response factors were assumed to be the same for all

monoterpenes in the product mixture. Liquid products were collected in an ice trap and analysed by the off-line GC.

6.2.1 Reaction time course

α -Pinene isomerisation was studied in the gas-phase, focussing on the formation of camphene and limonene. Preliminary investigations in terms of α -pinene conversion and camphene selectivity led to an optimum temperature of 200 °C.

Table 6.2 gives a summary of catalyst performance after 10 h on stream, displaying α -pinene conversion and the selectivity to camphene and limonene. Camphene was the main reaction product, with limonene, terpinolenes, terpinenes, β -pinene, p-cymene as well as unidentified monoterpene by-products also formed.

The reaction time-course is shown in Figures 6.1–6.6 and 6.9–6.11. Generally, the conversion of α -pinene decreased with the time on stream, revealing catalyst deactivation. This is probably due to coke formation on catalysts which is consistent with previous studies [1]. By monitoring the carbon balance, it was found that coke deposited mainly in the first 2–3 hours of reaction, and after that practically no coking was observed. The selectivity to camphene was increasing with the time on stream, along with catalyst deactivation. This indicates that the formation of camphene is favoured on moderate rather than strong catalyst acid sites. This is in agreement with the literature [2-4].

Table 6.2 α -Pinene conversion and product selectivity. (200°C, 0.1 g catalyst, 2.0 vol.% α -pinene in N₂, 20 ml/min flow rate, 10 h time on stream).^a

Catalyst	Conversion (%)	Selectivity (%)			C ^c (wt%)
		Camphene	Limonene	Other ^b	
H ₃ PW ₁₂ O ₄₀	80	55	9	36	0.7
Cs _{2.5} H _{0.5} PW ₁₂ O ₄₀	48	67	10	23	4.9
15% HPW/SiO ₂	100	27	0	73	
15% HPW/TiO ₂ -300	94	39	3	58	
15% HPW/TiO ₂ -500	88	56	7	37	5.4
15% HPW/Nb ₂ O ₅ -300	88	32	7	61	
15% HPW/Nb ₂ O ₅ -500	85	36	8	56	9.6
15% HPW/ZrO ₂ -300	74	55	19	26	
15% HPW/ZrO ₂ -500	75	51	18	31	3.0
Nb ₂ O ₅ -500	60	45	21	34	
ZrO ₂ -500	2	55	45	0	1.5
TiO ₂ -500	20	47	28	25	3.0

- a) Prior to reaction the catalysts were pre-treated in situ at 300 °C for 1 h in N₂ (20 ml/min).
- b) A mixture of terpinolenes, terpinenes, p-cymene, β -pinene and unidentified monoterpene isomers.
- c) Carbon deposition on catalysts after reaction from combustion elemental analysis.

6.2.2 Isomerisation of α -pinene over “standard” HPA catalysts

Bulk HPA and Cs_{2.5}H_{0.5}PW₁₂O₄₀, possessing very strong Brønsted acid sites with ammonia adsorption enthalpies of -195 and -164 kJ/mol, showed high initial catalytic activity (Figures 6.1 and 6.2). However, their catalytic activity quickly declined with the time on stream, especially in the case of Cs_{2.5}H_{0.5}PW₁₂O₄₀, probably

due to catalyst coking (Table 6.2). At the same time, their selectivity to camphene was increasing to achieve 57% with $\text{H}_3\text{PW}_{12}\text{O}_{40}$ and 70% with $\text{CS}_{2.5}\text{H}_{0.5}\text{PW}_{12}\text{O}_{40}$ in 17 h on stream, which was the highest camphene selectivity observed in this work. The selectivity to limonene was also increasing to reach 11 – 14%.

Silica-supported $\text{H}_3\text{PW}_{12}\text{O}_{40}$ exhibited almost 100% α -pinene conversion, which practically did not change within 20 h on stream (Figure 6.3). This catalyst gave a moderate camphene selectivity of 27%, with only traces of limonene formed. The high activity can arise from the strong acidity as well as from the large surface area and pore diameter of this catalyst (Table 6.1). The large pore diameter is also responsible for high production of undesired products (71% yield) [5].

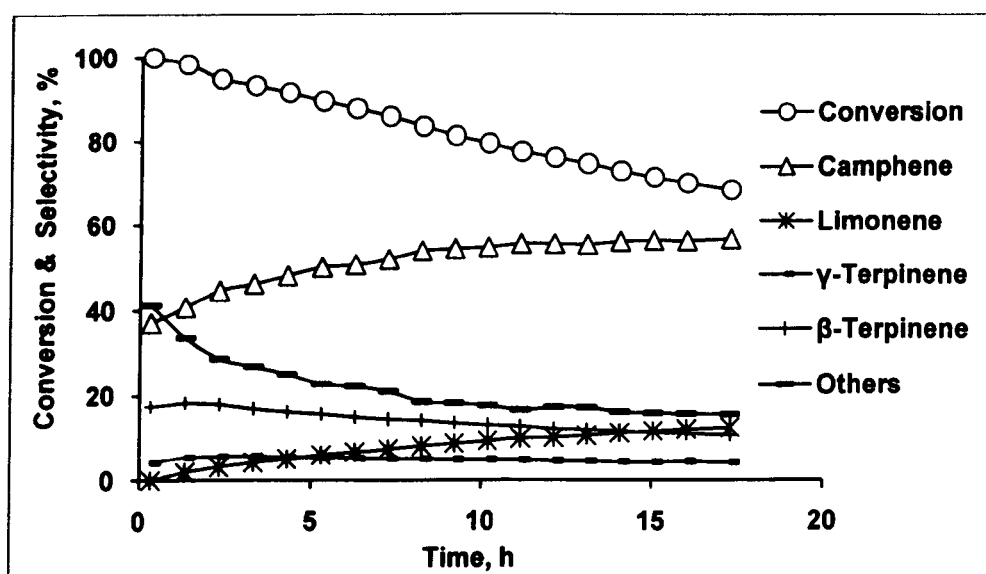


Figure 6.1 α -Pinene conversion and product selectivity over bulk HPW.

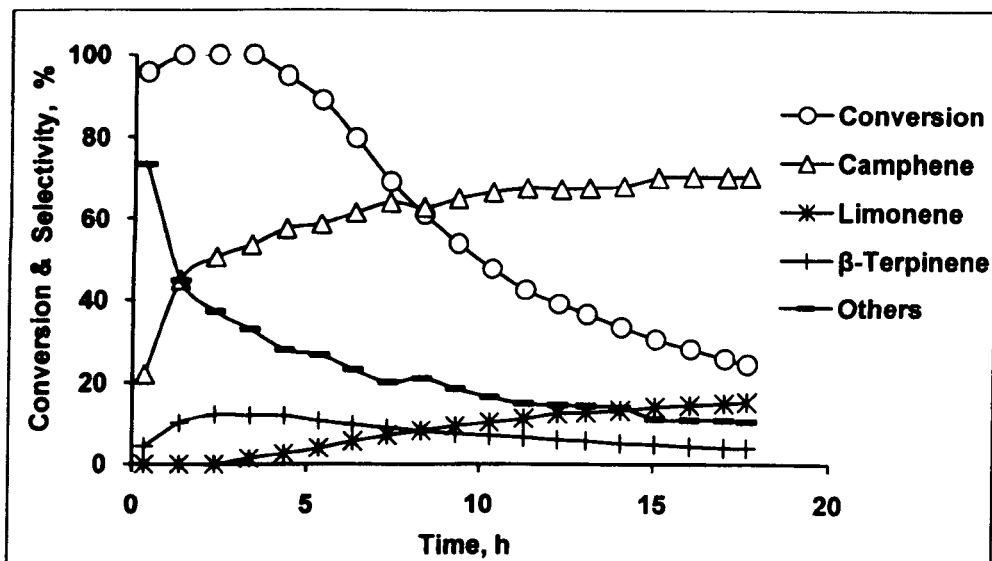


Figure 6.2 α -Pinene conversion and product selectivity over $Cs_{2.5}H_{0.5}PW_{12}O_{40}$.

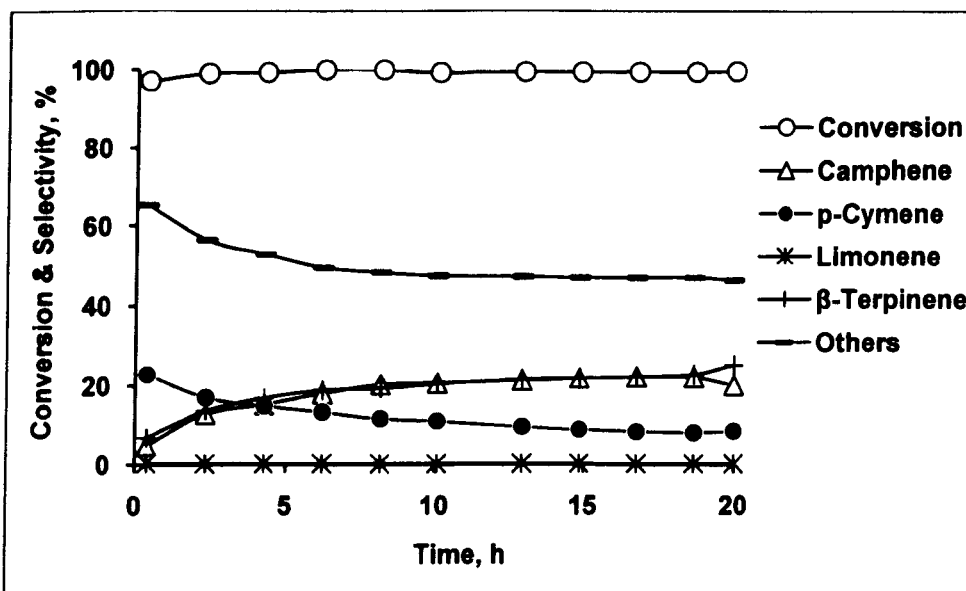


Figure 6.3 α -Pinene conversion and product selectivity over 15%HPW/SiO₂.

6.2.3 Isomerisation of α -pinene over HPW supported on Nb_2O_5 , ZrO_2 and TiO_2

The HPA catalysts supported on Nb_2O_5 , TiO_2 and ZrO_2 calcined at 500°C were all crystalline materials with fine amorphous HPA species on the catalyst surface (Section 3.5). Although weaker acids (Table 6.1), these catalysts performed better in α -pinene isomerisation regarding camphene selectivity and deactivation resistance (Figures 6.4-6.6) than the stronger acidic catalysts discussed above.

The pure niobium oxide, Nb_2O_5 -500, which possesses a relatively strong acidity [6], exhibited stable activity providing 45% camphene and 21% limonene selectivity at 60% conversion within 10 h on stream (Figure 6.4). Loading HPA on Nb_2O_5 increased the catalyst activity, albeit at the expense of camphene and limonene selectivity, providing 40% camphene and 10% limonene at 77% conversion in 20 h on stream.

The pure zirconia, ZrO_2 -500, showed a very small activity in α -pinene isomerisation, < 2% conversion (Figure 6.5). In contrast, the HPA catalyst 15%HPA/ ZrO_2 -500 performed well: 54% camphene and 20% limonene selectivity at 72% conversion in 20 h on stream (39% camphene yield). The catalyst exhibited very good resistance to deactivation, with a slight decrease in conversion from 81% to 72% in 20 h (Figure 6.5).

The pure titania, TiO_2 -500, showed a 100% initial α -pinene conversion, which, however, dropped down to 4% in 13 h on stream (Figure 6.6). The catalyst 15%HPA/ TiO_2 -500 exhibited the best performance amongst the catalysts studied, giving 59% camphene and 8% limonene selectivity at 81% conversion in 15 h on stream (51% camphene yield). It should be noted that it took about 10 h for the catalyst to reach that selectivity. This catalyst also showed good resistance to deactivation

(Figure 6.6). It is worth noting that acid treated TiO_2 is used as the catalyst in the commercial liquid-phase process of α -pinene isomerisation [1].

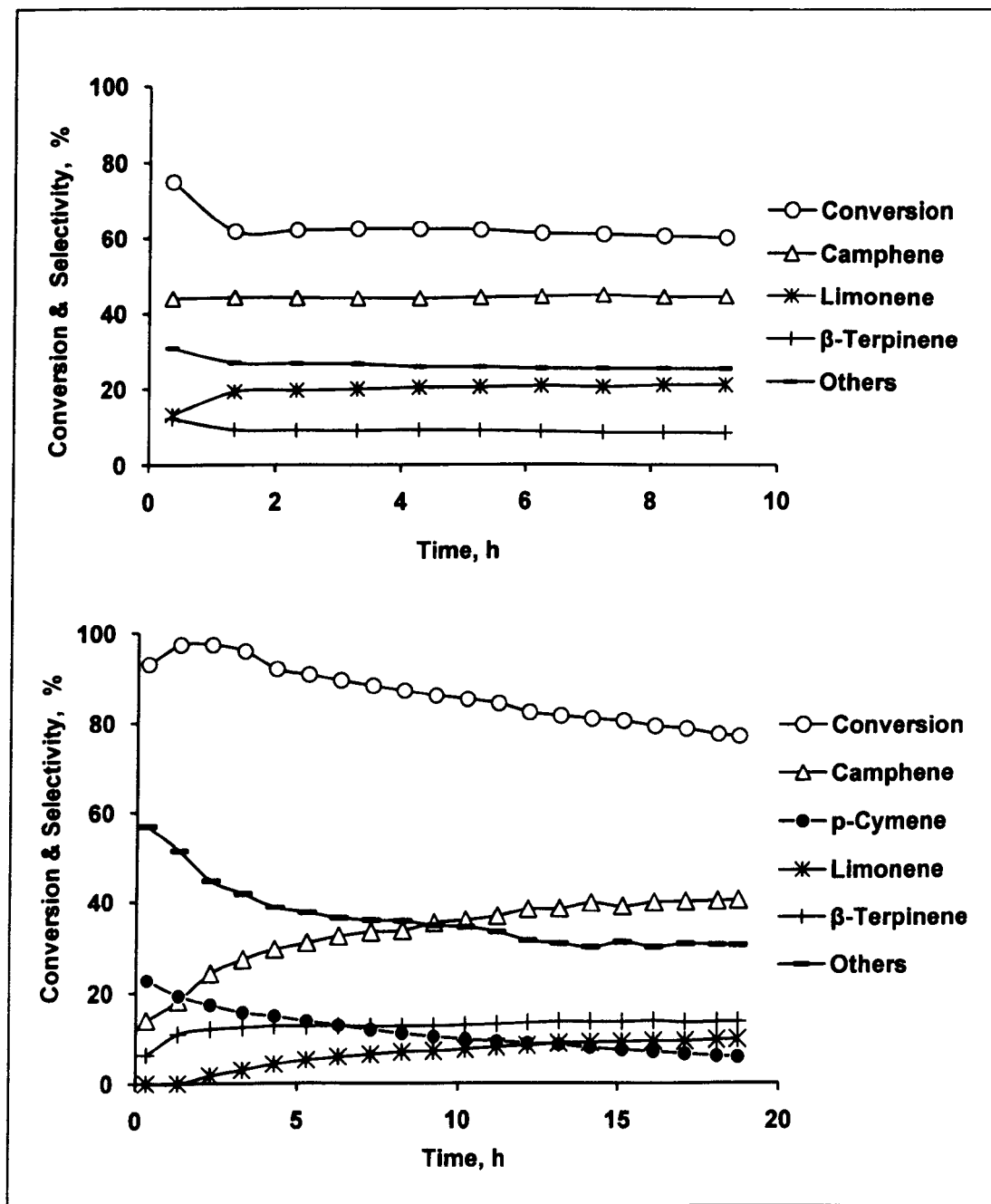


Figure 6.4 α -Pinene conversion and product selectivity over Nb_2O_5 -500 (top) and 15%HPW/ Nb_2O_5 -500 (bottom) at 200°C as a function of time on stream.

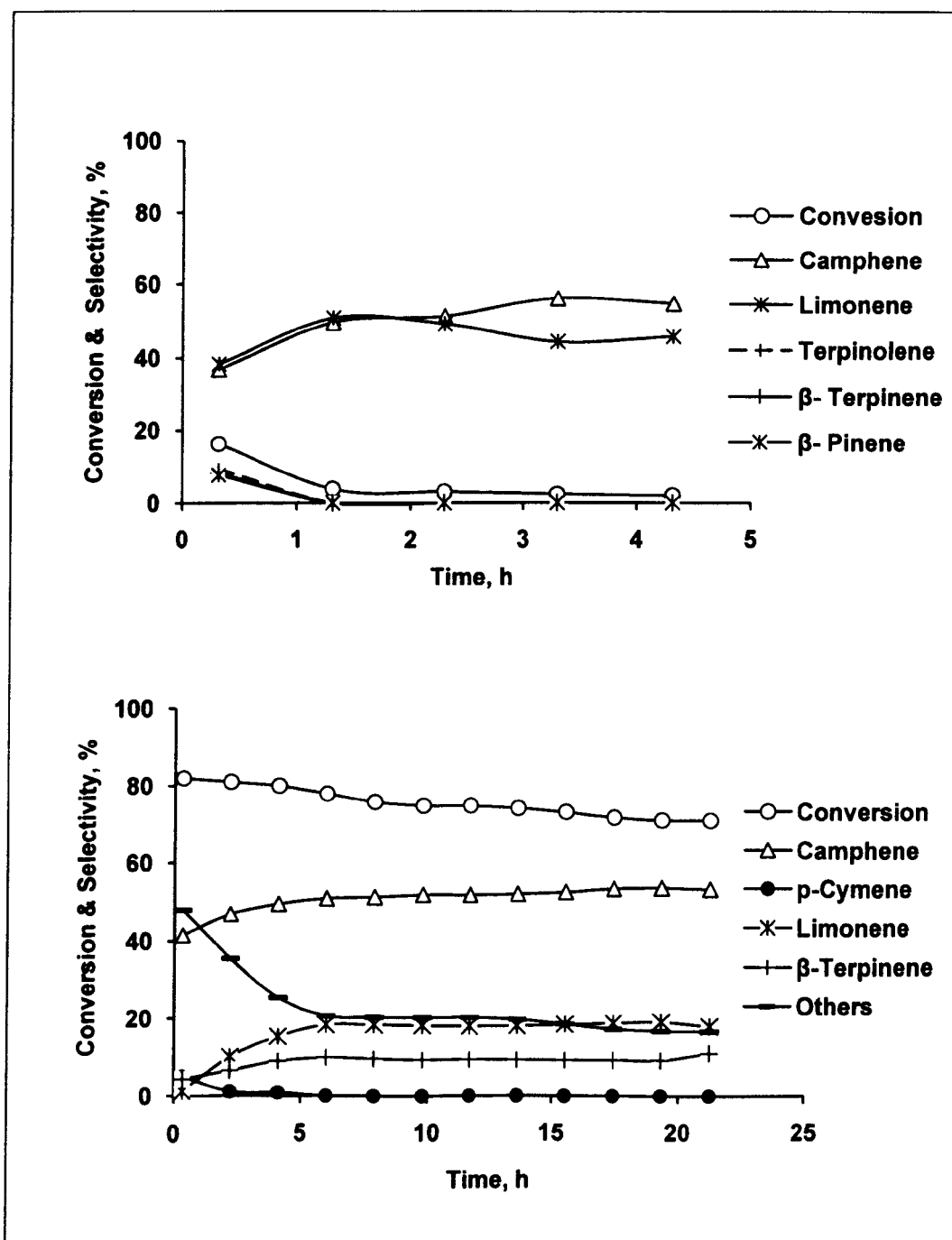


Figure 6.5 α -Pinene conversion and product selectivity over ZrO_2-500 (top) and $15\%HPW/ZrO_2-500$ (bottom) at $200^\circ C$ as a function of time on stream.

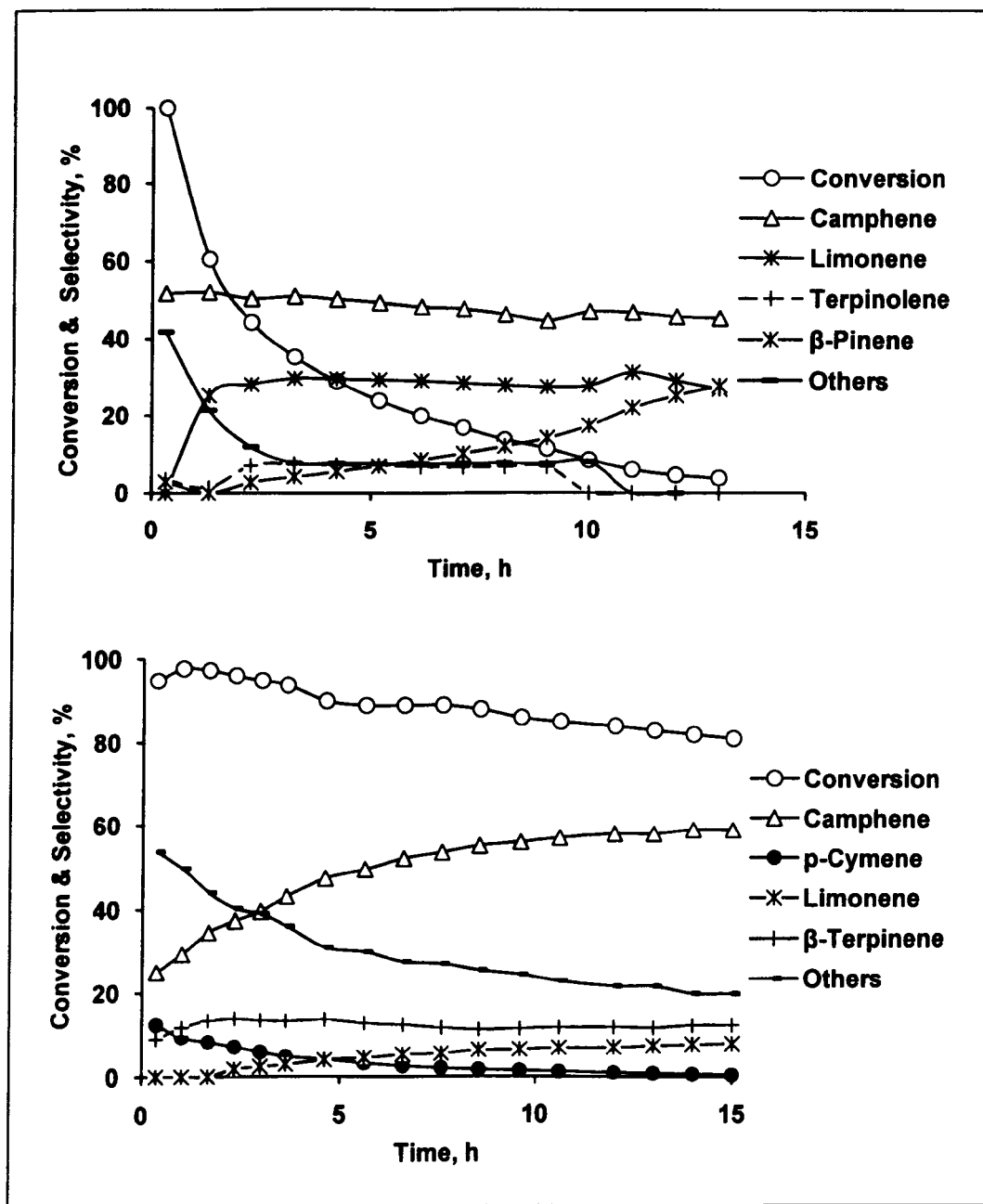


Figure 6.6 α -Pinene conversion and product selectivity over TiO₂-500 (top) and 15%HPW/TiO₂-500 (bottom) at 200°C as a function of time on stream.

6.2.4 Effect of reaction temperature

Figure 6.7 shows how the gas phase reaction results vary with increasing temperature (140-240 °C) for 15%HPW/ZrO₂-500 catalysts. The reactions were carried out for a period of 3 h, at the same conditions described above.

The α -pinene conversion rises steadily from around 47 % at 140 °C to approximately 95% at 220 °C. At the higher temperature of 240 °C α -pinene conversion decreases to 85%. Increasing reaction temperature from 140 °C to 160 °C led to a decrease in camphene and limonene selectivities from 51% to 46% and 13% to 9% respectively. Then, as the temperature further increased, the selectivities of camphene and limonene remain steady up to 200 °C. After that, a further decrease in selectivities was observed.

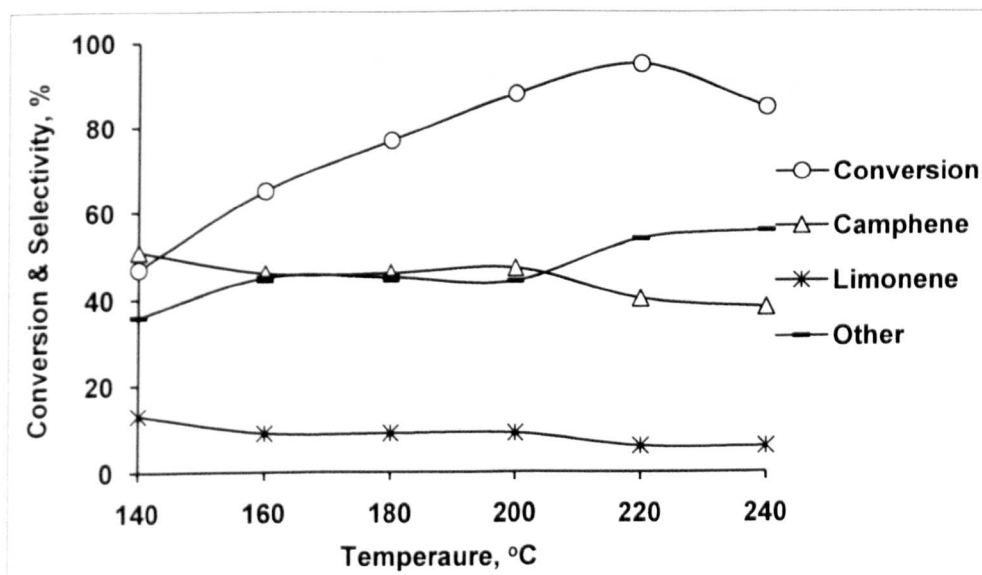


Figure 6.7 Effect of temperature on the catalytic performance of 15%HPW/ZrO₂-500

6.2.5 Effect of calcination temperature

The catalysts comprising HPA supported on Nb₂O₅, TiO₂ and ZrO₂ calcined at 300°C showed α -pinene conversions similar to that for the crystalline catalysts calcined at 500°C (Figures 6.8-6.10). In case of 15%HPA/ZrO₂ catalyst, the selectivity values did not depend on the calcination temperature. For the niobia and titania HPA catalysts, the selectivity to camphene was lower than that for the catalysts calcined at 500°C.

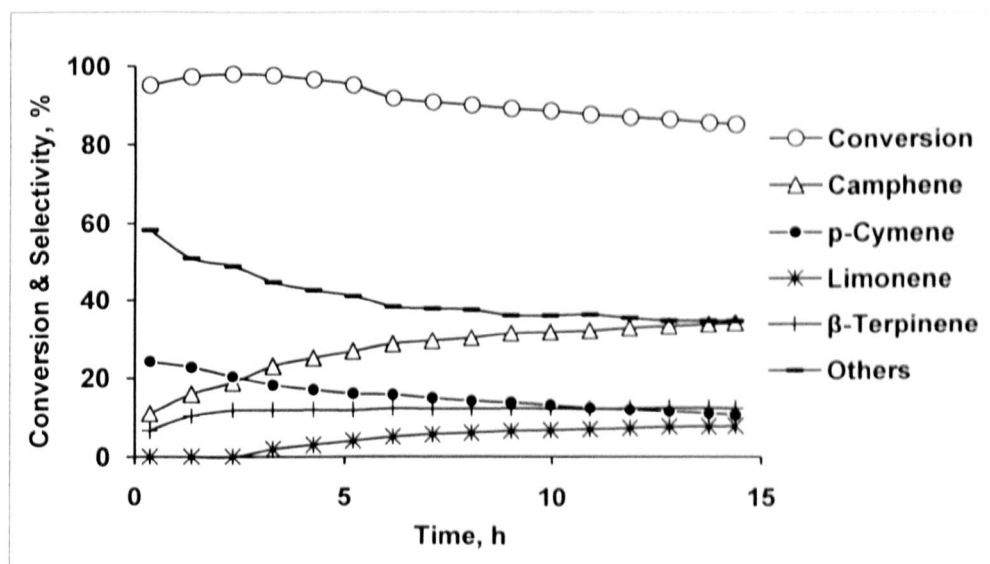


Figure 6.8 α -Pinene conversion and product selectivity over 15%HPW/Nb₂O₅-300 at 200°C as a function of time on stream.

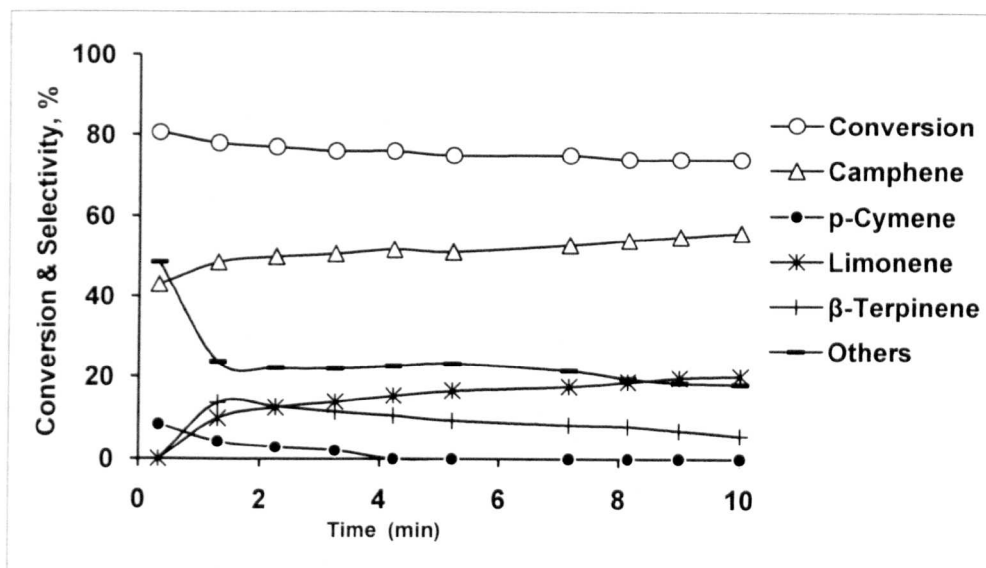


Figure 6.9 α -Pinene conversion and product selectivity over 15%HPW/ZrO₂-300 at 200°C as a function of time on stream.

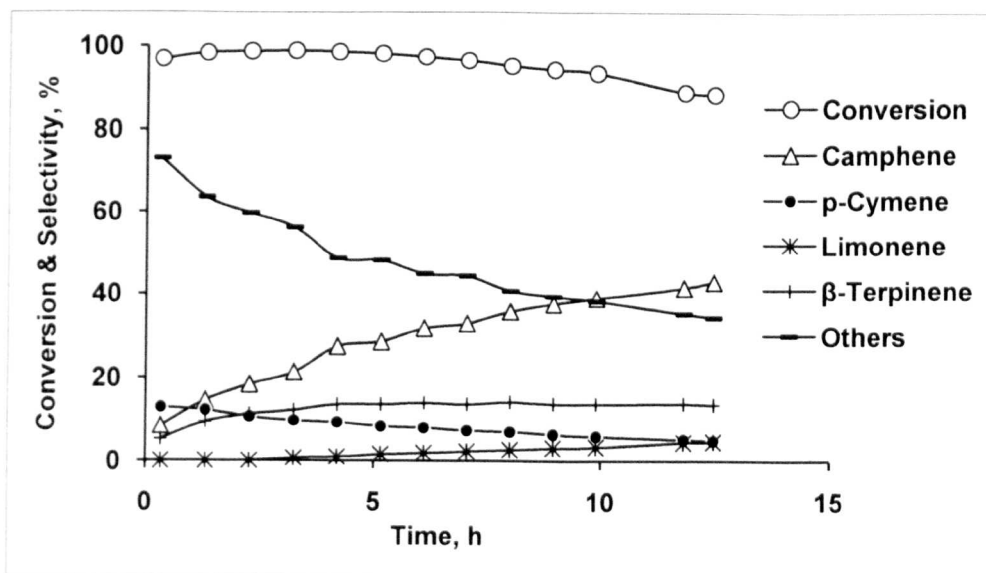


Figure 6.10 α -Pinene conversion and product selectivity over 15%HPW/TiO₂-300 at 200°C as a function of time on stream.

6.3 Conclusion

The acid-catalysed isomerisation of α -pinene is of industrial value to produce camphene and limonene, important industrial intermediates and ingredients. Here this reaction has been studied in the gas/solid system over a range of bulk and supported heteropoly acid catalysts based on $\text{H}_3\text{PW}_{12}\text{O}_{40}$ in a fixed bed flow reactor. Camphene is the main reaction product together with other monoterpenes such as limonene, terpinolenes, terpinenes, β -pinene, p-cymene, etc. The performance of these catalysts, regarding the product selectivity and catalyst resistance to deactivation, is profoundly dependent on the catalyst acidity. Thus, bulk $\text{H}_3\text{PW}_{12}\text{O}_{40}$ and $\text{Cs}_{2.5}\text{H}_{0.5}\text{PW}_{12}\text{O}_{40}$ possessing very strong Brønsted acid sites suffer from intense deactivation. Conversely, $\text{H}_3\text{PW}_{12}\text{O}_{40}$ supported on Nb_2O_5 , ZrO_2 and TiO_2 , although weaker acids, exhibit more stable as well as more selective performance in this reaction. The catalysts comprising $\text{H}_3\text{PW}_{12}\text{O}_{40}$ supported on ZrO_2 and TiO_2 give a camphene yield of 39% and 51% and a total camphene and limonene yield of 53% and 58% respectively after 15 h on stream.

References

- [1] A. Corma, S. Iborra, A. Velty, *Chem. Rev.* 107 (2007) 2411.
- [2] A. Severino, A. Esculcas, J. Rocha, J. Vital, L.S. Lobo, *Appl. Catal. A* 142 (1996) 255.
- [3] A. Stanislaus, L.M. Yeddanapalli, *Can. J. Chem.* 50 (1972) 61.
- [4] A. Stanislaus, L.M. Yeddanapalli, *Can. J. Chem.* 50 (1972) 113.
- [5] O. Akpolat, G. Gunduz, F. Ozkan, N. Besun, *Appl. Catal. A* 265 (2004) 11.
- [6] P. Carniti, A. Gervasini, S. Biella, A. Auroux, *Chem. Mater.* 17 (2005) 6128.

7. Conclusions

Heteropolyacids (HPAs) possess very strong Brønsted acidity, being stronger than conventional acids such as H_2SO_4 , mixed oxides, zeolites, etc. The Keggin type HPAs are more stable and easier to synthesise than other HPAs. Therefore, solid HPAs are promising catalysts for various reactions including selective oxidation and acid-catalysed reactions. However, HPAs are highly soluble in polar media which affects their application in liquid-phase reactions. Another drawback of HPAs is their low surface area ($1\text{--}10\text{ m}^2/\text{g}$). Thus, dispersing HPAs on solid supports with high surface areas is important for catalytic application.

Alternative fuels developed from renewable feedstocks have attracted much interest recently. Biodiesel is one of such alternative fuels produced from vegetable oils or animal fats. It is biodegradable, non-toxic and has a low emission profile. Low quality oils have been used in order to minimise cost of biodiesel production. Commercial production of biodiesel employs homogeneous alkali catalysts. These catalysts, although highly active, are sensitive to water and suffer from poisoning by fatty acids that are present in the feedstock. Their separation also presents an environmental problem. Homogeneous acid catalysts require high temperature, high molar ratio of alcohol to oil, difficult separation of the catalyst and corrosion. Solid acid catalysts have strong potential to replace liquid acids, eliminating separation, corrosion and environmental problems. The downside is that acid catalysts are significantly less active than the alkali catalysts.

α -Pinene is another important renewable feedstock. It is isomerised to produce camphene and limonene, important intermediates and ingredients in cosmetics, food and pharmaceutical industries. Commercially, α -pinene isomerisation is carried out in the liquid-phase over an acid-treated TiO₂ catalyst. The drawback to this process is its low rate and poor selectivity, hence there is a demand for new catalysts exhibiting higher activity and selectivity and a continuous process.

The aim of this work was to study homogeneous and heterogeneous catalysis by HPAs for conversion of renewable feedstocks to fuel and chemicals. Our main focus was on the HPW, the strongest acid among the Keggin HPAs. A range of catalysts based on HPW was prepared and tested for the liquid-phase transesterification and esterification reactions with methanol modeling biodiesel synthesis and gas-phase isomerisation of α -pinene to camphene. This is complemented by the characterisation of catalyst texture and chemical environment of HPA on the catalyst surface.

The composites under study comprised HPW (15 wt%) supported on Nb₂O₅, ZrO₂ and TiO₂. These were prepared by wet impregnation of oxide supports with aqueous HPW solution. These catalysts were compared to the “standard” bulk and supported HPA catalysts such as HPW, HPW/SiO₂ and CsPW as well as conventional acids such as H₂SO₄, zeolites and Amberlyst-15.

Catalyst texture, state of HPW on the surface, catalyst crystallinity, nature and strength of acid sites were investigated using different techniques including nitrogen adsorption using the BET method, Fourier transform infrared spectroscopy (FT-IR), X-ray diffraction (XRD), ³¹P MAS NMR and differential scanning calorimetry (DSC) as well as isopropanol dehydration as a test reaction.

The surface area analysis revealed that all the catalysts were mesoporous materials with average pore diameters of 22 – 230 Å. Changing the aging temperature did not affect the texture of supported HPW catalysts, while the surface area decreased significantly after increasing the calcination temperature. The supported HPA catalysts on Nb₂O₅ and ZrO₂ calcined at 300°C were amorphous. After calcination at 500°C, they became crystalline, exhibiting the patterns of the corresponding oxide supports. 15%HPW/TiO₂ after calcination at 300 and 500 °C exhibited the pattern of anatase TiO₂. The state of HPA on Nb₂O₅, ZrO₂ and TiO₂ was investigated by FT-IR and ³¹P MAS NMR using well-documented bulk and silica-supported HPA as reference materials. After calcination at 300 °C, only the 15%HPA/TiO₂ catalyst exhibited Keggin species (vibrations at 1080 and 983 cm⁻¹, and ³¹P NMR peak -14.9 ppm). After calcination temperature of 500 °C, none of the catalysts under study showed any Keggin species, which is explained by HPA decomposition and/or strong HPA/support interaction. In contrast to the parent acid, HPW, possessing strong Brønsted acid sites, the catalysts comprising HPW supported on Nb₂O₅, ZrO₂ and TiO₂ were found to possess both Brønsted and Lewis acid sites. The Brønsted/ Lewis site ratio (B/L) was higher in supported HPA catalysts than in the corresponding oxide supports. The relative number of Brønsted acid sites decreased with increasing calcination temperature due to catalyst dehydration. Their acid sites were weaker than those in HPW and CsPW.

The catalytic activity (turnover frequency) in isopropanol dehydration decreased in the order: HPW > CsPW > 15%HPW/SiO₂ > 15%HPW/TiO₂ >> 15%HPW/Nb₂O₅ > 15%HPW/ZrO₂, which is in line with the acid strength determined by NH₃ adsorption calorimetry. From the catalyst acid strength and catalyst characterisation by FTIR and ³¹P MAS NMR, the HPA/support interaction increases in the series: SiO₂ < TiO₂ <

Nb₂O₅, ZrO₂, which can be thought to cause the decrease of the catalyst acid strength in that order. Regarding their acid strength, the HPW catalysts supported on Nb₂O₅, ZrO₂ and TiO₂ oxides appear to be similar to acidic zeolites. These catalysts may have advantage over zeolite catalysts in the case of reactions involving large organic molecules that will not fit into zeolite micropores.

HPAs were found to be active catalysts for the esterification of hexanoic acid and transesterification of ethyl propanoate and ethyl hexanoate with methanol in both homogeneous and heterogeneous liquid-phase systems. The reactions were carried out at 60°C under atmospheric pressure at a substrate/methanol molar ratio of 1:20. In homogeneous system, HPAs were much more active than H₂SO₄ in terms of turnover frequency (TOF): HPW > HSiW > HPMo > H₂SO₄ which in line with the acid strength of these acids. In the heterogeneous systems, TOF for HPW supported on Nb₂O₅, ZrO₂ and TiO₂ was higher than that of the conventional solid acid catalysts such as Amberlyst-15, HY and H-Beta: 15%HPW/Nb₂O₅, 15%HPW/ZrO₂, 15%HPW/TiO₂ > HY, H-Beta > Amberlyst-15, which is explained by the greater acid strength of HPA compared to the other acids. However, these catalysts suffered from leaching and exhibited significant contribution of homogeneous catalysis by the leached HPA.

Isomerisation of α -pinene over HPW supported on Nb₂O₅, ZrO₂ and TiO₂ was carried out in the gas-phase at 200°C. The catalytic activity, selectivity and deactivation resistance of these catalysts were compared with “standard” HPAs such as bulk HPW, CsPW and HPW/SiO₂ and was found to be greatly dependent on the catalyst acidity. The catalysts possessing very strong Brønsted acid sites such as bulk HPW and CsPW suffered from intense deactivation. On the contrary, HPW supported on Nb₂O₅, ZrO₂ and TiO₂, possessing weaker acids, exhibited more stable as well as more selective performance in this reaction. The catalysts comprising HPW supported on ZrO₂ and

TiO₂ showed stable performance for at least 20 h on stream with 39% and 51% yield of camphene and 53% and 58% total yield of camphene and limonene respectively after 15 h on stream.

As HPA is an efficient catalyst for the esterification and transesterification reactions, as well as isomerisation of α -pinene, other renewable feedstocks such as carbohydrates and glycerol can also be tested to produce value added chemicals.

Further work is required to acquire thermally stable HPA compounds possessing strong acid sites and leaching resistance.